Lipidomics study in liver metabolic diseases
Singh, M.

Citation
Singh, M. (2024, June 13). *Lipidomics study in liver metabolic diseases*. Retrieved from https://hdl.handle.net/1887/3762800

Lipidomics Study
in
Liver Metabolic Diseases

Madhulika Singh

Lipidomics Study
in
Liver Metabolic Diseases

Proefschrift

ter verkrijging van de graad van doctor aan de Universiteit Leiden,

op gezag van rector magnificus prof.dr.ir. H. Bijl,

volgens besluit van het college voor promoties

te verdedigen op donderdag 13 juni 2024

klokke 16.15 uur

door

Madhulika Singh

geboren te Ballia, India

in 1990

Promotor

Prof. dr. T. Hankemeier

Co-promotor

Dr. A.C. Harms

Promotiecommissie:

Prof. dr. H. Irth

Prof. dr. E.C.M. de Lange

Prof. dr. J.M.F.G Aerts

Prof. dr. U. Spiekerkötter
   Universiteit Freiburg

Dr. B. Ramos Molina
   Biomedical Research Institute of Murcia

Dr. F. Vaz
   Amsterdam UMC

Contents

Chapter 1

General introduction and scope

Introduction

Liver metabolic diseases encompass a group of conditions arising from a multitude of factors including environmental, lifestyle choices, viral infections, or genetic mutations resulting in enzyme deficiencies, affecting the normal metabolic processes associated with the liver. Lipidomics, a branch of metabolomics, plays a pivotal role in advancing our understanding of liver metabolic diseases by identifying, quantifying and characterizing lipids in the liver. By examining the diverse lipid species present in the liver, elucidating their structural variations, and deciphering their functional implications, lipidomics provides valuable insights into the underlying mechanisms of these diseases. This approach not only aids in the identification of potential biomarkers but also provides a deeper comprehension of the complex interplay between lipids and metabolic dysregulation in the liver, paving the way for more targeted and effective therapeutic interventions.

Metabolomics and Lipidomics

Systems biology is a multidisciplinary approach that aims to understand the interactions in biological systems by interlinking biochemical networks from the molecular level to the entire organism level. The development of various omics technologies such as genomics, proteomics, transcriptomics and metabolomics advanced our understanding of the biological system. **Figure 1** shows the hierarchy of systems biology. Metabolomics serves as a reporter for downstream processes in systems biology and involves the measurements of small molecules (metabolites) which are end products of biological processes. Understanding changes in these metabolites can assist in unraveling the complex interactions between genes, transcriptional activators, proteins and enzymes, to gain insights into the overall functioning of biological systems [1,2]. Liquid-chromatography coupled to tandem mass spectrometry (LC-MS/MS) has been the most commonly used method for metabolomics studies as this technique provides high sensitivity, selectivity and broad coverage of metabolites such as amino acids, organic acids, amines, acylcarnitines, flavonoids, etc.
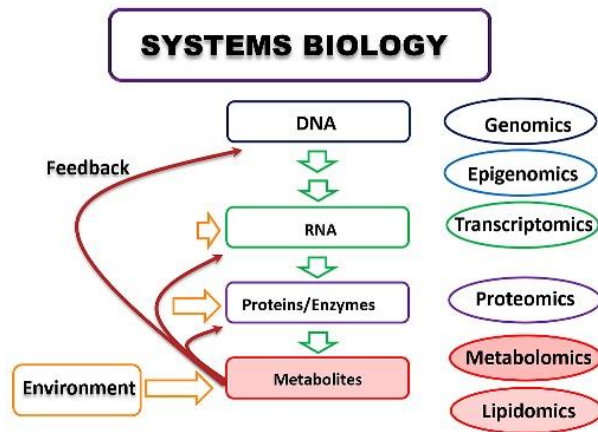
Figure 1. Hierarchy of systems biology showing the connection between different omics approaches [1]. Figure was reprinted under the Creative Commons Attribution License.

Lipidomics is a branch of metabolomics that focuses on the comprehensive analysis of lipids present in biological systems. A typical metabolomics/lipidomics workflow is depicted in **Figure 2**. The ultimate aim of lipidomics analysis is to identify and quantify the lipid biomarkers that can differentiate between healthy subjects and patients. These biomarkers can also contribute to understanding the biochemical and pathophysiological mechanisms of disease pathogenesis. Understanding deviations in the lipid profile due to a disease state is not only beneficial for diagnosis but also essential for monitoring the disease and evaluating a treatment's outcome [3,4].
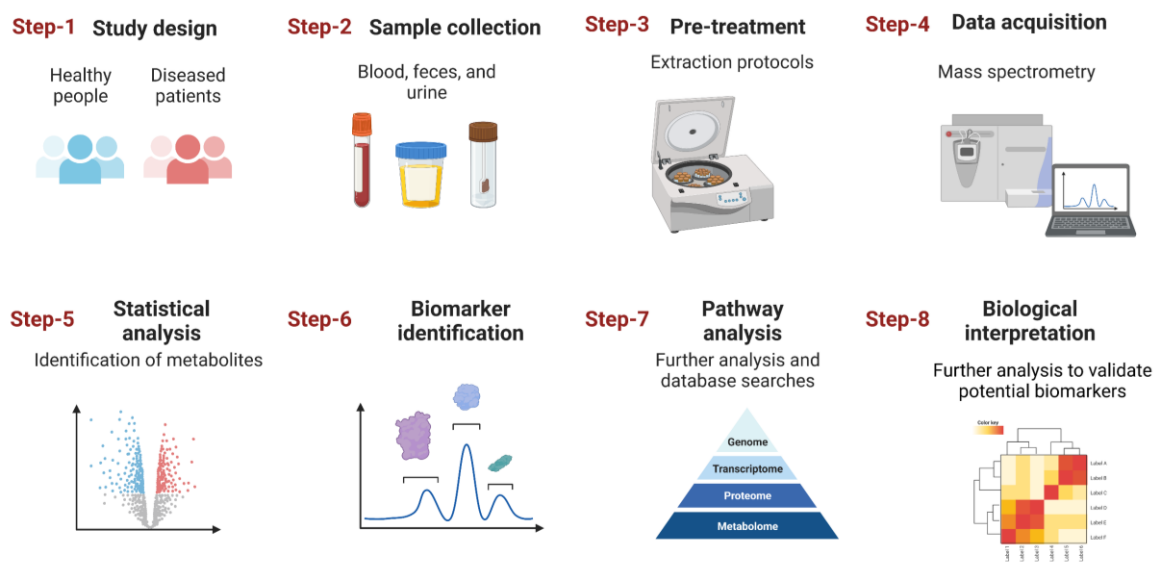
Figure 2. Metabolomics/lipidomics workflow for biomarker identification. (Figure designed with material from BioRender.com).

Advances in liquid chromatography coupled to mass spectrometry (LC-MS) techniques have facilitated lipidomics profiling in complex biological matrices, thus helping in the discovery of novel diagnostic biomarkers.

Lipids classification and biosynthetic pathway

Approximately 70% of entries in the Human Metabolome Database (HMDB) are classified as lipids [5]. The lipidome consists of tens to hundreds of thousands of entities that arise due to variations in the head groups, fatty acid chains, type of linkage, unsaturation, isomerism, etc. [6]. There are more than 44,800 lipid features present in the LIPID MAPS database [3]. The International Lipid Classification and Nomenclature Committee (ILCNC) under the LIPID MAPS consortium developed the ''Comprehensive Classification System for Lipids'' [7,8]. Based on the biosynthesis and structure of lipids, lipids are divided into eight categories including glycerolipids, glycerophospholipids, sphingolipids, sterol lipids, prenol lipids, saccharolipids, polyketides and fatty acyls. Saccharolipids and polyketides are found only in plants and bacteria while the other six classes are found in all organisms. This thesis will focus on five categories, glycerolipids, glycerophospholipids, sphingolipids, sterol lipids and fatty acyls. Each category is further divided into several classes and/or subclasses and typically consists of a backbone and fatty acid chain [6]. Glycerophospholipids consist of a polar head group, glycerol backbone and one or two fatty acid chains [8]. This category includes classes such as phosphatidylcholine, phosphatidylethanolamine, phosphatidylglycerol, etc. Glycerolipids consist of a glycerol backbone with one, two or three fatty acid chains esterified at the hydroxyl group of glycerol. Examples of this category include monoglycerides, diglycerides and triglycerides [8]. Sphingolipids are another category of complex lipids that contain a sphingosine backbone N-acylated with fatty acid chain and include classes such as ceramides and sphingomyelin [9]. Cholesteryl esters are members of sterol lipids and are formed by esterification of the hydroxyl group of cholesterol with the free fatty acids [10]. Acyl-coenzyme A (acyl-CoA) belongs to the group of thioester compounds and comes under the category of fatty acyl lipids [11]. Acyl-CoA molecules consist of a fatty acid chain linked to the coenzyme A moiety through a thioester bond. These molecules play a crucial role in fatty acid metabolism.

Lipids are involved in numerous physiological functions including important constituents for various tissues and organs, contributing to cell membrane structure, energy metabolism, signaling, cell-cell interactions, etc. [5,12]. The role of lipids has been established in various

diseases such as cancer, Alzheimer's, atherosclerosis, diabetes, obesity and also in the recent COVID-19 pandemic [13–17].

Lipid biosynthetic and catabolic pathways are highly influenced by dietary processes. In high glucose conditions, glycolysis in the cytosol converts glucose to pyruvate, which is then transformed into acetyl-CoA through oxidative decarboxylation [18]. Acetyl-CoA enters the Krebs cycle for ATP production. Citrate derived from the Krebs cycle returns to the cytosol where it regenerates acetyl-CoA via ATP citrate lyase. This acetyl-CoA serves as a precursor for fatty acid and lipid biosynthesis. In low glucose (starvation) conditions, lipids break down into free fatty acids which enter mitochondrial fatty acid beta-oxidation (FAO) to generate acetyl-CoA. **Figure 3** depicts the metabolic pathway of lipids and provides a clear depiction of the interconnected nature of lipid biosynthesis. The modification in the profile of one lipid class will significantly influence the profile of other classes. Therefore, comprehensive analysis of the majority of classes involved in the lipid metabolism pathway is crucial to gain a deeper understanding of the pathophysiology underlying behind various disorders.
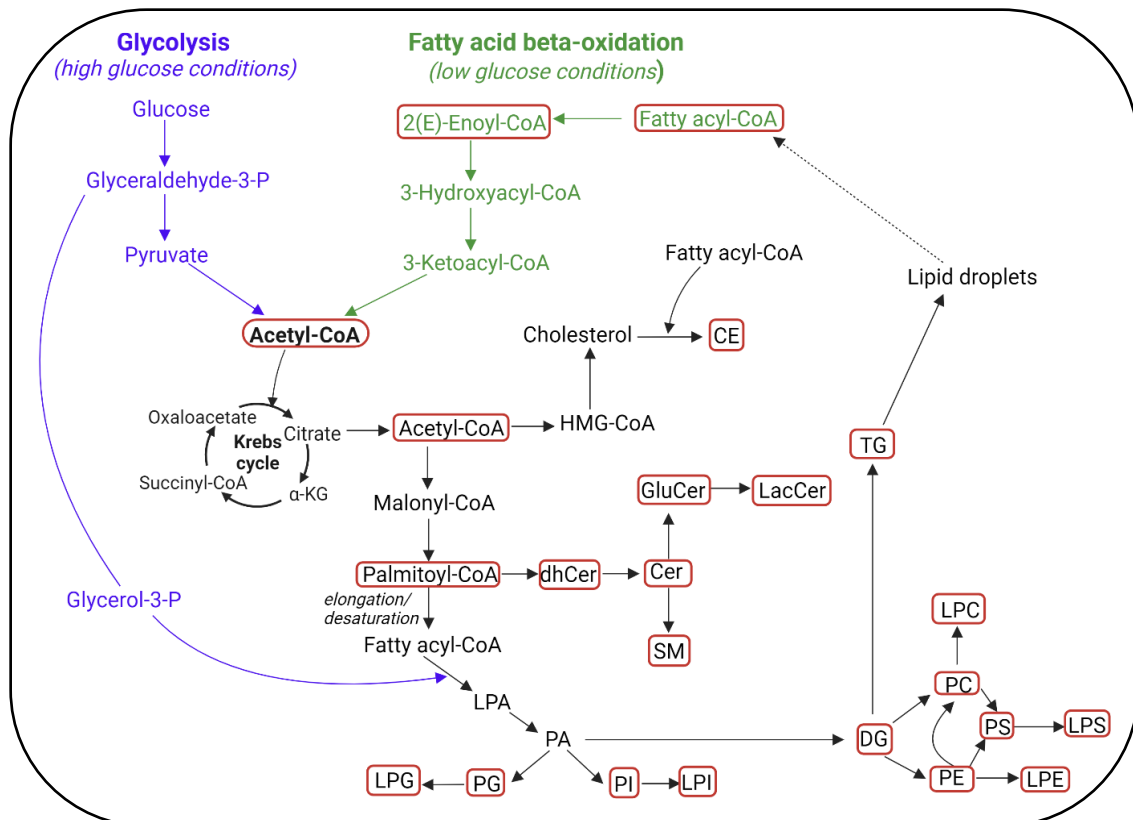
Figure 3. Lipid biosynthetic pathway. (Figure designed with material from BioRender.com).

In the cytosol, acetyl-CoA and malonyl-CoA combine to form longer fatty acyl-CoA through acetyl-CoA carboxylase. Glycerophospholipids are created by attaching fatty acyl groups to glycerol-3-phosphate, leading to LPA and PA in the endoplasmic reticulum. PA splits into pathways, one producing PI and PG, and the other generating DG, PC and PE via the Kennedy pathway. PG is formed in mitochondria, while the rest are synthesized

in the endoplasmic reticulum [19]. PC and PE can form PS through a base-exchange reaction with serine. Lysophospholipids are created through phospholipase-mediated hydrolysis [20]. TG is produced in the endoplasmic reticulum from DG through diacylglycerol transferase. Cholesterol synthesis starts with cytosolic acetyl-CoA, leading to cholesterol formation in the endoplasmic reticulum. CE results from cholesterol esterification with long-chain fatty acyl-CoA. Sphingolipid synthesis begins in the endoplasmic reticulum with serine and palmitoyl-CoA, progressing to ceramides [21], which then transform into SM, GluCer and LacCer in the Golgi apparatus [22–24].

Glyceraldehyde-3-P, Glyceraldehyde-3-Phosphate; α-KG, alpha-Ketogluatrate; HMG-CoA, 3-hydroxy-3-methyl glutaryl CoA; CE, Cholesteryl esters; Glycerol-3-P, Glycerol-3-Phosphate; LPA, Lysophosphatidic acids; PA, Phosphatidic acids; PG, Phosphatidylglycerol; LPG, Lysophosphatidylglycerol; PI, Phosphatidylinositol; LPI, Lysophosphatidylinositol; DG, Diglycerides; TG, Triglycerides; PC, Phosphatidylcholine; LPC, Lysophosphatidylcholine; PE, Phosphatidylethanolamine; LPE, Lysophosphatidylethanolamine; PS, Phosphatidylserine; LPS, Lysophosphatidylserine; dhCer, Dihydroceramides; Cer, Ceramides; SM, Sphingomyelin; GluCer, Glucosylceramides; LacCer, Lactosylceramides. The classes/species encircled in the red box are covered in this thesis.

Challenges in lipidomics analysis

Complex lipids

Complex lipids such as glycerophospholipids, glycerolipids and sphingolipids, differ significantly in their polarities. For instance, glycerolipids like TG require extremely non-polar conditions for extraction and analysis, while glycerophospholipids such as LPS require more polar conditions for the same processes. As a result, diverse analytical strategies are frequently utilized to effectively study and characterize different lipid classes. There are several types of LC-MS techniques that have been reported for the analysis of lipids. Reversed-phase chromatography (RPLC) [25], normal phase chromatography (NPLC) [26] and hydrophilic interaction liquid chromatography (HILIC) [27] have been used for the chromatographic separation of lipids but the existing methods have limitations in covering a broad range of lipid classes in one method. Mass spectrometry detection methods include both targeted and untargeted approaches. Triple quadrupole (QqQ) and quadrupole ion trap (QTRAP) instruments are typically employed for targeted analysis where multiple reaction monitoring (MRM) transitions are predetermined. Commonly used instruments for untargeted analysis include quadrupole time of flight (QTOF) and orbitrap, which acquire data across the entire mass range. The complexity in the structure of lipids is a major complication in lipidomics analysis which can lead to inaccurate identification and quantitation of lipid species. Multiple lipid species may share identical molecular masses, resulting from factors like isomers, isobars, adducts, in-source fragmentation, and variations in the position of fatty acyl chains and double bonds. In the absence of complete chromatographic resolution, this similarity in molecular mass can potentially lead to the misidentification of lipid species [28–30]. Ion-mobility mass

spectrometry, electron-activated dissociation (EAD) techniques, Ultra-Violet Photo-Dissociation (UVPD) are some of the techniques that have been introduced for characterization of isomeric lipid species and identification of double bonds positions in fatty acyl chains.

Absolute quantitation of metabolites is essential for accurately determining their concentrations in biological samples. However, in lipidomics, this can be challenging due to the vast number of existing endogenous lipids, and the limited availability of commercial standards. Experimental factors like extraction efficiency, ionization efficiency and matrix effects can influence the calculated concentrations of endogenous species. These factors are typically corrected using corresponding deuterated (internal) standards, however, the unavailability of these standards can lead to inaccurate correction, thus affecting the accuracy of the measured concentrations. As a result, achieving absolute quantitation for every lipid species is currently not feasible. The use of multiple standards enables the pairing of each endogenous species with the internal standards that closely match their fatty acyl chain composition and level of unsaturation. Although this approach does not provide absolute quantitation for each lipid species, it provides a practical and effective means of achieving accurate quantitation in lipidomics research [31–33]. Harmonization is another significant challenge in lipidomics studies as diverse extraction methods and analytical workflows across different laboratories can lead to variation in results making it difficult to compare data between research groups and hindering the reproducibility of findings.

Acyl-CoAs

Acyl-CoA species have distinct structures and properties as compared to complex lipids and are highly polar in nature. These compounds are not routinely used as diagnostic biomarkers for metabolic disorders due to several problems associated with their analysis such as instability and low endogenous level. The extreme variation in the physicochemical properties of acyl-CoA species often required multiple chromatographic methods [34,35], or other strategies such as derivatization [36] or ion pairing [37] to cover full range of species within this class. Moreover, measuring acyl-CoAs in readily available matrices such as plasma and urine is challenging due to their intracellular location. Consequently, tissue or biopsy samples are required for their analysis.

Lipidomics in liver metabolic diseases

The liver plays a central role in lipid metabolism and transport, making the lipidome responsive to genetic and environmental influences. Consequently, disorders related to the liver will

primarily affect the lipid metabolism pathway and as a result, will influence lipid levels in the body. There are numerous studies conducted to understand the role of lipids in various liver metabolic diseases. Metabolic dysfunction-associated steatotic liver disease (MASLD), previously known as non-alcoholic fatty liver disease (NAFLD) is one of the most common liver metabolic diseases with a global prevalence of 32% [38,39]. Although MASLD is mostly related to dietary factors, there are studies that have reported its genetic connection as well [40,41]. Fat accumulation in the liver is one of the important indications associated with MASLD. This condition arises due to several factors, including increased *de novo* lipogenesis, enhanced uptake of fatty acids and elevated *de novo* fatty acid synthesis in the liver due to insulin resistance [42,43]. The accumulated free fatty acids can either undergo fatty acid beta-oxidation to produce ATP or be esterified to form triglycerides (TG). These TGs are subsequently transported as very low-density lipoprotein (VLDL) to other tissues in the body [43]. The accumulation of triglycerides (TG), diglycerides (DG), cholesteryl esters (CE), ceramides (Cer) and decrease in phosphatidylethanolamine (PE), phosphatidylcholine (PC), phosphatidylinositol (PI), phosphatidylserine (PS) are common observations associated with development and progression of MASLD [44–48]. Liver biopsy is the gold standard for assessing the severity of MASLD. Yet, the prevalence of MASLD in large populations highlights the need for reliable non-invasive biomarkers to identify high-risk patients. Lipidomics holds promise in identifying these biomarkers, enhancing early detection and monitoring the progression of MASLD.

Inborn errors of metabolism (IEMs) are another major cause of liver metabolic diseases. The concept of IEMs was first introduced in 1908 by Sir Archibald Garrod [49]. IEMs are rare inherited genetic disorders occurring due to defects in the enzymes or transporters in the biological pathways and are most commonly inherited as autosomal recessive disorders [50,51]. These defects cause disruptions in metabolic pathways leading to the accumulation of toxic substances or deficiencies in essential metabolites. IEMs can vary depending on the affected enzymes, organelles and accumulated metabolites [50]. Based on pathophysiology, they are classified into three groups [52,53]:

1. IEMs leading to toxicity because of the accumulation of toxic substances resulting from defects in the biochemical metabolic pathway, eg., maple syrup urine disease;
2. IEMs causing deficiency in energy, eg., mitochondrial disorders;

3. IEMs involving the synthesis or catabolism of complex molecules in the cellular organelles, eg., lysosomal storage disorders.

Glycogen storage diseases (GSD) and fatty acid oxidation disorders (FAOD) are two of the most widely recognized metabolic disruptions associated with liver. GSD is a rare condition characterized by the impaired functioning of the enzyme responsible for glycogen metabolism, resulting in the accumulation of glycogen in the liver. There are 14 known types of GSD, with the most prevalent being Type I or von Gierke disease, Type III or Cori disease (or Forbes disease), and Type IV or Anderson disease. Complications associated with GSD include hypoglycemia pancreatitis and hepatic adenomas [54,55]. In GSD I, hyperlipidemia is a significant indication characterized by elevated levels of both cholesterol (hypercholesterolemia) and triglycerides (hypertriglyceridemia) [56]. Sidorina et al. have reported abnormal phospholipid metabolism in GSD II [57]. GSD III has been associated with hepatomegaly and hyperlipidemia as well [58]. Furthermore, a separate study has reported an increase in short-chain acylcarnitines in GSD I [59]. These findings shed light on the lipid metabolism disturbances in various types of GSDs and their potential implications in disease pathophysiology.

Mitochondrial fatty acid oxidation (FAO) is a crucial pathway that serves as an energy source during starvation or strenuous exercise. FAO generates acetyl-CoA, which plays a crucial role in ketogenesis, a vital energy source for the brain [60,61]. FAOD are inherited metabolic diseases resulting from deficiencies in certain enzyme activities and transporter proteins essential for mitochondrial fatty acid metabolism [62–64]. Consequently, there is an accumulation of acyl-CoAs and their carnitine and glycine conjugates. The accumulation of these compounds can result in lipid peroxidation, hepatic steatosis and impaired energy production. FAOD can also disrupt various metabolic pathways such as glucose metabolism, lipid synthesis and detoxification, thus compromising liver functions. The severity of symptoms associated with FAOD varies from mild hypoglycemia to sudden and unexpected death. Currently, the diagnosis for FAOD relies on analyzing the plasma acylcarnitines using tandem mass spectrometry alongwith genetic and enzyme analysis [65]. Acyl-CoA compounds are directly involved in the FAO pathway and are primary biomarkers associated with FAOD. However, there are several technical challenges associated with the analysis of acyl-CoA, which has led to the use of acylcarnitines as alternative biomarkers for FAOD. Different FAODs are characterized by distinct profiles of acylcarnitine species, allowing for differentiation and precise diagnosis of the specific disorder [66]. In cases of medium-chain acyl-CoA

dehydrogenase deficiency (MCADD), there have been reports of the accumulation of medium-chain acylcarnitines, including C6, C8, C10 and C10:1 [67,68]. On the other hand, very long-chain acyl-CoA dehydrogenase deficiency (VLCADD) is associated with the accumulation of long-chain acylcarnitines such as C12, C12:1, C14:1, C14:2, C16 and C16:1 [64,69]. In addition to acylcarnitines, other complex lipids have been reported to be altered in FAOD. For instance, in MCADD, the levels of oxidized phospholipids were found to be increased [70], whereas in VLCADD, phospholipids such as SM, PC, LPE and LPC were found to be elevated [71]. There have been limited reports regarding the analysis of complex lipids in FAOD. Most of the studies have used metabolomics approaches while lipidomics approaches were limited to specific lipid classes [72]. This shows further research is needed for comprehensive lipid analysis to unveil the lipid alterations in advancing and managing FAOD.

Diagnosis of liver metabolic diseases

Diagnosing liver metabolic diseases typically involves a combination of blood tests for liver function, liver enzymes and the lipid profile such as cholesterol and triglyceride levels, as well as imaging tests to assess structural liver changes. In some cases, a liver biopsy may be required for liver histology or the identification of accumulating metabolites. For inherited diseases such as FAOD, newborn screening (NBS) is recommended shortly after birth to screen for IEMs. The introduction of tandem mass spectrometry (MS/MS) has significantly improved the speed and accuracy of IEMs detection. Metabolite measurement using mass spectrometry remains so far the preferred method for newborn screening compared to genome sequencing due to several advantages. The metabolite measurements enable quick clinical decisions as after a metabolic disorder is detected, healthcare providers can immediately start treatment, dietary interventions, and additionally, these measurements can be used to monitor interventions. Whole-genome population screening has been reported to detect variants of uncertain clinical significance in the majority of people screened [73]. Currently, targeted next-generation sequencing is the first diagnostic tool to detect disorders for which a metabolite is not measurable [74]. The combination of genome sequencing with metabolite measurements has the potential of improving the diagnostic rate of IEMs.

Currently, the NBS program collects a small amount of blood samples from the baby's heel, followed by the detection of specific metabolites or the ratios between two metabolites. These metabolites or ratios serve as specific biomarkers for detecting and identifying the type of IEMs. The disorders targeted in the screening procedure vary across different regions. A single

MS/MS injection can diagnose approximately 45 different disorders [75]. The diagnosis of liver metabolic diseases can be further improved by discovering and analyzing a broader range of biomarkers that demonstrate changes in their concentration levels during the diseased condition, indicating the presence of the disease. Identifying a wide range of biomarkers can better capture disruptions in biochemical pathways and the interplay among multiple pathways. These biomarkers can guide the selection of appropriate treatments and monitor therapy responses. The biomarker profile should also help to understand how genetic variations affect disease progression and susceptibility, facilitating personalized diagnosis based on individual characteristics. Furthermore, these biomarkers should provide insights into complex disorders, adapt to emerging health conditions, and offer comprehensive metabolic profiles for early detection of issues, thus aiding in the prediction of future disease risks.

Scope and outline of the thesis

Liver metabolic diseases, influenced by genetic and environmental factors have a substantial impact on the lipid profile. Considering this, lipidomics can play a critical role in facilitating the diagnosis and monitoring of these diseases by identifying and quantifying disease-specific lipid biomarkers. The correlation of these biomarkers with metabolic pathways has the potential to offer valuable insights into the underlying disease mechanisms. Therefore, lipidomics can contribute to personalized diagnosis based on individual patient profiles, thereby assisting in treatment strategies through a 'systems medicine' approach.

The ideas underlying this thesis are that lipidomics may improve the diagnosis of liver metabolic diseases, and can provide further insights into the underlying pathophysiology of these diseases. However to achieve this, the measurement of lipids should be further improved by enabling comprehensive coverage, accurate identification and quantitation. Therefore, in this thesis, new analytical methodologies using LC-MS for the accurate detection and quantitation of lipids are developed. These methods are then applied to MCADD samples to identify lipid biomarkers, which are further correlated with gene expression analysis to understand the underlying biochemical pathways.

Firstly, we have developed an LC-MS/MS-based lipidomics method for comprehensive coverage of complex lipid classes in **Chapter 2**. The aim of this chapter was to develop a hydrophilic interaction liquid chromatography-tandem MS (HILIC-MS/MS)-based lipidomics method covering 1200 lipid features across 19-(sub) classes in human plasma, including both non-polar and polar lipid classes. Several cross-class and within-class interferences were

evaluated to avoid over-reporting and confirm lipid features. A strategy was developed to assign scores showing confidence in the identification of species. To optimize and validate accurate quantitation, SRM 1950 NIST plasma samples were analyzed using multi-internal standards per class and post hoc correction approach. This targeted lipidomics method was validated and applied to COVID-19 plasma samples for biomarker discovery. To evaluate whether this method is efficient in providing a comprehensive coverage of the lipidome, the method was applied in subsequent chapters.

The investigation of liver metabolic diseases requires a biological model that can mimic hepatocyte-like liver functions, helps to understand the pathophysiology associated with liver metabolic diseases and subsequently can assist in the development of novel therapies. In **Chapter 3,** we compared the metabolic capabilities of different *in vitro* models of human hepatocytes. Primary human hepatocytes (PHH) are the gold standard for conducting metabolic liver disease research. However, they have several limitations such as rapid de-differentiation, limited availability and donor-to-donor variation. These limitations show the need of hepatocyte-like cell lines that can replicate defects and dysfunctions associated with the diseases. In this chapter, we compared stem cell-derived hepatocytes (iPSC-Hep), HepG2 cells, upcyte-hepatocytes (Upcyte-Hep) and adult donor-derived liver organoids with PHH in terms of energy metabolism. The goal was to evaluate the production of secreted glucose and induction of gluconeogenesis-related genes in challenged (starvation) conditions. To assess the lipid profile of these matrices and the alterations in intracellular lipid composition in challenged conditions, the HILIC-MS/MS-based lipidomics method, developed in **Chapter 2,** was used.

In **Chapter 4**, the importance of acyl-CoAs in diagnosing FAOD was emphasized and this chapter delved into the evolution of analytical techniques for the identification and quantitation of these compounds. Acyl-CoAs serve as primary biomarkers for FAOD, however, there are several analytical challenges associated with their analysis which restrict their use as the diagnostic biomarker. This chapter highlights these technical difficulties, such as low endogenous levels, diverse physicochemical properties and instability. Further, the chapter describes how LC-MS techniques are advantageous in terms of sensitivity and selectivity for acyl-CoA measurements. This chapter also suggests measures that clinics and hospitals can adopt to overcome the challenges associated with the quantitation of acyl-CoAs.

As **Chapter 4** highlights the importance of acyl-CoAs as diagnostic biomarkers for FAOD, in **Chapter 5**, the development of an analytical method utilizing HILIC-MS/MS for acyl-CoA

analysis was described. The analytical method development of acyl-CoAs is challenging due to significant variations in their polarity leading to the need of multiple chromatographic methods for the coverage of their entire species, which consequently increases complexity and analysis time. To overcome this issue, we have developed a method to cover free CoA and short- to long-chain acyl-CoA species in a single analytical run with a zwitterionic HILIC column. Firstly, a high-resolution instrument (QTOF) was employed for species identification and targeting retention time. After initial optimization, a targeted HILIC-MS/MS method was created using a QTRAP instrument in scheduled multiple reaction monitoring (MRM) mode. This targeted method showed satisfactory performance for various validation parameters such as linearity, precision, recovery and matrix effect. This method was evaluated for the study of acyl-CoA profile in wildtype HepG2 cells cultured in supplemented and starved state. As the method demonstrated significant changes in the acyl-CoA profile in the starved state, the method was used in **Chapter 6** for the study of MCADD.

Further, in **Chapter 6** we applied the HILIC-MS/MS method (developed in **Chapter 5**) for studying CoA metabolism in medium-chain acyl-CoA dehydrogenase deficiency (MCADD), the most prevalent form of fatty acid oxidation disorder (FAOD). Within this chapter, we utilized *in silico*, *in vitro* and *in vivo* models to explore the systemic changes triggered by MCADD and the potential compensatory mechanisms involved. Our observations unveiled an accumulation of medium-chain acyl-CoA and acylcarnitine metabolites in MCADD models, along with a reduction in free CoA levels. These findings were further correlated with gene expression analysis followed by an *in silico* demonstration of the involvement of multiple compensatory mechanisms to mitigate the disorder.

The thesis concludes in **Chapter 7** with a summary of the work reported in this thesis, discussion of the results and includes future perspectives and potential avenues for further investigating the role of lipids in samples related to liver metabolic diseases.

References

[1] V. Tolstikov, Metabolomics: Bridging the Gap between Pharmaceutical Development and Population Health, Metabolites. 6 (2016) 20. https://doi.org/10.3390/metabo6030020.

[2] D.S. Wishart, Metabolomics for Investigating Physiological and Pathophysiological Processes, Physiological Reviews. 99 (2019) 1819–1875. https://doi.org/10.1152/physrev.00035.2018.

[3] M.A. Alves, S. Lamichhane, A. Dickens, A. McGlinchey, H.C. Ribeiro, P. Sen, F. Wei, T. Hyötyläinen, M. Orešič, Systems biology approaches to study lipidomes in health and disease, Biochimica et Biophysica Acta (BBA) - Molecular and Cell Biology of Lipids. 1866 (2021) 158857. https://doi.org/10.1016/j.bbalip.2020.158857.

[4] F. Wei, S. Lamichhane, M. Orešič, T. Hyötyläinen, Lipidomes in health and disease: Analytical strategies and considerations, TrAC Trends in Analytical Chemistry. 120 (2019) 115664. https://doi.org/10.1016/j.trac.2019.115664.

[5] K. Sandra, R. T'Kindt, L. Jorge, P. Sandra, The Art and Practice of Lipidomics, in: M. Lämmerhofer, W. Weckwerth (Eds.), Metabolomics in Practice, 1st ed., Wiley, 2013: pp. 137–176. https://doi.org/10.1002/9783527655861.ch7.

[6] T. Xu, C. Hu, Q. Xuan, G. Xu, Recent advances in analytical strategies for mass spectrometry-based lipidomics, Anal Chim Acta. 1137 (2020) 156–169. https://doi.org/10.1016/j.aca.2020.09.060.

[7] E. Fahy, S. Subramaniam, R.C. Murphy, M. Nishijima, C.R.H. Raetz, T. Shimizu, F. Spener, G. Van Meer, M.J.O. Wakelam, E.A. Dennis, Update of the LIPID MAPS comprehensive classification system for lipids, Journal of Lipid Research. 50 (2009) S9–S14. https://doi.org/10.1194/jlr.R800095-JLR200.

[8] E. Fahy, D. Cotter, M. Sud, S. Subramaniam, Lipid classification, structures and tools, Biochimica et Biophysica Acta (BBA) - Molecular and Cell Biology of Lipids. 1811 (2011) 637–647. https://doi.org/10.1016/j.bbalip.2011.06.009.

[9] B.M. Quinville, N.M. Deschenes, A.E. Ryckman, J.S. Walia, A Comprehensive Review: Sphingolipid Metabolism and Implications of Disruption in Sphingolipid Homeostasis, Int J Mol Sci. 22 (2021) 5793. https://doi.org/10.3390/ijms22115793.

[10] M.R. Tosi, V. Tugnoli, Cholesteryl esters in malignancy, Clin Chim Acta. 359 (2005) 27–45. https://doi.org/10.1016/j.cccn.2005.04.003.

[11] G. Liebisch, E. Fahy, J. Aoki, E.A. Dennis, T. Durand, C.S. Ejsing, M. Fedorova, I. Feussner, W.J. Griffiths, H. Köfeler, A.H. Merrill, R.C. Murphy, V.B. O'Donnell, O. Oskolkova, S. Subramaniam, M.J.O. Wakelam, F. Spener, Update on LIPID MAPS classification, nomenclature, and shorthand notation for MS-derived lipid structures, J Lipid Res. 61 (2020) 1539–1555. https://doi.org/10.1194/jlr.S120001025.

[12] A. Kvasnička, L. Najdekr, D. Dobešová, B. Piskláková, E. Ivanovová, D. Friedecký, Clinical lipidomics in the era of the big data, Clinical Chemistry and Laboratory Medicine (CCLM). 61 (2023) 587–598. https://doi.org/10.1515/cclm-2022-1105.

[13] Y. Liu, A. Thalamuthu, K.A. Mather, J. Crawford, M. Ulanova, M.W.K. Wong, R. Pickford, P.S. Sachdev, N. Braidy, Plasma lipidome is dysregulated in Alzheimer's disease and is associated with disease risk genes, Transl Psychiatry. 11 (2021) 1–18. https://doi.org/10.1038/s41398-021-01362-2.

[14] E.J. Kim, R. Ramachandran, A.S. Wierzbicki, Lipidomics in diabetes, Curr Opin Endocrinol Diabetes Obes. 29 (2022) 124–130. https://doi.org/10.1097/MED.0000000000000704.

[15] A. Poznyak, A.V. Grechko, P. Poggio, V.A. Myasoedova, V. Alfieri, A.N. Orekhov, The Diabetes Mellitus-Atherosclerosis Connection: The Role of Lipid and Glucose Metabolism and Chronic Inflammation, Int J Mol Sci. 21 (2020) 1835. https://doi.org/10.3390/ijms21051835.

[16] M. Pan, C. Qin, X. Han, Lipid Metabolism and Lipidomics Applications in Cancer Research, Adv Exp Med Biol. 1316 (2021) 1–24. https://doi.org/10.1007/978-981-33-6785-2_1.

[17] F. Schmelter, B. Föh, A. Mallagaray, J. Rahmöller, M. Ehlers, S. Lehrian, V. von Kopylow, I. Künsting, A.S. Lixenfeld, E. Martin, M. Ragab, R. Meyer-Saraei, F. Kreutzmann, I. Eitel, S. Taube, N. Käding, E. Jantzen, T. Graf, C. Sina, U.L. Günther, Metabolic and Lipidomic Markers Differentiate COVID-19 From Non-Hospitalized and Other Intensive Care Patients, Frontiers in Molecular Biosciences. 8 (2021). https://www.frontiersin.org/articles/10.3389/fmolb.2021.737039 (accessed July 18, 2023).

[18] L. Shi, B.P. Tu, Acetyl-CoA and the Regulation of Metabolism: Mechanisms and Consequences, Curr Opin Cell Biol. 33 (2015) 125–131. https://doi.org/10.1016/j.ceb.2015.02.003.

[19] N.J. Blunsom, S. Cockcroft, CDP-Diacylglycerol Synthases (CDS): Gateway to Phosphatidylinositol and Cardiolipin Synthesis, Frontiers in Cell and Developmental Biology. 8 (2020). https://www.frontiersin.org/articles/10.3389/fcell.2020.00063 (accessed July 22, 2023).

[20] Y. Hao, M. Guo, Y. Feng, Q. Dong, M. Cui, Lysophospholipids and Their G-Coupled Protein Signaling in Alzheimer's Disease: From Physiological Performance to Pathological Impairment, Frontiers in Molecular Neuroscience. 13 (2020). https://www.frontiersin.org/articles/10.3389/fnmol.2020.00058 (accessed July 24, 2023).

[21]   C. Gault, L. Obeid, Y. Hannun, An overview of sphingolipid metabolism: from synthesis to breakdown, Adv Exp Med Biol. 688 (2010) 1–23.

[22]   J.C.M. Holthuis, A.K. Menon, Lipid landscapes and pipelines in membrane homeostasis, Nature. 510 (2014) 48–57. https://doi.org/10.1038/nature13474.

[23]   A. Nohturfft, S.C. Zhang, Coordination of Lipid Metabolism in Membrane Biogenesis, Annual Review of Cell and Developmental Biology. 25 (2009) 539–566. https://doi.org/10.1146/annurev.cellbio.24.110707.175344.

[24]   Y.-Y. Liu, Y.-T. Li, Ceramide Glycosylation Catalyzed by Glucosylceramide Synthase and Cancer Drug Resistance, Adv Cancer Res. 117 (2013) 59–89. https://doi.org/10.1016/B978-0-12-394274-6.00003-0.

[25]   P.D. Rainville, C.L. Stumpf, J.P. Shockcor, R.S. Plumb, J.K. Nicholson, Novel application of reversed-phase UPLC-oaTOF-MS for lipid analysis in complex biological mixtures: a new tool for lipidomics, J Proteome Res. 6 (2007) 552–558. https://doi.org/10.1021/pr060611b.

[26]   H.K. Kotapati, P.D. Bates, Normal phase HPLC method for combined separation of both polar and neutral lipid classes with application to lipid metabolic flux, Journal of Chromatography B. 1145 (2020) 122099. https://doi.org/10.1016/j.jchromb.2020.122099.

[27]   E. Cífková, M. Holčapek, M. Lísa, M. Ovčačíková, A. Lyčka, F. Lynen, P. Sandra, Nontargeted quantitation of lipid classes using hydrophilic interaction liquid chromatography-electrospray ionization mass spectrometry with single internal standard and response factor approach, Anal Chem. 84 (2012) 10064–10070. https://doi.org/10.1021/ac3024476.

[28]   R.M. Gathungu, P. Larrea, M.J. Sniatynski, V.R. Marur, J.A. Bowden, J.P. Koelmel, P. Starke-Reed, V.S. Hubbard, B.S. Kristal, Optimization of Electrospray Ionization Source Parameters for Lipidomics To Reduce Misannotation of In-Source Fragments as Precursor Ions, Anal Chem. 90 (2018) 13523–13532. https://doi.org/10.1021/acs.analchem.8b03436.

[29]   H.C. Köfeler, R. Ahrends, E.S. Baker, K. Ekroos, X. Han, N. Hoffmann, M. Holčapek, M.R. Wenk, G. Liebisch, Recommendations for good practice in MS-based lipidomics, J Lipid Res. 62 (2021) 100138. https://doi.org/10.1016/j.jlr.2021.100138.

[30]   Y.H. Rustam, G.E. Reid, Analytical Challenges and Recent Advances in Mass Spectrometry Based Lipidomics, Anal Chem. 90 (2018) 374–397. https://doi.org/10.1021/acs.analchem.7b04836.

[31]   N.R. Zhang, N.G. Hatcher, K. Ekroos, K. Kedia, M. Kandebo, J.N. Marcus, S.M. Smith, K.P. Bateman, D.S. Spellman, Validation of a multiplexed and targeted lipidomics assay for accurate quantification of lipidomes, Journal of Lipid Research. 63 (2022). https://doi.org/10.1016/j.jlr.2022.100218.

[32]   M. Ghorasaini, Y. Mohammed, J. Adamski, L. Bettcher, J.A. Bowden, M. Cabruja, K. Contrepois, M. Ellenberger, B. Gajera, M. Haid, D. Hornburg, C. Hunter, C.M. Jones, T. Klein, O. Mayboroda, M. Mirzaian, R. Moaddel, L. Ferrucci, J. Lovett, K. Nazir, M. Pearson, B.K. Ubhi, D. Raftery, F. Riols, R. Sayers, E.J.G. Sijbrands, M.P. Snyder, B. Su, V. Velagapudi, K.J. Williams, Y.B. de Rijke, M. Giera, Cross-Laboratory Standardization of Preclinical Lipidomics Using Differential Mobility Spectrometry and Multiple Reaction Monitoring, Anal Chem. 93 (2021) 16369–16378. https://doi.org/10.1021/acs.analchem.1c02826.

[33]   J.J. Aristizabal-Henao, C.M. Jones, K.A. Lippa, J.A. Bowden, Nontargeted lipidomics of novel human plasma reference materials: hypertriglyceridemic, diabetic, and African-American, Anal Bioanal Chem. 412 (2020) 7373–7380. https://doi.org/10.1007/s00216-020-02910-3.

[34]   S. Wang, Z. Wang, L. Zhou, X. Shi, G. Xu, Comprehensive Analysis of Short-, Medium-, and Long-Chain Acyl-Coenzyme A by Online Two-Dimensional Liquid Chromatography/Mass Spectrometry, Anal Chem. 89 (2017) 12902–12908. https://doi.org/10.1021/acs.analchem.7b03659.

[35]   L. Abrankó, G. Williamson, S. Gardner, A. Kerimi, Comprehensive quantitative analysis of fatty-acyl-Coenzyme A species in biological samples by ultra-high performance liquid chromatography–tandem mass spectrometry harmonizing hydrophilic interaction and reversed phase chromatography, Journal of Chromatography A. 1534 (2018) 111–122. https://doi.org/10.1016/j.chroma.2017.12.052.

[36]   P. Li, M. Gawaz, M. Chatterjee, M. Lämmerhofer, Targeted Profiling of Short-, Medium-, and Long-Chain Fatty Acyl-Coenzyme As in Biological Samples by Phosphate Methylation Coupled to Liquid Chromatography–Tandem Mass Spectrometry, Anal. Chem. 93 (2021) 4342–4350. https://doi.org/10.1021/acs.analchem.1c00664.

[37]   S.M. Lam, T. Zhou, J. Li, S. Zhang, G.H. Chua, B. Li, G. Shui, A robust, integrated platform for comprehensive analyses of acyl-coenzyme As and acyl-carnitines revealed chain length-dependent disparity in fatty acyl metabolic fates across Drosophila development, Science Bulletin. 65 (2020) 1840–1848. https://doi.org/10.1016/j.scib.2020.07.023.

[38]   M.E. Rinella et al. "A multisociety Delphi consensus statement on new fatty liver disease nomenclature." *Annals of hepatology* vol. 29,1 (2024): 101133. doi:10.1016/j.aohep.2023.101133

[39]   M.L. Teng, C.H. Ng, D.Q. Huang, K.E. Chan, D.J. Tan, W.H. Lim, J.D. Yang, E. Tan, M.D. Muthiah, Global incidence and prevalence of nonalcoholic fatty liver disease, Clin Mol Hepatol. 29 (2023) S32–S42. https://doi.org/10.3350/cmh.2022.0365.

[40] S.A. Sulaiman, V. Dorairaj, M.N.H. Adrus, Genetic Polymorphisms and Diversity in Nonalcoholic Fatty Liver Disease (NAFLD): A Mini Review, Biomedicines. 11 (2022) 106. https://doi.org/10.3390/biomedicines11010106.

[41] Q.M. Anstee, C.P. Day, The Genetics of Nonalcoholic Fatty Liver Disease: Spotlight on PNPLA3 and TM6SF2, Semin Liver Dis. 35 (2015) 270–290. https://doi.org/10.1055/s-0035-1562947.

[42] M. Foretz, C. Guichard, P. Ferré, F. Foufelle, Sterol regulatory element binding protein-1c is a major mediator of insulin action on the hepatic expression of glucokinase and lipogenesis-related genes, Proc Natl Acad Sci U S A. 96 (1999) 12737–12742. https://doi.org/10.1073/pnas.96.22.12737.

[43] J.K. Dowman, J.W. Tomlinson, P.N. Newsome, Pathogenesis of non-alcoholic fatty liver disease, QJM. 103 (2010) 71–83. https://doi.org/10.1093/qjmed/hcp158.

[44] P. Puri, R.A. Baillie, M.M. Wiest, F. Mirshahi, J. Choudhury, O. Cheung, C. Sargeant, M.J. Contos, A.J. Sanyal, A lipidomic analysis of nonalcoholic fatty liver disease, Hepatology. 46 (2007) 1081–1090. https://doi.org/10.1002/hep.21763.

[45] K.-Y. Peng, M.J. Watt, S. Rensen, J.W. Greve, K. Huynh, K.S. Jayawardana, P.J. Meikle, R.C.R. Meex, Mitochondrial dysfunction-related lipid changes occur in nonalcoholic fatty liver disease progression, Journal of Lipid Research. 59 (2018) 1977–1986. https://doi.org/10.1194/jlr.M085613.

[46] S. Tiwari-Heckler, H. Gan-Schreier, W. Stremmel, W. Chamulitrat, A. Pathil, Circulating Phospholipid Patterns in NAFLD Patients Associated with a Combination of Metabolic Risk Factors, Nutrients. 10 (2018) 649. https://doi.org/10.3390/nu10050649.

[47] F. Chiappini, C. Desterke, J. Bertrand-Michel, C. Guettier, F. Le Naour, Hepatic and serum lipid signatures specific to nonalcoholic steatohepatitis in murine models, Sci Rep. 6 (2016) 31587. https://doi.org/10.1038/srep31587.

[48] Y.J. Yang, C.S. Bang, S.P. Shin, G.H. Baik, Clinical impact of non-alcoholic fatty liver disease on the occurrence of colorectal neoplasm: Propensity score matching analysis, PLOS ONE. 12 (2017) e0182014. https://doi.org/10.1371/journal.pone.0182014.

[49] C.R. Scriver, Garrod's Croonian Lectures (1908) and the charter "Inborn Errors of Metabolism": albinism, alkaptonuria, cystinuria, and pentosuria at age 100 in 2008, J Inherit Metab Dis. 31 (2008) 580–598. https://doi.org/10.1007/s10545-008-0984-9.

[50] F. Ezgu, Inborn Errors of Metabolism, in: Advances in Clinical Chemistry, Elsevier, 2016: pp. 195–250. https://doi.org/10.1016/bs.acc.2015.12.001.

[51] L. Ford, M. Mitchell, J. Wulff, A. Evans, A. Kennedy, S. Elsea, B. Wittmann, D. Toal, Clinical metabolomics for inborn errors of metabolism, in: Advances in Clinical Chemistry, Elsevier, 2022: pp. 79–138. https://doi.org/10.1016/bs.acc.2021.09.001.

[52] A.W. El-Hattab, Inborn Errors of Metabolism, Clinics in Perinatology. 42 (2015) 413–439. https://doi.org/10.1016/j.clp.2015.02.010.

[53] M. Agana, J. Frueh, M. Kamboj, D.R. Patel, S. Kanungo, Common metabolic disorder (inborn errors of metabolism) concerns in primary care practice, Ann Transl Med. 6 (2018) 469. https://doi.org/10.21037/atm.2018.12.34.

[54] T.G.J. Derks, M. van Rijn, Lipids in hepatic glycogen storage diseases: pathophysiology, monitoring of dietary management and future directions, Journal of Inherited Metabolic Disease. 38 (2015) 537–543. https://doi.org/10.1007/s10545-015-9811-2.

[55] S. Kanungo, K. Wells, T. Tribett, A. El-Gharbawy, Glycogen metabolism and glycogen storage disorders, Ann Transl Med. 6 (2018) 474. https://doi.org/10.21037/atm.2018.10.59.

[56] R.H. Bandsma, P.G. Smit, F. Kuipers, Disturbed lipid metabolism in glycogen storage disease type 1, Eur J Pediatr. 161 (2002) S65–S69. https://doi.org/10.1007/s00431-002-1007-8.

[57] A. Sidorina, G. Catesini, S. Levi Mortera, V. Marzano, L. Putignani, S. Boenzi, R. Taurisano, M. Garibaldi, F. Deodato, C. Dionisi-Vici, Combined proteomic and lipidomic studies in Pompe disease allow a better disease mechanism understanding, Journal of Inherited Metabolic Disease. 44 (2021) 705–717. https://doi.org/10.1002/jimd.12344.

[58] X.-H. Li, Q.-M. Gong, Y. Ling, C. Huang, D.-M. Yu, L.-L. Gu, X.-W. Liao, D.-H. Zhang, X.-Q. Hu, Y. Han, X.-F. Kong, X.-X. Zhang, Inherent lipid metabolic dysfunction in glycogen storage disease IIIa, Biochemical and Biophysical Research Communications. 455 (2014) 90–97. https://doi.org/10.1016/j.bbrc.2014.10.096.

[59] J.A. Hoogerland, F. Peeks, B.S. Hijmans, J.C. Wolters, S. Kooijman, T. Bos, A. Bleeker, T.H. van Dijk, H. Wolters, A. Gerding, K. van Eunen, R. Havinga, A.C.M. Pronk, P.C.N. Rensen, G. Mithieux, F. Rajas, F. Kuipers, D.-J. Reijngoud, T.G.J. Derks, M.H. Oosterveer, Impaired Very-Low-Density Lipoprotein catabolism links hypoglycemia to hypertriglyceridemia in Glycogen Storage Disease type Ia, Journal of Inherited Metabolic Disease. 44 (2021) 879–892. https://doi.org/10.1002/jimd.12380.

[60] S.M. Houten, R.J.A. Wanders, A general introduction to the biochemistry of mitochondrial fatty acid β-oxidation, J Inherit Metab Dis. 33 (2010) 469–477. https://doi.org/10.1007/s10545-010-9061-2.

[61] M.J. Bennett, P. Rinaldo, A.W. Strauss, Inborn errors of mitochondrial fatty acid oxidation, Crit Rev Clin Lab Sci. 37 (2000) 1–44. https://doi.org/10.1080/10408360091174169.

[62] M. Wajner, A.U. Amaral, Mitochondrial dysfunction in fatty acid oxidation disorders: insights from human and animal studies, Bioscience Reports. 36 (2016) e00281. https://doi.org/10.1042/BSR20150240.

[63] V.A. Vishwanath, Fatty Acid Beta-Oxidation Disorders: A Brief Review, Ann Neurosci. 23 (2016) 51–55. https://doi.org/10.1159/000443556.

[64] J.L. Merritt, E. MacLeod, A. Jurecka, B. Hainline, Clinical manifestations and management of fatty acid oxidation disorders, Rev Endocr Metab Disord. 21 (2020) 479–493. https://doi.org/10.1007/s11154-020-09568-3.

[65] J.L. Merritt, M. Norris, S. Kanungo, Fatty acid oxidation disorders, Ann Transl Med. 6 (2018) 473. https://doi.org/10.21037/atm.2018.10.57.

[66] C. Vianey-Saban, A. Fouilhoux, J. Vockley, C. Acquaviva-Bourdain, N. Guffon, Improving diagnosis of mitochondrial fatty-acid oxidation disorders, Eur J Hum Genet. 31 (2023) 265–272. https://doi.org/10.1038/s41431-022-01260-1.

[67] J.L. Merritt, I.J. Chang, Medium-Chain Acyl-Coenzyme A Dehydrogenase Deficiency, in: M.P. Adam, G.M. Mirzaa, R.A. Pagon, S.E. Wallace, L.J. Bean, K.W. Gripp, A. Amemiya (Eds.), GeneReviews®, University of Washington, Seattle, Seattle (WA), 1993. http://www.ncbi.nlm.nih.gov/books/NBK1424/ (accessed July 24, 2023).

[68] M.L. Couce, P. Sánchez-Pintos, L. Diogo, E. Leão-Teles, E. Martins, H. Santos, M.A. Bueno, C. Delgado-Pecellín, D.E. Castiñeiras, J.A. Cocho, J. García-Villoria, A. Ribes, J.M. Fraga, H. Rocha, Newborn screening for medium-chain acyl-CoA dehydrogenase deficiency: regional experience and high incidence of carnitine deficiency, Orphanet Journal of Rare Diseases. 8 (2013) 102. https://doi.org/10.1186/1750-1172-8-102.

[69] N.D. Leslie, S. Saenz-Ayala, Very Long-Chain Acyl-Coenzyme A Dehydrogenase Deficiency, in: M.P. Adam, G.M. Mirzaa, R.A. Pagon, S.E. Wallace, L.J. Bean, K.W. Gripp, A. Amemiya (Eds.), GeneReviews®, University of Washington, Seattle, Seattle (WA), 1993. http://www.ncbi.nlm.nih.gov/books/NBK6816/ (accessed July 24, 2023).

[70] L. Najdekr, A. Gardlo, L. Mádrová, D. Friedecký, H. Janečková, E.S. Correa, R. Goodacre, T. Adam, Oxidized phosphatidylcholines suggest oxidative stress in patients with medium-chain acyl-CoA dehydrogenase deficiency, Talanta. 139 (2015) 62–66. https://doi.org/10.1016/j.talanta.2015.02.041.

[71] E. Sklirou, A.N. Alodaib, S.F. Dobrowolski, A.-W.A. Mohsen, J. Vockley, Physiological Perspectives on the Use of Triheptanoin as Anaplerotic Therapy for Long Chain Fatty Acid Oxidation Disorders, Frontiers in Genetics. 11 (2021). https://www.frontiersin.org/articles/10.3389/fgene.2020.598760 (accessed July 20, 2023).

[72] I.M.S. Guerra, H.B. Ferreira, T. Melo, H. Rocha, S. Moreira, L. Diogo, M.R. Domingues, A.S.P. Moreira, Mitochondrial Fatty Acid β-Oxidation Disorders: From Disease to Lipidomic Studies—A Critical Review, Int J Mol Sci. 23 (2022) 13933. https://doi.org/10.3390/ijms232213933.

[73] T. Lancet, Genomic newborn screening: current concerns and challenges, The Lancet. 402 (2023) 265. https://doi.org/10.1016/S0140-6736(23)01513-1.

[74] R.B. Parad, S.G. Kaler, E. Mauceli, T. Sokolsky, L. Yi, A. Bhattacharjee, Targeted next generation sequencing for newborn screening of Menkes disease, Molecular Genetics and Metabolism Reports 24, (2020) 100625. https://doi.org/10.1016/j.ymgmr.2020.100625.

[75] D.C. Lehotay, P. Hall, J. Lepage, J.C. Eichhorst, M.L. Etter, C.R. Greenberg, LC–MS/MS progress in newborn screening, Clinical Biochemistry. 44 (2011) 21–31. https://doi.org/10.1016/j.clinbiochem.2010.08.007.

Chapter 2

Development of a targeted hydrophilic interaction liquid chromatography-tandem mass spectrometry based lipidomics platform applied to a coronavirus disease severity study

Abstract

The importance of lipids seen in studies of metabolism, cancer, the recent COVID-19 pandemic and other diseases has brought the field of lipidomics to the forefront of clinical research. Quantitative and comprehensive analysis is required to understand biological interactions among lipid species. However, lipidomic analysis is often challenging due to the various compositional structures, diverse physicochemical properties, and wide dynamic range of concentrations of lipids in biological systems. To study the comprehensive lipidome, a hydrophilic interaction liquid chromatography-tandem mass spectrometry (HILIC-MS/MS)-based screening method with 1200 lipid features across 19-(sub)classes, including both nonpolar and polar lipids, has been developed. HILIC-MS/MS was selected due to its class separation property and fatty acyl chain level information. 3D models of class chromatographic retention behavior were established and evaluations of cross-class and within-class interferences were performed to avoid over-reporting these features. This targeted HILIC-MS/MS method was fully validated, with acceptable analytical parameters in terms of linearity, precision, reproducibility, and recovery. The accurate quantitation of 608 lipid species in the SRM 1950 NIST plasma was achieved using multi-internal standards per class and post-hoc correction, extending current databases by providing lipid concentrations resolved at fatty acyl chain level. The overall correlation coefficients (R^2) of measured concentrations with values from literature range from 0.64 to 0.84. The applicability of the developed targeted lipidomics method was demonstrated by discovering 520 differential lipid features related to COVID-19 severity. This high coverage and targeted approach will aid in future investigations of the lipidome in various disease contexts.

Keywords

1. Introduction

Lipids play a critical role in defining cellular and sub-cellular structures, signaling, modifying metabolic processes and energy storage [1]. Imbalance of lipids in the body (dyslipidemia) has been linked to multiple disorders such as neurodegenerative diseases [2], cancer [3], metabolic syndrome [4] and dysregulation of the gut microbiome [5]. The role of lipids also showed an important role in the individuals affected by the recent pandemic caused by coronavirus (COVID-19). Several lipidomic investigations have documented a modified lipidome profile in individuals affected by COVID-19 [6–13]. In an initial study conducted during the pandemic by Shen et al., patients with varying degrees of COVID-19 severity exhibited reduced levels of sphingolipids and glycerophospholipids in their serum, while phosphatidylcholine (PC) levels were increased [6]. Another study found decreased plasma diglycerides (DG) and elevated levels of sphingomyelins (SM) in COVID-19 patients [12]. Other studies have indicated decreased serum levels of total cholesterol, HDL and LDL, with increased levels of triglycerides (TG) [13]. These findings suggest an overall disruption in lipid metabolism in COVID-19, highlighting how lipidomics is essential in understanding the role played by lipids in disease progression, and for developing prevention strategies in translational clinical studies.

Deciphering the interplay between the lipidome and other parts of the biological system requires a deep understanding of the complex pathways of lipid metabolism, the function of lipids, and how lipids are generated and interact with other molecules. This can only be achieved by analytical methods with exhaustive coverage and good quantitative performance. Consequently, two major challenges must be addressed by lipidomics methods: 1) elucidating the diverse compositional structures of lipids in detail, and 2) quantifying the biological concentrations of lipids over a wide dynamic range [14]. Mass spectrometry (MS)-based lipidomics methodologies can be divided into two groups, species-separation based and class-separation based, irrespective of their separation mechanisms. The class-based separations, like differential ion mobility, hydrophilic interaction chromatography (HILIC) [15,16], normal-phase liquid chromatography (NPLC) [17], and supercritical fluid chromatography (SFC), are powerful in resolving the isobars. These techniques also facilitate the co-elution of lipid species and their internal standards (ISs) for accurate quantitation. Species-separation based techniques like reverse phase liquid chromatography (RPLC) and trapped ion-mobility have limitations in achieving reliable quantitation, as ISs often do not co-elute with analytes and suffer from cross-class isobaric interference [18,19]. Multiple reaction monitoring (MRM) is frequently selected as the MS method due to its high sensitivity and additional acyl tail characterization of

phospholipid species [20]. The combination of separation techniques, such as HILIC, ion mobility, with MRM are often being used in large scale targeted lipidome profiling [21–25]. Direct infusion methods with or without ion mobility may encounter severe matrix effect, consume large amount samples, exhibit lower sensitivity and have limitation in the separation of isomers/isobars [22]. Another important aspect in the lipidomics study is the unambiguous identification of lipid species, as there are several sources of cross-class interference (isobars/isomers, in-source fragments) and within-class interference (isotopes and different ion types), which can lead to over-reporting of lipid species [26].

Achieving absolute quantitation is another challenge in lipidomics due to commercial unavailability of (internal) standards for all endogenous lipid species. Recognizing the difficulties in achieving absolute quantitation, we refer to all attempts to report data in molar concentrations as accurate quantitation. These efforts include using multiple internal standards with different chain length and double bond numbers per class and/or applying response correction factors for quantitation [27,28]. Although it must be noted that true accurate quantitation would require the systematic use of individual standards per species, a standardized analytical workflow with unambiguous identification resolving the complexity associated with lipidomics analysis can ensure highly reliable data that can also be correlated with other studies [29,30].

The comprehensive coverage of the lipidome is necessary for biomarker discovery and pathway mapping. HILIC-MS/MS is chosen in this study for large-scale metabolic profiling because of its superior quantitative performance due to close elution of ISs and corresponding lipid molecular species, thus diminishing differential matrix effects. The experimental design in this paper aims to screen lipid species to minimize over-reporting and enhancing confidence in lipid identification. This HILIC-MS/MS method targets 19 lipid (sub)classes in a 14 min analytical run. Firstly, a MS/MS library was built for routine lipid screening followed by assigning lipid identification confidence scores after evaluation of various cross-class and within-class interference correction. The method validation was performed according to the bioanalytical method validation guidelines as precisely as possible. The accurate quantitation was conducted using multiple internal standards per class and was performed on National Institute of Standards and Technology Standard Reference Material 1950 (NIST SRM 1950) plasma for lipid species with high confidence score. As a proof of applicability, the developed HILIC-MS/MS lipidomics method was used to characterize the lipidome of plasma samples from coronavirus disease 2019 (COVID-19) patients. The results showed a wide class-based changed lipidome

correlated with disease severity, indicating the potential for disease progression prediction using lipidomics.

2. Experimental section

2.1 Reagents and Materials

Acetonitrile, methanol (LC-MS grade), isopropanol, dichloromethane and chloroform (HPLC grade) were purchased from Biosolve Chimie (Dieuze, France). LiChropur™ quality ammonium acetate was purchased from Merck KGaA (Darmstadt, Germany). Water was purified by Milli-Q® reference water purification system purchased from Merck KGaA (Darmstadt, Germany). Two lipid standards from each class were used for HILIC-MS/MS method development. The standard mix for method development consists of the system suitability kit for the Lipidyzer platform (part no.5040407) purchased from AB Sciex (Framinghan MA, USA) and it includes ceramides (Cer), cholesterol esters (CE); diglycerides (DG); lysophosphatidylcholine (LPC); lysophosphatidylethanolamine (LPE); phosphatidylcholine (PC); phosphatidylethanolamine (PE); sphingomyelin (SM); triglycerides (TG); hexosylceramides (HexCer); lactosylceramdides (LacCer). Individual standards such as galactosyl ceramide, GalCer 18:1;O2/16:0; glucosyl ceramide GluCer 18:1;O2/16:0; phosphatidylglycerol, PG 14:0/14:0 and PG 17:0/17:0; Bis(Monoacylglycero) Phosphate, BMP 14:0/14:0 and BMP 18:1/18:1; phosphatidylserines, PS 14:0/14:0 and PS 16:0/16:0; phosphatidylinositols, PI 18:0/20:4 and PI 16:0/18:1; lysophosphatidylglycerol, LPG 17:1 and LPG 18:1; lysophosphatidylinositol, LPI 17:1 and LPI 20:4; lysophosphatidylserines, LPS 17:1 and LPS 18:1 were purchased from Avanti Polar Lipids (Alabaster, AL, USA).

The one-IS per class mix was used for the validation of the method and application in the COVID-19 plasma samples, consisting of SPLASH® LIPIDOMIX® Mass Spec Standard (330707-1EA), LPS 17:1; LPI 17:1; LPG 17:1 purchased from Avanti polar lipids and deuterated hexosylceramides (Hex-Cer 18:1;O2/16:0-d9) (part no.5040398) , deuterated lactosylceramide (Lac-Cer 18:1;O2/16:0-d9) (part no.5040399), deuterated dihydroceramide (Cer 18:0;O2/16:0-d9) (part no.5040397), deuterated ceramides (Cer 18:1;O2/16:0-d9) (part no.5040167) purchased from AB Sciex. The one-IS per class mix were also spiked in the COVID-19 samples as internal standard (as shown in **supplementary Table S1**).

The multi-ISs per class mix was used for accurate quantitation, consisting of UltimateSPLASH™ ONE (330820L-1EA), SPLASH® LIPIDOMIX® Mass Spec Standard

(330707-1EA), LPS 17:1, LPI 17:1, LPG 17:1 purchased from Avanti Polar lipids; Hex-Cer 18:1;O2/16:0-d9 (part no.5040398), Lac-Cer 18:1;O2/16:0-d9 (part no.5040399), Cer 18:0;O2/16:0-d9 (part no.5040397) purchased from AB Sciex were used for quantitation (as shown in **supplementary Table S2**). All stock solutions, standards and calibration solutions were prepared in acetonitrile-methanol mixture (3:7 v/v).

2.2 Plasma sample collection

Human K2 Ethylenediaminetetraacetic acid (EDTA) plasma was purchased from Innovative research (Novi, MI, USA) and used for method development and validation. NIST SRM 1950 human plasma for quantitation was purchased from Avanti Polar Lipids (Alabaster, AL, USA). The COVID-19 cohort consisted of 44 adults admitted to the regional Amphia hospital in Breda, the Netherlands, on 24 March 2020–14 April 2020, as published earlier [31,32]. **Supplementary Table S3** summarizes key characteristics of the 44 patients and 103 collected plasma samples. EDTA plasma samples were collected in intervals of 3–4 days throughout the study. All patients reported COVID-19 related complaints, tested positive for the SARS-CoV-2 by polymerase chain reaction (PCR), and gave consent to be included in the study. The study was performed in accordance with the guidelines for sharing of patient data of observational scientific research in case of exceptional health situations.

2.3 Sample preparation

Lipids were extracted from 25 μL of plasma (human K2 EDTA plasma/COVID-19 patient plasma) according to the methyl tert-butyl ether (MTBE) method [33]. A volume of 34 μL of the one-IS per class mix was added to 25 μL of plasma and vortexed. To this mixture, 231 μL of methanol (MeOH) and 770 μL of MTBE were added. The sample was incubated at room temperature on an orbital shaker for 1 h followed by the addition of 192.5 μL of water thus making final ratio MTBE:MeOH:Water (10:3:2.5, v/v/v). The mixture was again incubated at room temperature for 10 min and then centrifuged at 15800 rcf for 10 min. A volume of 520 μL of upper layer was collected and dried in a vacuum concentrator followed by reconstitution in 200 μL of acetonitrile:methanol (3:7). This mixture was vortexed and centrifuged for 10 min. The supernatant was collected and injected in the LC–MS for analysis.

The COVID-19 study batch design includes solvent blanks, procedure blanks (with IS), clinical study samples and quality control (QC) samples. These QC samples were a pool of all the study plasma samples and were analyzed at regular intervals in the study batch to determine the performance of the method.

2.4 Lipidomics profiling analysis

A QTRAP 6500+ (AB Sciex, Concord, ON, Canada) coupled to an Exion LC AD (AB Sciex, Concord, ON, Canada) was used for targeted lipid profiling to obtain lipid information including retention time (tR) and MS/MS fragments. The column used for the separation was a Luna amino column (100 mm × 2 mm, 3 μm, Phenomenex). The mobile phase A (MP-A) was 1 mM ammonium acetate in chloroform: acetonitrile (1:9), while mobile phase B (MP-B) was 1 mM ammonium acetate in acetonitrile: water (1:1). The gradient is shown in **supplementary Table S4(A)**. Two injections were made to accommodate all the MRM transitions of the targeted lipid features. The injection volume was 5 μL for the first acquisition run and 1 μL for the second acquisition run. The column temperature was kept at 35 °C. The injector needle was washed with isopropanol:water:dichloromethane (94:5:1, v/v/v) after each injection.

MS/MS experiments were done on QTRAP 6500+ mass spectrometer with a Turbo V source (AB Sciex, Concord, ON, Canada) operated with electrospray ionization (ESI) probe. The declustering potential (DP) and collision energy (CE) of lipid transitions were optimized to obtain the highest response for the mixture of lipid standards. The information about the precursor ion (Q1), characteristic product ion (Q3), lipid name (ID), optimized DP, and CE of all the lipid features were incorporated into the MS acquisition method before the screening in plasma samples. The parameters of the QTRAP 6500+ mass spectrometer were as follows: curtain gas (N2) was 20 psi; collision gas (N2) kept at medium, ion spray voltage was 5500 V and -4500 V for positive and negative mode respectively; source temperature was 400 °C, GS1 and GS2 were 30 and 35 psi respectively. Scheduled MRM (sMRM) was used for data acquisition for targeted analysis. sMRM window, ion transitions and tR are summarized in **supplementary Table S5 (sheet 1 and 2)**. The total scan time was 0.5 s. The lipids detected by the UHPLC-QTRAP based lipidomics profiling analysis were processed using AB Sciex OS (version 2.1.6, AB SCIEX, Concord, ON, Canada).

The method for accurate mass measurements was based on the previously reported RPLC-HRMS method [34]. An Acquity UPLC (Waters, Milford, MA, USA) was coupled to a SCIEX ZenoTOF 7600 system (Darmstadt, Germany). The column used was Waters Acquity HSS T3 column (2.1 × 100 mm, 1.8 μm, Waters, Milford, MA). The mobile phase A (MP-A) was 10 mM ammonium formate in acetonitrile: water (6:4), while mobile phase B (MP-B) was 10 mM ammonium formate in isopropanol: acetonitrile (9:1). This gradient is described in **supplementary Table S4(B)**. The following ion source parameters were used: ESI spray voltage was 5.2 kv and 4.5 kV in the positive and negative ionization mode respectively, a

capillary temperature of 550 °C, ion source gas 1 50 psi, ion source gas 2 50 psi, curtain gas of 35 psi and CAD gas of 7 psi. A survey TOF-MS scan was performed in the mass range of (300–1000) Da in Information Dependent Acquisition mode (IDA).

2.5 Method validation

The one-IS per class mix (specified in reagents and materials section) has been used to calculate the various validation parameters. An 8-point calibration line (cal-1 to cal-8) was made by serial dilution of IS present in the one-IS per class mix to determine the linear range. The concentrations of these calibration points are mentioned in the **supplementary Table S6**. The serially diluted standards of the one-IS per class mix were spiked in three different ways to prepare the calibration curves: a) in pure solvent (without matrix), b) spiking the standard in human K2 EDTA plasma before following the extraction described in the sample preparation section, c) spiking the standard in human K2 EDTA plasma after extraction. The calibration curves were prepared on three different days using freshly prepared standards. To determine the linear range, we used an unweighted linear regression model. The determination of various validation parameters was performed by spiking one-IS per class mix at low (L), medium (M) and high (H) concentration levels. Low levels (L) were chosen to be 3 times higher than the lower limit of quantitation (LLOQ). Medium levels (M) were set to be around (30–50)% of the calibration range. The high level (H) samples were spiked at close to 75% of the upper limit of quantitation (ULOQ). The details about the calculations of validation parameters such as carryover, precision, ion suppression and matrix effects are described in **supplementary information**. The limit of detection (LOD) and limit of quantitation (LOQ) were calculated based on the signal-to-noise ratio of 3 and 10 respectively. The equations used for the calculations of LOD and LOQ are described in **supplementary information**. The repeatability was evaluated to assess any deviation in analysis over time and is an important criteria to assess the performance of the method when running longer batches. We evaluated the repeatability of our method by calculating relative standard deviation (RSD %) of endogenous lipid features in QC samples of COVID-19 patients. In this work, the lipid species with RSD below 15% in QC samples were classified as high confidence metabolites while those in the range of (15–30)% were treated with caution as shown in **supplementary Table S5 (sheet 7)**. Since we are doing exploratory study, we considered metabolites with RSD up to 30% to accommodate variations due to class behavior.

2.6 Accurate quantitation in the NIST SRM 1950 plasma

NIST SRM 1950 plasma samples were used for the accurate quantitation of endogenous lipid

species. Six-point calibration lines were prepared by serially diluting the multi-ISs per class mix. These six points were spiked in NIST SRM 1950 plasma samples before extraction and lipid extraction was performed according to the protocol specified in **Section 2.3**. The details of the initial concentration of multi-ISs mix internal standards are specified in **supplementary Table S2**. The concentrations of these calibration lines (cal-1 to cal-6) are mentioned in **supplementary Table S5 (sheet 5).**

To estimate the concentrations of endogenous compounds in human plasma, an unweighted linear regression model (y = ax + b, where x represents the metabolite concentration) was used, based on the calibration curves. The model fitness was estimated using R^2. Where intercept 'b' was not significant (*p>0.05*) for the model fit, the intercept was set to 0 (y = ax + 0). The lipid concentrations were calculated in nmol mL^{-1} to compare with other reported studies. Type II isotopic correction was performed using LICAR [35]. The concentration calculation of the species with same fatty acyl chain will be influenced by the selection of MRM transition used for IS, hence post-hoc correction was used to correct for the metabolites with two same fatty acyl chains to remove the double signal.

2.7 Data processing and statistical analysis

A model establishing a relation between tR and the length of fatty acyl chains (carbon number, CN) as well as the number of double bond equivalents (DBEs) was generated for each lipid class using multivariate analysis. The models with error rates higher than 20% or $R^2 < 0.9$ were treated with caution. A linear regression model was used to find the most important biomarker candidates distinguishing the patients at ward from intensive care unit (ICU). All variables were cuberoot-transformed prior to statistical analyses. Differential analysis between ICU and ward patients incorporating all samples was performed using linear regression correcting for age, sex, and BMI, grouped by patient, and weighted by the inverse number of observations per patient. The p-values obtained in all tests were adjusted for multiple testing using the Benjamini– Hochberg method implemented in the p.adjust R function (v.4.0.3), and termed Qvalues. The statistical significance was set at *Q<0.05* to determine the lipid biomarkers related to COVID-19 disease severity between ICU patients and ward patients. Principal component analysis (PCA) and volcano plot visualization were conducted. All statistical analyses were performed in R (version 4.0.3), and graphs were plotted using the packages ggpubr and stats.

3. Results and discussion

The aim of the present study is to establish the HILIC-MS/MS-based targeted lipidomics method with high coverage that can be used for comprehensive profiling and quantitation of the plasma lipidome.

3.1 Construction of the lipid database

MRM transitions were split into two methods in polarity switching mode, depending on the biological concentration of the lipid classes. The first and second acquisition methods contained 602 and 598 ion pairs, respectively. The complete list is shown in **supplementary Table S5 (sheet 1 and 2)**. A total of 19 lipid subclasses could be summarized as DG, TG, CE, PC, PE, alkyl and alkenyl substituent PEs (PE-O) & (PE-P), PG, PS, PI, LPC, LPE, LPS, LPI, LPG, Cer, HexCer, LacCer and SM. The lipid naming convention used will follow the guidelines established by Liebisch et al. [36] and additionally, by the Lipid Maps Consortium. The complete lipid identifiers (Lipidmaps, Swisslipids, MetaNetX, CHEBI, PubChem, HMDB, LipidX, InChI and InChI key) are listed in **supplementary Table S5 (sheet 3)**. All classes of phospholipids and lysophospholipidswere measured in the negative mode as it enabled the identification of fragment ions corresponding to the fatty acyl chains (not positional information), e.g., PC 18:1_18:2. The phospholipids are analyzed using one fatty acyl chain, as the second chain can be characterized by measuring the total carbon count and subtracting the measured chain. The MRM transitions of TG and DG are generated using neutral loss of one fatty acyl tail in positive mode. Only one tail has been reported for TG, e.g. TG 16:1_51:2, where 16:1 will be one of the fatty acyl chain out of three chain in TG 51:2.

Five criteria were used for the confirmation of identification for all lipid features: **Class separation and cross-class interference**, Criteria 1: lipid features detected in the HILIC-MS/MS method; Criteria 2: lipid class chromatographically separated or has a diagnostic fragment in the case of overlapping chromatographic peaks; **Within-class separation and interference**, Criteria 3: lipid features confirmed by accurate mass using RPLC-HRMS; Criteria 4: lipid features with full chromatographic separation; Criteria 5: lipid features matched with retention time model; Criteria 6: lipid features showing non-zero concentration after isotopic and interfering adduct/ion type correction. The confidence of lipid identification will be indicated using confidence level scores, score 4 being the highest while score 1 the lowest. An overview of the lipid identification workflow and confidence level score is shown in **Figure 1(A) and 1(B)**.
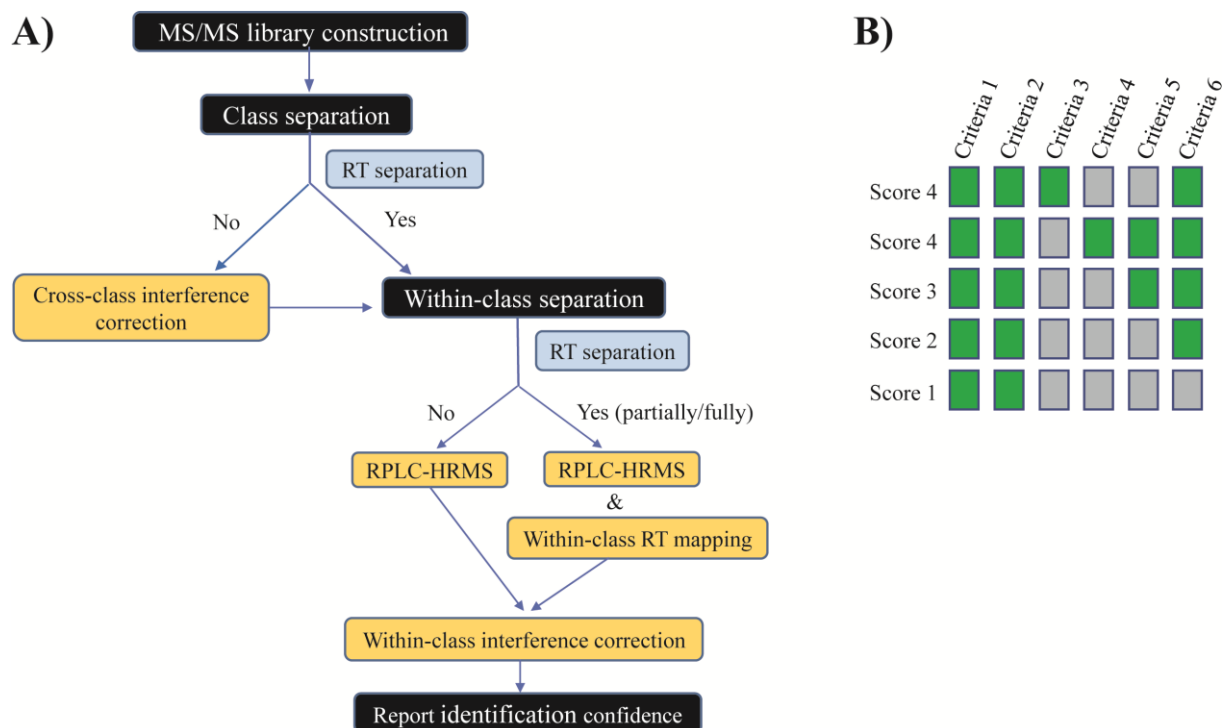
Figure 1. (A) Decision tree of lipid identification.; (B) Score levels of identification confidence. Criteria 1: lipid features detected in the HILIC-MS/MS method; Criteria 2: lipid class chromatographically separated or has a diagnostic fragment in the case of overlapping chromatographic peaks; Criteria 3: lipid features confirmed by accurate mass using RPLC-HRMS; Criteria 4: lipid features with full chromatographic separation; Criteria 5: lipid features matched with retention time model; Criteria 6: lipid features showing non-zero concentration after isotopic and interfering adduct/ion type correction. The green boxes represent the fulfillment of the criteria. RT, Retention time; RPLC-HRMS, Reversed-phase liquid chromatography-high resolution mass spectrometry.

3.2 Class separation and cross-class interference of lipids in the HILIC-MS/MS method

The UHPLC system coupled to the QTRAP 6500+ mass spectrometer was employed for targeted acquisition of lipids in MRM mode. XIC chromatograms of standards spiked in plasma are shown in **Figure 2(A).** The class retention time was confirmed by 3–5 standards per class with different chain length and carbon number. In HILIC chromatography, individual lipid classes are separated according to polarity of the head group. Therefore, the non-polar character of TG, DG and CE leads to the least retention for these classes, followed by Cer at the beginning of the chromatogram. The more polar lipid classes, such as PC, PE, PG, PI, HexCer, LacCer, SM, LPC, LPE, LPG elute over a wide tR range in the middle part of the chromatogram. The most polar lipids PS, LPI and LPS elute at the end of the chromatogram.
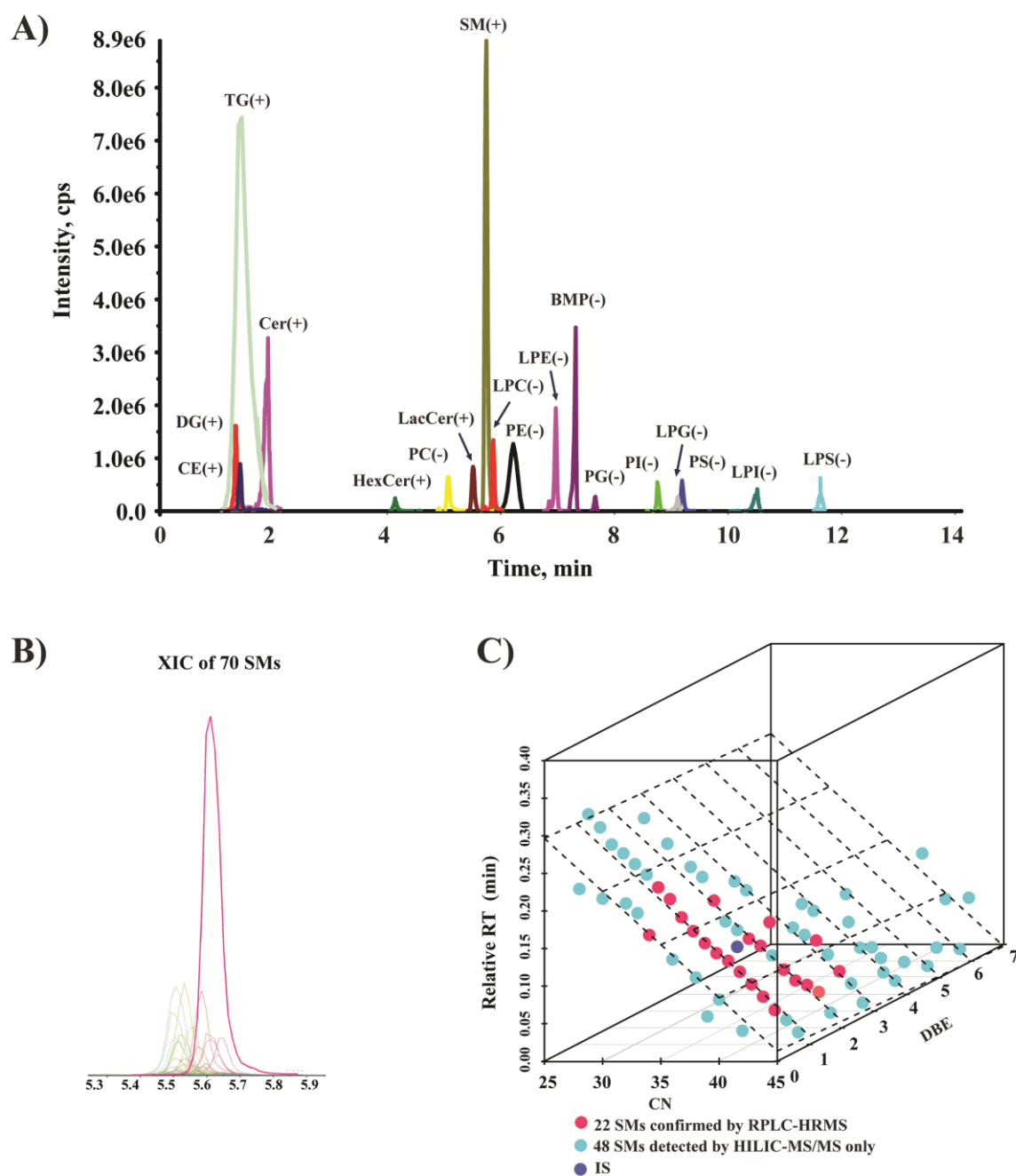
Figure 2. A) Representative XIC chromatograms of standards spiked in plasma by HILIC-MS/MS lipidomics analyses in switching polarity modes (positive (+) and negative (-)).; B) XIC chromatograms of 70 SMs detected in plasma using HILIC-MS/MS method.; C) 3D model for retention time mapping with carbon number (CN) and double bond equivalents (DBE) for 70 SMs detected by the HILIC-MS/MS method. 22 SMs confirmed by RPLC-HRMS are colored in red, the remaining SMs fitting the retention time model with error rates less than 20% are colored in light blue and SM 18:1;O2/18:1-d9 (IS) is in dark blue. Peak annotation: TG, Triglyceride; DG, Diglyceride; CE, Cholesteryl ester; Cer, Ceramide; HexCer, Hexosyl ceramide; PC, Phosphatidylcholine; LacCer, Lactosyl ceramide; SM, Sphingomyelin; LPC, Lysophosphatidylcholine; PE, Phosphatidylethanolamine; LPE, Lysophosphatidylethanolamine; BMP, Bis(Monoacylglycero)Phosphate; PG, Phosphatidylglycerol; PI, Phosphatidylinositol; LPG, Lysophosphatidylglycerol; PS, Phosphatidylserine; LPI, Lysophosphatidylinositol; LPS, Lysophosphatidylserine.

The first step (criteria 1) of the identification involves the detection of the lipid features in the

HILIC-MS/MS method. The limit of detection (LOD) was first determined for each class, and

features that were detected over the LOD threshold were further checked for interference from background signal. The repeatability of six replicates of the same plasma samples were examined, and the features with deviation above 30% in these replicates were excluded.

The next step (criteria 2) of identification was the evaluation of cross-class interferences. The classes should either be chromatographically separated or should have a diagnostic fragment for clear identification. GalCer and GluCer are an example of isomeric interferences that do not separate chromatographically and co-elute and hence, they are reported as HexCer. PG and BMP are another example of isomeric lipid classes which are chromatographically well-separated as seen in the standards in **Figure 2(A)** (the coverage of endogenous BMPs can be extended in the future). SM has been reported to have isobaric interference from PC as they generate the same product ion 184.1 from their headgroup in the positive ion mode, but this interference can be resolved as these two classes are separated by retention time.

There are also potential cross-class interferences due to in-source fragmentation. PC undergoes in-source fragmentation to generate PE in negative ionization mode [37]. Lysophospholipids and phospholipids will generate ions from their fatty acyl chains that can be misannotated as free fatty acids (FFAs) or they can also lose their head group and misannotated as lysophosphatidic acid (LPA) or phosphatidic acid (PA). In positive mode, glycosphingolipids could lose their head group, generating respective ceramide fragment [38]. But all of these potential cases of interferences due to in-source fragmentation are well separated by the chromatography. TG is a common in-source fragmentation source for DG, however ammonium adducts of TG in positive polarity mode undergoes neutral m/z loss of NH_3 and a fatty acid chain [39]. After the neutral loss, the remaining part of TG corresponds to the in-source fragment of DG $[M + H]^+$ (protonated form) instead of DG $[M + NH_4]^+$. Since the ammonium adduct of DG is used in our method for analysis, the problem with TG's in-source fragmentation is avoided. After cross-class interference screening, the lipid features was evaluated for within-class interference.

3.3 Within-class separation and interference of lipid features in HILIC-MS/MS method

The further identification (criteria 3) of lipid features from the HILIC-MS/MS method library was performed by their accurate mass determination by RPLC-HRMS method as reverse phase has superior performance in within-class species separation. Apart from accurate mass determination, the fatty acyl chain information was also checked for classes TG, DG, PC, PE and PI by using IDA mode **(supplementary Table S5, sheet 3).**

The next step for the identification of lipid features was through chromatographic tR in the HILIC-MS/MS method, which is a very important parameter for lipid identification. The individual lipid features within class are separated according to the carbon number and the double bond equivalents. The lipid features in the classes LPC, LPE, LPG, SM, PI, PS, PE and PC are partially separated and elute over a range of tR (0.2–0.4) min while features with different acyl chains in the classes LPI and LPS are fully separated and elute over a retention time range of 0.7 min and 1.13 min, respectively **(supplementary Table S7)**. The lipid features belonging to the classes TG, DG, CE, Cer, HexCer, LacCer and PG, show no separation and elute at a range spanning less than 0.05 min. Criteria 4 was assigned to the features belonging to the fully separated classes. Further, retention time models were built for partially/fully separated classes to match retention pattern with lipid features (criteria 5). To study the retention behavior of lipid features within each class in HILIC, relative dependencies of tR on the CN and the DB number are fitted using a multiple linear regression model using the unambiguously identified lipid features. As seen in **Figure 2(B) and 2(C)**, SM features are separated over a range of 0.31 min. In **supplementary Table S5 (sheet 3)**, out of the 71 SM features, 70 features detected in the HILIC method and 22 SM features unambiguously identified using RPLC-HRMS were utilized to create a 3D model. In total, 70 SMs fit in the model with error rates of 11.9% and an R^2 of 0.97, after removal of the outliers with error rates higher than 20% or $R^2 <$ 0.9 **(Figure 2(C))**. The PS class had higher error rates (23.94%) due to fewer number of features (data not shown). In general, the higher carbon number in fatty acyl chains corresponds to decreased tR in HILIC **(Figure S1)**. Double bond equivalents contribute little in the separation of different lipid features in SM, PC, PE classes and result in partial or full separation in the tR of LPC, LPE, PI, LPG, PS, LPI, LPS.
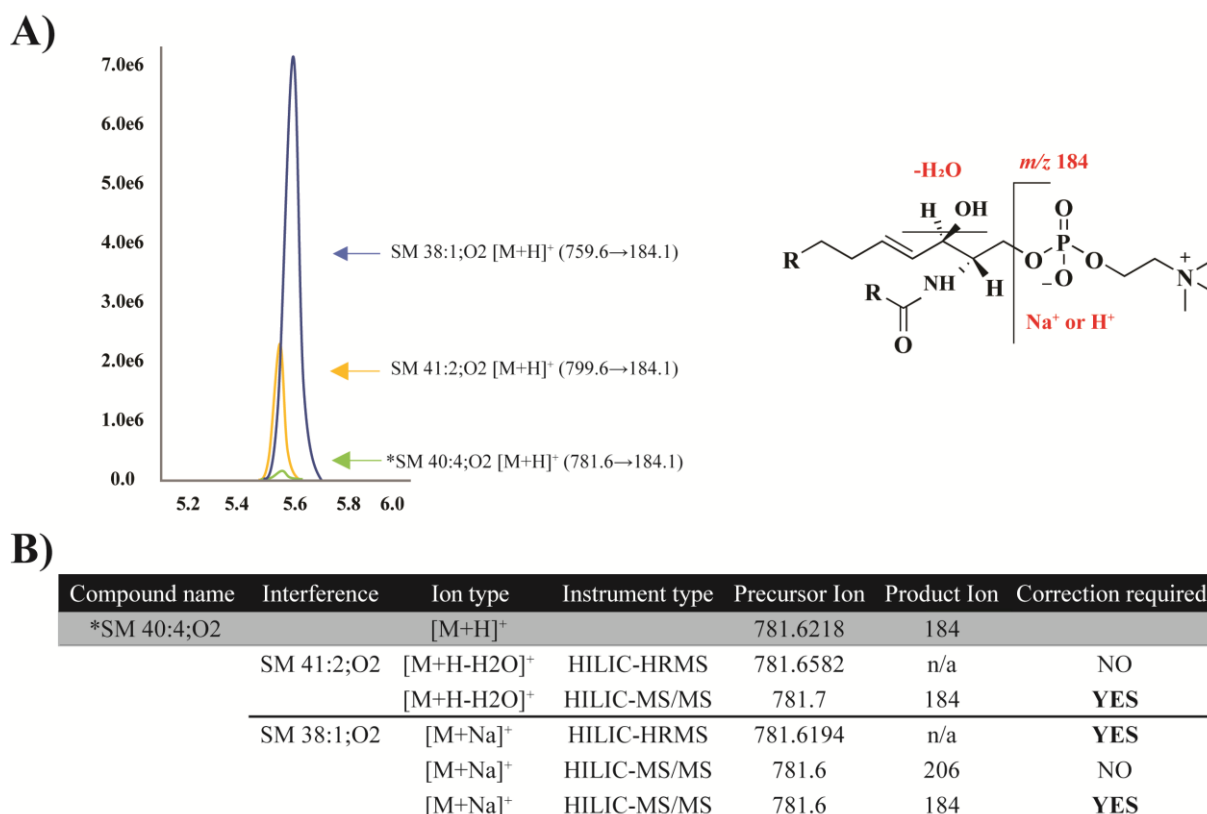
Figure 3. A) An example of XICs of monoisotopic peaks of three SMs and structure of different ion type (+H$^+$, +Na$^+$, -H2O) of SM in positive mode.; B) The possible interference from different ion types of SM in HILIC-HRMS and MRM analysis. (* *putatively annotated SM with score 2*)

All detected features with no/partial separation went through the quantifying corrections for different ion types and isotopes. We will take an example of SM for illustration of ion type interference. The primary observed ion types generated in positive mode for SMs are [M+H]$^+$, [M+Na]$^+$, and [M+H-H$_2$O]$^+$, with [M+H]$^+$ being the most intense peak. If we consider SM 40:4;O2, the primary ion type interference for [M+H]$^+$ could be caused by [M+Na]$^+$ of SM 38:1;O2 and [M+H-H$_2$O]$^+$ of SM 41:2;O2. The accurate masses of [M+H]$^+$ and [M+Na]$^+$ of SM 38:1;O2 are 759.6374 and 781.6194 respectively. The [M+Na]$^+$ of SM 38:1;O2 has almost the same mass as [M+H]$^+$ of SM 40:4;O2 (m/z 781.6218) and thus, is the main interference of SM 40:4;O2 in the HRMS method **(Figure 3(A)).** However, in the MRM method, SM 38:1;O2 will form a product ion of 206 which corresponds to the sodium phosphocholine headgroup instead of 184.07. The transitions of [M+Na]$^+$ of SM 38:1;O2 will be 781.6 → 206 instead of 781.6 → 184.07 and no correction is required in MRM method **(Figure 3(B)).** Another source of interference could be [M+H-H$_2$O]$^+$ of SM 41:2;O2 which has the transition of 781.6582 → 184.07, accounting for 0.05% of the signal of [M+H]$^+$ of SM 41:2;O2. The ion type interference for all other lipid classes are specified in **supplementary Table S8**.

The example of isotopic interference can be demonstrated by using sphingolipids classes such as Cer, LacCer and HexCer. These classes are dominated by the sphingoid backbone fragments 266, 264, 262 corresponding to the backbone d18:0, d18:1, d18:2 respectively [40]. These fragments can lead to interference, as the product ion of M+2 of d18:2 can contribute to the response of d18:1. Likewise, M+2 product ion of d18:1 can contribute to the response of d18:0. Hence, these kinds of interferences should be corrected.

The corresponding type II isotopic correction for all no/partially separated lipid features was performed by LICAR [35]. Criteria 6 was met for the features with non-zero concentration after isotopic and interfering adduct/ion type correction.

3.4 Report confidence

The scores are assigned based on the attainment of criteria as described in **Figure 1(B)**. For fully separated classes, features that at least meet the criteria 1+2+4+5+6 receive a score 4. For no/partially separated classes, score 4 is assigned to the features meeting at least the criteria 1+2+3+6. For no/partially separated classes, the features fulfilling criteria 1+2+5+6 are given a score of 3. All other features irrespective of no/partial/full separation, meeting criteria 1+2+6 are given score 2, while ones fulfilling criteria 1+2 get score 1. Depending on the fulfillment of criteria, each lipid feature has been given a score as shown in **supplementary Table S5 (sheet 3)**.

Names are assigned to the highest confidence features with score 4. The features with scores 3 and 2 are considered putatively annotated, while the features with score 1 are designated as unknowns.

3.5 Validation in human K2 EDTA plasma

The in-house human K2 EDTA plasma was used as matrix and one-IS per class mix was used for assessing the performance of HILIC-MS/MS method. The calibration lines of IS spiked in pure solvent and in plasma (before and after extraction) are shown in **Figure S2**. Linearity, LOD, LOQ, carryover, precision, recovery, ion suppression and matrix effect were assessed and reported in **Table 1 and supplementary Table S5 (sheet 4)**. The LODs and LOQs were as low as 0.60 pmol mL^{-1} and 1.31 pmol mL^{-1} respectively (except for CE) which makes our method sensitive enough to detect the lipids at low concentrations in 25 μL of plasma. The linear regression coefficients (R^2) were above 0.98 for most of the lipid classes except for CE where it was 0.97. The carryover was analyzed in the blank samples placed right after the plasma

samples (spiked with highest calibration point before extraction). Apart from PS and LPS, all lipid classes showed a carryover of below 2%. The intraday and interday precisions were determined at L, M and H concentration levels. Almost all the classes have RSD (%) below 15% except for DG, Cer and CE. The recovery was in the range of (53–112)% for most of the lipid classes but for the polar classes such as LPG, LPS and LPI, the recovery is poor which may reflect the current extraction method is less suited for polar lipids and these classes may need a dedicated extraction method. It was observed that non-polar classes such as DG and CE show severe ion suppression and matrix effects as these classes elute at the same retention time as TG. The TG class has very high endogenous concentrations which may lead to the ion suppression of DG and CE. The polar classes such PC and LPC also show significant ion suppression that may be due to the interference from the matrix. LPG, LPI and LPS show severe matrix effects at L and M level concentration. In our HILIC method, the internal standards co-elute with the endogenous compounds, hence the issues related to poor recovery, severe ion suppression and matrix effects can be compensated by the use of appropriate internal standards. The repeatability of our HILIC-MS/MS method was determined by measuring the RSD of endogenous lipid features in 12 QC samples. These QC samples were inserted at an interval of every 10 samples in the covid patient samples batch. It was found that 20 lipid features showed RSD below 5% while 360 and 380 lipid features showed RSD in between (5–10)% and (10–15)% respectively. 227 had RSD in the range of (15–20)% while 75 have RSD in between (20–30)%. In total, 1062 endogenous lipid features show an RSD below 30% (**Figure 5(A)**) which in accordance with the metabolomics study requirements.

Table 1. Summary of the validation parameters for human K2 EDTA plasma samples using one-IS per class mix.

Lipid class	Internal standards	Linearity	LOD (nmol mL⁻¹)	LOQ (nmol mL⁻¹)	Intraday Precision (%)			Interday Precision (%)		
					low	medium	high	low	medium	high
Phosphatidylcholine	PC 15:0/18:1-d7	0.995	0.0306	0.071	2.69	2.43	3.13	7.09	9.16	8.72
Phosphatidylethanolamine	PE 15:0/18:1-d7	0.995	0.0006	0.0013	3.67	7.08	3.67	8.23	6.99	6.04
Phosphatidylserine	PS 15:0/18:1-d7	0.999	0.0014	0.0041	8.41	4.81	5.22	8.29	5.75	5.26
Phosphatidylglycerol	PG 15:0/18:1-d7	0.997	0.001	0.0024	0.75	1.83	1.79	7.34	3.47	3.46
Phosphatidylinositol	PI 15:0/18:1-d7	0.994	0.0051	0.016	5.87	4.48	1.88	4.56	5.78	3.17
Lysophosphatidylcholine	LPC 18:1-d7	0.992	0.0032	0.0089	0.36	1.02	2.4	4.97	5.57	6.76
Lysophosphatidylethanolamine	LPE 18:1-d7	0.992	0.0011	0.0021	2.14	1.43	5.49	7.13	6.83	6.79
Cholesteryl esters	CE 18:1-d7	0.970	2.0202	6.6603	16.89	10.76	7.82	12.87	13.01	19.99
Diglycerides	DG 15:0/18:1-d7	0.982	0.0495	0.129	2.44	8.29	8.32	15.89	33.26	29.25
Triglycerides	TG 15:0/18:1-d7/15:0	0.992	0.0086	0.0247	0.88	3.19	0.51	12.73	11.84	8.62
Sphingomyelin	SM 18:1;O2/18:1-d9	0.990	0.0013	0.0033	2.85	1.59	1.87	3.7	12.86	7.46
Lysophosphatidylglycerol	LPG 17:1	0.992	0.0011	0.0035	2.99	3.18	3.83	5.25	9.03	8.92
Lysophosphatidylinositol	LPI 17:1	0.992	0.0007	0.0021	3.52	2.04	5.87	14.16	13.67	14.91
Lysophosphatidylserine	LPS 17:1	0.991	0.0036	0.005	7.21	5.57	4.87	9.92	5.71	7.38
Ceramides	Cer 18:1;O2/16:0-d9	0.981	0.0241	0.0581	9.63	29.68	34.15	21.76	21.37	18.59
Ceramides	Cer 18:0;O2/16:0-d9	0.989	0.0057	0.008	2.91	0.57	2.22	4.51	5.65	7.21
Hexosylceramides	Hex-Cer 18:1;O2/16:0-d9	0.998	0.0053	0.0108	16.46	6.74	11.16	11.82	8.87	8.69
Lactosylceramides	Lac-Cer 18:1;O2/16:0-d9	0.993	0.0056	0.0119	9.78	12.96	4.98	15.34	14.29	23.51

3.6 Accurate quantitation in NIST SRM 1950 plasma

In NIST SRM 1950 plasma, 608 lipid species across 19 classes with score 4 were quantified. The quantitation strategies are listed in **Figure 4(A)**. The unavailability of commercial standards for all endogenous lipid species leads to limitations in achieving absolute quantitation, but HILIC has an advantage over other separation techniques as the elution of species occurs according to their head group, so all species in a particular class elute at almost the same time and have similar ionization efficiencies. Since we lack individual standards for each endogenous lipid species, we are using multiple internal standards per class to achieve quantitation as accurate as possible. Here, we further use the multi-ISs per class strategy to correct for the response factor to report measured lipid concentrations for the NIST SRM 1950 plasma.

Another factor to be taken into account is the different response of sn-1 and sn-2 of phospholipids in MRM experiments [41]. Determining ratios between fragment ions of positional isomers can help determine the sn-positions of fatty acyl chains in glycerophospholipids [14]. Using this strategy, we defined the positional isomers of lipid species and then assigned internal standards for quantitation. The response of both fatty acyl chains at sn-1 and sn-2 position of phospholipid species were examined to determine the position of the chains. **Supplementary Table S9** illustrates the ratios of the sn-1/sn-2 carboxylate anion of phospholipids ISs at different collision energies. At collision energies of 30, 40, and 50 eV, the sn-1/sn-2 response ratios of PI and PS are above 1, whereas those of PC, PE, and PG are below 1. There is an exception where the ratio is more than 1 when the sn-2 chain is 22:4 at collision energy of 60 eV. Further, we determined the ratio of two transitions of fatty acid chains of endogenous species in the NIST plasma samples to identify the dominant isomers. We took sn-1/sn-2> 1 or sn-1/sn-2< 1 to define the dominant isomer.

After determining the sn-1 and sn-2 ratios, we used calibration lines using multi-ISs per class. The calibration lines with $R^2 < 0.98$ were dropped, except for CE and DG with criteria of $R^2 > 0.96$. The next step was to assign an IS based on total carbon number and double bond equivalents of endogenous compounds. If the total carbon number was same, then the double bond equivalents was also taken into account **supplementary Table S5 (sheet 5)**. The sn-1 and sn-2 information of endogenous metabolites was considered while assigning the ISs and post-hoc correction was used to correct for metabolites with two of the same fatty acyl chains, e.g. PC 18:1_18:1.

The TG classes with three fatty acyl chains are more complex and it is difficult to determine their fatty acyl chain position with our current method. Hence, their quantitation was performed considering only the total carbon number and double bond equivalents of the fatty acyl chains. The concentration values of the lipid species in the NIST plasma samples are specified in **supplementary Table S5 (sheet 6)**. The correlation of the NIST SRM 1950 data with that from published consensus values [42,43,21] shows overall good correlation with R^2 ranging from 0.64 to 0.84 (**Figure 4(B)**).

Although we applied several strategies to achieve the accurate quantitation, our method is still limited due to the lack of a suitable model to correct the response factor for the sn-1/sn-2 isomer ratio and lack of (internal) standards for individual compounds.
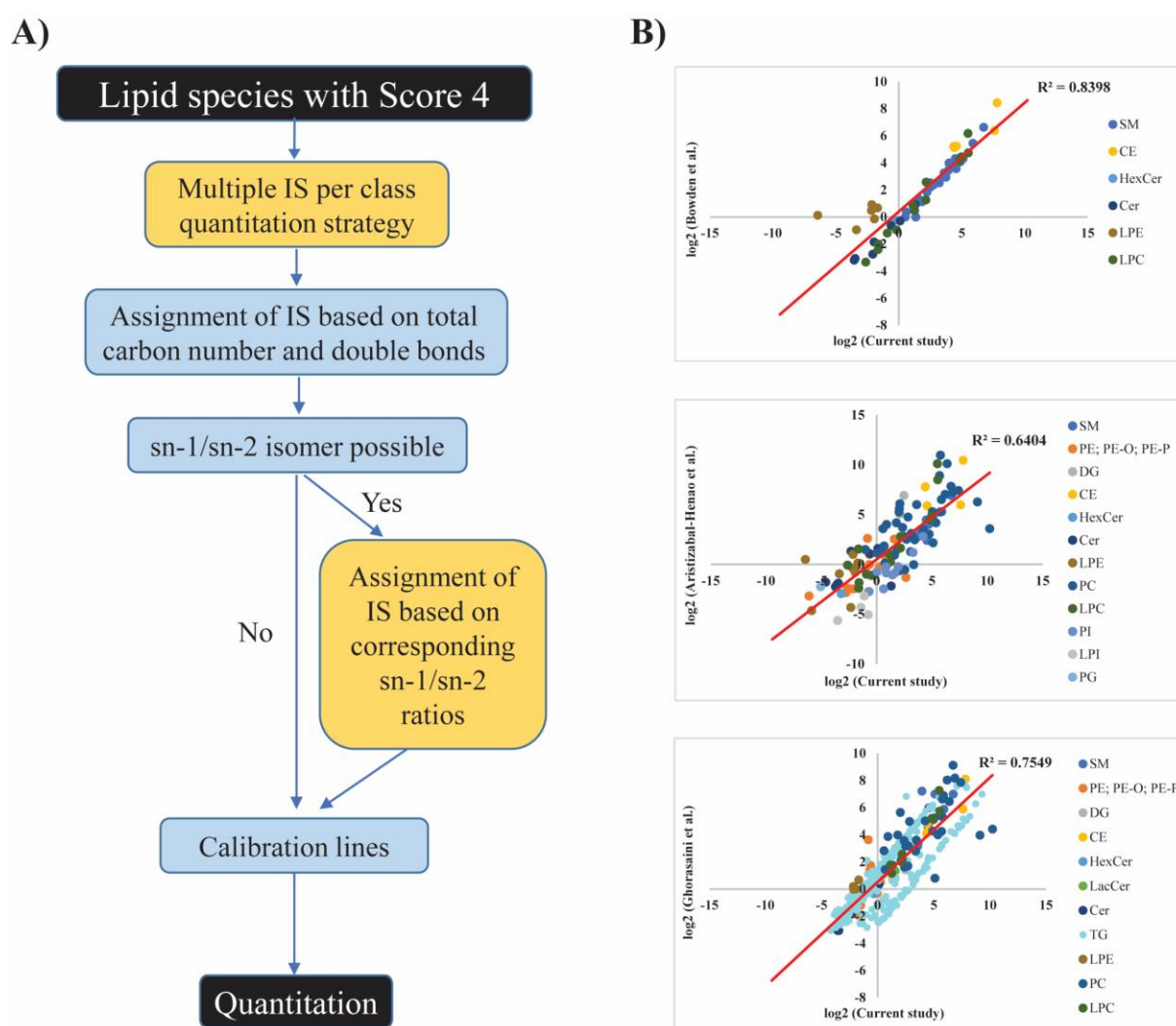

Figure 4. A) Decision tree of lipid quantitation.; B) Correlation of lipid concentrations (nmol mL^{-1}, base 2 logarithm) between our HILIC-MS/MS method and reported literature values (a. Bowden et al, 2017; b. Aristizabal-Henao et al, 2020, c. Ghorasaini et.al, 2021).

3.7 Application of HILIC-MS/MS lipidomics method in COVID-19 plasma samples

Next, we applied this method to discover plasma lipid biomarkers for COVID-19 severity using all the lipid features irrespective of their confidence scores. The plasma lipid extracts of 25 patients housed in the hospital ward and 78 patients in ICU were analyzed in a random order by this HILIC-MS/MS method. QC samples were inserted between every 10 study samples for data quality control and batch correction. After peak integration, 1062 lipid features with a QC RSD < 30% and with a distribution of the coefficient of variation (%) shown in **Figure 5(A)** were selected for subsequent statistical analyses.

The PCA plot shows good separation between the ward and ICU patients (**Figure 5(B)**), which indicates a widely changed lipidome in severe COVID-19 patients. A linear regression model was used to find out the most important biomarker candidates distinguishing the patients in the ward from ICU. The modeling results showed that a total of 511 identified lipid features (score 2, 3&4) and 9 unknowns (score 1) across 18 lipid (sub)classes with *FC ≥ 1.3* or *FC ≤ 0.7* as well as false discovery rate (FDR) *Q<0.05* were significant **(supplementary Table S5, sheet 7)**. The volcano plot of these significantly changed lipid metabolites is shown in **Figure 5(C)**. In general, Cers, glycerophospholipids, DGs, TGs, short-chain SMs, and plasmalogen phosphoethanolamines were significantly increased, and six saturated/monounsaturated PIs, one LacCer, four SMs, one plasmalogen phosphoethanolamine (PE O-16:0/20:4) and two CEs were significantly (≥30% median fold change, and *Q<0.05*) decreased in ICU patients as compared to the those in the ward.

Specifically, TGs were identified as having higher abundance in the ICU patients compared with those in the ward. TGs are an important source of energy metabolism in the liver and many COVID-19 patients showed liver function abnormalities [8,44]. This is also supported by the lower total CE, which is often observed in liver damage [45].

Glycerophospholipids and sphingolipids are the major components of cell membranes and play a key role of maintaining the balance of the *in vivo* energy metabolism. Reports showed that phospholipids were significantly decreased in severe covid patients [7]. However, increased glycerophospholipid levels, including PC, PE, PI, PG, PS, and corresponding lysophospholipids were observed in our results. This may be because 80% of the patients of this cohort had chloroquine treatment, which has been reported to increase phospholipid levels [46]. Sphingolipids are also essential components of biomembrane lipid rafts which mediate signal transduction and immune activation processes. Critical patients are characterized by a

decrease in SMs and elevated levels of Cers, HexCers. In severe patients, the altered lipidome of lipid rafts compositions may lead to cell apoptosis and immunoescape [10].

The application of our method in the COVID-19 plasma samples shows mainly class-based changes in the lipid profiles. There are also strong associations observed between severity of disease progression with fatty acid chain composition and saturation degree. Although a biological interpretation is not the aim of this paper, our results demonstrate that the HILIC-MS/MS-based targeted lipidomics method with wide coverage is very promising for disease biomarker discovery.
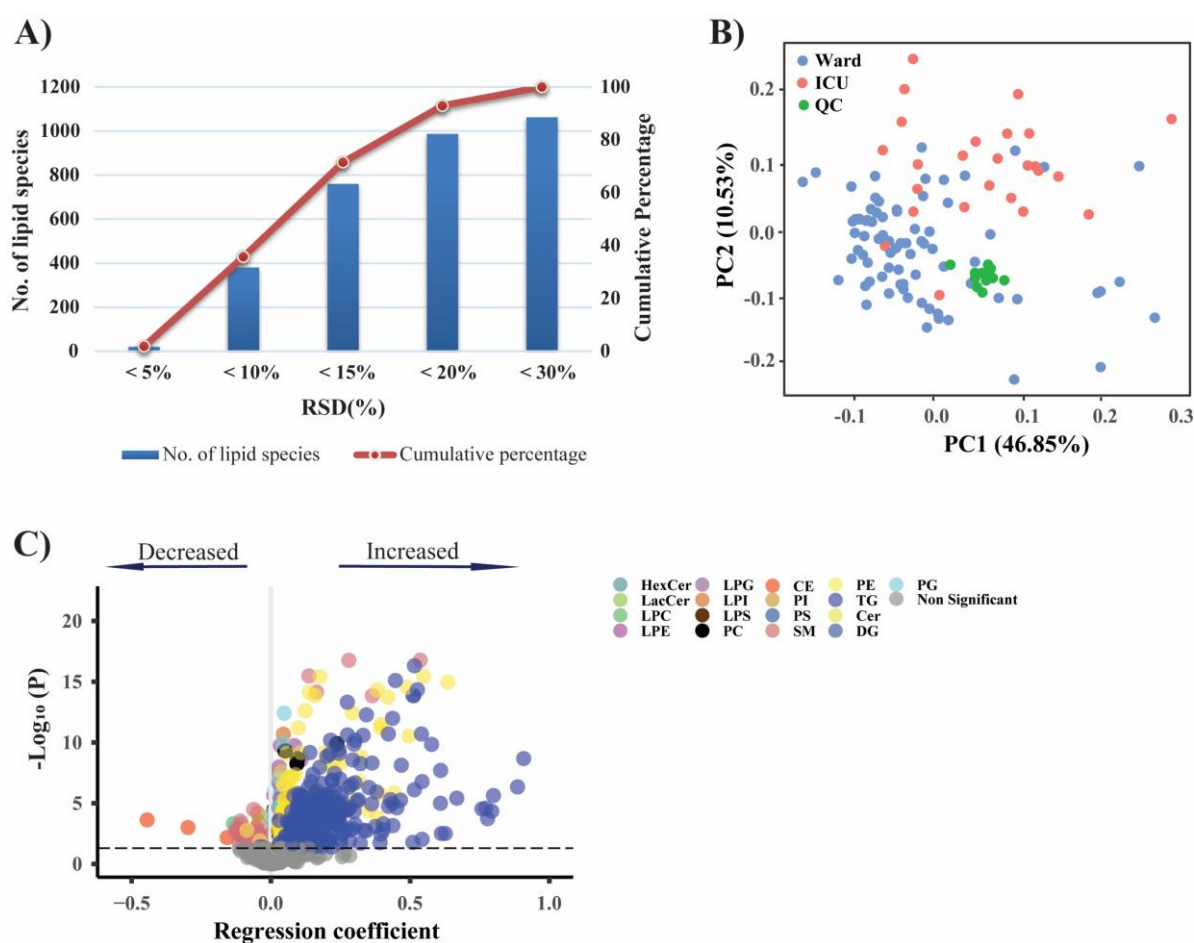
Figure 5. Application in COVID-19 patients to distinguish the disease severity. A) Repeatability of lipid features in pooled QC samples of COVID-19 patients.; B) PCA scores plot of samples from patients admitted to ward, or ICU and QCs, based on all metabolite data (cube-root transformed and Pareto-scaled).; C) Volcano plot comparing plasma metabolites of patients in ICU with ward. Significantly altered metabolites with FDR < 0.05 are highlighted with different colors for different classes. Negative values indicate decreased and positive values indicate increased levels in ICU patients.

4. Conclusion

The lipidomics field is continuously evolving and a significant amount of work has been done in this area in recent years. But still two important aspects have been missing, comprehensive coverage spanning non-polar to polar lipid classes and quantifying the different lipid species at fatty acyl chain level. To achieve this, it is crucial to follow the standardized workflow as proposed by Lipidomics Standards Initiative to avoid over-reporting and false identification [29]. Herein, we describe a HILIC-MS/MS method with the initial target list of 1200 lipid features across 19 lipid (sub)classes. These lipid features were evaluated using various cross-class and within-class interference criteria for confirmation of their identification. Scores have been assigned to all these features showing the confidence in their identification. Further, we provided accurate quantitation of 608 lipid species with score 4 in NIST SRM plasma using multiple-ISs per class and a post-hoc correction strategy. This HILIC-MS/MS-based lipidomics method was validated and applied to COVID-19 patient samples. All detected features were used for biomarker discovery in COVID-19 plasma samples and features with high confidence were used for quantitation and comparison with other reported studies. Around 1062 detected lipid features from 25 μL of plasma were reported in COVID-19 patient plasma and dramatic class-based lipidome alterations indicated the changes in energy metabolism.

In conclusion, we have applied several strategies for high confidence lipid identification to avoid over-reporting of lipid species. This method has the competence of comprehensive lipidome coverage and can be used to extend the existing libraries of lipid features. Despite the fact that several strategies were applied to provide lipid concentrations at the fatty acyl chain level, limitations remain due to lack of a suitable model to correct for response factor for fatty acyl chain positional isomers. Nevertheless, this work has demonstrated potential in biomarker discovery to help in improving clinical lipidomics studies and will also encourage lipidomics researchers to use methods reporting lipids at a detailed structural level.

Author contributions

Z.Z. and M.S. contributed equally to this manuscript. Z.Z and M.S.- Conceptualization, Data curation, Investigation, Writing-original draft and editing; A.K.- Investigation, Writing-Review & editing; A.B.W.- Investigation, Review & editing; M.J.P.-Investigation; A.A.- Supervision, Review & editing; A.H.- Supervision, Review & editing; P.B.- Conceptualization, Supervision, Review & editing; T.H.- Funding acquisition, Conceptualization, Supervision, Review & editing. The manuscript was written through contributions of all authors. All authors have given approval to the final version of the manuscript.

Declaration of competing interests

The authors declare that they have no known competing financial interests or personal relationships that could have appeared to influence the work reported in this paper.

Acknowledgements

References

[1] M.R. Wenk, Lipidomics: new tools and applications, Cell 143 (2010) 888-895,https://doi.org/10.1016/j.cell.2010.11.033.

[2] C.E. Stokes, J.N. Hawthorne, Reduced phosphoinositide concentrations in anterior temporal cortex of Alzheimer-diseased brains, J. Neurochem. 48 (1987) 1018–1021, https://doi.org/10.1111/j.1471-4159.1987.tb05619.x.

[3] A. Mukherjee, Y. Ma, F. Yuan, Y. Gong, Z. Fang, E.M. Mohamed, E. Berrios, H. Shao, X. Fang, Lysophosphatidic acid up-regulates hexokinase II and glycolysis to promote proliferation of ovarian cancer cells, Neoplasia 17 (2015) 723–734, https://doi.org/10.1016/j.neo.2015.09.003.

[4] R.W. Gross, X. Han, Lipidomics in diabetes and the metabolic syndrome. Methods Enzymol, Elsevier, 2007, pp. 73–90, https://doi.org/10.1016/S0076-6879(07) 33004-8.

[5] P. G´erard, The crosstalk between the gut microbiota and lipids, OCL 27 (2020) 70, https://doi.org/10.1051/ocl/2020070.

[6] B. Shen, X. Yi, Y. Sun, X. Bi, J. Du, C. Zhang, S. Quan, F. Zhang, R. Sun, L. Qian, W. Ge, W. Liu, S. Liang, H. Chen, Y. Zhang, J. Li, J. Xu, Z. He, B. Chen, J. Wang, H. Yan, Y. Zheng, D. Wang, J. Zhu, Z. Kong, Z. Kang, X. Liang, X. Ding, G. Ruan, N. Xiang, X. Cai, H. Gao, L. Li, S. Li, Q. Xiao, T. Lu, Y. Zhu, H. Liu, H. Chen, T. Guo, Proteomic and metabolomic characterization of COVID-19 patient sera, Cell 182 (2020) 59–72, https://doi.org/10.1016/j.cell.2020.05.032, e15.

[7] M.A. Hussein, N.E.M. Ismail, A.H. Mohamed, R.M. Borik, A.A. Ali, Y.O. Mosaad, Plasma phospholipids: a promising simple biochemical parameter to evaluate COVID-19 infection severity, Bioinform. Biol. Insights 15 (2021), https://doi.org/10.1177/11779322211055891, 117793222110558.

[8] D. Wu, T. Shu, X. Yang, J.-X. Song, M. Zhang, C. Yao, W. Liu, M. Huang, Y. Yu, Q. Yang, T. Zhu, J. Xu, J. Mu, Y. Wang, H. Wang, T. Tang, Y. Ren, Y. Wu, S.-H. Lin, Y. Qiu, D.-Y. Zhang, Y. Shang, X. Zhou, Plasma metabolomic and lipidomic alterations associated with COVID-19, Natl. Sci. Rev. 7 (2020) 1157–1168, https://doi.org/10.1093/nsr/nwaa086.

[9] M Abdalla, N.E.M Ismail, ah mohamed, R.M. Borik, Aa ali, Y.O Mosaad, Plasma Levels of Phospholipids in Patients With COVID-19; A Promising Simple Biochemical Parameter to Evaluate the Disease Severity, Research Square (2020), https://doi.org/10.21203/rs.3.rs-57302/v1.

[10] E. Torretta, M. Garziano, M. Poliseno, D. Capitanio, M. Biasin, T.A. Santantonio, M. Clerici, S.L. Caputo, D. Trabattoni, C. Gelfi, Severity of COVID-19 patients predicted by serum sphingolipids signature, Int. J. Mol. Sci. 22 (2021) 10198, https://doi.org/10.3390/ijms221910198.

[11] M. Abu-Farha, T.A. Thanaraj, M.G. Qaddoumi, A. Hashem, J. Abubaker, F. Al- Mulla, The role of lipid

metabolism in COVID-19 virus infection and as a drug target, Int. J. Mol. Sci. 21 (2020) 3544, https://doi.org/10.3390/ijms21103544.

[12]   J.-W. Song, S.M. Lam, X. Fan, W.-J. Cao, S.-Y. Wang, H. Tian, G.H. Chua, C. Zhang, F.-P. Meng, Z. Xu, J.-L. Fu, L. Huang, P. Xia, T. Yang, S. Zhang, B. Li, T.-J. Jiang, R. Wang, Z. Wang, M. Shi, J.-Y. Zhang, F.-S. Wang, G. Shui, Omics-driven systems interrogation of metabolic dysregulation in COVID-19 pathogenesis, Cell Metab. 32 (2020) 188–202, https://doi.org/10.1016/j.cmet.2020.06.016, e5.

[13]   J.F. Osuna-Ramos, H. Rend´on-Aguilar, L.A.D. Jes´us-Gonz´alez, J.M. Reyes-Ruiz, A. M. Espinoza-Ortega, L.A. Ochoa-Ramírez, A. Romero-Utrilla, E. Ríos-Burgue˜no, A. Soto-Almaral, J.J. Ríos-Tostado, J.G. Romero-Quintana, H. Ponce-Ramos, C.N. Farfan-Morales, R.M. del ´Angel, H. Barajas-Martínez, J. Rodríguez-Mill´an, J.S. Velarde-F´elix, Serum lipid profile changes and their clinical diagnostic significance in COVID-19 Mexican patients, Infectious Diseases (except HIV/AIDS), 2020. http://medrxiv.org/lookup /doi/10.1101/ 2020.08.24. 20169789 (accessed September 25, 2022).

[14]   M. Holˇcapek, G. Liebisch, K. Ekroos, Lipidomic analysis, Anal. Chem 90 (2018) 4249–4257, https://doi.org/10.1021/acs.analchem.7b05395.

[15]   B. Buszewski, S. Noga, Hydrophilic interaction liquid chromatography (HILIC)-a powerful separation technique, Anal. Bioanal. Chem. 402 (2012) 231–247, https://doi.org/10.1007/s00216-011-5308-5.

[16]   E. Cífkov´a, M. Holˇcapek, M. Lísa, D. Vr´ana, B. Melichar, V. ˇStudent, Lipidomic differentiation between human kidney tumors and surrounding normal tissues using HILIC-HPLC/ESI–MS and multivariate data analysis, J. Chromatogr. B 1000 (2015) 14–21, https://doi.org/10.1016/j.jchromb.2015.07.011.

[17]   H.K. Kotapati, P.D. Bates, Normal phase HPLC method for combined separation of both polar and neutral lipid classes with application to lipid metabolic flux, J. Chromatogr. B 1145 (2020), 122099, https://doi.org/10.1016/j. jchromb.2020.122099.

[18]   P.D. Rainville, C.L. Stumpf, J.P. Shockcor, R.S. Plumb, J.K. Nicholson, Novel application of reversed-phase UPLC-oaTOF-MS for lipid analysis in complex biological mixtures: a new tool for lipidomics, J. Proteome Res. 6 (2007) 552–558, https://doi.org/10.1021/pr060611b.

[19]   C.G. Vasilopoulou, K. Sulek, A.D. Brunner, et al., Trapped ion mobility spectrometry and PASEF enable in-depth lipidomics from minimal sample amounts, Nat. Commun. 11 (2020) 331, https://doi.org/10.1038/s41467-019- 14044-x.

[20]   U. Loizides-Mangold, On the future of mass-spectrometry-based lipidomics, FEBS J.280 (2013) 2817–2829, https://doi.org/10.1111/febs.12202.

[21]   M. Ghorasaini, Y. Mohammed, J. Adamski, L. Bettcher, J.A. Bowden, M. Cabruja,K. Contrepois, M. Ellenberger, B. Gajera, M. Haid, D. Hornburg, C. Hunter, C. M. Jones, T. Klein, O. Mayboroda, M. Mirzaian, R. Moaddel, L. Ferrucci, J. Lovett, K. Nazir, M. Pearson, B.K. Ubhi, D. Raftery, F. Riols, R. Sayers, E.J.G. Sijbrands, M.P. Snyder, B. Su, V. Velagapudi, K.J. Williams, Y.B. de Rijke, M. Giera, Crosslaboratory standardization of preclinical lipidomics using differential mobility spectrometry and multiple reaction monitoring, Anal. Chem. 93 (2021) 16369–16378, https://doi.org/10.1021/acs.analchem.1c02826.

[22]   Z. Cao, T.C. Schmitt, V. Varma, D. Sloper, R.D. Beger, J. Sun, Evaluation of the performance of lipidyzer platform and its application in the lipidomics analysis in mouse heart and liver, J. Proteome Res. 19 (2020) 2742–2749, https://doi.org/10.1021/acs.jproteome.9b00289.

[23]   R. Lerner, D. Baker, C. Schwitter, S. Neuhaus, T. Hauptmann, J.M. Post, S. Kramer, L. Bindila, Four-dimensional trapped ion mobility spectrometry lipidomics for high throughput clinical profiling of human blood samples, Nat. Commun. 14 (2023) 937, https://doi.org/10.1038/s41467-023-36520-1.

[24]   J. Medina, R. Borreggine, T. Teav, L. Gao, S. Ji, J. Carrard, C. Jones, N. Blomberg, M. Jech, A. Atkins, C. Martins, A. Schmidt-Trucksass, M. Giera, A. Cazenave-Gassiot, H. Gallart-Ayala, J. Ivanisevic, Omic-scale high-throughput quantitative LC–MS/MS approach for circulatory lipid phenotyping in clinical research, Anal. Chem. 95 (2023) 3168–3179, https://doi.org/10.1021/acs.analchem.2c02598.

[25]   N.R. Zhang, N.G. Hatcher, K. Ekroos, K. Kedia, M. Kandebo, J.N. Marcus, S.M. Smith, K.P. Bateman, D.S. Spellman, Validation of a multiplexed and targeted lipidomics assay for accurate quantification of lipidomes, J. Lipid Res. 63 (2022), 100218, https://doi.org/10.1016/j.jlr.2022.100218.

[26]   H.C. Kofeler, T.O. Eichmann, R. Ahrends, J.A. Bowden, N. Danne-Rasche, E. A. Dennis, M. Fedorova, W.J. Griffiths, X. Han, J. Hartler, M. Holˇcapek, R. Jir´asko, J.P. Koelmel, C.S. Ejsing, G. Liebisch, Z. Ni, V.B. O'Donnell, O. Quehenberger, D. Schwudke, A. Shevchenko, M.J.O. Wakelam, M.R. Wenk, D. Wolrab, K. Ekroos, Quality control requirements for the correct annotation of lipidomics data, Nat. Commun. 12 (2021) 4771, https://doi.org/10.1038/s41467-021-24984-y.

[27]   S.M. Lam, H. Tian, G. Shui, Lipidomics, en route to accurate quantitation, Biochim. Biophys. Acta (BBA) - Mol. Cell Biol. Lipids 1862 (2017) 752–761, https://doi.org/ 10.1016/j.bbalip.2017.02.008.

[28]   K. Yang, X. Han, Accurate quantification of lipid species by electrospray ionization mass spectrometry-meets a key challenge in lipidomics, Metabolites 1 (2011) 21–40, https://doi.org/10.3390/metabo1010021.

[29]   G. Liebisch, R. Ahrends, M. Arita, M. Arita, J.A. Bowden, C.S. Ejsing, W.J. Griffiths, M. Holˇcapek, H.

K¨ofeler, T.W. Mitchell, M.R. Wenk, K. Ekroos, Lipidomics standards initiative consortium, lipidomics needs more standardization, Nat. Metab. 1 (2019) 745–747, https://doi.org/10.1038/s42255-019-0094-z.

[30] V.B. O'Donnell, G.A. FitzGerald, R.C. Murphy, G. Liebisch, E.A. Dennis, O. Quehenberger, S. Subramaniam, M.J.O. Wakelam, Steps toward minimal reporting standards for lipidomics mass spectrometry in biomedical research publications, Circ. Genom. Precis. Med. (2020) 13, https://doi.org/10.1161/CIRCGEN.120.003019.

[31] N. Karu, A. Kindt, A.J. van Gammeren, A.A.M. Ermens, A.C. Harms, L. Portengen, R.C.H. Vermeulen, W.A. Dik, A.W. Langerak, V.H.J. van der Velden, T. Hankemeier, Severe COVID-19 is characterised by perturbations in plasma amines correlated with immune response markers, and linked to inflammation and oxidative stress, Metabolites 12 (2022) 618, https://doi.org/10.3390/ metabo12070618.

[32] N. Karu, A. Kindt, L. Lamont, A.J. van Gammeren, A.A.M. Ermens, A.C. Harms, L. Portengen, R.C.H. Vermeulen, W.A. Dik, A.W. Langerak, V.H.J. van der Velden, T. Hankemeier, Plasma oxylipins and their precursors are strongly associated with COVID-19 severity and with immune response markers, Metabolites 12 (2022) 619, https://doi.org/10.3390/metabo12070619.

[33] V. Matyash, G. Liebisch, T.V. Kurzchalia, A. Shevchenko, D. Schwudke, Lipid extraction by methyl-tert-butyl ether for high-throughput lipidomics, J. Lipid Res. 49 (2008) 1137–1146, https://doi.org/10.1194/jlr.D700041-JLR200.

[34] C. Hu, J. van Dommelen, R. van der Heijden, G. Spijksma, T.H. Reijmers, M. Wang, E. Slee, X. Lu, G. Xu, J. van der Greef, T. Hankemeier, RPLC-ion-trap-FTMS method for lipid profiling of plasma: method validation and application to p53 mutant mouse model, J. Proteome Res. 7 (2008) 4982–4991, https://doi.org/10.1021/ pr800373m.

[35] L. Gao, S. Ji, B. Burla, M.R. Wenk, F. Torta, A. Cazenave-Gassiot, LICAR: an application for isotopic correction of targeted lipidomic data acquired with classbased chromatographic separations using multiple reaction monitoring, Anal. Chem. 93 (2021) 3163–3171, https://doi.org/10.1021/acs.analchem.0c04565.

[36] G. Liebisch, E. Fahy, J. Aoki, E.A. Dennis, T. Durand, C.S. Ejsing, M. Fedorova, I. Feussner, W.J. Griffiths, H. K¨ofeler, A.H. Merrill, R.C. Murphy, V.B. O'Donnell, O. Oskolkova, S. Subramaniam, M.J.O. Wakelam, F. Spener, Update on LIPID MAPS classification, nomenclature, and shorthand notation for MS-derived lipid structures, J. Lipid Res. 61 (2020) 1539–1555, https://doi.org/10.1194/jlr. S120001025.

[37] R.M. Gathungu, P. Larrea, M.J. Sniatynski, V.R. Marur, J.A. Bowden, J.P. Koelmel, P. Starke-Reed, V.S. Hubbard, B.S. Kristal, Optimization of electrospray ionization source parameters for lipidomics to reduce misannotation of in-source fragments as precursor ions, Anal. Chem. 90 (2018) 13523–13532, https://doi.org/10.1021/ acs.analchem.8b03436.

[38] A. Criscuolo, M. Zeller, M. Fedorova, Evaluation of lipid in-source fragmentation on different orbitrap-based mass spectrometers, J. Am. Soc. Mass Spectrom. (2020) 4.

[39] O.L. Knittelfelder, B.P. Weberhofer, T.O. Eichmann, S.D. Kohlwein, G. N. Rechberger, A versatile ultra-high performance LC–MS method for lipid profiling, J. Chromatogr. B 951–952 (2014) 119–128, https://doi.org/10.1016/j. jchromb.2014.01.011.

[40] A. Singh, M. Del Poeta, Sphingolipidomics: an important mechanistic tool for studying fungal pathogens, Front. Microbiol. 7 (2016), https://doi.org/10.3389/fmicb.2016.00501.

[41] J. Pi, X. Wu, Y. Feng, Fragmentation patterns of five types of phospholipids by ultra-high-performance liquid chromatography electrospray ionization quadrupole time-of-flight tandem mass spectrometry, Anal. Methods 8 (2016) 1319–1332, https://doi.org/10.1039/C5AY00776C.

[42] J.A. Bowden, A. Heckert, C.Z. Ulmer, C.M. Jones, J.P. Koelmel, L. Abdullah, L. Ahonen, Y. Alnouti, A.M. Armando, J.M. Asara, T. Bamba, J.R. Barr, J. Bergquist, C.H. Borchers, J. Brandsma, S.B. Breitkopf, T. Cajka, A. Cazenave-Gassiot, A. Checa, M.A. Cinel, R.A. Colas, S. Cremers, E.A. Dennis, J.E. Evans, A. Fauland, O. Fiehn, M.S. Gardner, T.J. Garrett, K.H. Gotlinger, J. Han, Y. Huang, A.H. Neo, T. Hy¨otyl¨ainen, Y. Izumi, H. Jiang, H. Jiang, J. Jiang, M. Kachman, R. Kiyonami, K. Klavins, C. Klose, H.C. K¨ofeler, J. Kolmert, T. Koal, G. Koster, Z. Kuklenyik, I. J. Kurland, M. Leadley, K. Lin, K.R. Maddipati, D. McDougall, P.J. Meikle, N. A. Mellett, C. Monnin, M.A. Moseley, R. Nandakumar, M. Oresic, R. Patterson, D. Peake, J.S. Pierce, M. Post, A.D. Postle, R. Pugh, Y. Qiu, O. Quehenberger, P. Ramrup, J. Rees, B. Rembiesa, D. Reynaud, M.R. Roth, S. Sales, K. Schuhmann, M.L. Schwartzman, C.N. Serhan, A. Shevchenko, S.E. Somerville, L.St. John-Williams, M.A. Surma, H. Takeda, R. Thakare, J.W. Thompson, F. Torta, A. Triebl, M. Tr¨otzmüller, S.J.K. Ubhayasekera, D. Vuckovic, J.M. Weir, R. Welti, M.R. Wenk, C.E. Wheelock, L. Yao, M. Yuan, X.H. Zhao, S. Zhou, Harmonizing lipidomics: NIST interlaboratory comparison exercise for lipidomics using SRM 1950–metabolites in frozen human plasma, J. Lipid Res. 58 (2017) 2275–2288, https://doi.org/ 10.1194/jlr.M079012.

[43] J.J. Aristizabal-Henao, C.M. Jones, K.A. Lippa, J.A. Bowden, Nontargeted lipidomics of novel human plasma reference materials: hypertriglyceridemic, diabetic, and African–American, Anal. Bioanal. Chem. 412 (2020) 7373–7380, https://doi.org/10.1007/s00216-020-02910-3.

[44] C. Zhang, L. Shi, F.-S. Wang, Liver injury in COVID-19: management and challenges, Lancet Gastroenterol.

Hepatol. 5 (2020) 428–430, https://doi.org/10.1016/S2468-1253(20)30057-1.

[45] B. Francesco, P. Daniele, F. Domenico, C. Giovanna, T. Giulia, A. Francesco, V. Francesco, D.B. Maria, Reduced lysosomal acid lipase activity: a new marker of liver disease severity across the clinical continuum of non-alcoholic fatty liver disease? World J. Gastroenterol. 25 (2019) 4172–4180, https://doi.org/10.3748/wjg.v25.i30.4172.

[46] K.Y. Hostetler, M. Reasor, P.J. Yazaki, Chloroquine-induced phospholipid fatty liver. Measurement of drug and lipid concentrations in rat liver lysosomes, J. Biol.Chem. 260 (1985) 215–219, https://doi.org/10.1016/S0021-9258(18)89718-6.

Supplementary Material

Method validation calculations

LOD and LOQ were calculated by using the equation S1 and equation S2 respectively.

$$LOD = \frac{3 \times SD_{areaC_{low}} + area_{blank}}{\frac{area_{Clow}}{[C_{low}]}} \qquad (S1)$$

$$LOQ = \frac{10 \times SD_{areaC_{low}} + area_{blank}}{\frac{area_{Clow}}{[C_{low}]}} \qquad (S2)$$

where $SD_{areaC_{low}}$ represents the standard deviation of the lowest concentration with signal to noise ratio greater than $3(C_{low})$, $area_{blank}$ are the peak area of the blank and $\frac{area_{Clow}}{[C_{low}]}$ represents the ratio between peak area and concentration at C_{low} [1].

Carryover is the presence of analytes in the blank samples after injection of high concentration standards [2]. The carryover is calculated by assessing the peak area of analytes in the blank solvents to the peak area of plasma sample analyzed before the blank.

The precision is determined by calculating the RSD (%) three consecutive measurements of samples at L, M and H concentration level. The intraday precision is measured on the same day while interday precision is calculated from the samples measured on 3 different days. The precision can be calculated by equation S3.

$$RSD\ (\%) = \frac{Standard\ deviation}{Mean} \times 100 \qquad (S3)$$

The recovery, ion suppression and matrix effects were calculated in L, M, H levels (prepared in triplicates). The recovery was calculated by comparing the response of samples spiked before and after extraction (equation S4).

$$Recovery(\%) = \frac{Response\ of\ IS\ in\ plasma\ before\ extraction}{Response\ of\ IS\ in\ plasma\ after\ extraction} \times 100 \qquad (S4)$$

The ion suppression and matrix effects are common problems related to mass spectrometry measurements in which response of the analyte may be suppressed or enhanced due to the presence of matrix or other components interfering with the ionization of compounds. The ion suppression and matrix effects were calculated from equation S5 and S6 respectively.

$$Ion\ suppression(\%) = \frac{Response\ of\ IS\ in\ plasma\ after\ extraction}{Response\ of\ IS\ in\ neat\ standards} \times 100 \qquad (S5)$$

$$Matrix\ effect(\%) = \frac{Response\ of\ IS\ in\ plasma\ before\ extraction}{Response\ of\ IS\ in\ water\ before\ extraction} \times 100 \qquad (S6)$$

References

[1] T. van der Laan, A.-C. Dubbelman, K. Duisters, A. Kindt, A.C. Harms, T. Hankemeier, High-Throughput Fractionation Coupled to Mass Spectrometry for Improved Quantitation in Metabolomics, Anal. Chem. 92 (2020) 14330–14338. https://doi.org/10.1021/acs.analchem.0c01375.

[2] D. Wolrab, M. Chocholoušková, R. Jirásko, O. Peterka, M. Holčapek, Validation of lipidomic analysis of human plasma and serum by supercritical fluid chromatography–mass spectrometry and hydrophilic interaction liquid chromatography–mass spectrometry, Anal. Bioanal. Chem. 412 (2020) 2375–2388. https://doi.org/10.1007/s00216-020-02473-3.
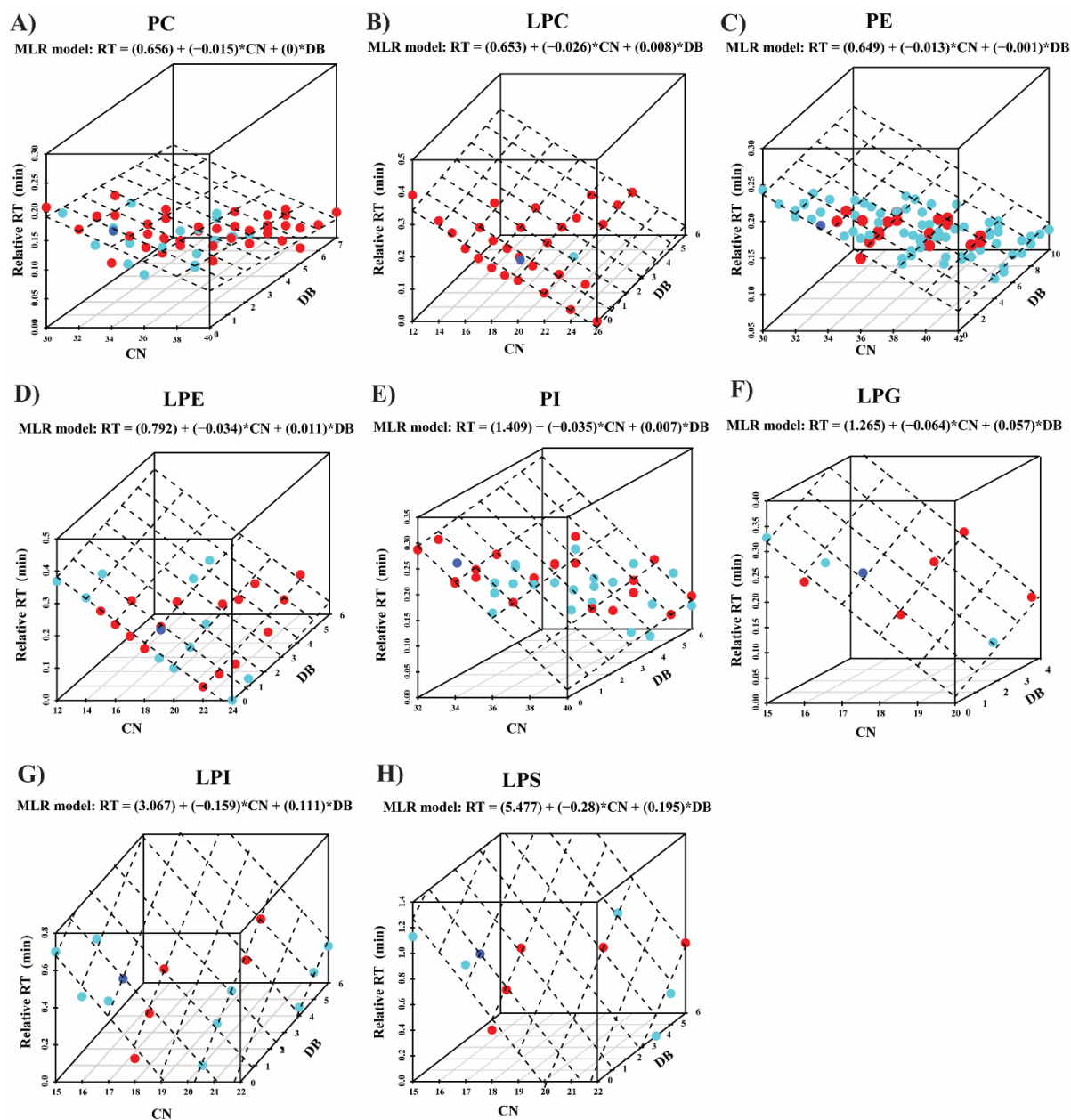
Figure S1. Multivariate linear regression analysis (MLR) of the relative retention time against the acyl chain carbon number (CN) and double bond number (DB) for each lipid features (red dots) within each lipid class depicted as 3D plot. A) PC; B) LPC; C) PE; D) LPE; E) PI; F) LPG; G) LPI; H) LPS. Lipids confirmed by RPLC-HRMS are colored in red, the remaining lipids fitting the retention time model with error rates less than 20% are colored in light blue and internal standards in dark blue.
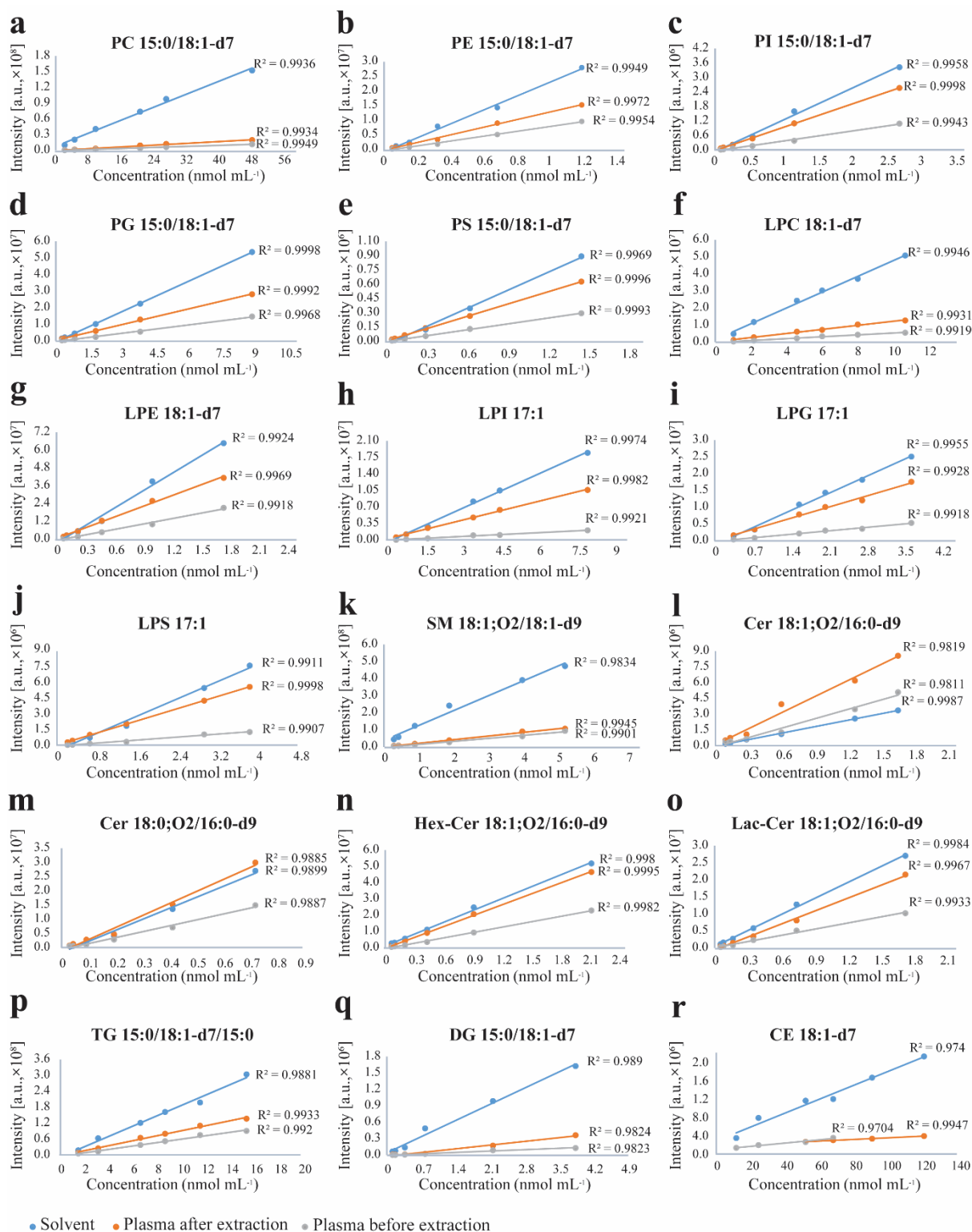
Figure S2. Calibration curves of deuterated or odd chain standards. a. PC 15:0/18:1-d7; b. PE 15:0/18:1-d7; c. PI 15:0/18:1-d7; d. PG 15:0/18:1-d7; e. PS 15:0/18:1-d7; f. LPC 18:1-d7; g. LPE 18:1-d7; h. LPI 17:1; i. LPG 17:1; j. LPS 17:1; k. SM 18:1;O2/18:1-d9; l. Cer 18:1;O2/16:0-d9; m. Cer 18:0;O2/16:0-d9; n. Hex-Cer 18:1;O2/16:0-d9; o. Lac-Cer 18:1;O2/16:0-d9; p. TG 15:0/18:1-d7/15:0; q. DG 15:0/18:1-d7; r. CE 18:1-d7. Calibration standards prepared in the pure solvent (blue), spiked in plasma after extraction (orange), and spiked in plasma before extraction (grey).

Table S1. The spiked concentration of lipid internal standard mixture in the COVID-19 plasma samples.

Internal standard	Source	Concentration (nmol mL^{-1})
TG 15:0/18:1-d7/15:0	SPLASH® LIPIDOMIX® Mass Spec Standard	8.55
CE 18:1-d7	SPLASH® LIPIDOMIX® Mass Spec Standard	65.80
SM 18:1;O2/18:1-d9	SPLASH® LIPIDOMIX® Mass Spec Standard	5.28
PC 15:0/18:1-d7	SPLASH® LIPIDOMIX® Mass Spec Standard	26.31
PE 15:0/18:1-d7	SPLASH® LIPIDOMIX® Mass Spec Standard	0.98
PG 15:0/18:1-d7	SPLASH® LIPIDOMIX® Mass Spec Standard	4.60
PS 15:0/18:1-d7	SPLASH® LIPIDOMIX® Mass Spec Standard	0.66
DG 15:0/18:1-d7	SPLASH® LIPIDOMIX® Mass Spec Standard	1.97
PI 15:0/18:1-d7	SPLASH® LIPIDOMIX® Mass Spec Standard	1.32
LPI 17:1	odd chain single standard	3.39
LPS 17:1	odd chain single standard	3.29
LPG 17:1	odd chain single standard	1.31
LPC 18:1-d7	SPLASH® LIPIDOMIX® Mass Spec Standard	5.92
LPE 18:1-d7	SPLASH® LIPIDOMIX® Mass Spec Standard	1.32
Cer 18:0;O2/16:0-d9	Lipidyzer®	0.96
Hex-Cer 18:1;O2/16:0-d9	Lipidyzer®	0.56
Lac-Cer 18:1;O2/16:0-d9	Lipidyzer®	0.75
Cer 18:1;O2/16:0-d9	Lipidyzer®	0.96

Table S2. Internal standard lipid mixture made of UltimateSPLASH™ ONE and SPLASH® LIPIDOMIX® with the insertion of additional standards for accurate quantitation.

Class	Internal standard	Source	mol wt.	Concentration (nmol mL^{-1})
TG	TG-d5 14:0/13:0/14:0	UltimateSPLASH™ ONE	714.18	10.50
	TG-d5 14:0/15:1/14:0	UltimateSPLASH™ ONE	740.22	20.26
	TG-d5 14:0/17:1/14:0	UltimateSPLASH™ ONE	768.27	29.29
	TG-d5 16:0/15:1/16:0	UltimateSPLASH™ ONE	796.33	37.67
	TG-d5 16:0/17:1/16:0	UltimateSPLASH™ ONE	824.38	45.49
	TG-d5 16:0/19:2/16:0	UltimateSPLASH™ ONE	850.42	35.28
	TG-d5 18:1/17:1/18:1	UltimateSPLASH™ ONE	876.46	25.67
	TG-d5 18:1/19:2/18:1	UltimateSPLASH™ ONE	902.47	16.62
	TG-d5 18:1/21:2/18:1	UltimateSPLASH™ ONE	930.53	8.06
	TG 15:0/18:1-d7/15:0	SPLASH® LIPIDOMIX® Mass Spec Standard	812.35	20.31
CE	CE-d7 14:1	UltimateSPLASH™ ONE	602.04	12.46
	CE-d7 16:1	UltimateSPLASH™ ONE	630.09	23.81
	CE-d7 18:1	UltimateSPLASH™ ONE	658.14	34.19
	CE-d7 20:3	UltimateSPLASH™ ONE	682.16	21.99
	CE-d7 22:4	UltimateSPLASH™ ONE	708.2	10.59
	CE 18:1-d7	SPLASH® LIPIDOMIX® Mass Spec Standard	658.14	159.54
	Cer 18:1;O2-d7/16:1	UltimateSPLASH™ ONE	542.93	41.44
	Cer 18:1;O2-d7/18:1	UltimateSPLASH™ ONE	570.98	26.27
Cer	Cer 18:1;O2-d7/20:1	UltimateSPLASH™ ONE	599.03	12.52
	Cer 18:1;O2-d7/22:1	UltimateSPLASH™ ONE	627.09	23.92
	Cer 18:1;O2-d7/24:1	UltimateSPLASH™ ONE	655.14	34.34

	Cer 18:1;O2/16:0-d9	Lipidyzer®	546.97	3.90
	Cer 18:0;O2/16:0-d9	Lipidyzer®	548.99	1.28
SM	SM-d9 18:1;O2/16:1	UltimateSPLASH™ ONE	710.08	31.69
	SM-d9 18:1;O2/18:1	UltimateSPLASH™ ONE	738.14	20.32
	SM-d9 18:1;O2/20:1	UltimateSPLASH™ ONE	766.19	9.79
	SM-d9 18:1;O2/22:1	UltimateSPLASH™ ONE	794.24	18.89
	SM-d9 18:1;O2/24:1	UltimateSPLASH™ ONE	822.28	27.36
	SM 18:1;O2/18:1-d9	SPLASH® LIPIDOMIX® Mass Spec Standard	738.12	12.19
PC	PC-d5 17:0/14:1	UltimateSPLASH™ ONE	723.04	20.75
	PC-d5 17:0/16:1	UltimateSPLASH™ ONE	751.09	39.94
	PC-d5 17:0/18:1	UltimateSPLASH™ ONE	779.15	57.76
	PC-d5 17:0/20:3	UltimateSPLASH™ ONE	803.17	37.35
	PC-d5 17:0/22:4	UltimateSPLASH™ ONE	829.21	18.09
	PC 15:0/18:1-d7	SPLASH® LIPIDOMIX® Mass Spec Standard	753.09	63.74
PE	PE-d5 17:0/14:1	UltimateSPLASH™ ONE	680.96	11.01
	PE-d5 17:0/16:1	UltimateSPLASH™ ONE	709.01	21.16
	PE-d5 17:0/18:1	UltimateSPLASH™ ONE	737.07	30.53
	PE-d5 17:0/20:3	UltimateSPLASH™ ONE	761.09	19.71
	PE-d5 17:0/22:4	UltimateSPLASH™ ONE	787.13	9.53
	PE 15:0/18:1-d7	SPLASH® LIPIDOMIX® Mass Spec Standard	711.01	2.11
PG	PG-d5 17:0/14:1	UltimateSPLASH™ ONE	733.95	10.22
	PG-d5 17:0/16:1	UltimateSPLASH™ ONE	762.01	19.68
	PG-d5 17:0/18:1	UltimateSPLASH™ ONE	790.06	28.48
	PG-d5 17:0/20:3	UltimateSPLASH™ ONE	814.08	18.43
	PG-d5 17:0/22:4	UltimateSPLASH™ ONE	840.12	8.93
	PG 15:0/18:1-d7	SPLASH® LIPIDOMIX® Mass Spec Standard	764.01	11.78
PS	PS-d5 17:0/14:1	UltimateSPLASH™ ONE	746.95	10.04
	PS-d5 17:0/16:1	UltimateSPLASH™ ONE	775	19.35
	PS-d5 17:0/18:1	UltimateSPLASH™ ONE	803.06	28.02
	PS-d5 17:0/20:3	UltimateSPLASH™ ONE	827.08	18.14
	PS-d5 17:0/22:4	UltimateSPLASH™ ONE	853.12	8.79
	PS 15:0/18:1-d7	SPLASH® LIPIDOMIX® Mass Spec Standard	777	1.93
DG	DG-d5 17:0/14:1	UltimateSPLASH™ ONE	557.91	13.44
	DG-d5 17:0/16:1	UltimateSPLASH™ ONE	585.97	25.60
	DG-d5 17:0/18:1	UltimateSPLASH™ ONE	614.02	36.64
	DG-d5 17:0/20:3	UltimateSPLASH™ ONE	638.04	23.51
	DG-d5 17:0/22:4	UltimateSPLASH™ ONE	664.08	11.29
	DG 15:0/18:1-d7	SPLASH® LIPIDOMIX® Mass Spec Standard	587.97	5.10
PI	PI-d5 17:0/14:1	UltimateSPLASH™ ONE	817.06	9.18
	PI-d5 17:0/16:1	UltimateSPLASH™ ONE	845.12	17.75
	PI-d5 17:0/18:1	UltimateSPLASH™ ONE	873.17	25.77
	PI-d5 17:0/20:3	UltimateSPLASH™ ONE	897.19	16.72
	PI-d5 17:0/22:4	UltimateSPLASH™ ONE	923.23	8.12
	PI 15:0/18:1-d7	SPLASH® LIPIDOMIX® Mass Spec Standard	847.12	3.54
LPI	LPI-d5 15:0	UltimateSPLASH™ ONE	580.66	12.92
	LPI-d5 17:0	UltimateSPLASH™ ONE	608.72	24.64
	LPI-d5 19:0	UltimateSPLASH™ ONE	636.77	11.78
	LPI 17:1	odd chain single standard	601.66	17.38

LPS	LPS-d5 15:0	UltimateSPLASH™ ONE	510.55	14.69
	LPS-d5 17:0	UltimateSPLASH™ ONE	538.61	27.85
	LPS-d5 19:0	UltimateSPLASH™ ONE	566.66	13.24
	LPS 17:1	odd chain single standard	531.55	18.81
LPG	LPG-d5 15:0	UltimateSPLASH™ ONE	497.55	15.07
	LPG-d5 17:0	UltimateSPLASH™ ONE	525.61	28.54
	LPG-d5 19:0	UltimateSPLASH™ ONE	553.66	13.55
	LPG 17:1	odd chain single standard	518.55	9.32
	LPC-d5 15:0	UltimateSPLASH™ ONE	486.63	15.41
LPC	LPC-d5 17:0	UltimateSPLASH™ ONE	514.7	29.14
	LPC-d5 19:0	UltimateSPLASH™ ONE	542.75	13.82
	LPC 18:1-d7	SPLASH® LIPIDOMIX® Mass Spec Standard	528.71	14.19
LPE	LPE-d5 15:0	UltimateSPLASH™ ONE	444.55	16.87
	LPE-d5 17:0	UltimateSPLASH™ ONE	472.61	31.74
	LPE-d5 19:0	UltimateSPLASH™ ONE	500.67	14.98
	LPE 18:1-d7	SPLASH® LIPIDOMIX® Mass Spec Standard	486.63	3.08
HexCer	Hex-Cer 18:1;O2/16:0-d9	Lipidyzer®	709.11	2.82
LacCer	Lac-Cer 18:1;O2/16:0-d9	Lipidyzer®	871.25	2.30

Table S3. Demographics of the COVID-19 patients in the lipidomics study. Values are n (%) or median [full range].

	Patients (n=44)	Samples (n=103)
Age, years	73 [49-87]	71 [49-87]
Male (%)	30 (68%)	65 (63%)
BMI	27 [19-42]	27 [19-42]
Admitted to ward	37 (84%)	78 (76%)
Admitted to ICU	7 (16%)	25 (24%)
Deceased	9 (20%)	
post-admission chloroquine	35 (80%)	

Table S4.
A. LC gradient table showing parameters for HILIC-MS/MS chromatographic separation of lipid classes.

Time (min)	Flow rate (mL/min)	MP-A (%)	MP-B (%)
0.00	0.2	100	0
2.00	0.2	100	0
2.10	1.0	100	0
11.00	1.0	50	50
11.50	1.0	30	70
12.50	1.0	30	70
12.60	0.2	100	0
14.00	0.2	100	0

B. LC gradient table showing parameters for RPLC-HRMS chromatographic separation of lipid classes.

Time (min)	Flow rate (mL/min)	MP-A (%)	MP-B (%)
0.00	0.4	50	50
0.50	0.4	50	50
10.00	0.4	3	97
13.00	0.4	3	97
13.10	0.4	50	50
16.00	0.4	50	50

Table S5. In supplementary excel.

Sheet 1. The first acquisition method including 602 transitions in switch polarity mode. The internal standards are highlighted in yellow.

Sheet 2. The second acquisition method including 598 transitions in switch polarity mode. The internal standards are highlighted in yellow.

Sheet 3. Report confidence scores of lipid features and corresponding lipid identifiers. "✓" represents the corresponding lipid feature fulfill the corresponding criteria; * represents the fatty acyl chain information is confirmed by the IDA.

Sheet 4. Summary of the validation parameters for human K2 EDTA plasma samples using one-IS per class mix.

Sheet 5. Parameters of the multi-internal standards(ISs) per class mix standards used for accurate quantitation.

Sheet 6. Quantitation results for NIST SRM 1950 plasma samples using multi-ISs per class mix.

Sheet 7. Significantly changed metabolites with FDR<0.05 in COVID-19 plasma samples of ICU patients compared to ward patients.

Table S6. Concentrations of the standard mix used in making the calibration curves for validation.

Standard (nmol mL^{-1})	cal-1	cal-2	cal-3	cal-4	cal-5	cal-6	cal-7	cal-8
PC 15:0/18:1-d7	1.48	2.18	4.61	9.77	20.69	27.09	36.12	48.16
PE 15:0/18:1-d7	0.05	0.07	0.15	0.32	0.68	0.90	1.20	1.59
PS 15:0/18:1-d7	0.04	0.07	0.14	0.30	0.63	0.82	1.09	1.46
PG 15:0/18:1-d7	0.27	0.40	0.85	1.81	3.82	5.01	6.68	8.90
PI 15:0/18:1-d7	0.08	0.12	0.26	0.54	1.15	1.51	2.01	2.68
LPC 18:1-d7	0.33	0.48	1.03	2.17	4.61	6.03	8.04	10.72
LPE 18:1-d7	0.07	0.11	0.22	0.47	1.00	1.31	1.75	2.33
CE 18:1-d7	3.71	5.45	11.55	24.46	51.80	67.80	90.41	120.54
DG 15:0/18:1-d7	0.12	0.17	0.37	0.78	1.66	2.17	2.89	3.86
TG 15:0/18:1-d7/15:0	0.47	0.69	1.47	3.11	6.59	8.63	11.51	15.35
SM 18:1;O2/18:1-d9	0.28	0.42	0.88	1.87	3.96	5.18	6.91	9.21
LPG 17:1	0.11	0.17	0.35	0.74	1.57	2.05	2.74	3.65
LPI 17:1	0.24	0.36	0.76	1.60	3.39	4.44	5.92	7.90
LPS 17:1	0.21	0.31	0.65	1.38	2.92	3.83	5.10	6.80
Cer 18:1;O2/16:0-d9	0.09	0.13	0.28	0.60	1.27	1.66	2.21	2.95
Cer 18:0;O2/16:0-d9	0.03	0.04	0.09	0.20	0.41	0.54	0.72	0.96
Hex-Cer 18:1;O2/16:0-d9	0.07	0.10	0.20	0.43	0.92	1.20	1.60	2.13
Lac-Cer 18:1;O2/16:0-d9	0.05	0.08	0.17	0.35	0.75	0.98	1.30	1.73

Table S7. Estimated error for the retention time model with carbon number and unsaturated bond combination.

Class	Retention time range (min)	Adjusted R^2	Error rates
PE	0.24	0.94	7.80%
PC	0.21	0.89	17.92%
PI	0.29	0.93	11.97%
PS	0.23	0.93	23.94%
LPE	0.37	0.95	14.05%
LPC	0.39	0.95	10.53%
LPI	0.7	0.96	13.54%
LPG	0.33	0.93	9.79%
LPS	1.13	0.91	15.20%
SM	0.31	0.97	11.92%

Table S8. Transitions of interference from different ion types within the class and their average relative abundances in positive/negative-ion ESI MS/MS mass spectra of IS.

IS	Elemental formula	Observed ion	MS/MS Q1	MS/MS Q3	Relative abundance [%]*
PC 15:0/18:1-d7	$C_{41}H_{73}D_7NO_8P$	[M-H]⁻	751.6	288.3	n/a
		[M+OAc]⁻	811.6	288.3	100
		[M+Cl]⁻	787.6	288.3	306
		[M-15]⁻	737.6	288.3	28
PE 15:0/18:1-d7	$C_{38}H_{67}D_7NO_8P$	[M-H]⁻	709.6	288.3	100
PS 15:0/18:1-d7	$C_{39}H_{66}D_7NNaO_{10}P$	[M-H]⁻	752.5	288.3	100
PG 15:0/18:1-d7	$C_{39}H_{67}D_7NaO_{10}P$	[M-H]⁻	739.5	288.3	100
PI 15:0/18:1-d7	$C_{42}H_{75}D_7NO_{13}P$	[M-H]⁻	845.6	288.3	100
LPC 18:1-d7	$C_{26}H_{45}D_7NO_7P$	[M-H]⁻	527.4	288.3	n/a
		[M+OAc]⁻	587.4	288.3	100
LPE 18:1-d7	$C_{23}H_{39}D_7NO_7P$	[M-H]⁻	485.3	288.3	100
LPG 17:1	$C_{23}H_{45}O_9P$	[M-H]⁻	495.3	267.4	100
LPI 17:1	$C_{26}H_{49}O_{12}P$	[M-H]⁻	583.4	267.4	100
LPS 17:1	$C_{23}H_{44}NO_9P$	[M-H]⁻	508.3	267.4	100
CE 18:1-d7	$C_{45}H_{71}D_7O_2$	[M+H]⁺	658.7	369.4	3.4
		[M+Na]⁺	680.6	369.4	n/a
		[M+NH₄]⁺	675.7	369.4	100
DG 15:0/18:1-d7	$C_{36}H_{61}D_7O_5$	[M+H]⁺	588.6	346.3	22.84
		[M+NH₄]⁺	605.6	346.3	100
		[M+Na]⁺	610.5	346.3	n/a
		[M+K]⁺	626.5	346.3	n/a
TG 15:0/18:1-d7/15:0	$C_{51}H_{89}D_7O_6$	[M+H]⁺	812.8	570.5	0.32
		[M+NH₄]⁺	829.8	570.5	100
SM 18:1;O2/18:1-d9	$C_{41}H_{72}D_9N_2O_6P$	[M+H]⁺	738.6	184.1	100
		[M+Na]⁺	760.6	184.1	n/a
		[M+K]⁺	776.6	184.1	n/a
		[M+NH₄]⁺	755.7	184.1	0.05
		[M+H-H₂O]⁺	720.6	184.1	0.06
Cer 18:0;O2/16:0-d9	$C_{34}H_{60}D_9NO_3$	[M+H]⁺	549.6	266.4	100
		[M+Na]⁺	571.6	266.4	n/a
		[M+H-H₂O]⁺	531.6	266.4	2647.6
		[M+H-2H₂O]⁺	513.6	266.4	323.6
Cer 18:1;O2/16:0-d9	$C_{34}H_{58}D_9NO_4$	[M+H]⁺	547.6	264.4	100
		[M+Na]⁺	569.6	264.4	n/a

		[M+H-H₂O]⁺	529.6	264.4	3583.3
		[M+H-2H₂O]⁺	511.6	264.4	435.82
Hex-Cer 18:1;O2/16:0-d9	C₄₀H₆₈D₉NO₈	[M+H]⁺	709.6	264.4	100
		[M+Na]⁺	731.6	264.4	n/a
		[M+K]⁺	747.6	264.4	n/a
		[M+H-H₂O]⁺	691.6	264.4	414.35
		[M+H-Hex]⁺	529.6	264.4	143.61
Lac-Cer 18:1;O2/16:0-d9	C₄₆H₇₈D₉NO₁₃	[M+H]⁺	871.7	264.4	100
		[M+Na]⁺	893.7	264.4	n/a
		[M+K]⁺	909.6	264.4	n/a
		[M+H-H₂O]⁺	853.7	264.4	112.73

*100% represents the main peak used for the method construction. Percentage was calculated by the intensity of interference of other ion type or isotope divided by the main ion form for method construction; n/a means below the LOD.

Table S9. The sn-1/sn-2 ratios of fatty acyl tails of five phospholipid classes at different collision energies (30 eV, 40 eV, 50 eV and 60 eV) in ESI (−) mode.

		sn-1/sn-2, (Collision Energy, eV)			
Lipid class	ESI mode	30	40	50	60
PC 15:0/18:1-d7	(-)	0.36	0.37	0.36	0.35
PC-d5 17:0/14:1	(-)	0.41	0.39	0.50	0.69
PC-d5 17:0/16:1	(-)	0.51	0.46	0.49	0.57
PC-d5 17:0/18:1	(-)	0.96	0.82	0.80	0.80
PC-d5 17:0/20:3	(-)	0.79	0.78	0.71	0.84
PC-d5 17:0/22:4	(-)	0.87	0.88	0.85	1.24
PE 15:0/18:1-d7	(-)	0.39	0.43	0.46	0.37
PE-d5 17:0/14:1	(-)	0.35	0.38	0.50	0.67
PE-d5 17:0/16:1	(-)	0.36	0.37	0.42	0.53
PE-d5 17:0/18:1	(-)	0.39	0.40	0.43	0.46
PE-d5 17:0/20:3	(-)	0.44	0.44	0.54	0.75
PE-d5 17:0/22:4	(-)	0.54	0.54	0.75	1.40
PI 15:0/18:1-d7	(-)	2.53	2.84	1.93	1.42
PI-d5 17:0/14:1	(-)	1.44	1.17	1.21	1.27
PI-d5 17:0/16:1	(-)	1.41	1.18	1.11	1.10
PI-d5 17:0/18:1	(-)	1.26	1.17	1.06	1.04
PI-d5 17:0/20:3	(-)	1.27	1.04	1.08	1.22
PI-d5 17:0/22:4	(-)	1.49	1.10	1.15	1.52
PS 15:0/18:1-d7	(-)	1.75	2.20	2.82	2.78
PS-d5 17:0/14:1	(-)	1.97	2.19	2.80	3.60
PS-d5 17:0/16:1	(-)	2.10	2.20	2.54	2.94
PS-d5 17:0/18:1	(-)	1.99	2.04	2.39	2.67
PS-d5 17:0/20:3	(-)	1.95	2.04	2.91	3.54
PS-d5 17:0/22:4	(-)	2.50	2.52	3.62	5.36
PG 15:0/18:1-d7	(-)	0.44	0.43	0.39	0.37
PG-d5 17:0/14:1	(-)	0.46	0.45	0.52	0.66
PG-d5 17:0/16:1	(-)	0.49	0.43	0.43	0.51
PG-d5 17:0/18:1	(-)	0.50	0.46	0.44	0.46
PG-d5 17:0/20:3	(-)	0.50	0.49	0.51	0.66
PG-d5 17:0/22:4	(-)	0.48	0.60	0.69	1.11

Chapter 3

A comparison between different human hepatocyte models reveals profound differences in net glucose production, lipid composition and metabolism *in vitro*

Abstract

Hepatocytes are responsible for maintaining a stable blood glucose concentration during periods of nutrient scarcity. The breakdown of glycogen and *de novo* synthesis of glucose are crucial metabolic pathways deeply interlinked with lipid metabolism. Alterations in these pathways are often associated with metabolic diseases with serious clinical implications. Studying energy metabolism in human cells is challenging. Primary hepatocytes are still considered the golden standard for *in vitro* studies and have been instrumental in elucidating key aspects of energy metabolism found *in vivo*. As a result of several limitations posed by using primary cells, a multitude of alternative hepatocyte cellular models emerged as potential substitutes. Yet, there remains a lack of clarity regarding the precise applications for which these models accurately reflect the metabolic competence of primary hepatocytes. In this study, we compared primary hepatocytes, stem cell-derived hepatocytes, adult donor-derived liver organoids, immortalized upcyte-hepatocytes and the hepatoma cell lines HepG2 in their response to a glucose production challenge. We observed the highest net glucose production in primary hepatocytes, followed by organoids, stem-cell derived hepatocytes, upcyte-hepatocytes and HepG2 cells. Gluconeogenic gene induction was observed in all tested models, as indicated by an increase in *G6PC* and *PCK1* expression. Lipidomics revealed considerable differences across the models, with organoids showing the closest similarity to primary hepatocytes in the common lipidome, comprising 347 lipid species across 17 classes. Changes in lipid profiles as a result of the glucose production induction suggest that only primary hepatocytes and organoids activate the fatty acid beta-oxidation pathway, resulting in decreased triglyceride content.

Keywords

1. Introduction

Maintaining a stable blood glucose concentration through periods of nutrient availability or fasting is an essential physiological equilibrium [1]. Much of this balance is orchestrated by hepatocytes in the liver, which control several metabolic pathways to regulate glucose blood levels, such as glycogenesis, glycogenolysis, glycolysis, and gluconeogenesis [2]. During periods when a dietary glucose supply is not available, hepatocytes can secrete large quantities of glucose into the blood. Glucose is produced and released either via breakdown of stored glycogen (glycogenolysis and glycophagy) [3,4] or *de novo* synthesis using carbon substrates such as pyruvate, lactate and amino acids (gluconeogenesis) [5].

Lipid metabolism plays a crucial role in maintaining energy homeostasis and is deeply interlinked with glucose metabolism [6]. Gluconeogenesis is an energy-demanding process, which is primarily derived from the beta-oxidation of fatty acids (FAs). These FAs are stored in hepatocytes as triglycerides (TGs) or delivered by the adipose tissue via the blood circulation during periods of starvation [7]. The breakdown of FAs produces molecules such as acetyl-CoA and NADH, which can enter the Krebs cycle and the electron transport chain, respectively, to generate ATP that is necessary for the production of glucose [7]. While the link between fatty acid beta-oxidation and gluconeogenesis is widely accepted and characterized, the metabolic connection with other lipids, such as phospholipids and sphingolipids is complex and partially unknown.

Unsurprisingly, impaired or dysregulated glucose production and lipid metabolism, often associated with pathologies such as diabetes, obesity and inborn errors of metabolism, can lead to severe and life-threatening medical conditions [8–15]. Studying the process of glucose and lipid metabolism during periods of nutrient deprivation is crucial to understand how metabolic disorders lead to potentially life-threatening scenarios. Consequently, *in vitro* glucose production assays, in which hepatocytes are stimulated to secrete glucose under controlled conditions are central biological readouts that hold immense importance in the field. These assays rely on metabolically competent human hepatocyte models, experimental conditions that simulate the physiological nutrient availability oscillations found *in vivo* and robust assay to quantify molecular targets.

Primary human hepatocytes (PHH) are still considered as the gold standard in metabolic disease research but present several limitations, such as their limited availability, donor-to-donor variation, rapid de-differentiation and high costs. Hence, researchers have been exploring the

possibility to use alternative hepatocyte sources. Studies have reported comparison of PHH with iPSC-derived hepatocytes (iPSC-Hep) and HepG2 [16]. Glucose production has been measured for PHH, iPSC-derived hepatocytes and hepatoma cell lines and typically involve a prolonged period of starvation (3-24 h) in which the cells are cultured in absence (or reduced levels) of glucose but in presence of gluconeogenic substrates, such as glycerol, lactate or pyruvate [16–20].

Recently, expandable primary hepatocytes (Upcyte-Hep) have been generated by inducing low expression of the human papilloma virus [21,22] but their competence for energy metabolism studies remains doubtful [23]. Furthermore, hepatic organoids (Orgs) emerged as an exciting possibility to generate patient-derived expandable hepatocytes and recent progress started to determine their exact application landscape to study liver metabolism and disease [24,25]. Yet, more research is needed in order to identify specific applications of alternatives to primary hepatocytes in metabolism studies. Direct comparisons are needed for specific assays in order to evaluate the biological response of non-primary hepatocytes exposed to a metabolic challenge.

With this study, we aimed to characterize and compare the metabolic capabilities of various *in vitro* models of human hepatocytes such as iPSC-Hep, HepG2, Upcyte-Hep and organoids with PHH. Specifically, we challenged the models with a glucose production assay by measuring secreted glucose levels and induction of gluconeogenesis-related genes. Finally, we used a highly sensitive targeted lipidomics method to study the lipid profile of these hepatocyte models to monitor the modulation of intracellular lipid composition as a result of the glucose production challenge. This study aimed to further characterize and evaluate alternatives to primary hepatocyte models for energy metabolism studies.

2. Materials and methods

2.1 Cell culture
HepG2

HepG2 cells (Passage 3) were kindly provided by University of Groningen (order number: ATCC-HB-8065, ATCC, Manasses, Virginia, USA) and plated at 50000 cell/well in a 24 well plate. Cells were grown for 5 days in DMEM (Gibco, 11965092) + 10% Fetal Bovine Serum (FBS, Gibco, 16140071) + 1% Penicillin / Streptomycin with a full medium change every 2-3 days.

iPSC-Hep

iPSC-derived Hepatocytes (iCell Hepatocytes 2.0, Fujifilm) were cultured for 5 days in DMEM F12 (Thermo, 11039-021) supplemented with B27 (Thermo, 17504-044), 100 nM Dexamethasone (Sigma, D4902) and Gentamicin (Thermo, 15750-060). Then, cells were gently dissociated with TrypLE™ Express Enzyme (Thermo, 12604021) and seeded at 100000 cells/well in a collagen-I coated 24 well plates. Cells were grown for 5 days with a full medium change every 2-3 days.

PHH

Primary human hepatocytes (BIOIVT, M00995, Lot: MLS) were seeded at 700000 cells/well in a collagen-I coated 24 well plate after thawing in INVITROGRO CP Medium (BIOIVT, Z99029). Cells were kept in culture for 5 days in INVITROGRO HI Medium (BIOIVT, Z99009) with a medium change every 2-3 days.

Upcyte-Hep

Human upcyte® Hepatocytes (BIOIVT, CHE002, Lot 151.03.20180822.1) were thawed in Thawing Medium (Upcyte technologies, MHE001) seeded at a density of 10000 cells/cm^2 in collagen-type I-coated T75 flasks (Thermo, 156499) and cultured in High-Performance Medium (HPM, Upcyte technologies, MHE003). Cells were then dissociated with TrypLE™ Express Enzyme (Thermo, 12604021) and cryopreserved. Cells were then subsequently thawed and plated at 100000 cells/well in a collagen-I coated 24 well plate and kept in culture for 5 days in High-Performance Medium (HPM, Upcyte technologies, MHE003) with a medium change every 2-3 days.

Organoids

Primary adult stem cell-derived liver organoids are expanding adult bile duct-derived bipotent progenitor cells that can be differentiated into functional hepatocytes. The organoid line (M17-00060) was obtained from the Hubrecht Organoid Technology and was isolated from a healthy 43-year old male. Prior differentiation, organoids were maintained in HepatiCult^{TM} Growth Medium (STEMCELL Technologies, 100-0385) in droplets of 70% Matrigel GFR (7.2 mg/mL, Corning, 356237) and 30% HepatiCult Organoid Growth Medium (OGM, STEMCELL Technologies, 100-0385) with 50 µg/mL Primocin® (Invitrogen, ANT-PM-2) in 24-well suspension plates (Greiner Bio-One, 662102) in a humidified incubator at 37 °C, 5% CO_2 with an additional 500 µL per well of HepatiCult OGM [26]. Medium was refreshed every 2-3 days. Organoids were passaged by mechanical dissociation every 7-10 days. For passaging, the

Matrigel GFR droplets were broken using media from two wells and transferred to a 15 mL tube with a P1000 tip pre-coated with DBSA consisting of Dulbecco's Modified Eagle medium +4.5 g/L D-Glucose, L-Glutamine (Thermo, 31966047) with additional 1:100 v/v of PEN/STREP (Thermo, 15140122) and 1:100 v/v of 10% BSA (A2153, Sigma-Aldrich) in DPBS (Thermo, 14190144). A maximum of 12 wells were pooled in one 15 mL tube followed by filling it up to 12 mL with ice-cold DBSA and pipetting up and down 10 times using a 10 mL plastic pipette. The organoids were centrifuged at 450 rcf for 5 min at 8 °C (Eppendorf® Centrifuge 5910 R) and the supernatant was aspirated. The pellets were resuspended in 1 mL of AdDF+++, prepared by adding 1:100 v/v of GlutaMAX™ Supplement (Thermo, 35050061), 1:100 v/v of PEN/STREP (Thermo, 15140122), and 1:100 1M HEPES (15630080, Thermo Fisher) to Advanced DMEM/F-12 (12634028, Thermo Fisher). Organoids were sheared mechanically by pipetting up and down 10-20 times depending on donor and drop density with a P10 pipette tip fitted on a P1000 tip. AdDF+++ was added up to 12 mL and the tube was centrifuged at 450 rcf for 5 min at 8 °C. The supernatant was aspirated, and the pellet placed on ice before it was resuspended in OGM followed by addition of Matrigel GFR in a 30%-70% v/v ratio respectively, with a total volume of 50 µL per well to be seeded. Organoids were seeded in 50 µL droplets by pipetting them in the center of 24-well suspension plates that were pre-warmed at least 24 h in the incubator. After 5 min at room temperature (RT) the 24-well plates were placed upside down in the incubator for 1 h to solidify the droplets. Organoids used for this study were at passage 7.

Prior differentiation, organoids were cultured for 7 days in HepatiCult™ Growth Medium which was then replaced for additional 7 days with HepatiCult™ Differentiation Medium (STEMCELL Technologies, 100-0383). Full medium change was performed every 2-3 days. The research described here has been performed according to applicable Dutch national ethics regulations. The use of liver organoid line was approved by the medical ethical committee of the UMC Utrecht, the Netherlands in compliance with guidelines from Ethical Committee and European Union legislation.

2.2 Glucose production assay

2D cell cultures

To initiate the glucose production assay, the cell culture medium was replaced by pre-starvation medium comprised of DMEM + 2 mg/mL D-glucose (Sigma, G7021), 1 mM Sodium Pyruvate (Thermo, 11360070), 100 nM Dexamethasone (Sigma, D4902) and 1% Penicillin-Streptomycin (Sigma, P4333). Cells were cultured in pre-starvation medium for 2 h. Cells were

then washed 3 times with 1 mL glucose-free DMEM (Thermo, A1443001) to remove any residual glucose. Cells were then cultured for 12 h in either Glucose Production (GP) medium comprised of glucose-free DMEM supplemented with 1 mM Sodium Pyruvate, 20 mM Sodium Lactate (Sigma, L7022), GlutaMAX (Thermo, A1286001), 100 nM Dexamethasone (Sigma, D4902), 10 µM Forskolin (Tocris, 66575-29-9v), and 1% Penicillin-Streptomycin or, Fed medium comprised of DMEM supplemented with 2 mg/mL glucose, 1 mM Sodium Pyruvate, GlutaMAX, ITS (Thermo, 41400045), 100 nM Dexamethasone and and 1% Penicillin-Streptomycin.

3D cell culture

Organoids were extracted from Matrigel domes by mechanical dissociation in combination with cold Advanced DMEM/F-12 (Thermo, 12634028). Organoids were then collected in a 15 mL tube and more cold Advanced DMEM/F-12 was added for a final volume of 15 mL. The organoids were then centrifuged for 5 min at 450 g and 8 ℃. Matrigel layer was aspirated without disrupting the organoid pellet. 15 mL cold Advanced DMEM/F-12 was added to the tube, centrifuged and aspirated for a total of 2 washes. Matrigel-free organoids were then resuspended in 15 mL pre-starvation medium and incubated at 37 ℃ for 2 h. After that, organoids were centrifuged, and pre-starvation medium was removed and replaced with 15 mL glucose-free DMEM. Organoids were washed with 15 mL glucose-free DMEM for 3 times and were then distributed across multiple 1.5 mL tubes in 1 mL glucose-free DMEM. Tubes were centrifuged at 300 g for 5 min at 8 ℃. Organoids were then resuspended in 200 µL of Fed (comprised of DMEM supplemented with 2 mg/mL glucose, 1 mM Sodium Pyruvate, GlutaMAX, ITS, 100 nM Dexamethasone and and 1% Penicillin-Streptomycin) or GP medium (comprised of glucose-free DMEM supplemented with 1 mM Sodium Pyruvate, 20 mM Sodium Lactate , GlutaMAX, 100 nM Dexamethasone, 10 µM Forskolin and 1% Penicillin-Streptomycin) for 12 h.

Glucose Measurement

To measure extracellular glucose, 250 µL of conditioned medium was collected in a 96 well-plate. 31.25 µL of 0.6 N HCl was added to inactivate endogenous enzyme activity and degrade NAD(P)H. After 5 min, 31.25 µL of 121 mg/mL Trizma base (Sigma, T1503) was added to neutralize the solution. To the remaining cells, 0.6 N HCl was added to extract intracellular glucose and was neutralized after 20 min using 121 mg/mL Trizma Base. Glucose was then measured by using Glucose-Glo (Promega, J6021) following manufacturer's instructions.

2.3 Protein quantification

Cells cultured in either GP medium or Fed medium for 12 h were lysed using 200 µL RIPA buffer (Thermo, 89900) for 10 min at room temperature. Total protein was then quantified using DC™ Protein Assay (BIO-RAD, 5000112).

2.4 qPCR

Total RNA was isolated from hepatocytes using RNeasy Mini Kit (Qiagen) and reverse transcribed using M-MLV Reverse Transcriptase (Invitrogen, 28025013) at 37 °C for 50 min in a - LightCycler® 96 Instrument (Roche, 05815916001). qPCR was performed using SYBR Green according to manufacturer's protocol. The primers used for the analysis were following: *G6PC* forward 5'-GCTGCTCATTTTCCTCATCAA-3', reverse 5'-TTCTGTAACAGCAATGCCTGA-3'; *PCK1* forward 5'-GGTCAGTGAGAGCCAACCAG-3', reverse 5'-AGATGGAGGAAGAGGGCATT-3'; *FBP1* forward 5'-GAGGCGTACGCTAAGGACTTT-3', reverse 5'-GAGGCGTACGCTAAGGACTTT-3'; *ACTB* forward 5'-CTCTTCCAGCCTTCCTTCCT-3', reverse 5'-AGCACTGTGTTGGCGTACAG3'.

2.5 Lipidomics analysis

Sample preparation

Cells cultured in either GP medium or Fed medium for 12 h were washed once with 1 mL cold PBS. Then, 250 µL of cold MeOH:Water 8:2 (v/v) was added. Adherent cells were scraped from the wells using a pipet tip, organoids were resuspended and disrupted and 100 µL was transferred to a tube. Samples were immediately frozen at -80 ºC.

Liquid chromatography-mass spectrometry (LC-MS) reagents and materials

The LC-MS grade acetonitrile and methanol and HPLC grade chloroform were purchased from Biosolve (Biosolve Chimie SARL), Dieuze, France. The ammonium acetate was of LC-MS grade (LiChropur™) and was purchased from Sigma-Aldrich (St.Louis, MO, USA). The Milli-Q® reference water purification system (Merck KGaA, Darmstadt, Germany) was used for purifying the water. The internal standard for lipidomics study was a mixture of splash lipidomix mix (330707-1EA); lysophosphatidylserine, LPS (17:1); lysophosphatidylinositol, LPI (17:1); lysophosphatidylglycerol, LPG (17:1) purchased from Avanti polar lipids. This internal standard mix also contained deuterated hexosyl ceramides, Hex-Cer 18:1;O2/16:0-d9 *(part no.-5040398)*; deuterated lactosyl ceramides, Lac-Cer 18:1;O2/16:0-d9 *(part no.-5040399)*; deuterated dihydroceramides, Cer 18:0;O2/16:0-d9 *(part no.-5040397)*; deuterated

ceramides, Cer 18:1;O2/16:0-d9 *(part no.-5040167)* purchased from AB Sciex. The splash lipidomics mix contains deuterated internal standards mixture of phosphatidylcholine (PC); phosphatidylethanolamine (PE); phosphatidylserine (PS); phosphatidylglycerol (PG); phosphatidylinositol (PI); lysophosphatidylcholine (LPC); lysophosphatidylethanolamine (LPE); cholesteryl esters (CE); diglycerides (DG); triglycerides (TG); sphingomyelin (SM). The internal standard mixture was prepared in acetonitrile:methanol (3:7, v/v).

Lipid extraction

The lipids were extracted using Matyash method [27] with slight modifications. The tubes containing cells have 100 µL of methanol:water (80:20, v/v) were used for lipid extraction. 34 µL of the internal standard mix was added to each tube followed by the addition of 115 µL of methanol and 650 µL methyl *tert*-butyl ether (MTBE) and vortexed for 5 min. This mixture was then incubated at room temperature on an orbital shaker for 1 h. After the addition of water (143 µL), making the final ratio of MTBE:MeOH:Water to 10:3:2.5, v/v/v, the mixture was again incubated at room temperature for 10 min and centrifuged at 15800 rcf for 10 min at 4 °C. 550 µL of organic (upper) layer was collected and dried in a vacuum concentrator. Samples were then reconstituted with 150 µL of acetonitrile:methanol (3:7), vortexed and centrifuged for 10 min. The supernatant was taken and injected in LC-MS for analysis.

Lipid profiling through LC-MS analysis

Hydrophilic interaction chromatography with electrospray ionization-tandem mass spectrometry (HILIC-MS/MS) experiments were performed on an Exion LC AD (Sciex, Concord, ON,Canada) according to our previously published study [28]. The LC was coupled to QTRAP 6500+ mass spectrometer with a Turbo V source (Sciex, Concord, ON,Canada). Separations was performed on Luna amino column (100 mm × 2 mm, 3 µm, Phenomenex). The organic phase (MP-A) contains 1mM ammonium acetate in choroform: acetonitrile (1:9) and aqueous phase (MP-B) contains 1mM ammonium acetate in acetonitrile: water (1:1). The injection volume was kept 5 µL for all the classes except for TG and PE where it was kept at 1 µL. The temperature of the column was 35 °C. The rinsing solvent for the injector needle was isopropanol:water:dichloromethane (94:5:1, v/v/v). The mass spectrometer was operated at ionspray voltage of 5500 V and -4500 V for positive and negative mode respectively. The curtain gas was 20 psi, collision gas was kept at medium. The source temperature was 400 °C, GS1 and GS2 were 30 and 35 psi respectively. The data acquisition was done in scheduled MRM (sMRM) mode. The details about the sMRM window, ion transitions, retention times,

collision energy and declustering potential can be found in previous publication [28] and is summarized in **Table S2, sheet 1**. The total scan time was set at 0.5 sec. One internal standard per class has been used for the quantitation of lipid species. **Table S1** shows the concentration of internal standards spiked in the samples. Based on these concentrations and response of internal standards, the concentration of endogenous lipid species was calculated.

2.6 Data/Statistical analysis

Statistical analysis of glucose production rates was performed using GraphPad Prism 6.01. Significant differences at $p<0.05$ were determined using One-Way Anova, Dunnett's multiple comparison test. 'n' represents different well replicates. Gene expression analysis was performed using LightCycler®96. For lipidomics data, Sciex OS (v2.1.6) was used for peak integration and all statistical analyses were performed in R (version 4.2.0), and the packages such as ggplots, ggpubr, ComplexHeatmap were used to plot the graphs. The statistical significance was calculated using Kruskal-Wallis test followed by Dunnett's test.

3. Results

3.1 Hepatocyte glucose production

To compare the net glucose production of the hepatocyte models, we pre-cultured PHH, iPSC-Hep, Upcyte-Hep, HepG2 and organoids between 5 and 10 days under normal growth conditions. Then, medium was replaced with serum-free DMEM supplemented with 2 mg/mL glucose for 2 h prior to glucose production challenge as serum starvation has been shown to stimulate the induction of gluconeogenic genes [29]. The cells were then incubated with glucose production (GP) medium consisting of glucose-free and serum-free DMEM medium containing 20 mM lactate, 1 mM pyruvate, glutamine, 100 nM Dexamethasone and 10 µM Forskolin for 12 h (**Figure 1A**). Glucose levels were then measured both extracellularly and intracellularly. While detectable levels of extracellular glucose were measured for all hepatocyte models, PHH showed greater net glucose production and secretion (**Figure 1B**) followed by organoids, iPSC-Hep, Upcyte-Hep and HepG2. Similarly, intracellular levels were highest in PHH, followed by

organoids and iPSC-Hep while glucose concentration was below the detectable limit for Upcyte-Hep and HepG2 (**Figure 1B**).
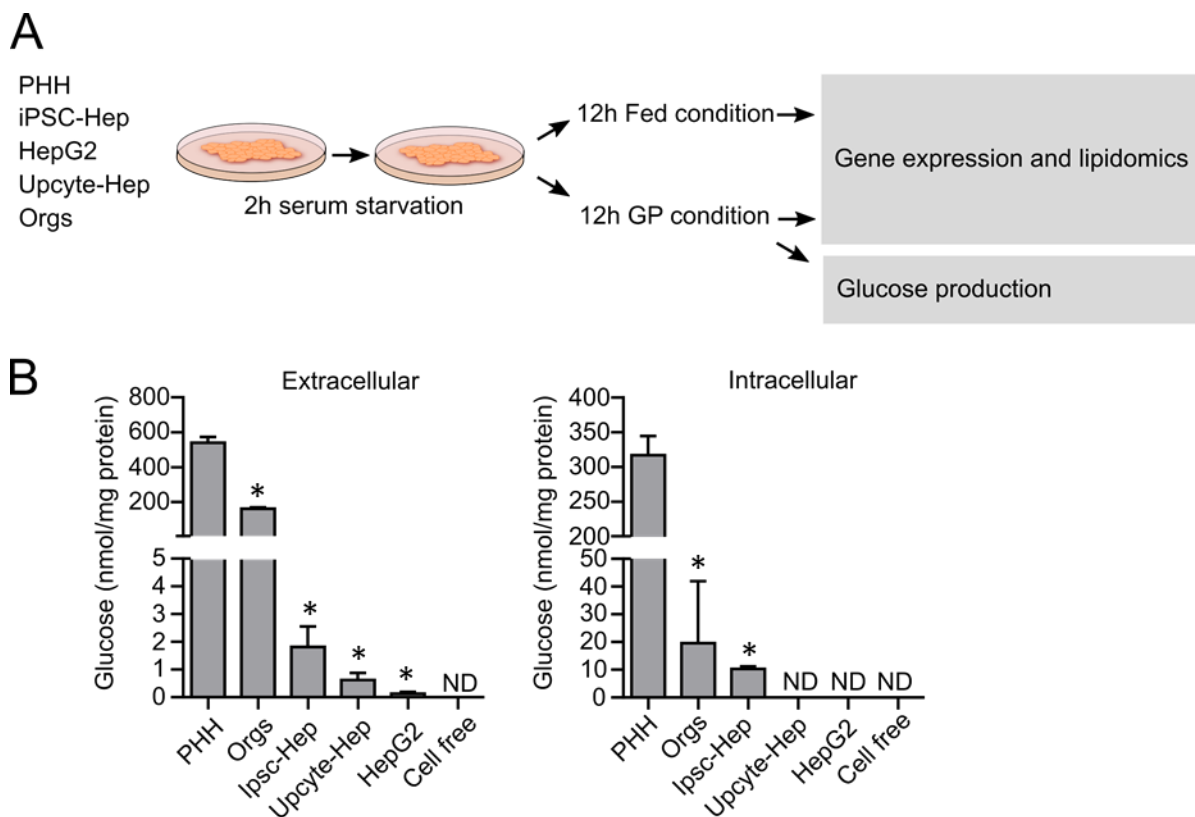

Figure 1. Experimental procedure and glucose production: (A) Scheme of the experimental procedure.; (B) Glucose production normalized to protein content after 12 h in GP medium. (n = 3-6; mean ± SD; *$p<0.05$, PHH Versus organoids (Orgs), iPSC-Hep, Upcyte-Hep, HepG2). n represents different well replicates.

3.2 Gluconeogenic genes induction

Gluconeogenesis is one of the main metabolic pathways for generation of glucose and becomes the dominant source of endogenously produced glucose after glycogen storages are depleted [7]. Gluconeogenesis is highly regulated on multiple levels including gene transcription [5]. Glucose-6-phosphatase (G6PC) hydrolyses the terminal step of gluconeogenesis and glycogenolysis. Phosphoenolpyruvate carboxykinase 1 (PCK1) is the rate-limiting enzyme of gluconeogenesis [30]. Fructose 1,6-biphosphatase (FBP1) converts fructose-1,6-biphosphate to fructose-6-phosphate in another rate-limiting reaction [5]. We assessed the gene expression levels of these key enzymes by qPCR for each hepatocyte model after 12 h of either GP medium or Fed medium. Overall, expression and induction of *G6PC* and *PCK1* were observed in all hepatocyte models (**Figure 2A**). *FBP1* appears to be the least regulated at a gene expression level and has notably low expresssion in HepG2 cells compared to the other gluconeogenic genes. PHH showed approximately 100-fold induction of *G6PC* and *PCK1* when cultured in

GP medium compared to Fed medium (**Figure 2B**). iPSC-Hep and Upcyte-Hep appear to regulate their gene expression levels in a comparable way to PHH while organoids showed overall reduced induction.
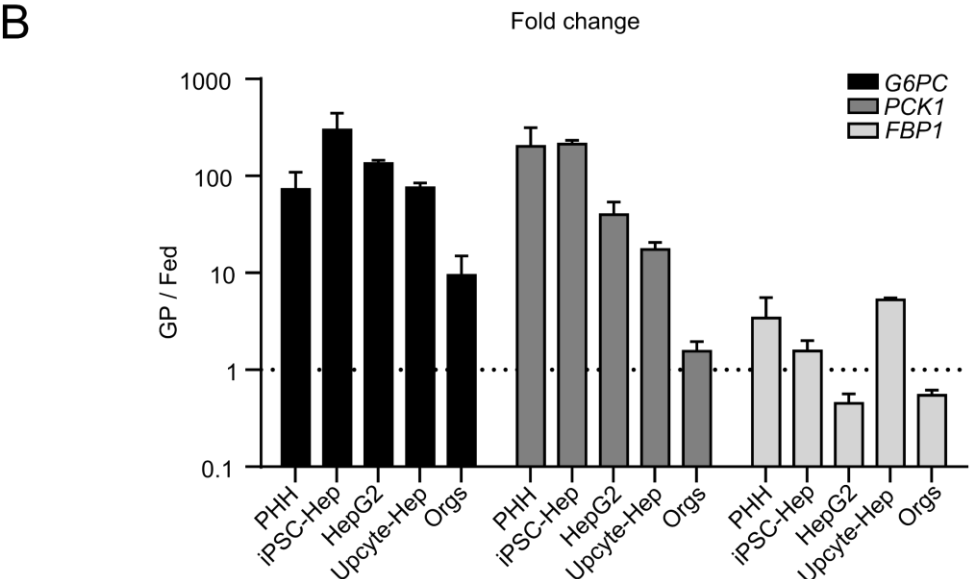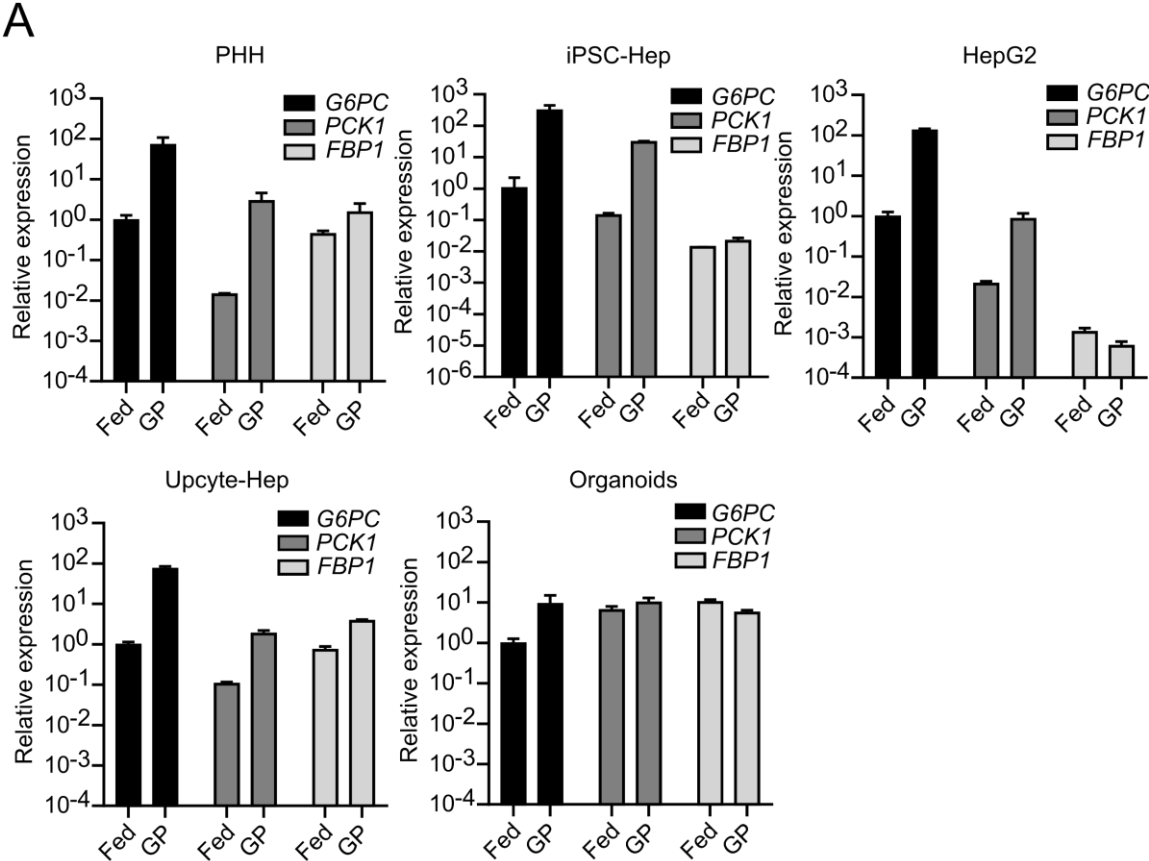

Figure 2. Gluconeogenesis gene induction as a result of glucose production challenge: (A) Expression of gluconeogenic genes in PHH, iPSC-Hep, HepG2 cells, Upcyte-Hep and organoids (Orgs) after 12 h incubation in GP or Fed medium. Genes of interest were normalized to the houskeeping gene ACTB and expression levels are

shown as relative to G6PC in Fed condition (n=3).; (B) Fold change of gene expression relative to the Fed condition for all hepatocyte models (n=3). n represents different well replicates.

3.3 Lipid profile of hepatocytes

Lipidomics analysis has been extensively used in metabolic studies of hepatocytes to profile entire cells or isolated lipid droplets [31–33]. We have used a HILIC-MS/MS method targeting 1200 lipid features for lipidomics analysis, where each feature represents one or more lipid species with certain chemical (sub)structures (i.e can include possible isomers). **Table 1** shows the total number of detected lipid species across 19 lipid (sub)classes in the hepatocyte models cultured with Fed or GP medium. These classes include phospholipids (LPE, PC, LPC, PI, PS, LPG, LPI, LPS, PG, PE, PE with alkyl ether (PE-O) and alkenyl ether substituents (PE-P)), sphingolipids (SM, HexCer, LacCer, Cer), glycerolipids (DG, TG) and sterol lipids (CE). We were able to detect 691 lipid species in PHHs, 624 in organoids, 433 in iPSC-Hep, 565 in Upcyte-Hep and 645 in HepG2 cells.

Table 1. The number of detected lipid species across 19 lipid (sub)classes in different hepatocyte models measured using HILIC-MS/MS.

Lipid class	HepG2	Upcyte-Hep	iPSC-Hep	PHH	Organoids	Common
LPE	16	18	11	24	24	8
PC	70	56	59	72	57	50
LPC	4	4	4	11	18	4
PI	35	26	21	59	48	20
PS	30	22	9	32	27	9
LPG	3	3	2	9	9	2
LPI	3	5	1	10	12	1
LPS	2	3	1	10	14	1
PG	47	43	39	55	42	33
SM	56	53	39	68	55	37
HexCer	9	10	3	18	14	3
LacCer	12	12	2	9	3	2
Cer	9	9	9	18	16	7
TG	253	207	174	169	171	123
PE	74	57	39	87	68	34
PE-O	14	18	8	20	22	6
PE-P	8	19	12	14	20	7
DG	0	0	0	4	2	0
CE	0	0	0	2	2	0
Total	*645*	*565*	*433*	*691*	*624*	*347*

First, we compared the total lipidome found in each hepatocyte model in Fed medium and divided the lipid species according to their chain length and amount of double bonds in

glycerolipids and phospholipids. **Figure 3A** shows abundance of lipid species containing chain lengths of 16, 18, 20 and 22 carbon atoms in glycerolipids and phospholipids (as these four were the most abundant fatty acid chains). In glycerolipids, PHH cells exhibit the greatest prevalence of FA chain lengths comprising 18 carbon atoms, followed by FA chain lengths containing 16 carbon atoms. For iPSC-Hep, the dominant FA chain length is 16 carbon atoms, followed by 18 carbon atoms. HepG2, Upcyte-Hep and organoids have comparable levels of abundance for 16 and 18 carbon containing FA chains. PHH cells also display lipid species with longer chain lengths like C20 and C22. Within phospholipids, species with 18 carbon chain length emerges as the most abundant across all cell types. The FA chain with 20 carbons is the second abundant chain in all the hepatocyte models except HepG2 where 16 carbons are the second abundant. C22 remains the least abundant chain length across all cell types, with PHH cells exhibiting the highest prevalence among the five hepatocyte models. **Figure 3B** illustrates the distribution of lipid species in glycerolipids and phospholipids based on the presence of monounsaturated fatty acids (MUFA), polyunsaturated fatty acids (PUFA), and saturated fatty acids (SFA) across the five cell models. Among glycerolipids, all hepatocyte models show higher prevalence of MUFA compared to primary hepatocytes and a lower content in PUFA. In phospholipids, PHH and iPSC-Hep cells shows the highest abundance in PUFA, while HepG2, Upcyte-Hep, and organoids have a higher presence of MUFA, followed by PUFA. Across all hepatocyte models, SFA shows a lower level of abundance in phospholipids. We also performed this analysis in the GP medium to investigate the variation in the composition of fatty acyl chains in lipids under glucose-deprived conditions. However, we observed a similar abundance of species in the GP medium as in the Fed medium.
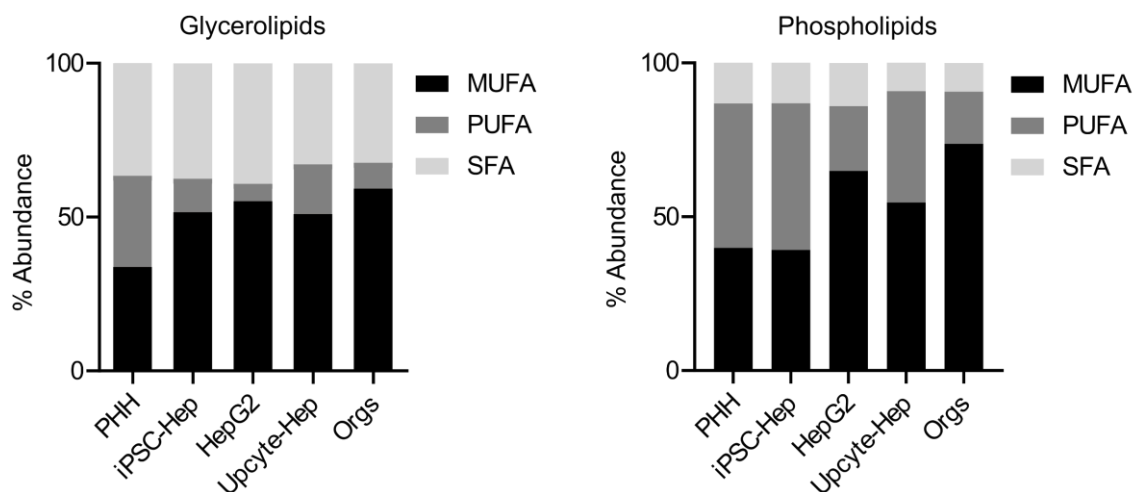
A
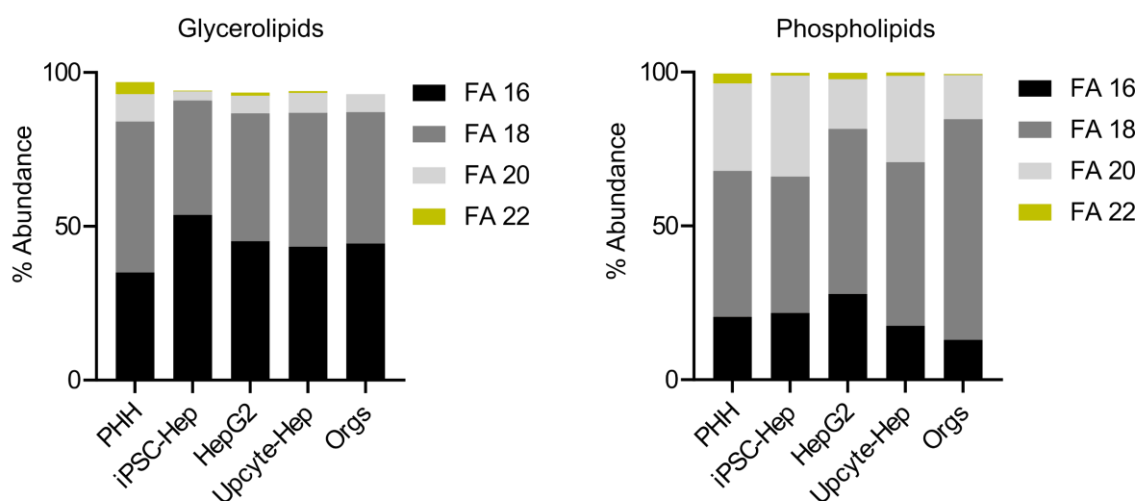
B

Figure 3. Fatty acyl chain composition of glycerolipids and phospholipids in five hepatocyte models in Fed medium. (A) Abundance (%) of lipids with fatty acid chain length containing 16, 18, 20 and 22 carbon atoms.; (B) Abundance (%) of lipids containing monounsaturated fatty acid (MUFA), polyunsaturated fatty acid (PUFA) and saturated fatty acid (SFA). In Figure 3A, the total does not add up to 100%, as there are also minor contributions from other chain lengths.

Since our aim was to identify similarities and differences of alternative hepatocyte models to PHH, we confined the consequent analysis only to the common species across the different models and samples reducing the number to 347 lipid species that were distributed across 17 lipid (sub)classes. The concentration of all the species in Fed and GP state are specified in **Table S2, sheet 2.** The accurate concentration of endogenous lipid species was calculated based on the concentration of internal standards spiked in the samples. The relative abundance of each class was calculated based on these concentrations. For this, we considered the amount of lipids in each distinct class divided by the total amount of lipids (as the sum of all species across all classes). In terms of relative abundance expressed in mol% across all common species, we found that in PHH the TG class constitutes the largest proportion of lipid species in both Fed

and GP conditions totaling approximately 60% followed by PC with about 22%, while PE, PI, SM and PS constitute approximately 6%, 5%, 4% and 2.5% of the common lipidome, respectively. Other lipid classes account for the remaining percentage. A similar ranking was observed for all hepatocyte models with the exception of Upcyte-Hep, where we found TGs to account for only 31%, with PC being the most abundant (34%). An extensive summary of the relative abundance is presented in **Table 2**.

Table 2. Composition of the lipidome of tested hepatocyte models under Fed and GP conditions expressed as mol% from the accurate amount of common lipid molecular species obtained by HILIC-MS/MS analysis.

mol%	Fed medium				
	PHH	**iPSC-Hep**	**HepG2**	**Upcyte-Hep**	**Organoids**
LPE	0.136 ± 0.003	0.145 ± 0.018	0.122 ± 0.005	0.256 ± 0.018	0.081 ± 0.007
PC	21.621 ± 1.038	15.421 ± 0.221	30.768 ± 0.758	33.6 ± 0.449	11.968 ± 0.501
LPC	0.141 ± 0.014	0.144 ± 0.011	0.086 ± 0.006	0.157 ± 0.015	0.102 ± 0.01
PI	4.725 ± 0.133	2.527 ± 0.03	4.833 ± 0.106	6.895 ± 0.584	2.656 ± 0.153
PS	2.455 ± 0.089	1.57 ± 0.048	5.39 ± 0.357	6.75 ± 0.313	1.578 ± 0.121
LPG	0.007 ± 0.001	0.007 ± 0.001	0.008 ± 0.001	0.03 ± 0.001	0.003 ± 0.001
LPI	0.041 ± 0.01	0.039 ± 0.004	0.023 ± 0.003	0.218 ± 0.035	0.018 ± 0.005
LPS	0.065 ± 0.012	0.034 ± 0.003	0.015 ± 0.002	0.123 ± 0.014	0.044 ± 0.01
PG	0.745 ± 0.051	0.6 ± 0.036	0.992 ± 0.043	2.189 ± 0.054	0.909 ± 0.039
SM	3.578 ± 0.056	2.279 ± 0.037	3.318 ± 0.042	5.579 ± 0.11	0.897 ± 0.052
HexCer	0.006 ± 0.001	0.013 ± 0.001	0.007 ± 0.001	0.034 ± 0.001	0.001 ± 0
LacCer	0.022 ± 0.003	0.003 ± 0	0.024 ± 0.001	0.039 ± 0.003	0.001 ± 0
Cer	0.67 ± 0.026	0.222 ± 0.012	0.112 ± 0.008	1.303 ± 0.17	0.26 ± 0.028
TG	59.664 ± 0.797	71.585 ± 0.883	45.623 ± 0.831	30.644 ± 0.577	77.948 ± 2.299
PE*	6.124 ± 0.176	5.411 ± 0.174	8.678 ± 0.198	12.184 ± 0.342	3.533 ± 0.17

mol%	Glucose production (GP) medium				
	PHH	**iPSC-Hep**	**HepG2**	**Upcyte-Hep**	**Organoids**
LPE	0.177 ± 0.004	0.145 ± 0.018	0.083 ± 0.001	0.282 ± 0.009	0.082 ± 0.008
PC	23.775 ± 0.374	15.421 ± 0.221	31.985 ± 0.929	34.478 ± 0.199	11.63 ± 0.503
LPC	0.202 ± 0.01	0.144 ± 0.011	0.105 ± 0.007	0.163 ± 0.008	0.113 ± 0.005
PI	4.993 ± 0.104	2.527 ± 0.03	4.723 ± 0.211	6.547 ± 0.347	2.874 ± 0.123
PS	2.547 ± 0.088	1.57 ± 0.048	6.872 ± 0.191	5.974 ± 0.108	1.414 ± 0.063
LPG	0.009 ± 0.001	0.007 ± 0.001	0.01 ± 0.001	0.039 ± 0	0.006 ± 0.001
LPI	0.042 ± 0.006	0.039 ± 0.004	0.031 ± 0.001	0.296 ± 0.041	0.017 ± 0.005
LPS	0.083 ± 0.015	0.034 ± 0.003	0.017 ± 0.001	0.124 ± 0.009	0.045 ± 0.015
PG	0.804 ± 0.032	0.6 ± 0.036	1.018 ± 0.019	2.064 ± 0.06	0.908 ± 0.099

SM	3.636 ± 0.057	2.279 ± 0.037	3.518 ± 0.075	5.672 ± 0.079	0.869 ± 0.045
HexCer	0.009 ± 0	0.013 ± 0.001	0.004 ± 0	0.025 ± 0	0.001 ± 0
LacCer	0.021 ± 0.001	0.003 ± 0	0.019 ± 0.002	0.033 ± 0.001	0.001 ± 0
Cer	0.688 ± 0.036	0.222 ± 0.012	0.12 ± 0.024	1.293 ± 0.034	0.253 ± 0.008
TG	58.298 ± 2.584	71.585 ± 0.883	45.166 ± 1.216	32.095 ± 0.572	78.607 ± 1.555
PE*	4.716 ± 0.068	5.411 ± 0.174	6.328 ± 0.264	10.917 ± 0.09	3.181 ± 0.149

* The abundance of PE-O and PE-P were included in PE.

Principal component analysis (PCA) reveals a high degree of agreement between replicates but also distinct separation between the different models in both experimental conditions (**Figure 4**). This analysis suggests diverse lipid profiles for PHH and Organoids which appear to be constituting distinctly isolated, and iPSC-Hep, HepG2 and Upcyte-Hep which tend to cluster together in another separate group. Within this group, iPSC-Hep, HepG2 and Upcyte-Hep can further be distinguished from each other (**Figure 4**, insert) revealing closest similarity between iPSC-Hep and Upcyte-Hep, while HepG2 tends to cluster separately. Overall, we observed distinct separation between all hepatocyte models. In comparison to the difference across separate hepatocyte models, distinction between Fed and GP conditions within each model appear to be relatively limited. This suggests a small alteration of the lipidome as a result of the glucose production challenge in the condition studied.
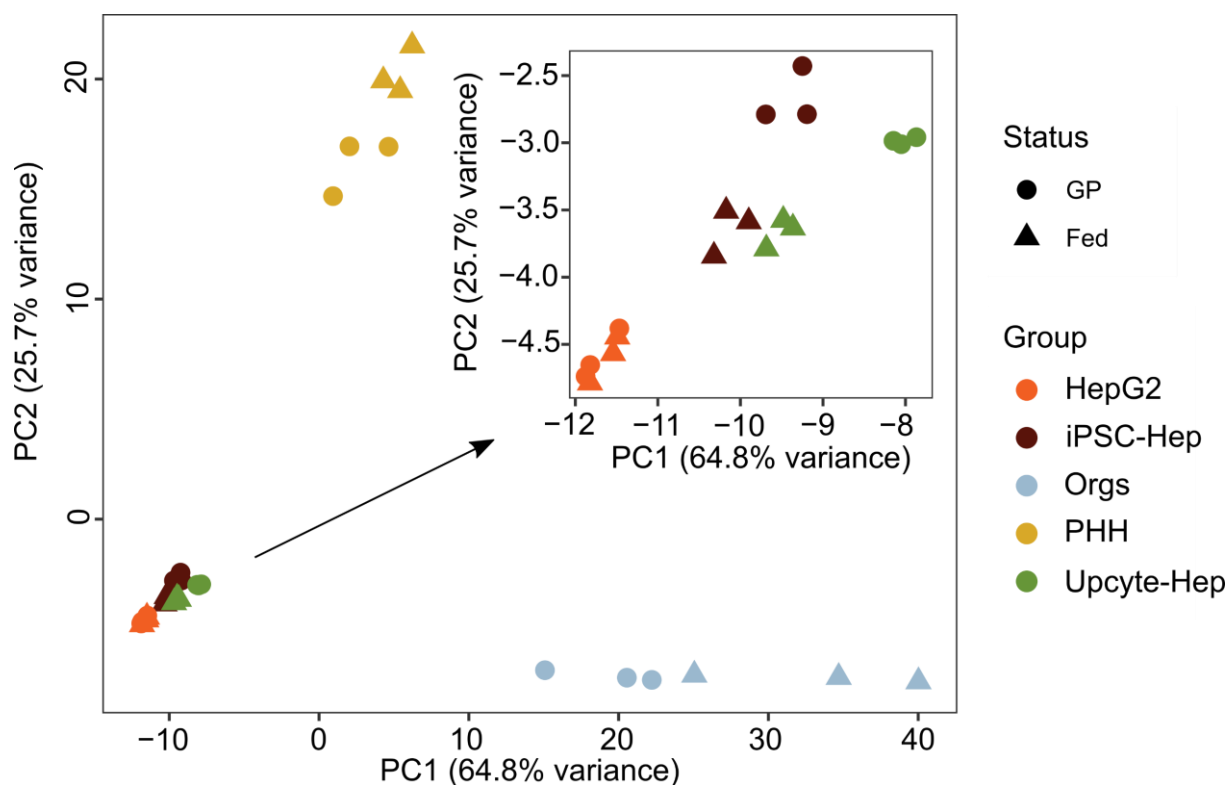

Figure 4. PCA plot showing the separation between hepatocyte models based on their lipid profile.

Further, we used a heatmap to visualize the abundance of lipid species. We confirmed the association between the hepatocytes by performing hierarchical clustering on the whole dataset (**Figure 5**). Overall, organoids show the highest lipid concentration across the lipidome, followed by PHH. The heatmap reveals closest similarity between the datasets of PHH and organoids, while confirming the separation of iPSC-Hep, HepG2 and Upcyte-Hep as a distinct group. **Table S2, sheet 3** presents the statistical significance of individual species, indicating the variation in their profiles across all four hepatocyte models when compared to PHH.
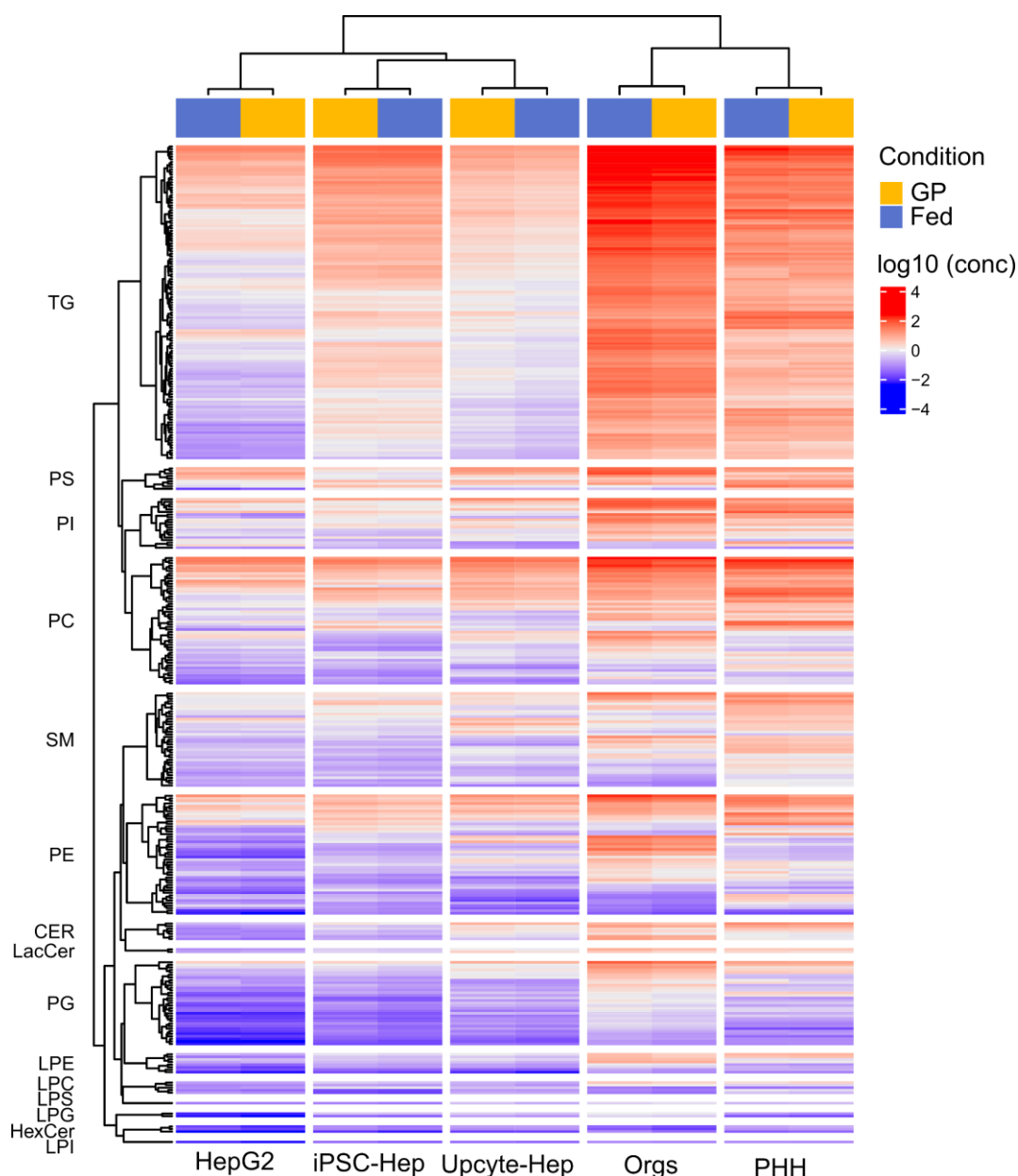

Figure 5. Heatmap of lipid species concentration, divided into their classes and associated dendograms. Each row represents a lipid species and color scale indicates log10 of the concentration normalized to protein content.

Experimental conditions, GP and Fed, did not cause drastic changes in the lipid profiles of the tested models. To evaluate significant changes in lipid species concentrations resulting from glucose production induction conditions, we conducted a statistical analysis (using *FC ≥ 1.5 or FC ≤ 0.7* and *p<0.05*). **Table 3** shows the lipid species that have been altered during GP conditions. Here we observed significant downregulation of 18 TG species and 21 PE species in PHH while there were no significant changes in the other lipid classes. This was in strong contrast with the other hepatocyte models where we observed a diverse response to the culture conditions. iPSC-Hep show an increase in several classes while no change in TG was observed. HepG2 cells revealed only minimal significant changes with a possible exception of a few species in PE, LPE, PI and PC. Upcyte-Hep shows a marked increase in several classes, most notably PC and TG. In contrast, organoids showed a significant decrease across most of the species in the lipidome including 18 PC species, 28 TG species and 32 PE species. The identity of the species that have been altered in the GP medium has been provided in **Table S2, sheet 4.** We noted that GP medium caused a reduction of saturated species in organoids like PC 18:0_18:0, PE 16:0_16:0 and PC 16:0_16:0. Conversely, we observed an elevation in species containing PUFA such as PC 16:0_20:4, PC 18:1_20:4 and PG 18:2_20:4 in iPSC-Hep, HepG2 and Upcyte-Hep. This might indicate an overall preference for saving PUFAs in fasting conditions to preserve essential building blocks for membrane synthesis or provide substrate for enzymatic reactions to produce signaling molecules.

Table 3. Lipidome alterations during GP conditions listing the number of lipid species that have been either increased or decreased during the GP state.

Lipid classes	Increased					Decreased				
	PHH	iPSC-Hep	HepG2	Upcyte-Hep	Organoids	PHH	iPSC-Hep	HepG2	Upcyte-Hep	Organoids
LPE	0	0	0	1	0	0	0	4	0	3
PC	0	6	3	12	0	0	0	0	0	18
LPC	0	0	0	2	0	0	0	0	0	1
PI	0	1	0	3	0	0	0	4	0	1
PS	0	0	1	0	0	0	0	0	0	5
LPG	0	1	0	1	0	0	0	0	0	0
LPI	0	0	0	1	0	0	0	0	0	0
LPS	0	0	0	0	0	0	0	0	0	0
PG	0	13	0	1	0	0	0	2	0	7
SM	0	1	0	1	0	0	0	0	0	9
HexCer	0	2	0	0	0	0	0	2	0	3
LacCer	0	0	0	0	0	0	0	0	0	1
Cer	0	2	1	1	0	0	0	1	0	3
TG	0	0	2	31	0	18	0	1	0	28

PE; PE-O; PE-P	0	3	0	0	0	21	0	9	0	32

4. Discussion

This study reaffirmed the distinct responses that different hepatocyte models may produce under a metabolic challenge *in vitro*. We challenged primary hepatocytes, iPSC-derived hepatocytes, upcyte hepatocytes, hepatic organoids and HepG2 with a glucose production condition, in which the cells were starved of glucose for 12 h but stimulated with forskolin to induce expression of gluconeogenic genes and supplied with the gluconeogenic precursors pyruvate, lactate and amino acids. Forskolin directly stimulates the cyclic adenosine monophosphate (cAMP) signalling pathway which has been shown to mimic the action of glucagon on primary hepatocytes [34]. Glucose production assays rely on a net-positive balance between production and consumption, where glucose is measured in the conditioned medium after an incubation period.

Due to their metabolic competence and despite their limitations, primary hepatocytes have been routinely used in energy metabolism studies, including *in vitro* glucose production capacity and dose-dependent response to either insulin or glucagon [16]. In this study, we confirmed that primary hepatocytes are indeed capable of positive net glucose production and showed the highest value compared to all other tested models. Hepatoma cell line HepG2, a widely used hepatocyte model, showed the least net glucose production of the models tested. This is in line with evidence suggesting an aberrant phenotype in terms of glucose metabolism that doesn't represent liver energy metabolism [35]. Indeed, a study shows 14-fold greater glucose incorporation compared to primary hepatocytes after incubation with ^{14}C glucose suggesting a much higher consumption rate compared to primary hepatocytes. The same study also shows a decreased capacity of fatty acid oxidation [17].

iPSC-derived hepatocytes emerged as a promising alternative to primary hepatocytes as iPSCs are a virtually illimited source of cells, they carry the genetic profile of the donor and can differentiate into hepatocyte-like cells. iPSC has been proposed as a valid alternative and several studies show similar metabolic competence as primary hepatocytes including glucose production [20,32,36]. Yet, concerns remain about iPSC-derived hepatocytes to resemble adult hepatocytes and several reports suggest a fetal phenotype instead [37,38]. In an attempt to improve maturation and differentiation efficiency, several protocols and culture settings have been proposed but there is yet no consensus on a standardized approach to generate functional,

mature hepatocytes [39]. In this study, we used a commercially available iPSC-derived hepatocyte model which was capable of net glucose production, although considerably less than primary hepatocytes. This could indeed be due to a fetal phenotype that reflects in a decreased capacity for net glucose production. Indeed, gluconeogenesis is known to be absent in the fetal liver but it increases rapidly in the liver of newborns [40]. Although in our experimental model glucose production probably arises from a combination of glycogenolysis and gluconeogenesis, the reduced net output could be attributed to decreased gluconeogenesis compared to primary hepatocytes due to an immature phenotype of the cells.

Upcyte hepatocytes were initially generated to overcome the limitations of primary hepatocytes by inducing their proliferation and re-differentiation showing many basic hepatocyte markers and functionality [21,22,41]. Initial comparison to HepG2 cells revealed an increase expression of gluconeogenesis-related genes *G6PC* and *PEPCK* and the authors hypothesized that these cells would be better capable of gluconeogenesis and glycogen synthesis [41]. A recent study showed that upcyte hepatocytes display similarities with HepG2 in terms of energy metabolism including increased glucose uptake, lactate secretion, reduced glycogen levels and signaling pathway activation associated with hepatocellular carcinoma [23]. This is in line with our observations that although upcyte hepatocytes were capable of glucose net production, this was at levels similar to HepG2 cells.

Hepatic organoids emerged as an exciting possibility to generate patient-derived expandable hepatocytes and recent progress started to determine their exact application landscape to study liver metabolism and disease [24,25]. In this work, we used epithelial organoids established from adult intrahepatic cholangiocytes. These bipotent cells possess a primarily cholangiocyte phenotype but retain the potential to, at least partially, transdifferentiate towards hepatocyte-like cells [25]. Recently a study showed that under optimized culture conditions, adult-derived liver organoid expression levels of *G6PC* and *PCK1* are similar to primary hepatocytes. The same study showed the possibility to perform a glucose production assay in Matrigel-embedded HepG2 clusters [42]. However, no clear protocol has been established for these measurements, as scaffold-embedded organoids cultures present several challenges compared to cells grown as monolayers. The repeated washing of the cells prior to glucose production initiation is imperative, as any residual glucose present from the previous culture phase might lead to an overestimation of glucose released by the cells. This is especially challenging when culture wells contain Matrigel domes, which could potentially release glucose traces also after repeated

washing steps. Furthermore, normalization can be difficult. For this study we opted to normalize metabolic readouts with total protein amount which is clearly challenging when the cells are cultured in biological, protein-rich scaffold such as Matrigel. Determining the total amount of cells also revealed to be challenging for organoids, as these cells grow in compact, three-dimensional structures and an accurate estimation of the total amount of cells remains difficult. Total DNA normalization has been proposed as a valid alternative for metabolomics studies [43]. Despite this, considering the high degree of aneuploidy in HepG2 cells [44], as well as the known polyploidy generally observed in hepatocytes [45], we questioned the utility of this approach for this study. For these reasons, we decided to extract the organoids from the scaffold prior to the 12 h incubation, which was conducted in Eppendorf tubes after repeated washing, from which we could lyse the cells and measure the total protein amount. Despite these challenges, we were capable of measuring net glucose production from liver organoids which was notably higher than all hepatocyte models, with the exception of primary hepatocytes. Yet, concerns about glucose and Matrigel traces during the incubation period remain, and further research needs to be conducted to establish robust glucose production assays in scaffold-embedded organoids.

Glucose production is a highly regulated process, as hepatocytes quickly respond to hormonal stimulation, substrate availability and intracellular molecular changes to maintain glucose homeostasis [2,5,8]. We observed clear induction of gluconeogenic genes *G6PC* and *PCK1* after incubation in GP medium compared to Fed medium, in which glucose was abundant and in the presence of insulin. This was noticeable in all hepatocyte models, with primary hepatocytes increasing the expression of both genes approximately 100-fold. This trend was not observed for the expression of *FBP1*, which was upregulated only 2-fold in primary hepatocytes and upcyte hepatocytes, while we observed a downregulation in organoids and HepG2 cells. This can be explained by the fact that FBPase has been shown to be mainly regulated allosterically, rather than at the transcription level, such as by AMP mediated inhibition [46].

Glucose and lipid metabolism are connected in a multitude of ways and disturbances of glucose metabolism can in turn lead to pathological changes in lipids. Examples include dyslipidemia often found in patients with diabetes [47] or fatty liver disease caused by glycogen storage diseases [48]. In turn, disorders of lipid metabolism are often associated with dysregulation in glucose metabolism [49]. Comparing the total lipidome of different hepatocyte models is challenging due to profound differences in the starting material, donor-to-donor variations,

growing and differentiation medium composition and subsequent substrate availability that can greatly alter the lipid composition. Furthermore, biological differences in metabolic pathways can result in drastic differences. It has been shown, for example, that de-differentiation of primary hepatocytes as a result of *in vitro* culture results in marked increase in SFA and MUFA with a decrease in PUFA over time [50]. Overall, we observed a similar trend in glycerolipids when comparing primary hepatocytes to the other hepatocyte models possibly indicating that they possess a de-differentiated phenotype. When comparing individual lipid species, it has been shown that iPSC-derived hepatocytes possess a closer lipid profile to primary hepatocytes compared to HepG2 [32]. In our study, we observed closest similarity with organoids, a model that was not tested in that study. We note however that comparing the total lipid profile in terms of concentration poses challenges. This is because of the uneven abundance of the different classes, where the highest abundant ones, primarily triglycerides, are largely responsible for the most pronounced differences between the models. In our multivariate analysis, we attributed the same weight to each class and lipid species. Different multivariate techniques could potentially elucidate other associations between different models.

The most direct link between lipid and glucose metabolism is reflected in the hepatic synthesis or breakdown of fatty acids, stored as triglycerides, as a response of nutrient availability. Fatty acid beta-oxidation is a key process to release the energy needed for the production of glucose during gluconeogenesis [7]. Alternatively, *de novo* lipogenesis converts excess carbohydrates into fatty acids, later incorporated into triglycerides [51]. Overall, our experimental glucose production condition seems to induce a downregulation of several TG species in primary hepatocytes and organoids. This could be attributed to an activated beta-oxidation pathway which could in turn explain the increase in net glucose production compared to iPSC-Hep and HepG2 in which TG content was minimally altered. In this study we did not directly assess beta-oxidation, and further studies and direct assays are needed to provide a functional proof. In contrast to primary hepatocytes and organoids, Upcyte-Hep significantly increased several TG species under the same conditions. We hypothesize that our glucose production condition, which contained no glucose but abundant amounts of lactate and pyruvate could lead to a great availability of acetyl-CoA, a major lipogenic precursor. Decreased gluconeogenic flux and energy demand could therefore lead Upcyte-Hep to utilize acetyl-CoA for *de novo* lipogenesis, rather than breakdown via the Krebs pathway. It is possible, therefore, that decreased glucose production rates in iPSC-Hep, HepG2 and Upcyte-Hep correlate with decreased fatty acid beta-oxidation. Indeed it has been reported that HepG2 possess a significantly lesser basal oxidation

rate compared to primary hepatocytes rates [17]. Overall, our data suggest that this experimental approach does not seem to induce TG breakdown in iPSC-Hep, HepG2 and Upcyte-Hep. Further studies are needed to identify experimental conditions that are compatible with these hepatocyte models to induce fatty acid beta-oxidation in combination with glucose production. This could include a pre-starvation period to deplete stored glycogen reserves or a period of fatty acid treatments to increase the TG content in the cells prior to the glucose production challenge.

Triglycerides are stored inside of lipid droplets in the cytoplasm of the cells that act as dynamic organelles, alternating between periods of growth and consumption [52]. Triglycerides are also secreted by hepatocytes in very low-density lipoproteins (VLDL) in a highly regulated process to meet energetic demands of extrahepatic tissues. Indeed, glucagon has been reported to decrease VLDL release in hepatocytes [53]. It has been observed that changes in cell membrane composition, as a result of dietary or environmental factors, can alter cell permeability and receptor stability that can contribute to pathologies such as insulin resistance and other metabolic disorders. Cell membrane components, such as phospholipid and sphingolipids are an integral part of lipid droplets and VLDL and their synthesis, breakdown or release is interlinked with the metabolic processes to maintain energy homeostasis in the organism. The two most abundant phospholipids, PC and PE were highly abundant in all hepatocyte models compared to other lipid classes, with the exception of TGs. Glucose production conditions significantly decreased several PE species in primary hepatocytes and, to a lesser extent, in HepG2 cells while PC species did not show any significant change. A change in PE could partially be explained by an alteration in VLDL synthesis and release, or structural changes of lipid droplets that would result in an alteration of the synthesis and breakdown of membrane components. Organoids showed significantly decreased PE and PC species in the glucose production condition while an increase was observed in iPSC-Hep and Upcyte-Hep.

Overall, a great diversity of response was observed across all lipid classes, indicating profound differences between the hepatocyte models. Further studies and fundamental research is needed to identify the links between lipid metabolism in conjunction with energy homeostasis. Our data seem to suggest a closer relationship in lipid composition and changes between primary hepatocytes and organoids compared to iPSC-Hep, Upcyte-Hep and HepG2. This was ultimately also reflected in the glucose production rates.

5. Conclusion

With this study, we aimed at further advancing the scientific community's pursuit of establishing and characterizing an accurate and dependable cellular tool that can substitute primary hepatocytes for *in vitro* studies. Hepatocytes are responsible for a plethora of functions and a complete cellular model with *in vivo*-like accuracy has yet to be developed. Hence, researchers are trying to identify and categorize different hepatocyte models for their suitability on specific applications. Here, we focused on energy metabolism, comparing several hepatocyte models to primary hepatocytes on glucose production, gluconeogenic gene regulation and lipid content. This study suggests that for glucose production studies, liver organoids might possess the highest net production capacity after primary hepatocytes. Other models also show net production but at lower levels. In terms of gene regulation, we observed induction of key gluconeogenic genes in all models, suggesting that, although net glucose production might drastically differ, all models could be useful to study gluconeogenesis gene regulation. Finally, lipidomics analysis revealed promising similarity between primary hepatocytes and liver organoids compared to other models. However, further studies need to be conducted to confirm organoid models as representative of fully mature, differentiated and metabolically competent hepatocytes.

6. Limitations of this study

In this section, we would like to explicitly address the limitations of this study. The first notable limitation is the use of cells derived from a single donor which may limit the extrapolation of some of the conclusions to a broader population. Donor-to-donor variation is an important variable that can drastically influence cell metabolism. Furthermore, the differentiation process of organoids and iPSC-derived hepatocytes can vary between donors and experiment. A bigger donor cohort of all hepatocyte models (with exception of HepG2 as it represents a single donor line) should be included in future studies. Gene expression analysis revealed high degree of regulation, yet this was not confirmed at the protein level. Subsequent protein expression profile should be addressed in future studies. Similarly, hepatocyte phenotype characterization was performed on gene expression. Yet, although indicative of the cell's phenotype, functional proof is not included in this work and should be addressed in follow-up characterization.

Author contributions

Flavio Bonanini and Madhulika Singh contributed equally to this manuscript. Flavio Bonanini: Conceptualization, Data curation, Formal analysis, Investigation, Methodology, Visualization,

Writing – original draft, Writing – review and editing. Madhulika Singh: Conceptualization, Data curation, Formal analysis, Investigation, Methodology, Visualization, Writing – original draft, Writing – review and editing. Hong Yang: Formal analysis, Data curation. Dorota Kurek: Funding acquisition, Project administration, Supervision, Writing – review and editing. Amy Harms: Funding acquisition, Project administration, Supervision, Writing – review and editing. Adil Mardinoglu: Funding acquisition, Project administration, Supervision. Thomas Hankemeier: Funding acquisition, Project administration, Writing – review and editing.

Declaration of competing interests

Flavio Bonanini and Dorota Kurek are employees of Mimetas BV, which markets advanced *in vitro* system for drug development. The authors declare they have no additional conflict of interests.

References

[1]   Sharabi K, Tavares CDJ, Rines AK, Puigserver P. Molecular pathophysiology of hepatic glucose production. Vol. 46, Molecular Aspects of Medicine. Elsevier Ltd; 2015. p. 21–33.

[2]   Nordlie RC, Foster JD, Lange AJ. Regulation of glucose production by the liver. Annu Rev Nutr. 1999;19:379–406.

[3]   Koutsifeli P, Varma U, Daniels LJ, Annandale M, Li X, Neale JPH, et al. Glycogen-autophagy: Molecular machinery and cellular mechanisms of glycophagy. Vol. 298, Journal of Biological Chemistry. American Society for Biochemistry and Molecular Biology Inc.; 2022.

[4]   Adeva-Andany MM, González-Lucán M, Donapetry-García C, Fernández-Fernández C, Ameneiros-Rodríguez E. Glycogen metabolism in humans. Vol. 5, BBA Clinical. Elsevier B.V.; 2016. p. 85–100.

[5]   Zhang X, Yang S, Chen J, Su Z. Unraveling the regulation of hepatic gluconeogenesis. Vol. 10, Frontiers in Endocrinology. Frontiers Media S.A.; 2019.

[6]   Chen L, Chen XW, Huang X, Song BL, Wang Y, Wang Y. Regulation of glucose and lipid metabolism in health and disease. Vol. 62, Science China Life Sciences. Science in China Press; 2019. p. 1420–58.

[7]   Rui L. Energy metabolism in the liver. Compr Physiol. 2014;4(1):177–97.

[8]   Petersen MC, Vatner DF, Shulman GI. Regulation of hepatic glucose metabolism in health and disease. Vol. 13, Nature Reviews Endocrinology. Nature Publishing Group; 2017. p. 572–87.

[9]   Weinstein DA, Steuerwald U, De Souza CFM, Derks TGJ. Inborn Errors of Metabolism with Hypoglycemia: Glycogen Storage Diseases and Inherited Disorders of Gluconeogenesis. Vol. 65, Pediatric Clinics of North America. W.B. Saunders; 2018. p. 247–65.

[10]   Jiang S, Young JL, Wang K, Qian Y, Cai L. Diabetic-induced alterations in hepatic glucose and lipid metabolism: The role of type 1 and type 2 diabetes mellitus (Review). Vol. 22, Molecular Medicine Reports. Spandidos Publications; 2020. p. 603–11.

[11]   Gastaldelli A, Baldi S, Pettiti M, Toschi E, Camastra S, Natali A, et al. Influence of Obesity and Type 2 Diabetes on Gluconeogenesis and Glucose Output in Humans A Quantitative Study [Internet]. Vol. 49, DIABETES. 2000. Available from: http://diabetesjournals.org/diabetes/article-

pdf/49/8/1367/365058/10923639.pdf

[12] Roh E, Song DK, Kim MS. Emerging role of the brain in the homeostatic regulation of energy and glucose metabolism. Vol. 48, Experimental and Molecular Medicine. Nature Publishing Group; 2016.

[13] Van Den Berghe G. Disorders of gluconeogenesis. Vol. 19, J. Inher. Metab. Dis. 1996.

[14] Özen H, Bayraktar Y. Glycogen storage diseases: New perspectives Professor, Series Editor. World J Gastroenterol [Internet]. 2007;13(18):2541–53. Available from: www.wjgnet.comhttp://www.wjgnet.com/1007-9327/13/2541.asp

[15] Lee CH, Olson P, Evans RM. Minireview: Lipid metabolism, metabolic diseases, and peroxisome proliferator-activated receptors. In: Endocrinology. 2003. p. 2201–7.

[16] Zou H, Liu Q, Meng L, Zhou J, Da C, Wu X, et al. Chemical genetic-based phenotypic screen reveals novel regulators of gluconeogenesis in human primary hepatocytes. NPJ Genom Med. 2018 Dec 1;3(1).

[17] Nagarajan SR, Paul-Heng M, Krycer JR, Fazakerley DJ, Sharland AF, Andrew X, et al. Lipid and glucose metabolism in hepatocyte cell lines and primary mouse hepatocytes: a comprehensive resource for in vitro studies of hepatic metabolism. Am J Physiol Endocrinol Metab [Internet]. 2019;316:578–89. Available from: http://www.ajpendo.org

[18] Kalemba KM, Wang Y, Xu H, Chiles E, McMillin SM, Kwon H, et al. Glycerol induces G6pc in primary mouse hepatocytes and is the preferred substrate for gluconeogenesis both in vitro and in vivo. Journal of Biological Chemistry. 2019 Nov 29;294(48):18017–28.

[19] Matsumoto M, Sakai M. Glucose Production Assay in Primary Mouse Hepatocytes [Internet]. Vol. 2, Iss. 2012. Available from: http://www.bio-protocol.org/e284

[20] Mitani S, Takayama K, Nagamoto Y, Imagawa K, Sakurai F, Tachibana M, et al. Human ESC/iPSC-Derived Hepatocyte-like Cells Achieve Zone-Specific Hepatic Properties by Modulation of WNT Signaling. Molecular Therapy. 2017 Jun 7;25(6):1420–33.

[21] Tolosa L, Gómez-Lechón MJ, López S, Guzmán C, Castell J V., Donato MT, et al. Human upcyte hepatocytes: Characterization of the hepatic phenotype and evaluation for acute and long-term hepatotoxicity routine testing. Toxicological Sciences. 2016 Jul 1;152(1):214–29.

[22] Levy G, Bomze D, Heinz S, Ramachandran SD, Noerenberg A, Cohen M, et al. Long-term culture and expansion of primary human hepatocytes. Nat Biotechnol. 2015 Dec 1;33(12):1264–71.

[23] Scheffschick A, Babel J, Sperling S, Nerusch J, Herzog N, Seehofer D, et al. Primary-like Human Hepatocytes Genetically Engineered to Obtain Proliferation Competence as a Capable Application for Energy Metabolism Experiments in In Vitro Oncologic Liver Models. Biology (Basel). 2022 Aug 1;11(8).

[24] Lehmann V, Schene IF, Ardisasmita AI, Liv N, Veenendaal T, Klumperman J, et al. The potential and limitations of intrahepatic cholangiocyte organoids to study inborn errors of metabolism. J Inherit Metab Dis. 2022 Mar 1;45(2):353–65.

[25] Huch M, Gehart H, Van Boxtel R, Hamer K, Blokzijl F, Verstegen MMA, et al. Long-term culture of genome-stable bipotent stem cells from adult human liver. Cell. 2015 Jan 15;160(1–2):299–312.

[26] Broutier L, Andersson-Rolf A, Hindley CJ, Boj SF, Clevers H, Koo BK, et al. Culture and establishment of self-renewing human and mouse adult liver and pancreas 3D organoids and their genetic manipulation. Nat Protoc. 2016;11(9):1724–43.

[27] Matyash V, Liebisch G, Kurzchalia T V., Shevchenko A, Schwudke D. Lipid extraction by methyl-terf-butyl ether for high-throughput lipidomics. J Lipid Res. 2008;49(5):1137–46.

[28] Zhang Z, Singh M, Kindt A, Wegrzyn AB, Pearson MackenzieJ, Ali A, et al. Development of a targeted hydrophilic interaction liquid chromatography-tandem mass spectrometry based lipidomics platform applied to a coronavirus disease severity study. J Chromatogr A [Internet]. 2023;464342. https://www.sciencedirect.com/science/article/pii/S0021967323005678

[29] Sefried S, Häring HU, Weigert C, Eckstein SS. Suitability of hepatocyte cell lines HepG2, AML12 and THLE-2 for investigation of insulin signalling and hepatokine gene expression. Open Biol. 2018 Oct 1;8(10).

[30] Yu S, Meng S, Xiang M, Ma H. Phosphoenolpyruvate carboxykinase in cell metabolism: Roles and mechanisms beyond gluconeogenesis. Vol. 53, Molecular Metabolism. Elsevier GmbH; 2021.

[31] Hartler J, Köfeler HC, Trötzmüller M, Thallinger GG, Spener F. Assessment of lipidomic species in hepatocyte lipid droplets from stressed mouse models. Sci Data. 2014 Dec 23;1.

[32] Kiamehr M, Alexanova A, Viiri LE, Heiskanen L, Vihervaara T, Kauhanen D, et al. hiPSC-derived hepatocytes closely mimic the lipid profile of primary hepatocytes: A future personalised cell model for studying the lipid metabolism of the liver. J Cell Physiol. 2019 Apr 1;234(4):3744–61.

[33] Huggett ZJ, Smith A, De Vivo N, Gomez D, Jethwa P, Brameld JM, et al. A Comparison of Primary Human Hepatocytes and Hepatoma Cell Lines to Model the Effects of Fatty Acids, Fructose and Glucose on Liver Cell Lipid Accumulation. Nutrients. 2023 Jan 1;15(1).

[34] Xu H, Wang Y, Kwon H, Shah A, Kalemba K, Su X, et al. Glucagon changes substrate preference in gluconeogenesis. Journal of Biological Chemistry. 2022 Dec 1;298(12).

[35] Molinaro A, Becattini B, Solinas G. Insulin signaling and glucose metabolism in different hepatoma cell lines deviate from hepatocyte physiology toward a convergent aberrant phenotype. Sci Rep. 2020 Dec 1;10(1).

[36] Holmgren G, Ulfenborg B, Asplund A, Toet K, Andersson CX, Hammarstedt A, et al. Characterization of human induced pluripotent stem cell-derived hepatocytes with mature features and potential for modeling metabolic diseases. Int J Mol Sci. 2020 Jan 2;21(2).

[37] Kvist AJ, Kanebratt KP, Walentinsson A, Palmgren H, O'Hara M, Björkbom A, et al. Critical differences in drug metabolic properties of human hepatic cellular models, including primary human hepatocytes, stem cell derived hepatocytes, and hepatoma cell lines. Biochem Pharmacol. 2018 Sep 1;155:124–40.

[38] Raju R, Chau D, Notelaers T, Myers CL, Verfaillie CM, Hu WS. In vitro pluripotent stem cell differentiation to hepatocyte ceases further maturation at an equivalent stage of e15 in mouse embryonic liver development. Stem Cells Dev. 2018 Jul 1;27(13):910–21.

[39] Graffmann N, Scherer B, Adjaye J. In vitro differentiation of pluripotent stem cells into hepatocyte like cells – Basic principles and current progress. Vol. 61, Stem Cell Research. Elsevier B.V.; 2022.

[40] Girard J. Glueoneogenesis in Late Fetal and Early Neonatal Life [Internet]. Vol. 50, Biol. Neonate. 1986. Available from: http://karger.com/neo/article-pdf/50/5/237/2273521/000242605.pdf

[41] Tolosa L, Gómez-Lechón MJ, López S, Guzmán C, Castell J V., Donato MT, et al. Human upcyte hepatocytes: Characterization of the hepatic phenotype and evaluation for acute and long-term hepatotoxicity routine testing. Toxicological Sciences. 2016 Jul 1;152(1):214–29.

[42] Gamboa CM, Wang Y, Xu H, Kalemba K, Wondisford FE, Sabaawy HE. Optimized 3d culture of hepatic cells for liver organoid metabolic assays. Cells. 2021 Dec 1;10(12).

[43] Silva LP, Lorenzi PL, Purwaha P, Yong V, Hawke DH, Weinstein JN. Measurement of DNA concentration as a normalization strategy for metabolomic data from adherent cell lines. Anal Chem. 2013 Oct 15;85(20):9536–42.

[44] Zhou B, Ho SS, Greer SU, Spies N, Bell JM, Zhang X, et al. Haplotype-resolved and integrated genome analysis of the cancer cell line HepG2. Nucleic Acids Res. 2019 May 7;47(8):3846–61.

[45] Wang MJ, Chen F, Lau JTY, Hu YP. Hepatocyte polyploidization and its association with pathophysiological processes. Vol. 8, Cell Death and Disease. Springer Nature; 2017.

[46] Liu GM, Zhang YM. Targeting FBPase is an emerging novel approach for cancer therapy. Vol. 18, Cancer Cell International. BioMed Central Ltd.; 2018.

[47] Sargsyan A, Herman MA. Regulation of Glucose Production in the Pathogenesis of Type 2 Diabetes. Vol. 19, Current Diabetes Reports. Current Medicine Group LLC 1; 2019.

[48] Leuzinger Dias C, Maio I, Brandão JR, Tomás E, Martins E, Santos Silva E. Fatty Liver Caused by Glycogen Storage Disease Type IX: A Small Series of Cases in Children. GE Port J Gastroenterol. 2019 Oct 1;26(6):430–7.

[49] Wanders RJA, Visser G, Ferdinandusse S, Vaz FM, Houtkooper RH. Mitochondrial fatty acid oxidation disorders: Laboratory diagnosis, pathogenesis, and the complicated route to treatment. Vol. 9, Journal of Lipid and Atherosclerosis. Korean Society of Lipid and Atherosclerosis; 2020. p. 313–33.

[50] Kiamehr M, Heiskanen L, Laufer T, Düsterloh A, Kahraman M, Käkelä R, et al. Dedifferentiation of primary hepatocytes is accompanied with reorganization of lipid metabolism indicated by altered molecular lipid and miRNA profiles. Int J Mol Sci. 2019 Jun 2;20(12).

[51] Ameer F, Scandiuzzi L, Hasnain S, Kalbacher H, Zaidi N. De novo lipogenesis in health and disease. Vol. 63, Metabolism: Clinical and Experimental. W.B. Saunders; 2014. p. 895–902.

[52] Olzmann JA, Carvalho P. Dynamics and functions of lipid droplets. Vol. 20, Nature Reviews Molecular Cell Biology. Nature Publishing Group; 2019. p. 137–55.

[53] Guettet ' C, Mathe D, Riottot ' M, Lutton ' C. Effects of chronic glucagon administration on cholesterol and bile acid metabolism. Vol. 963, Biochimica et Biophyka Acta. 1988.

Supplementary Material

Table S1. Concentration of internal standard mix spiked in liver cell matrices.

Internal standards mix	Concentration (nmol mL^{-1})
PC 15:0/18:1-d7	17.00
PE 15:0/18:1-d7	0.56
PS 15:0/18:1-d7	0.51
PG 15:0/18:1-d7	3.14
PI 15:0/18:1-d7	0.94
LPC 18:1-d7	3.78
LPE 18:1-d7	0.82
CE 18:1-d7	42.54
DG 15:0/18:1-d7	1.36
TG 15:0/18:1-d7/15:0	5.42
SM 18:1;O2/18:1-d9	3.25
LPG 17:1	0.16
LPI 17:1	0.31
LPS 17:1	0.22
Cer 18:1;O2/16:0-d9	1.83
Cer 18:0;O2/16:0-d9	0.73
Hex-Cer 18:1;O2/16:0-d9	0.38
Lac-Cer d18:1;O2/16:0-d9	1.03

Table S2. In supplementary excel.

Sheet 1. Lipid targets in HILIC-MS/MS acquisition method. The internal standards are highlighted in yellow.
Sheet 2. Lipid concentration expressed in μM per mg of protein.
Sheet 3. Statistical significance (p-value) of endogenous lipid species in four matrices with PHH as reference.
Sheet 4. Lipid species that have been altered significantly ($FC \geq 1.5$ or $FC \leq 0.7$, p-value < 0.05) in the GP medium.

Chapter 4

Recent developments in the analytical approaches of acyl-CoAs to assess their role in mitochondrial fatty acid oxidation disorders

Abstract

Fatty acid oxidation disorders (FAOD) are inborn errors of metabolism that occur due to deficiency of specific enzyme activities and transporter proteins involved in the mitochondrial metabolism of fatty acids, causing a deficiency in ATP production. The identification of suitable biomarkers plays a crucial role in predicting the future risk of disease and monitoring responses to therapies. Acyl-CoAs are directly involved in the steps of fatty acid oxidation and are the primary biomarkers associated with FAOD. However, acyl-CoAs are not used as diagnostic biomarkers in hospitals and clinics as they are present intracellularly with low endogenous levels. Additionally, the analytical method development of acyl-CoAs is quite challenging due to diverse physicochemical properties and instability. Hence, secondary biomarkers such as acylcarnitines are used for the identification of FAOD. In this review, the focus is on the analytical techniques that have evolved over the years for the identification and quantitation of acyl-CoAs. Among these techniques, liquid chromatography-mass spectrometry clearly has an advantage in terms of sensitivity and selectivity. Stable isotope labeling by essential nutrients in cell culture (SILEC) enables the generation of labeled internal standards. Each acyl-CoA species has a distinct pattern of instability and degradation, and the use of appropriately matched internal standards can compensate for such issues. Although significant progress has been made in measuring acyl-CoAs, more efforts are needed for bringing these technical advancements to hospitals and clinics. This review also highlights the difficulties involved in the routine use of acyl-CoAs as a diagnostic biomarker and some of the measures that can be adopted by clinics and hospitals for overcoming these limitations.

1. Introduction

Mitochondrial fatty acid oxidation disorders (FAOD) are inborn errors of metabolism resulting from defects in the mitochondrial fatty acid oxidation (FAO) pathway. These disorders are presented through various symptoms affecting the quality of life of patients and often lead to sudden death of infants. The diagnosis of FAOD is done through newborn screening and novel diagnostic biomarkers can help for the detection of the disorder at an early stage of life and subsequently provide a suitable personalized treatment. Acyl-Coenzyme A (Acyl-CoAs) are intermediate compounds formed during the process of FAO, and their profiles can be used as biomarkers for FAOD. Coenzyme A (CoASH, also called as free CoA) is synthesized naturally from pantothenic acid, also known as vitamin B5 or pantothenate [1,2]. Pantothenate is an essential nutrient present in foods such as eggs, milk, beef, vegetables and grains [3]. Pantothenate is used to synthesize CoASH through five enzymatic steps which further leads to the formation of acyl-CoA thioesters as mentioned in **Figure 1** [2,4]. Acyl-CoAs are generated from the actions of acyl-CoA synthetase or ketoacid dehydrogenase [4,5]
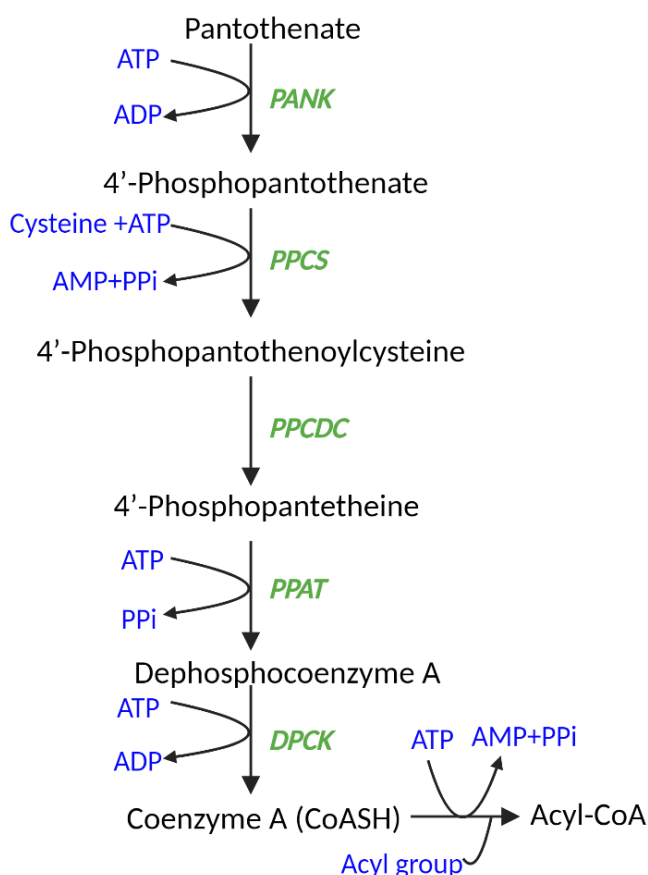

Figure 1. Biosynthetic pathway of CoASH and acyl-CoAs. ATP, adenosine triphosphate; ADP, adenosine diphosphate; AMP, adenosine monophosphate; PPi, pyrophosphate; PANK, pantothenate kinase; PPCS, phosphopantothenoylcysteine synthetase; PPCDC, phosphopantothenoylcysteine decarboxylase; PPAT, phosphopantetheine adenylyltransferase; DPCK, dephosphocoenzyme A kinase.

In FAOD, acyl-CoA molecules accumulate depending on the type of disorder and result in energy deficiency and other toxic effects. However, due to several analytical challenges associated with acyl-CoAs, acylcarnitines are commonly employed as diagnostic biomarkers for these disorders. Acyl-CoAs are quite diverse in their physicochemical structures due to varying fatty acyl chain length, unsaturation index and functional groups. They lack resonance stabilization of the energy-rich thioester bond which makes them prone to hydrolysis [6], hence they degrade in alkaline and strongly acidic solutions [7]. Also, these molecules have thiols in their structure which are prone to oxidation or other intra and extracellular reactions [8]. Apart from chemical instability, acyl-CoA species are also unstable in biological samples and often lower signals are reported as they can form anhydrides [9] or S-acyl glutathione [10,11] in tissue samples. Therefore, analysis of these molecules is quite challenging and requires careful sample handling and measurement strategies. Nevertheless, it is important to be able to measure concentrations of these molecules as CoASH and acyl-CoAs have numerous important roles in various biological processes. CoASH is an important co-factor in various cellular oxidative reactions and biosynthetic processes [4] and acts as an activator of carboxylic acids for biochemical transformation and carrier of acyl groups [12]. CoASH and acyl-CoAs are involved in fatty acid synthesis and complex lipid synthesis and also reported to have an important role in cancer [13,14], diabetes [15,16], xenobiotics metabolism [4,17], pantothenate kinase-associated neurodegeneration [18], etc.

This review considers the important role of acyl-CoAs as these are directly involved in the FAO pathway. Developing analytical techniques to enable the detection of acyl-CoAs is quite important to assess their roles in FAOD. The detection and measurement of acyl-CoAs, in addition to acylcarnitines, can enable researchers and clinicians to gain insight into defective enzymes responsible for FAOD and hence, provide for appropriate and timely treatments. In this review, the focus is on the analytical techniques that have evolved over the years for identification and quantitation of acyl-CoAs, limitations involved in the routine use of acyl-CoAs as the diagnostic biomarker for FAOD and efforts that can be taken to bridge the gap between technological advancement and routine diagnosis.

2. Role of CoASH (free CoA) and acyl-CoAs in FAO

2.1 Mechanism of mitochondrial FAO: an essential process for survival

During prolonged fasting and strenuous exercise, the blood glucose level decreases and the body needs compensatory mechanisms to replenish energy sources. In the first few hours of

fasting, the glycogen reserve is used to maintain the blood glucose level and after its depletion, fats are used as the energy source, where FAO is a key pathway for energy supply [19–21]. Peroxisomes and mitochondria are the two sites for FAO, where mitochondrial FAO pathway facilitates the oxidation of fatty acids (FA) with ≤20 carbons while peroxisomal FAO involves the oxidation of very long-chain FA with >20 carbons and branched-chain FA [22]. Peroxisomal beta-oxidation is involved in biosynthetic pathways while mitochondrial beta-oxidation is involved in the production of ATP [23]. Most tissues such as heart, skeletal muscles and liver, with the exception of the brain, can use FAO as an energy source and it has been reported that approximately 80% of the total requirement of energy during fasting is provided by FAO [21,24,25]. Brain, on the other hand, can use ketone bodies produced by the liver during FAO as the major source of energy during periods of fasting [26,27].

In the presence of insulin, excess glucose from the diet is stored in the form of glycogen, which acts as a reserve for glucose for brain and other tissues [28,29]. In the initial few hours of fasting, the insulin level will decrease, activating glycogenolysis in liver and muscles to maintain the normal blood glucose level [27,29]. As the fasting period continues, the hepatic glycogen stores deplete and at this stage gluconeogenesis and FAO play an important role in maintaining energy balance. Gluconeogenesis is a process of glucose synthesis from non-carbohydrate sources, occurring primarily in the liver and kidney [30]. As the main focus of this review is on disorders related to FAO, we will describe FAO pathway in a detailed way.

FA serves as substrate for FAO and can be taken up by cells through multiple pathways. These pathways include dietary intake, the synthesis of FA within the body (*de novo* synthesis), or the breakdown of triglycerides stored in adipose tissues, resulting in the release of free fatty acids [19,31–33]. The FAO pathway is driven by multiple enzymes involved at different stages of this pathway. The medium- (C6-C10) and short-chain (<C6) fatty acids can diffuse freely across the plasma and mitochondrial membrane and subsequently enter inside the mitochondrial matrix where they get activated to acyl-CoA esters [34]. The long-chain (C12-C20) fatty acids are transported across the plasma membrane by protein carriers such as fatty acid transport proteins, fatty acid translocase and fatty acid-binding proteins [21,34]. After entering inside the cytosol, the long-chain FA are converted to fatty acyl-CoA esters via a thioesterification reaction with the help of cofactor CoASH by the action of acyl-CoA synthetase enzymes [35]. The mitochondrial membrane is impermeable to acyl-CoA esters, hence the transport of long-chain fatty acyl-CoA esters into the mitochondria requires the carnitine cycle **(Figure 2A)**. The carnitine cycle is mediated through different membrane bound proteins. Carnitine transporter

(OCTN2) will facilitate the entry of carnitine to the cell. This carnitine will be taken up by the carnitine palmitoyltransferase 1 (CPT1) present in the mitochondrial outer membrane, which is responsible for converting acyl-CoAs into acylcarnitines [36]. CPT1 catalyzes the rate limiting step of FAO in liver [37]. During the fasting state, malonyl-CoA (an inhibitor of CPT1) decreases, thus activating CPT1 which subsequently enhances FAO, while the opposite happens during the fed state [38]. Carnitine-acylcarnitine translocase (CACT) promotes the transfer of these acylcarnitines into the mitochondrial matrix. Long-chain acylcarnitine molecules are then re-esterified into their corresponding acyl-CoA esters by carnitine palmitoyltransferase 2 (CPT2) present on the mitochondrial inner membrane. Inside the mitochondrial matrix, the activated fatty acids in the form of acyl-CoA thioesters will undergo FAO (**Figure 2A**), which consists of four steps with different enzymes as depicted in **Figure 2B.**

Step-1 Acyl-coenzyme A dehydrogenases (ACAD) are the first set of enzymes involved in the cyclic process of FAO. Depending on the fatty acid chain length, there are different members in this class of enzymes which include very long-chain acyl-CoA dehydrogenase (VLCAD), long-chain acyl-CoA dehydrogenase (LCAD), medium-chain acyl-CoA dehydrogenase (MCAD), and short-chain acyl-CoA dehydrogenase (SCAD). These enzymes dehydrogenate the acyl-CoA ester to yield a trans-2-enoyl-CoA.

Step-2 The next enzyme involved in the process, 2-enoyl-CoA hydratase, is responsible for the hydration of the double bond, resulting in a 3-hydroxyacyl-CoA.

Step-3 In the third step, 3-hydroxyacyl-CoA is dehydrogenated to 3-ketoacyl-CoA by the action of the enzyme 3-hydroxyacyl-CoA dehydrogenase.

Step-4 The final step of this cycle is thiolytic cleavage of the 3-ketoacyl-CoA by enzyme 3-ketoacyl-CoA thiolase resulting in one molecule of acetyl-CoA and a two carbon chain-shortened acyl-CoA [21].

The acetyl-CoA formed at the end of this cycle will enter the Krebs cycle while the two carbon shortened acyl-CoA re-enters the FAO cycle for further oxidation. One round of mitochondrial beta-oxidation forms one $FADH_2$, one NADH, one acetyl-CoA and an acyl-CoA with two carbons less than the initial acyl-CoA [17]. The functions of 2-enoyl-CoA hydratase, 3-hydroxyacyl-CoA dehydrogenase and 3-ketoacyl-CoA thiolase are executed by mitochondrial trifunctional protein (MTP), located in the mitochondrial inner membrane [39].

The odd chain fatty acids undergo the same steps of FAO but the last cycle with five carbon chain will form one molecule each of acetyl-CoA and propionyl-CoA. This propionyl-CoA is carboxylated to form D-methylmalonyl-CoA which further racemizes to form L-

methylmalonyl-CoA and undergoes isomerization to form succinyl-CoA, an intermediate for the Krebs cycle [40,41]. The unsaturated fatty acyl-CoA esters need additional auxiliary enzymes 2,4-dienoyl-CoA reductase and Δ^3-Δ^2-enoyl-CoA isomerase to act on the double bonds [42,43]. 2,4-dienoyl-CoA reductase reduces polyunsaturated fatty acid chains having double bonds at 2,4 positions (using NADPH) to form trans-3-enoyl-CoA, while Δ^3-Δ^2-enoyl-CoA isomerase catalyzes cis or trans double bonds at position 3 of fatty acyl-CoA to a trans double bond at position 2.

Acetyl-CoA, generated from FAO, combines with oxaloacetate in the Krebs cycle. In low glucose conditions, oxaloacetate is directed towards gluconeogenesis while acetyl-CoA is redirected towards the production of ketone bodies [44]. The ketogenesis in liver increases with an increase in FAO due to enhanced production of acetyl-CoA. In the mitochondrial matrix of liver cells, the acetyl-CoA molecules generated from the FAO pathway are used for ketogenesis (**Figure 2A**). Two acetyl-CoA molecules condense to form acetoacetyl-CoA by enzyme acetoacetyl-CoA thiolase. Further, mitochondrial 3-hydroxy-3-methylglutaryl-CoA (HMG-CoA) synthase mediates the formation of HMG-CoA from acetoacetyl-CoA. HMG-CoA is further cleaved by HMG-CoA lyase to forms acetoacetate and is further reduced to 3-hydroxybutyrate by 3-hydroxybutyrate dehydrogenase. The decarboxylation of acetoacetate will yield acetone. Acetoacetate and 3-hydroxybutyrate are transported to the brain and other extrahepatic tissues through the bloodstream where they are further converted back to acetyl-CoA for entering in the Krebs cycle to generate ATP [44].

(A)
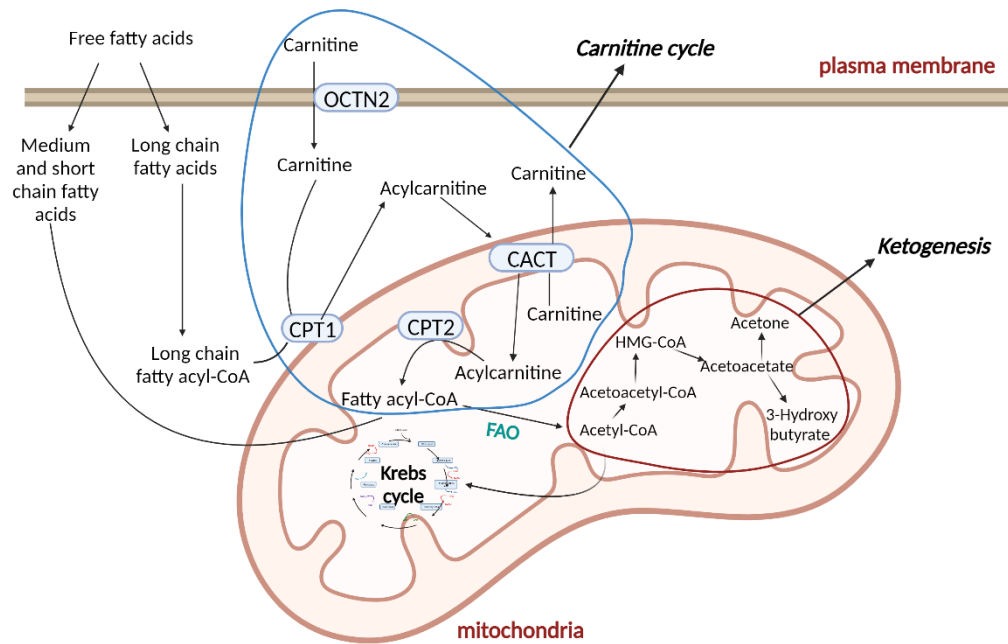
(B)
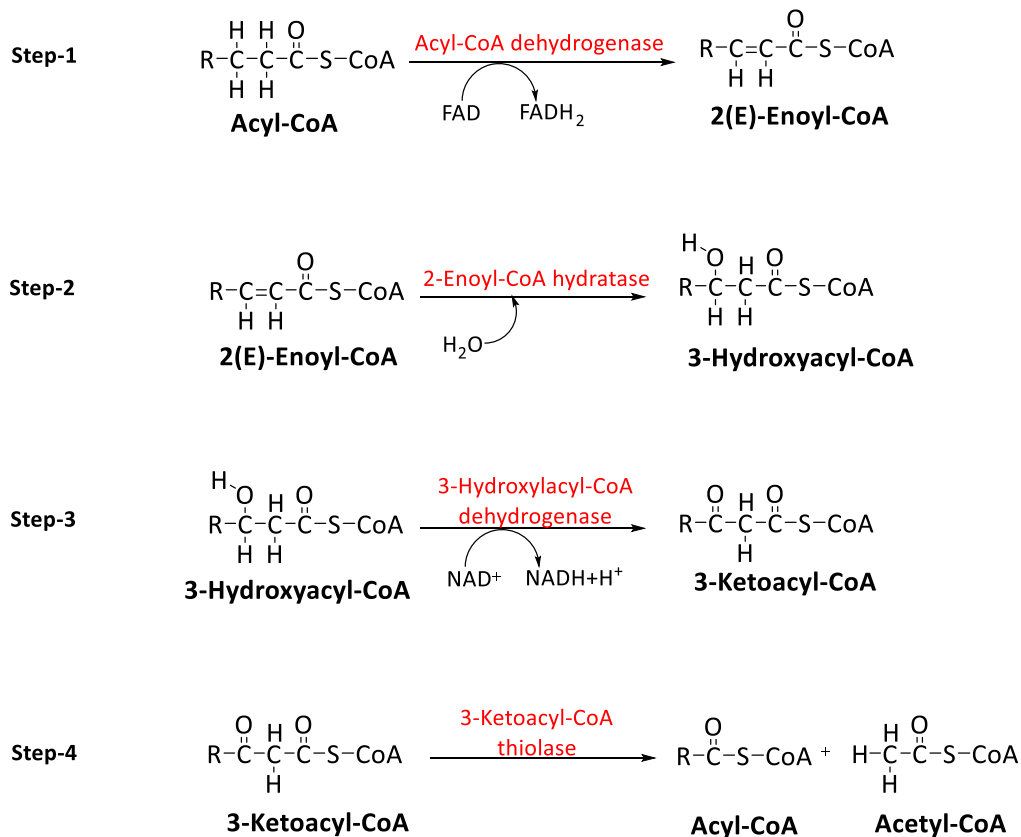
Figure 2. (A) Illustration of different stages involved in fatty acid oxidation cycle.; (B) Four key enzymatic steps of fatty acid oxidation. The first step is the uptake and activation of fatty acids followed by transport of fatty acids inside the mitochondria by the carnitine cycle. The activated fatty acids, in the form of acyl-CoA undergo fatty acid oxidation. OCTN2, carnitine transporter; CPT1, carnitine palmitoyltransferase 1; CACT, carnitine-acylcarnitine translocase; CPT2, carnitine palmitoyltransferase 2; FAD, flavin adenine dinucleotide; FADH$_2$, reduced flavin adenine dinucleotide; NAD, nicotinamide adenine dinucleotide; NADH, reduced nicotinamide adenine dinucleotide.

2.2 Disorders of fatty acid oxidation

FAOD are group of rare diseases that occur due to autosomal recessive inheritance that can lead to deficiency in energy. There are several types of FAO defects. Depending on the enzyme deficiency, they are divided in different categories [34,45,46] as shown in **Table 1**.

Table 1. Types of FAOD.

Categories of disorders	Enzyme Deficiency
Related to plasma membrane	Carnitine transporter (OCTN2)
	Long-chain fatty acid transporter protein (FATP1)
	Long-chain fatty acyl-CoA synthetase (LACS)
Related to transport through mitochondrial membrane	Carnitine palmitoyltransferase 1 (CPT1)
	Carnitine-acylcarnitine translocase (CACT)
	Carnitine palmitoyltransferase 2 (CPT2)
Beta-oxidation of long-chain inside mitochondria	Very long-chain acyl-CoA dehydrogenase (VLCAD)
	Long-chain acyl-CoA dehydrogenase (LCAD)
	Mitochondrial trifunctional protein (MTP)
	Long-chain 3-hydroxyacyl-CoA dehydrogenase (LCHAD)
	Long-chain 2-enoyl-CoA hydratase (LCEH)
	Long-chain 3-ketoacyl-CoA thiolase (LCKAT)
Beta-oxidation of medium-chain inside mitochondria	Medium-chain acyl-CoA dehydrogenase (MCAD)
	Medium-chain 3-hydroxyacyl-CoA dehydrogenase (MCHAD)
	Medium-chain 3-ketoacyl-CoA thiolase (MCKAT)
Beta-oxidation of short-chain inside mitochondria	Short-chain acyl-CoA dehydrogenase (SCAD)
	Short-chain 3-hydroxyacyl-CoA dehydrogenase (SCHAD)
	Short-chain 2-enoyl-CoA hydratase (SCEH)
Related to deficiency of electron transfer flavoproteins	Multiple acyl-CoA dehydrogenase (MAD)

The prevalence of these disorders is approximately one in 5000-10000 births, and may cause severe life threatening complications in infants within a few hours of fasting and in adults after 48 h of fasting [46,47]. The clinical onset of symptoms is quite variable depending on the patient's age. In newborns and infants, the basal energy need is higher, their brains need more glucose, hence they are most susceptible for these disorders compared to older children and adults [48–50]. Hypoglycemia, hepatic steatosis and liver dysfunction are associated with all types of FAODs [20,33,39,46]. Several long-chain FAODs and disorders related to fatty acid transport across the mitochondrial membrane impact the cardiac muscle (symptoms include

cardiomyopathy, arrhythmia and sudden death) and skeletal muscles (myopathy and rhabdomyolysis). Other organs affected rarely include the retina in LCHAD and kidney in VLCADD. Due to defects in the FAO, the intracellular accumulation of fatty acyl-CoA species and corresponding carnitine or glycine conjugates will increase in liver, skeletal muscle and heart, leading to impaired functionality of these organs [51,52]. The impaired functioning of liver results in a decrease in the production of ketones, which are an important energy source for the brain in glucose deficit conditions. The combined effects of reduced glucose production and impaired hepatic ketogenesis result in depletion of available energy substrates, thus hampering the normal functioning of brain.

3. Acyl-CoA as a diagnostic biomarker for FAOD

Newborn screening (NBS) is performed after birth for the diagnosis of FAOD. The current approach in hospitals and clinics is based on the routine profiling of secondary biomarkers such as acylcarnitines. Different types of FAOD can be distinguished based on the nature of acylcarnitines accumulated. Acyl-CoAs are directly involved in the steps of the FAO pathway and hence they are the primary biomarkers associated with these FAOD [53]. However, they are not routinely used, and instead acylcarnitines are the first choice as biomarkers for FAOD due to various reasons. Acylcarnitines can be analyzed from easily available matrices of patients such as plasma, blood, serum and urine, while acyl-CoAs are present only intracellularly, requiring tissue samples for their analysis which causes difficulties, especially in the case of newborns and infants. Additionally, acyl-CoAs are relatively unstable compounds, are present at low concentrations, and often require complicated chromatographic separations due to the wide polarity range between short- and long-chain species. Nevertheless, acyl-CoAs can provide more accurate insights as they are primarily located within the cellular matrix and are directly involved in the metabolic processes, making them more specific markers of cellular metabolic status. The changes in their levels can directly reflect changes in enzymatic activity and metabolic flux. Although acylcarnitines indicate changes in fatty acid metabolism, they are not central to the metabolic pathways like acyl-CoAs and can be influenced by factors such as carnitine availability. Hence, profiling of both acyl-CoA and acylcarnitines are quite important in interpreting the pathophysiological pathway associated with them. **Table 2** shows the reported biomarkers of acylcarnitines and acyl-CoAs for different types of FAOD. It is evident that more research and development has been done for analyzing acylcarnitines as biomarkers for FAOD while relatively fewer studies report the role of acyl-CoA compounds. The upcoming

sections in this review will focus on the analytical advances and strategies that have been adopted over the years for improving the detection and quantitation of acyl-CoA compounds.

Table 2. Diagnostic acylcarnitine and acyl-CoA biomarkers for FAOD.

| Deficiency | Biomarker | | Reference | |
	Free carnitines (C0); Acylcarnitines (Plasma/Dried blood spot)[#]	Acyl-CoA (matrix is defined in the corresponding rows)[#]	Acylcarnitines	Acyl-CoA
CT	Decrease: C0, C2, C3, C16, C18, C18:1	NA	[34,39,54]	NA
CPT1	Increase: C0, C0/(C16 + C18) Decrease: C16, C18, C18:1, C18:2, (C16 + C18:1)/C2	**Matrix**: Human Fibroblasts Increase: C16	[34,39,46,55]	[56,57]
CACT	Increase: C14, C16, C16:1, C18, C18:1, C18:2, C14:1/C2, (C16 + C18:1)/C2 Decrease: C0, C2, C3/C16, C0/(C16 + C18)	**Matrix**: Human Fibroblasts Decrease: C16	[34,39,46,55]	[57]
CPT2	Increase: C12, C14, C16, C16:1, C18, C18:1, C18:2, C14:1/C2, (C16 + C18:1)/C2 Decrease: C0, C2, C3/C16, C0/(C16 + C18)	NA	[34,39,46,55]	NA
VLCAD	Increase: C12, C12:1, C14:2, C14:1, C14, C16:1 C16, C18, C18:1, C18:2 C14:1/C2, C14:1/C12:1, C14:1/C16 Decrease: C0	**Matrix**: Human Fibroblasts Increase: C16/C12 Decrease: C12	[34,39,46,55]	[56]
LCAD	NA	**Matrix**: Human Fibroblasts Increase: C16/C12 Decrease: C12	NA	[56]
MTP	Increase: C14, C14-OH, C14:1, C14:2, C16:1, C16-OH, C16:1-OH, C18-OH, C18:1-OH, C18:2-OH, C14:1/C2, C14:1/C16, C16-OH/C16, C18-OH/C18 Decrease: C0	**Matrix**: Human Fibroblasts Increase: C16:1, C16-OH Decrease: C12, C14	[25,34,35,46]	[57]

LCHAD	Increase: C14, C14:1, C14:2, C14-OH, C14:1-OH, C16:1, C16-OH, C16:1-OH, C18, C18:1, C18:2, C18-OH, C18:1-OH, C18:2-OH, C14:1/C2, C14:1/C16, C16-OH/C16, C18-OH/C18	**Matrix**: Human Fibroblasts Increase: C14:1, C16:1, C16-OH	[34,39,46,55]	[58]
	Decrease: C0			
LCEH	NA	NA	[34]	NA
LCKAT	Increase: C14:1, C16:1, C16-OH, C18-OH	NA	[34,39]	NA
MCAD	Increase: C6, C8, C10, C10:1, C8/C2, C8/C10, C8/C16, C8/C8:1	**Matrix**: Human Fibroblasts Increase: C8, C10	[34,39,46,55]	[57,58]
	Decrease: C0, C2	Decrease: C12, C14		
M/SCHAD*	Increase: C4-OH, C6-OH, C8-OH	NA	[25,34,35]	NA
MCKAT	NA	NA	[39]	NA
SCAD	Increase: C4, C4/C2, C4/C3, C4/C8	**Matrix**: Mouse liver	[34,39,46,55]	[53]
	Decrease: C0	Increase: C4, C6		
SCHAD*	Increase: C4-OH	**Matrix**: Mouse liver Increase: C4-OH, C6, C6-OH, C8:1, C8	[34,39,46,55,59]	[53]
		Decrease: C2		
SCEH	NA	NA	[60]	NA
MAD	Increase: C4, C5, C6, C8, C10:1, C12, C14, C14:1, C16, C16:1, C18, C18:1, C16-OH, C16:1-OH, C18-OH, C18:1-OH, C4/C2, C4/C3, C5/C0, C5/C2, C5/C3, C8/C2, C14:1/C2, C14:1/C16, (C16 + C18:1)/C2	NA	[39,46]	NA
	Decrease: C0			

NA; not available.

*3-Hydroxyacyl-CoA dehydrogenase (HAD) deficiency term is now used to represent both short-chain hydroxyacyl-CoA dehydrogenase (SCHAD) deficiency and medium- & short-chain hydroxyacyl-CoA dehydrogenase (M/SCHAD), as this dehydrogenase enzyme encoded by single gene has chain length specificity for C4-C10 substrates [46,61].

Acylcarnitine biomarkers are reported in plasma or dried blood spots while acyl-CoA biomarkers are reported in different matrices as mentioned in the table.

4. Analytical advances for the measurement of Acyl-CoAs

4.1 Extraction of Acyl-CoAs from biological samples

Sample preparation is an important step for the quantitative determination of any compound and should be optimized to extract and recover the maximum quantity of compounds from the biological samples. As summarized by Rivera et al. [62], various methodologies such as protein precipitation, liquid-liquid extraction (LLE) and solid-phase extraction (SPE) have been employed for the extraction of acyl-CoAs. Acyl-CoA species vary significantly in their polarity. Although soluble in polar solvents, long-chain acyl-CoAs can migrate into the non-polar organic layer during LLE which can result in the poor recovery of these compounds from the aqueous layer. The organic and aqueous layers can be combined to improve recovery, however this will introduce lipids in the sample and thus can cause matrix effects. For these reasons, researchers have also used the combination of LLE-SPE [63,64]. LLE followed by SPE is quite efficient in removing endogenous interferences such as phospholipids from the matrices and can provide better purification. On the other hand, these techniques can have a negative impact on recoveries, and are time-consuming and expensive. Hence, some studies completely eliminated LLE/SPE extraction and have used protein precipitation [65,66]. Fu et al. used 0.4 M perchloric acid containing 0.5 mM EGTA [65] while Pearce et al. used acidified methanol (5% acetic acid in cold methanol) [66] for extraction of acyl-CoAs. The selection of the extraction technique depends on the type of acyl-CoA species. Short-chain species are well-extracted at strongly acidic pH while long-chain species are not soluble under the same conditions [67]. Therefore, studies covering all short- to long-chain species employ weakly acidic solvents. **Table 3** summarizes various extraction strategies that have been used for acyl-CoAs since 2018.

Table 3. Sample preparation techniques for the extraction of acyl-CoAs from biological samples.

Extraction Techniques	Biological Samples	Extraction solvents	Recovery (%)	Reference
Protein precipitation	Mouse liver	0.4 M $HClO_4$ containing 0.5 mM EGTA followed by neutralization with 0.5 M K_2CO_3	84.44-112	[65]
	HepG2 cells, Bone marrow-derived macrophages from mice	2.5% (w/v) 5-sulfosalicylic acid solution	59-80	[2]
	Betaproteobacterium "Aromatoleum" sp. strain HxN1	2 mL MeOH, 0.5 mL of ice-cold 10 mM $HCOONH_4$ (pH 7)	NA	[68]
	Human liver adenocarcinoma cells (SK-HEP-1)	5% acetic acid in cold MeOH	79.5-133.1	[66]
	Rabbit heart, liver brain, spleen and kidney	80% aqueous MeOH (pre-cooled at -80 °C)	NA	[69]
	Rat liver, kidney, brain and heart	80% MeOH	NA	[70]
	Mouse liver	Ice-cold MeOH:H_2O (80:20)	NA	[71]
	Human whole blood	MeOH: 2.5 mM CH_3COONH_4 (80:20) (pH 6.5) (pre-cooled at -80 °C)	~100	[72]
	Saccharomyces cerevisiae, HEK-293T cells, single rice seed, mouse kidney glomeruli, single *Arabidopsis thaliana* seed	*Saccharomyces cerevisiae,* HEK-293T cells, single rice seed: 80% MeOH Mouse kidney glomeruli: 50 mM borate buffer solution (pH 7) Single *Arabidopsis thaliana* seed: 50 mM borate buffer solution (pH 7)	77.1-112.4	[73]
LLE	Drosophila larva and pupa	Extraction buffer (IPA, 50 mmol/L KH_2PO_4, glacial acetic acid and bovine serum albumin), petroleum ether, saturated ammonium sulfate and $CHCl_3$: MeOH (1:2)	86.4 ± 1.3	[74]
	Rat hepatic stellate cells (HSCs) T6; Human embryonic kidney cells 293T	Extraction buffer (IPA, 50 mmol/L KH_2PO_4, glacial acetic acid and bovine serum albumin), ethyl ether, $CHCl_3$: MeOH (1:2)	NA	[75]

Protein Precipitation-SPE	HepG2 cells	**Protein precipitation:** 1 mL of ice-cold 10% (w/v) trichloroacetic acid in H_2O **SPE:** *Cartridge:* Oasis HLB 1 cc (30 mg) SPE columns (Waters). *Pre-conditioning solvent:* 1 mL H_2O *Washing solvent:* 1 mL MeOH, *Elution solvent:* 1 mL MeOH containing 25 mM CH_3COONH_4	NA	[76]
LLE-SPE	Human cervical HeLa cells, Human platelet samples	**LLE:** ACN:IPA (3:1), KH_2PO_4 buffer (0.1 M, pH 6.7), acetic acid **SPE:** *Cartridge:* Oasis WAX (Waters, Milford, MA) *Pre-conditioning solvent:* MeOH:H_2O:acetic acid (3:1:1) *Washing solvent:* MeOH:H_2O:acetic acid (3:1:1); 50% MeOH *Elution solvent:* IPA:MeOH:3% ammonia (6:3:1)	43.4-76.1	[64]

$HClO_4$, perchloric acid; K_2CO_3, potassium carbonate; MeOH, methanol; $HCOONH_4$, ammonium formate; H_2O, (ultra-pure) water; CH_3COONH_4, ammonium acetate; IPA, isopropanol; $CHCl_3$, chloroform; KH_2PO_4, potassium phosphate monobasic; ACN, acetonitrile.

4.2 Methods for separation and detection of CoASH (free CoA) and acyl-CoA thioesters

There are various techniques employed for analyzing CoASH and acyl-CoA thioesters. The details of changes in the analytical techniques over the years are described in sections below.

4.2.1   Enzymatic methods

The two most common enzymatic assays that were employed for determination of CoASH and acyl-CoA compounds were: (i) endpoint assays: measurement of the end products of a reaction; (ii) recycling assays: multiple enzyme catalyzed reactions are involved for recycling of CoASH or acyl-CoAs and product is formed. The rate of formation of this product is proportional to the CoASH/acyl-CoA concentration. The detection for these enzymatic methods was through spectrophotometric, fluorometric and radioactive assays. **Table 4** shows the methods that were

commonly used to measure CoASH and acyl-CoAs. The details and principle of these assays are described comprehensively by Bieber et al. [77] and Tsuchiya et al. [67].

Table 4. Enzymatic methods for the determination of CoASH (free CoA) and acyl-CoAs.

Type of assays	Detection technique	Species analyzed	Sensitivity (Limit of detection)	Reference
Endpoint	Fluorometric	CoASH; C2:0-CoA; long-chain fatty acyl-CoA	50 µmol	[78,79]
	Radioisotopic	Malonyl-CoA	10 pmol (approx.)	[80,81]
	Radioisotopic	CoASH; C2:0-CoA	10 pmol	[82]
Recycling	Spectrophotometric/ Fluorometric	CoASH; C2:0-CoA	<40 pmol per mL of tissue extract	[67,77,83]
	Spectrophotometric	C2:0-CoA	Not defined	[84]
	Fluorometric	CoASH; C2:0-CoA	0.04 pmol	[85]
	Spectrophotometric	C2:0-CoA; Malonyl-CoA	1 pmol	[86]

Although these enzymatic assays were very useful for determination of individual acyl-CoAs, their targets were mainly limited to CoASH, acetyl-CoA and malonyl-CoA. They lack the broad coverage and are considered less reliable due to interferences. Therefore, techniques that can resolve and identify multiple acyl-CoA species and are sensitive enough to detect these compounds in cells and tissues were needed.

Analytical methods coupling separation and detection techniques

To overcome the limitations associated with enzymatic methods, researchers started using methods that involve the combination of separation techniques such as liquid chromatography (LC) or gas chromatography (GC) with detection techniques such as ultraviolet (UV) absorption or mass spectrometry (MS).

4.2.2 Liquid chromatography-ultraviolet (LC-UV) detection methods

High-performance liquid chromatography (HPLC) started gaining popularity due to high speed and good resolution of separation. The first separation of acyl-CoA species was described by Baker and Schooley with the application of ion-pairing reversed-phase liquid chromatography (IPRP-LC) interfaced with a UV detector [87]. Ammonium-based counter ions were used as ion-pairing agents. Later, other studies employed reversed-phase chromatography with mobile phases containing (10-100) mM phosphate salts such as potassium phosphate monobasic (KH_2PO_4) [63,88–91] and sodium phosphate monobasic (NaH_2PO_4) at pH range of (4.5-5.3) [92]. Isocratic elution with 100 mM of NaH_2PO_4 had also been used for detection of CoASH

and acetyl-CoA species [93,94]. The most optimum wavelength for UV detection of acyl-CoA species is in the range of 254-260 nm [63,89,90,92–97]. The detection limit for long-chain acyl-CoA esters was reported to be 12 pmol [90] while that of CoASH and short-chain acyl-CoAs were reported over a wide range of 3-12000 pmol [91–94]. The major limitation associated with methods using LC-UV detection is their inability to resolve co-eluting peaks (specificity) [63]. There might be interference from other compounds which do not belong to the acyl-CoA species at the same absorbance and retention time. To ensure that peaks detected in the chromatogram belong to CoASH or acyl-CoA species, additional experiments had to be performed. Shurubor et al. spiked CoASH and acetyl-CoA standards in the deproteinized biological samples to match them with peaks appearing in experimental samples [94]. Additionally, biological samples were subjected to acidic and enzymatic treatments to breakdown CoASH and acetyl-CoA. Since these acidic and enzymatic treatments will specifically target CoASH and acetyl-CoA peaks [85], the disappearance of their peaks will confirm their identification [94]. These additional experiments required for confirmation of acyl-CoA species in LC-UV detection increase the time required for analysis. Apart from specificity, the sensitivities of these techniques were also lower which is critical considering the low endogenous levels of acyl-CoAs. These shortcomings prompted the use of other more sensitive and specific analytical techniques.

4.2.3 Gas chromatography (GC) methods

Gas chromatography has also been employed for quantitative determination of acyl-CoAs. In GC, typically a derivatization agent is used to convert the analytes to their volatile forms for their separation and detection. Some of the studies have used sodium borohydride to convert long-chain acyl-CoA esters to their alcohol forms [98,99]. Further, these alcohols are treated with t-butyldimethylchlorosilane to form t-butyldimethylsilyl ethers and are detected with flame ionization [99] or converted to pentafluorobenzoyl ester by treating the alcohol with pentafluorobenzoyl chloride and detected with negative ion chemical ionization mass spectrometry [98]. Tamvakopoulos et al. developed a method in which acyl-CoA esters are treated with glycine, the resulting N-acyl glycinates derivatized with pentafluorobenzyl bromide to form N-acylpentafluorobenzylglycinates, which are then quantified with negative ion chemical ionization mass spectrometry [100]. Long-chain acyl-CoA esters are also detected as methyl esters by treating them with a boron trifluoride methanol reagent [101]. In another study, propionyl-CoA was detected as pentafluorobenzyl derivative mediated via the formation of N-propionylsarcosine (reaction of propionyl-CoA with sarcosine), while methylmalonyl-

CoA and succinyl-CoA were detected as tert-butyl dimethylsilyl derivatives mediated by the formation of corresponding acids [102]. Kopka et al. derivatized acyl-CoA esters with n-butyl amine thus forming acyl butylamide derivatives and the detection was performed with electron ionization mass spectrometry [103]. It has been reported in several studies that the sensitivity for detection of acyl-CoAs can be increased by use of gas chromatography-mass spectrometry [98,102,103]. The lowest detection limits of acyl-CoA esters reported by this technique were in the range (0.4-500) fmol [98,100,103]. But gas chromatography requires derivatization of acyl-CoAs which makes the method lengthy and tedious [104]. There might also be a chance of cross reactions due to the reaction of acyl chains that do not belong to the acyl-CoA group (e.g.,fatty acids), which can in turn affect the accuracy of quantitation [105].

4.2.4 Liquid chromatography-mass spectrometry (LC-MS) methods

Compared to previously reported techniques for identification and quantitation of acyl-CoA, methods using LC-MS prove to be the most effective due to their better sensitivity, resolution and high coverage compared to enzymatic assays and LC-UV detection. Additionally, they do not need the derivatization steps required for gas chromatography. The first liquid-chromatography technique used for separation of acyl-CoAs was IPRP-LC [87]. Since then, numerous liquid chromatography techniques and methods have come into use which include normal phase, hydrophilic-interaction chromatography (HILIC), 2DLC, etc.

The detection by MS can be targeted or untargeted. In targeted mass spectrometry analysis, the information about the analytes is known and method parameters (such as mass and retention time) are set based on this available information whereas in untargeted analysis, instead of pre-defining a target mass or multiple reaction monitoring (MRM) transition, an entire mass range is acquired so that the information of both known and unknown analytes present in a sample can be collected. Triple quadrupole (QqQ) and quadrupole ion traps (QTRAP) are the common instruments employed in targeted analysis, while quadrupole time of flight (QTOF) and orbitrap instruments are mostly employed for untargeted analysis. The most common fragment ion for the identification and quantitation of acyl-CoAs is the neutral loss of 507 in positive ionization mode, occurring due to the loss of 3'-phosphonucleoside diphosphate from the precursor ion **(Figure 3).**
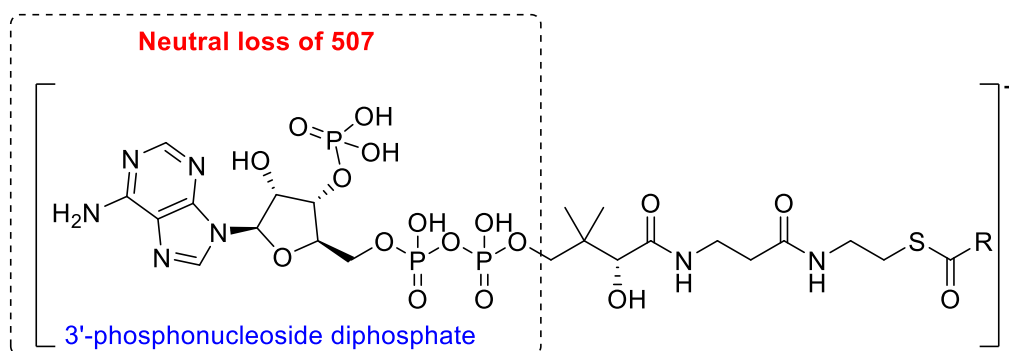
Figure 3. Neutral loss of 507 occurring due to the loss of 3'-phosphonucleoside diphosphate from precursor ion of acyl-CoAs.

Various methodologies have been used for the determination of acyl-CoAs using LC-MS. Reversed-phase liquid chromatography coupled to tandem mass spectrometry (RPLC-MS/MS) [62,104–106] has been used more frequently and is suitable for long-chain compounds. The short-chain acyl-CoAs need slightly acidic mobile phases in RPLC conditions [11,107] while long-chain acyl-CoAs have serious peak tailing problems under these conditions. Therefore, an alkaline mobile phase was preferred for long-chain acyl-CoAs [106,108,109]. Rivera et al. has summarized comprehensively the major advances in the chromatographic techniques coupled with mass spectrometry of acyl-CoA species till 2018 [62]. The upcoming sections will explain the various approaches that have been used for improving the LC-MS analytical approaches of acyl-CoAs since 2018. These approaches include ion-pairing, derivatization, native chemical ligation as well as the efforts that have been taken to improve the current existing experimental databases of these compounds. **Table 5** lists the LC-MS parameters that have been employed for the detection of CoASH and acyl-CoA species.

Table 5. LC-MS techniques employed for measurement of acyl-CoAs.

Method	Chromatography	Instrument	Targets: CoA SH (free CoA)	Short-, medium-, long- and very long-chain#	Other species*	Column	Mobile phase	Sensitivity	Reference
Method **i**	RPLC-MS/MS	QTRAP 5500 (Sciex)	✓	Short to long	Malonyl; Acetoacetyl; 3-Hydroxybutyryl; Succinyl; Glutaryl; HMG; C12:1; C14:1; C16:1; C18:1; C18:2	Waters CSH C18 (50×2.1 mm, 1.8 µm)	**Aqueous Phase:** 10 mM NH_4HCO_3 (pH 9) **Organic Phase:** ACN: H_2O (95:5)	LOD: (0.24-3.41) ng/mL LOQ: (5-10) ng/mL	[66]
Method **ii**	IPRP-LC-MS/MS	Exion UPLC (Sciex) coupled to QTRAP 6500+ (Sciex)	✓	Short to long	Malonyl; Succinyl; Glutaryl; HMG; Acetoacetyl; Crotonoyl; 3-Hydroxybutyryl; C14:1; C14:2; C15:0; C16:1; C16:2; C18:1; C18:2; C18:3; C20:1; C20:3; C20:4; C20:5; C22:6	Phenomenex Kinetex-EVO-C18 (100×2.1 mm, 1.7 µm)	**Aqueous Phase:** 0.005% TEA in 2 mmol/L CH_3COONH_4 **Organic Phase:** 0.1% TEA in ACN:H_2O (4:1)	LOD: (0.15-62.5) pg LOQ: (0.5-10)** ng/mL	[74]
Method **iii**	IPRP-LC-MS; IPRP-LC-MS/MS	1290 UHPLC system (Agilent) coupled to 6530 QTOF mass spectrometer (Agilent); LC-30A system (Shimadzu) coupled to QTRAP 6500+ (Sciex)	✓	Short to medium	Crotonoyl; Tiglyl; Acetylacetyl; Malonyl; Succinyl; Glutaryl; 3-Hydroxybutyryl; HMG; Benzoyl; Phenylacetyl	Acquity BEH C18 (100×2.1 mm, 1.7 µm)	**Aqueous Phase:** 5 mM hexylamine in H_2O (pH was adjusted to 10.2 using acetic acid) **Organic Phase:** MeOH containing 10% of 10 mM CH_3COONH_4 (pH 8.5)	NA	[69]

Method	Derivatization	Instrument	Acyl-CoA	Targets	Column	Mobile Phase	LOD/LOQ	Ref
Method **iv** IPRP-LC-MS/MS	✗	LC-20AD (Shimadzu) coupled to API 3200 triple-quadrupole mass spectrometer (Sciex)	Short: C2:0; C3:0	Malonyl; Succinyl	Waters xBridge C18 (150×2.1 mm, 3 µm)	*Aqueous Phase*: H₂O:MeOH (95:5) with 4 mM DBAA; *Organic Phase*: H₂O:ACN (25:75)	LOQ: (10-50)** ng/mL	[65]
Method **v** IPRP-LC-MS/MS	✓	1290 UHPLC (Agilent) coupled to 5500 QTRAP (Sciex)	Short: C2:0; C3:0; C5:0	Malonyl; Succinyl	Phenomenex Kinetex UHPLC C18 (150×2.1 mm, 2.6 µm)	*Aqueous Phase*: 5 mM CH₃COONH₄ with 2.5 mM DMBA (pH 5.6); *Organic Phase*: 95% ACN, 5% H₂O with 5 mM CH₃COONH₄	LOD: (1-3) pmol; LOQ: (3.7-7.4) pmol	[2]
Method **vi** Derivatization-RPLC-MS/MS	✓	1290 Infinity UHPLC system (Agilent) coupled to QTRAP 4500 (Sciex)	Short to very long	Malonyl; C18:1; C18:2; C18:3; C20:4; C20:5; C22:6	Acquity UPLC CSH C18 (100× 2.1 mm, 1.7 µm)	*Aqueous Phase*: 10 mM CH₃COONH₄; *Organic Phase*: MeOH	LOD: (1.2-4.6) nM; LOQ: (4.2-16.9) nM	[64]
Method **vii** Derivatization-RPLC-MS/MS	✗	LC-30AD UHPLC system (Shimadzu) coupled to MS-8050 mass spectrometer (Shimadzu)	Short: C2:0	Succinyl	Acquity UPLC BEH C18 (100×2.1 mm, 1.8 µm)	*Aqueous Phase*: 2 mM NH₄HCO₃; *Organic Phase*: ACN	LOD: 36 pg/mL; LOQ: 100 pg/mL	[73]

Method		Instrument		Chain length	Analytes	Column	Mobile phases	LOD	Ref.
Method **viii**	RPLC-MS/MS	Acquity UPLC I-Class system (Waters) coupled to Xevo TQ-S QqQ mass spectrometer (Waters)	✗	Short to long; very long: C22:0	Malonyl; Succinyl; Glutaryl; HMG; 3-Hydroxybutyryl; C5:1; C6:1; C7:0; C7:1; C8:1; C9:0; C9:1; C10:1; C10:2; C11:0; C11:1; C12:1; C12:2; C13:0; C13:1; C14:1; C14:2; C15:0; C15:1; C16:1; C16:2; C16:3; C17:0; C17:1; C18:1; C18:2; C18:3; C18:4; C19:0; C19:1; C20:1; C20:2; C20:3; C20:4; C20:5; C21:0; C21:1; C22:2; C22:3; C22:4; C22:5; C22:6	Acquity UPLC BEH C18 (50×1 mm, 1.7 μm)	*Aqueous Phase:* 5% ACN with 0.1% HCOOH; *Organic Phase:* 90% ACN with 0.1% HCOOH	LOD: (2-50) fmol of injected product	[70]
Method **ix**	RPLC-MS	Vanquish Flex UHPLC system (ThermoFisher Scientific) coupled to Orbitrap Fusion mass spectrometer (ThermoFisher Scientific)	✗	Short to medium	3-Hydroxypropionyl; Malonyl; Succinyl; Methylmalonyl; Glutaryl; Methylsuccinyl; Ethylmalonyl; Acetoacetyl; 3-Hydroxybutyryl; HMG; Crotonoyl; 3-Oxohexanoyl; 3-Hydroxyhexanoyl; 2-Methylbutyryl; Benzoyl; Phenylacetyl; Mesaconyl; 3-Methylmalyl; C6:1	Phenomenex Gemini C18 (150×2.0 mm, 3 μm)	*Aqueous Phase:* 10 mM $HCOONH_4$ (pH 8.1); *Organic Phase:* ACN	LOD: (100-200) fM	[68]

Method	Technique	Instrument		Chain length	Analytes	Column	Mobile phase	LOD/LOQ	Ref.
Method **x**	RPLC-MS (MS/MS data was generated in data-dependent acquisition mode)	1290 UHPLC system (Agilent) coupled to 6550 iFunnel QTOF mass spectrometer (Agilent)	✓	Short to long	Glutathione; Succinyl; 3-Hydroxybutyryl; 3-Phenylpropanoyl; 2-Methylhexanoyl; Perillyl; C14:1; C16:1 ; C18:1; C18:2; C18:3; C20:3 C20:4; C22:6	Phenomenex Kinetex C18 (100×2.1 mm, 1.7 μm)	**Aqueous Phase:** 10 mM CH_3COONH_4 **Organic Phase:** ACN	NA	[71]
Method **xi**	RPLC-MS; RPLC-MS/HRMS	Ultimate 3000 Quaternary UHPLC (ThermoFisher Scientific) coupled to Q Exactive Plus (ThermoFisher Scientific)	✗	✗	Lactoyl	Waters XBridge C18 (150×2.1 mm, 3.5 μm)	**Aqueous Phase:** 5 mM CH_3COONH_4 **Organic Phase:** ACN:H_2O (95:5) with 5 mM CH_3COONH_4	LOD: 0.2 fmol on column	[76,110]
Method **xii**	RPLC-MS/MS	Exion UPLC (Sciex) coupled to QTRAP 6500+ (Sciex)	✗	Long	C14:1; C15:0; C15:1; C16:1; C16:2; C17:0; C18:1; C18:2; C18:3; C20:1; C20:2; C20:3; C20:4; C20:5; C22:1; C22:2; C22:3; C22:4; C22:5; C22:6	NA	NA	NA	[75]
Method **xiii**	RPLC-MS/MS	Acquity UPLC system (Waters) coupled to QTRAP 6500+ (Sciex)	✗	Short: C2:0	✗	Merck Chromolith Performance RP8e (100×4.6 mm)	**Aqueous Phase:** 2.5 mM CH_3COONH_4 (pH 6.5) **Organic Phase:** ACN:IPA (98:2)	LOD: 1.95 ng/mL LOQ: 3.91 ng/mL	[72]

107

Method xiv									
RPLC-MS/MS	Ultimate 3000 LC system (ThermoFisher Scientific) coupled to QqQ TSQ Quantum Ultra (ThermoFisher Scientific)	✓	Short: C2:0; C3:0	Succinyl; Methylmalonyl	Acquity Premier HSS T3 (50×2.1 mm, 1.8 μm)	**Aqueous Phase:** 25 mM CH_3COONH_4 **Organic Phase:** ACN:H_2O (80:20) with 25 mM CH_3COONH_4	NA	[111]

✓ - included in the target list; ✗ - not included in the target list.

The common species in short-chain are C2:0-CoA; C3:0-CoA; C4:0-CoA; C5:0 CoA. Medium-chain includes C6:0-CoA; C8:0-CoA; C10:0-CoA, long-chain consists of C12:0-CoA; C14:0-CoA; C16:0-CoA; C18:0-CoA; C20:0-CoA and very-long includes C22:0-CoA and C24:0-CoA. If fewer species are observed within these chains, they are individually listed in the corresponding columns.

*Remaining acyl-CoA species as well as the unsaturated form of common short-, medium-, long- and very long-chain acyl-CoAs are mentioned under the column of other species.

**lowest value defined in the linear range of the method.

RPLC-MS/MS, reversed-phase liquid chromatography coupled to tandem mass spectrometry; IPRP-LC-MS/MS, ion-pairing reversed-phase liquid chromatography coupled to tandem mass spectrometry; LOD, limit of detection; LOQ, limit of quantitation; NH_4HCO_3, ammonium bicarbonate; ACN, acetonitrile; H_2O, (ultra-pure) water; TEA, triethylamine; CH_3COONH_4, ammonium acetate; MeOH, methanol; DBAA, dibutylamine acetate; DMBA, N,N-dimethylbutylamine; HCOOH, formic acid; $HCOONH_4$, ammonium formate; IPA, isopropanol; NA, not available.

Acyl-CoAs have negatively charged phosphate groups in their structure which are responsible for peak tailing as they can bind to the stainless steel surface of HPLC columns and tubings in the instruments [112]. One of the considerations for improving the peak shape was the use of phosphate buffers [87,113,114], that can bind to these surfaces and thus decrease the interaction between the phosphate groups of acyl-CoA moiety with column and HPLC surfaces. But these phosphate buffers, on the other hand, are non-volatile and can contaminate the mass spectrometer. Most studies performing LC-MS have used buffers with ammonium as the counter ion (such as ammonium acetate and ammonium formate) in conjunction with other strategies, such as phosphoric acid wash or other ion-pairing agents. Pearce et al. reported a simple method using reversed-phase liquid chromatography coupled to electrospray ionization tandem mass spectrometry (RPLC-ESI MS/MS) that involves a phosphoric acid wash **(Table 5, Method i)** to improve the peak shape and reduce the peak tailing and carryover problem commonly associated with acyl-CoAs [66]. The wash consists of acetonitrile: water: phosphoric acid (60:40:5 v/v/v) and was introduced during the column washing phase of each gradient cycle in 10 repeats of 50 μL injections. This method was able to semi-quantify 21 acyl-CoA species in human adenocarcinoma cells.

Ion-pairing

Lam et al. used a well-known ion-pairing reagent triethylamine (TEA) for the simultaneous quantitation of all short-, medium- and long-chain acyl-CoAs and acylcarnitines [74]. RPLC was used and TEA was incorporated in both organic and aqueous phases **(Table 5, Method ii)**. The extraction protocol of acyl-CoAs is described in **Table 3**. Acyl-CoAs were analyzed in both positive and negative mode while acylcarnitines were analyzed in positive mode. TEA maintains the pH as well as acts as an ion-pairing reagent to improve the peak shape of acyl-CoAs. This method was applied on wild-type Drosophila strain w^{1118} to estimate isotope incorporation into intra- and extra mitochondrial acyl-CoAs after being supplied with labeled fatty acids. The limits of detection were reported in the picogram (pg) range with medium- to long-chain acyl-CoAs in the range of 0.15 to 0.43 pg while short-chain acyl-CoAs were from 3.75 to 7.51 pg.

Another method using IPRP-LC coupled with mass spectrometry was reported by Hu et al. **(Table 5, Method iii)** [69]. Firstly, full scan analysis was performed on a QTOF instrument to identify retention times which were subsequently used for the construction of a quantitative structure-retention relationship model for the prediction of retention times. These measured and predicted retention times were then used to construct a scheduled multiple reaction monitoring

(sMRM) method on a QTRAP for the quantitation of metabolites. Hexylamine was used as the ion-pairing reagent. The pH of hexylamine greatly influences the MS responses and retention times of the metabolites. A pH of 10-10.3 was chosen as 80% of hexylamine is ionized at this range, which will help in the strong electrostatic interaction with the analyte. The phosphate groups on the coenzyme-A moiety are expected to be completely ionized at pH 10, resulting in the negative charge which facilitates the strong electrostatic interactions with hexylamine. Additionally, hydrophobic interactions also play a role as retention times of acyl-CoA esters increase with an increase in the acyl chain length.

Fu et al. used dibutylamine acetate (DBAA) as an ion-pairing reagent in an RPLC-ESI MS/MS method (**Table 5, Method iv**) [65]. This method was suitable to analyze short-chain acyl-CoAs such as acetyl-, malonyl-, succinyl- and propionyl-CoA simultaneously with nucleotides and pyridine dinucleotides in the positive ion mode. Various parameters such as concentration, effect on retention time and MS signal to choose the optimum concentration of DBAA were studied. Jones et al. proposed another IPRP-LC method with a simple sample preparation and simultaneous measurement of short-chain acyl-CoAs and precursors in the biosynthetic pathway of CoASH in one single run (**Table 5, Method v**) [2]. N,N-dimethylbutylamine (DMBA) as an ion-pairing reagent was added to ammonium acetate solution (pH adjusted to 5.6). 5-sulfosalicylic acid was used for sample deproteinization and extraction of acyl-CoAs as well as for their reconstitution. This eliminates the need of SPE, a well-known procedure for purification and enrichment of acyl-CoAs from mammalian cells and tissues [115–117]. Crotonoyl-CoA was found to be suitable as internal standard (IS) to control the variation during the extraction procedure.

Although ion-pairing reagents can improve the separation, they are well known for causing contamination in the mass spectrometer and deterioration of its performance over the long run. Often, dedicated instrumentation is required for ion-pairing chromatography.

Derivatization

Derivatization is another approach which assists in the separation of a broad range of acyl-CoAs without impairing the mass spectrometer's efficiency and has the following advantages while developing an acyl-CoA method:

1. Neutralizing the negative charge present on the phosphate moiety of acyl-CoAs,
2. One condition optimal for the elution of all chain length,
3. Improving the peak shape,

4. No carryover or instrument contaminations, which eliminates the need of extra washing steps after multiple injections.

Li et al. introduced the derivatization of acyl-CoAs that involves the methylation of their phosphate groups **(Figure 4)** [64]. After extraction of acyl-CoAs from biological samples **(Table 3)** the dried extracts were reconstituted in methanol followed by derivatization using tert-butyl methyl ether/methanol/water (10:3:2.5, v/v/v) and trimethylsilyl diazomethane (TMS-DM, 2 M in hexane). The methanol acts as the proton donor for the formation of *in situ* diazomethane (CH_2N_2) and CH_3OTMS **(Figure 4).**
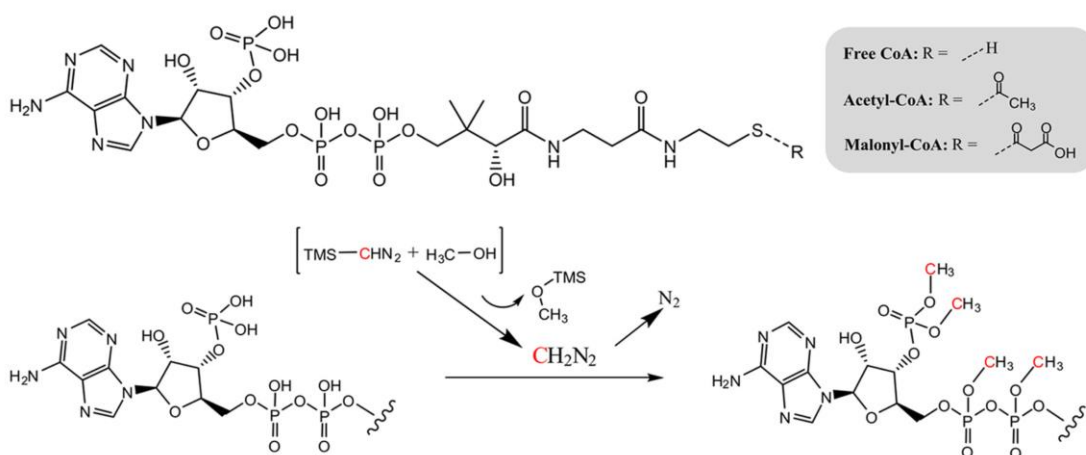
Figure 4. Phosphate methylation mechanism of acyl-CoAs using trimethylsilyl diazomethane. TMS-CHN$_2$ (TMS-DM), trimethylsilyl diazomethane; CH_3OH, methanol; CH_2N_2, diazomethane; N_2, nitrogen gas. Reprinted with permission from, Li et al. Targeted Profiling of Short-, Medium-, and Long-Chain Fatty Acyl-Coenzyme As in Biological Samples by Phosphate Methylation Coupled to Liquid Chromatography–Tandem Mass Spectrometry, Anal. Chem. 93 (2021) 4342–4350 [64], Copyright (2021).

The methylation of phosphate groups eliminates the negative charge. Different derivatization times were optimized and 30 min at ambient temperature was found to be the most suitable. After this derivatization step, the acyl-CoAs were separated by RPLC-MS/MS conditions in one single analytical run **(Table 5, Method vi)**. These methylated acyl-CoAs were stable for 48 h at 4 °C in the autosampler. Neutral loss of 507 Da is the most abundant fragment present for underivatized acyl-CoA species **(Figure 3),** but for this study a neutral loss of 563 Da was considered as all the phosphate groups of CoASH moiety were methylated (**Supplementary Figure S1**).

Another derivatization strategy was proposed with the use of 2-(diazo-methyl)-*N*-methyl-*N*-phenyl-benzamide [73]. This derivatization reaction was based on simple acid-base interactions without any requirement of catalysts. In this study, a pair of light and heavy isotope labeled, 2-

(diazo-methyl)-*N*-methyl-*N*-phenyl-benzamide and d$_5$-2-(diazo-methyl)-*N*-methyl-*N*-phenyl-benzamide were used. 2-(diazo-methyl)-*N*-methyl-*N*-phenyl-benzamide can derivatize the endogenous compounds while its d$_5$-isotope can produce the corresponding isotopic IS for accurate quantitation. The synthetic pathway of these derivatizing agents are defined by Liu et al. [118]. The derivatized internal standards were produced by treating the target standards with borate buffer and d$_5$-2-(diazo-methyl)-*N*-methyl-*N*-phenyl-benzamide. After the extraction of biological samples as specified in **Table 3**, the derivatization of endogenous compounds was performed by adding 50 mM borate buffer (pH 7) and 2-(diazo-methyl)-*N*-methyl-*N*-phenyl-benzamide in *Saccharomyces cerevisiae,* HEK-293T cells, and single rice seed while, in mouse kidney glomeruli and single *Arabidopsis thaliana* seed, this agent was directly added to the extracted samples. The reaction solution for all the matrices was vortexed and kept for the reaction for 1 h at 30 °C. The LC-MS/MS analysis was performed according to the conditions specified in **Table 5, Method vii.**

Derivatization can be quite beneficial for enhancing the sensitivity and detection of acyl-CoA compounds. But the limitations associated with it such as specificity, stability, loss of analyte, time, formation of byproduct or interference with the detection of target should be considered while developing the derivatization protocol for acyl-CoAs [119].

Increasing the acyl-CoA stability for its detection

Native chemical ligation of acyl-CoAs is a process that can spontaneously occur, acyl-CoAs can form anhydrides [9] or S-acyl glutathiones [10,11]. James et al. [70] adapted this process to stabilize and augment detection of acyl-CoAs. For this purpose, the authors developed a molecular probe CysTPP ([5-(2-amino-3-mercaptopropanoylamino)pentyl]triphenyl phosphonium) which changes acyl-CoA masses and fragmentation patterns. Incubating samples with CysTPP will cause a thioester exchange reaction generating S-acyl CysTPP intermediate, which undergoes further intramolecular rearrangement to form N-acyl CysTPP. The remaining S-acyl intermediates were removed by adding dithiothreitol (DTT) and free thiols of CysTPP and N-acyl-CysTPP were blocked by subsequent derivatization with iodoacetamide (IAM). This step will form N-acylated and S-carbamidomethylated (CAM) (N-acyl-CysTPP-CAM) as the final product. The species thus formed were considered to be stable for quantitation. With this strategy, the acyl moiety of acyl-CoAs attached to the N-terminal amine of cysteine residues were used to detect acyl-CoA thioesters **(Figure 5).** The positive charge on the TPP cation is known to enhance the MS detection [120,121] which enables the

quantitation of N-acylated CysTPP in the femtomole range. The diagnostic fragment in this case will be the neutral loss of 91 Da, arising due to the fragmentation of the relatively weak C-S bond to generate a dehydroalanine derivative. Approximately, 60 acyl-CoA species were identified *in vivo* (liver, brain, kidney and heart) with the application of this native chemical ligation technique **(Table 5, Method viii)**.
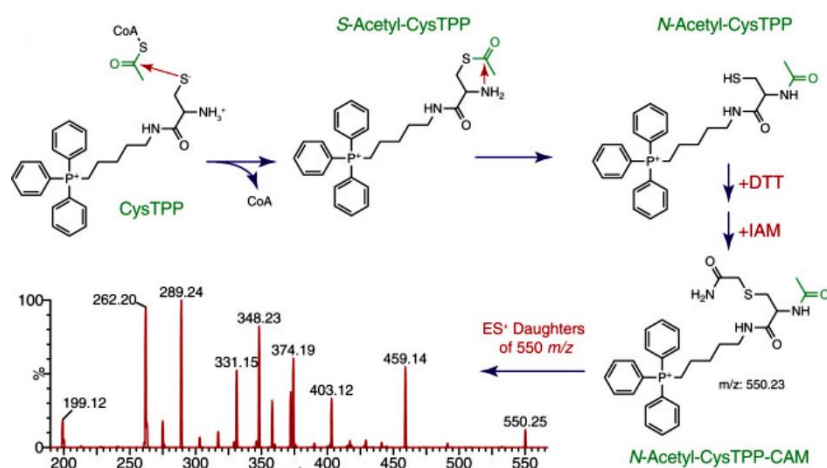

Figure 5. Detection of acetyl-CoA by CysTPP. CysTPP, [5-(2-amino-3-mercaptopropanoyl amino)pentyl]triphenylphosphonium; DTT, dithiothreitol; IAM, iodoacetamide; CAM, carbamidomethylated. Reprinted from, James et al. Native chemical ligation approach to sensitively probe tissue acyl-CoA pools, Cell Chem Biol. 29 (2022) 1232-1244.e5 [70], under the terms of the Creative Commons CC-BY license.

Expansion of current database of acyl-CoA species

Limited experimental acyl-CoA data is available in libraries such as NIST and MoNA, while ≥2000 are reported throughout the literature. These acyl-CoAs originate from conventional synthesis but also from enzyme promiscuity targeting yet unknown or unexpected carboxylic acid group containing compounds including pharmaceuticals [71]. Novel approaches are ongoing to find and identify these different acyl-CoAs to extend the experimental coverage beyond the existing databases.

Cakić et al. proposed a screening method using chromatography able to separate the isomeric species of short-chain acyl-CoAs **(Table 5, Method ix)**, including thioesters of linear and branched alkanoic acids and dicarboxylic acids **(Supplementary Figure S2)** [68]. Two detection strategies employed were based on in-source fragmentation (ISF) and data-dependent MS/MS experiments (ddMS^2) performed on a high resolution Orbitrap Fusion Tribrid mass spectrometer. For the ISF method, a full scan method was optimized to include the precursor and two major fragments, m/z 428.0365 and neutral loss of 506.9952. The precursor ions of

(unknown) acyl-CoAs with these two fragments were further evaluated on following criteria: a targeted mass trigger at m/z 428.0365, intensity filter to avoid false-positive selection and ensure MS^2 spectral quality, dynamic exclusion filter to narrow ion detection time range and limit scan repetitions, and finally targeted mass difference to confirm the neutral loss fragment. The molecular ions fulfilling all these conditions were sent for ddMS^2 scanning to (re)affirm the fragmentation pattern and accurate mass. The acyl-CoA species obtained from this screening process were incorporated in the inclusion list for targeted analysis. In the ddMS^2 method, the fragments originated from the high energy collisional dissociations scan instead of ISF. The selection criteria of molecular ions in this method were similar to the settings of the ISF experiment. Finally, the ISF method was preferred for its improved detection at lower concentrations and a list was compiled for targeted analysis. This targeted method was applied to detect targets in the degradation pathway of hexanoic acid to acetyl-CoA in betaproteobacterium "Aromatoleum" sp. strain HxN1. The extraction process of acyl-CoAs for these samples are defined in **Table 3**. In these bacterial cells, 35 species were identified, out of which eleven were confirmed by commercially available standards, thirteen by in-house synthesized standards, and eleven could not be confirmed.

To bridge the current gap between available experimental and theoretical acyl-CoA fragmentation data, Keshet et al. generated and validated an *in silico* library containing the predicted MS/MS data of unknown/hypothetical acyl-CoAs. They termed it as *in silico* CoA-Blast tandem mass spectral library and made it publicly available (github.com/urikeshet/CoA-Blast) as an online resource for annotating features in untargeted workflows [71]. The construction of the comprehensive list of *in silico* acyl-CoA compounds is described in this section. Eighteen hundred forty acyl-CoA compound structures were generated by compiling and curating targets from PubChem which contained the CoASH substructure, incorporating carboxylic acid-containing drugs to account for hypothetical acyl-CoAs and adding the odd chain fatty acyl-CoAs. Fragmentation rules were formulated using the limited existing data combined with fragmentation prediction software packages. These rules were used to model MS/MS spectra and generate predicted fragmentation patterns for these compounds in both MS polarities. The CoA-Blast MS/MS library was validated by matching spectra with the NIST MS/MS experimental library. Caution was given for the isomers as they can generate similar *in silico* MS/MS spectra. The library was further validated by acquiring MS/MS data from acyl-CoA synthetic standards in both positive and negative mode using a LC-QTOF. Apart from accurate precursor mass and MS/MS spectra, the additional dimension of retention time was

added to further strengthen the confidence of species identification. A linear regression model was developed based on the distribution coefficient (logD) of the chemical structure of the compounds. With the help of this CoA blast library, 23 acyl-CoAs (including 8 novel species) were identified in the mouse liver and annotated. **(Table 5, Method x).**

4.3 Importance of correct internal standards for absolute quantitation of acyl-CoAs

The use of an internal standard (IS) is obligatory for unstable compounds like acyl-CoAs for precise quantitation. Fu et al. highlighted the importance of using correct IS for quantitation as they can compensate for any analyte-related instability and degradation [65]. They observed degradation of >20% when neutralized extracts of acyl-CoAs were stored at room temperature for a day, degraded at -20 °C within a few days of storage or within 2 weeks of storage of acidified extracts in -80 °C. This study used labeled IS such as $[1,2-^{13}C_2]$ acetyl-CoA for the quantitation of acetyl-CoA and $[1,2,3-^{13}C_3]$ malonyl-CoA for the quantitation of malonyl, succinyl and propionyl-CoA. The ratio between analyte and IS shows that acetyl-CoA and malonyl-CoA can be quantified upto 28 days, as the rate of degradation was similar when IS used are the same as the analyte, while succinyl and propionyl-CoA show a higher variability, hence demonstrating the use of correct IS is important to compensate for degradation and to increase the useful time window for analysis **(Supplementary Figure S3)**.

Stable isotope analogs are the most suitable IS for LC-MS analysis because they have the same chemical properties as the target analytes and can be distinguished by their masses. But the chemical synthesis of labeled standards can be laborious and challenging, as it is not easy to incorporate labels at the desired site. Due to the commercial unavailability of most of the required labeled standards, structurally similar analytes are most commonly used for routine analysis. However, these IS can lead to over- or under-estimation due to different ionization efficiency in the ESI source, matrix effect, or different stabilities of the analyte and IS during the sample preparation process. Therefore, the use of isotope labeled IS is quite important for accurate estimation of these CoASH and acyl-CoA species. A fully and uniformly labeled $^{13}C(U-^{13}C)$ cell extract has been used by some studies as a potential source of IS for the quantitation of acyl-CoAs [64,107,122]. For the generation of labeled IS using this method, yeast *Pichia pastoris* was cultured on fully ^{13}C labeled glucose (sole carbon source in fed batch cultivation). This labeling strategy was not specifically targeted for CoASH and acyl-CoA thioesters, but it aimed at multiple intracellular metabolites such as organic acids, amino acids,

nucleotides, etc. As mentioned previously, acyl-CoAs are unstable molecules, hence a dedicated technique which can provide high isotopic purity for their IS is crucial.

4.3.1 SILEC for absolute quantitation of acyl-CoAs

Basu et al. developed stable isotope labeling by essential nutrients in cell culture (SILEC) for the generation of stable isotope labels for CoASH and short-chain acyl-CoA species [115,123]. SILEC leads to the generation of labeled CoASH and acyl-CoAs IS which are chemically identical, have the same stability to their corresponding endogenous CoASH and acyl-CoAs and enables their accurate quantitation as there will be parallel degradation of both unlabeled and labeled species. The approach of SILEC is based on the concept of SILAC (stable isotope labeling by amino acids in cell culture) [124], where labeled protein IS were formed by incubating cells in presence of isotope labeled essential amino acids.

Pantothenate is an essential nutrient that cannot be *de novo* synthesized by mammals and is one of the co-factors required in the cell culture medium. The biosynthetic generation of stable isotope labeled CoASH and acyl-CoAs occurs by replacing unlabeled pantothenate with labeled pantothenate ($[^{13}C_3^{15}N]$-pantothenate) in the cell culture medium (**Figure 6**). The murine hepatocytes (Hepa1c1c7) were cultured in the RPMI media containing 10% serum and $[^{13}C_3^{15}N]$-pantothenate. The serum is the major source of contamination of unlabeled pantothenate, therefore to minimize the contamination, specialized serum such as dialyzed fetal bovine serum (dFBS) or charcoal-dextran–stripped fetal bovine serum (csFBS) should be used. The labeling efficiency (ratio of unlabeled to labeled CoASH) was monitored for five passages at 0,1,3,6,12,18 and 24 h. The optimal condition for the labeling was found with a medium containing 3% csFBS and 3 mg/L $[^{13}C_3^{15}N]$-pantothenate after three passages resulting in ≥99.5% of the CoASH species being labeled, with labeling plateau achieved at 12 h. The labeling percentage was determined by equation 1.

$$\%Lmax = L/(L + U) \times 100 \qquad (1)$$

where %Lmax = fraction of labeled CoASH; L = labeled supplemented pantothenate; U = unlabeled pantothenate. The concentrations of endogenous acyl-CoA species were determined from calibration standard curves by serially diluting unlabeled CoASH and acyl-CoA species. The same concentrations of SILEC-labeled IS were spiked in the calibration curves and experimental biological samples, followed by extraction and LC-MS analysis. The area ratios (peak area of unlabeled standard to peak area of respective SILEC IS) were used to calculate the amount of each of the CoASH and acyl-CoA species in the sample.
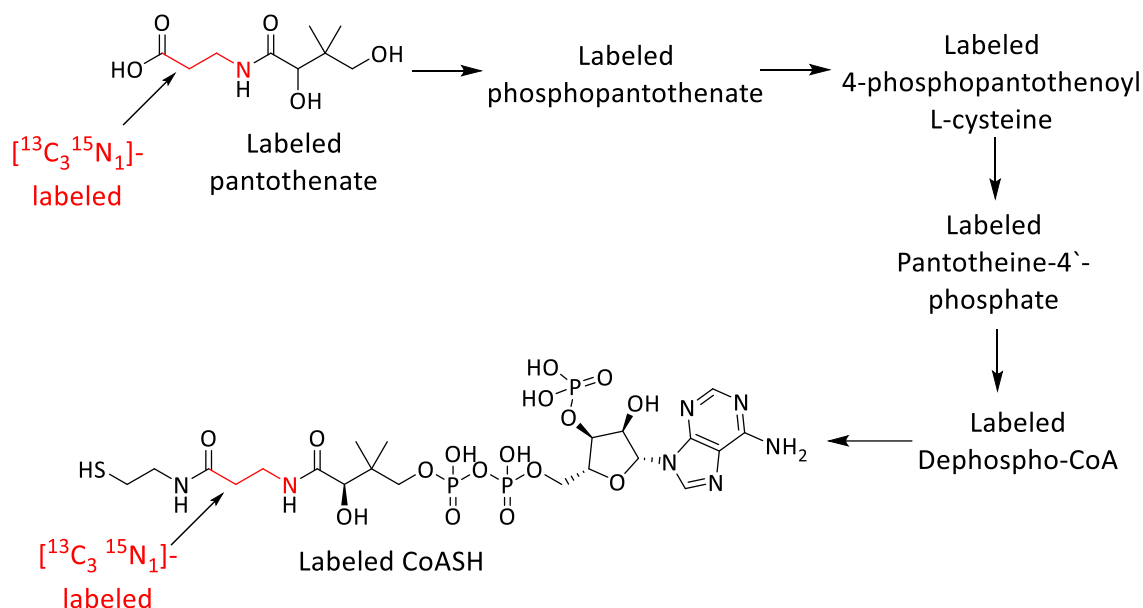
Figure 6. Metabolic pathway for biosynthesis of labeled CoASH using labeled pantothenate. The atoms marked in red are [^{13}C] and [^{15}N].
Figure is adapted from Basu et al. Stable Isotope Labeling by Essential Nutrients in Cell Culture for Preparation of Labeled Coenzyme A and Its Thioesters, Anal Chem. 83 (2011) 1363–1369. https://doi.org/10.1021/ac1027353 [115].

This assay was further expanded for the generation of stable isotope labeled medium- and long-chain acyl-CoA thioesters in Hepa1c1c7 cells by passaging cells for seven times in labeling media with 10% csFBS [6]. After establishing the labeled cell line, a 24 h passage was performed for ultra-labeling by completely removing csFBS to have the optimal acyl-CoA stable isotope labeling. Afterwards, Pan-6 deficient yeast cells were used to generate isotope labeled CoASH and acyl-CoA thioesters [125]. This yeast SILEC method was more efficient, less time consuming and more consistent as compared to mammalian SILEC method. Yeast cells can perform *de novo* biosynthesis of pantothenate. Hence, pan6 (gene responsible for synthesis of pantothenate in yeast) deficient yeast cells were used for SILEC generation. These pan6 deficient cells were cultured with [^{13}C$_3$^{15}N$_1$] pantothenic acid and was the only source for isotopically labeled pantothenate, CoASH and all the acyl-CoA thioesters. This yeast cell culture typically does not require any serum which further increases its labeling efficiency. With this technique, just after 2 days of yeast SILEC culture, ≥99% of labels were incorporated. This was a major improvement over mammalian cell culture as they have a slower growth rate compared to the yeast cells. The freeze-thaw stability of these isotope labeled standards was also tested for five cycles (each cycle was for 24 h). It was found that there was some degradation after the second cycle but after the fifth cycle, a significant degradation was

observed. This shows that calibration standard curves from the same aliquot of same batch should be considered for absolute quantitation. Many researchers have highlighted the importance of using SILEC technology for generating CoASH/acyl-CoA thioester IS [2,76,110] and have adopted this technique for carrying out the absolute quantitation in their studies [110]. The development of SILEC technology over the years has been shown in **Supplementary Figure S4.**

4.3.2 SILEC-SF: Quantitation of acyl-CoA species in subcellular compartments

Although the SILEC technology has a huge potential for defining the absolute quantities of acyl-CoAs in the biological samples, it is also important to understand the distribution of metabolites in the subcellular fractions (SF) to have deeper insight about metabolism. Trefely et al. developed another technique, SILEC-SF for quantitation of acyl-CoA thioesters in subcellular compartments [126]. SILEC has the ability to correct for many parameters such as loss of analyte, processing variation, ion-suppression and inefficient extraction. SILEC-SF technology has an added advantage for compensation of metabolic disruptions and sample losses that occur during the cell fractionation process. Using the SILEC-SF technique, the IS was included in the subcellular compartments which resulted in accurate relative quantitation of these metabolites. With this strategy, the IS was present in whole cells as well as in all the subcellular compartments after fractionation. Very distinctive profiles of acyl-CoAs were observed in the mitochondria and cytosol of cultured adipocytes, fibroblasts, mouse liver and human heart with the application of this technology.

SILEC-SF can be helpful in evaluating the acyl-CoA profiles in metabolic disorders such as FAOD at a subcellular level and thereby can assist in understanding the underlying pathophysiology by establishing a relationship between acyl-CoA supply and outcome of its metabolism.

5. Limitations in employing analytical advances for routine use of acyl-CoAs as diagnostic biomarkers

The developments of electrospray ionization and tandem mass spectrometry in 1980s and 1990s have led to rapid developments in the diagnosis of inborn errors of metabolism through the NBS program. Over the past decades, many classes of inborn errors have been included in newborn screening, as with a single injection, approximately 45 different disorders can be diagnosed [127]. Flow injection analysis-MS/MS is the most common technique that has been used for NBS. Some laboratories have started incorporating LC coupled to triple-quadrupole

mass spectrometer for expansion of the NBS as is summarized by Gelb et al. [128]. There are several methods reported for diagnosing FAOD by using LC-MS/MS, as it enables to better distinguish between compounds thus increasing the selectivity of the assays. High resolution mass spectrometers such as orbitrap, QTOF, etc. can increase the biomarker coverage as these instruments can detect a wide range of analytes and may also lead to the detection of novel metabolites. Yang and Herold summarized the current developments and advancements in the field of clinical mass spectrometry [129]. In the context of FAOD, acylcarnitines [130–133] are most commonly used as biomarkers followed by organic acids [134], acylglycines [135] and fatty acids [136,137]. The diagnosis of these FAOD at an early stage is crucial for a timely and effective therapy. Although acyl-CoAs are directly involved in the process of FAO, they are not routinely analyzed in clinics and hospitals. There are several techniques reported in literature related to LC-MS/MS for detecting and quantifying acyl-CoAs, but the problems associated with the analysis, like low endogenous level, requirement of tissue samples, instability and extreme variation in the physicochemical properties of different species, restricts their application as a biomarker for diagnosing FAOD. Measuring acyl-CoAs requires invasive sampling procedures to collect tissues or biopsies for cell culture. Few studies have reported the analysis of acyl-CoA species in human whole blood [72], platelets [138] and skin fibroblasts [56,58] but these have not been studied extensively. Another major concern associated in working with acyl-CoAs is the instability. Mostly they need a dedicated time-consuming sample preparation method and their extraction and analysis from the tissue samples should be done as soon as possible. In clinics, there is always a huge workload for sample screening and if analysis of these compounds is not performed carefully and timely, it may lead to faulty diagnosis. The well-known biomarkers of FAOD such as acylcarnitines, organic acid, acylglycines can be measured and integrated in one single method which also enables the diagnosis of other inherited metabolic disorders [139], while multiple methods or additional parameters such as ion-pairing are required to cover all acyl-CoA species, thus making the analysis more complicated.

Since analytical technologies are continuously evolving, there is a hope that in the near future, the current problems in the analysis of acyl-CoAs can be resolved. Moreover, the use of LC-MS/MS techniques enables the analysis of molecules in picomolar or even femtomolar range, which is a major advantage considering the low endogenous level of acyl-CoAs. There have been rapid and continuous advances in the analytical instrumentation and many vendors are trying their best to improve the technologies to make them user friendly.

6. Future perspectives and conclusion

Current strategies for diagnosing FAOD are based on the analysis of secondary biomarkers. Acyl-CoAs are more directly involved in the FAO pathway and are true indicators of the pathophysiology behind these disorders. Since these compounds are located intracellularly, most methods use cell or tissue samples. More research has to be performed especially on human samples to have alternative easily available matrices such as whole blood and fibroblasts, as these are easy to sample and can be more readily used for therapy monitoring. Determining the plasma levels of acylcarnitines are a routine way of diagnosing FAOD in the hospitals but the intracellular and extracellular level of metabolites may vary considerably during stress conditions. The inclusion of acyl-CoAs with the acylcarnitines in diagnosing FAOD will be of higher significance as the co-relation in profile of these compounds can help in understanding the pathophysiology behind FAOD.

A reference range has to be established from healthy individuals and should include representative subjects with a range of body mass index, age, gender, lifestyles, etc. as well as different metabolic stages such as fed and fasted state. LC-MS is clearly the most appropriate technique for sensitivity and selectivity. More efforts can be done in improving the chromatographic approaches like employing HILIC chromatography instead of using an ion-pairing reagent (can cause contamination in the mass spectrometers and subsequently diminish their performance) or two types of chromatography (lengthy and tedious approach). HILIC chromatography is more appropriate for polar compounds like acyl-CoAs. Although some of the earlier reported studies have used combinations of HILIC and reversed-phase chromatography for the coverage of a wide range of chain lengths of acyl-CoA compounds, future developments should be in the direction of using a single column and one method for comprehensively covering all side chains of acyl-CoAs. Zwitterionic stationary phase HILIC columns can be tried for their efficiency in analyzing acyl-CoA compounds. Chemical ligation is another interesting way to analyze these compounds. Implementation of SILEC in assays can further strengthen the absolute quantitation for acyl-CoAs. Creation of new libraries can help to extend databases for identification and confirmation of new species arising due to enzyme promiscuity. Once a standard protocol is established for routine analysis of these compounds, then clinicians and researchers should come together for the full integration of these techniques in the routine clinical practice. Developing a deeper understanding about the acyl-CoAs as biomarkers of FAOD can be of significant importance and has a huge potential in characterizing these disorders.

In this review, we have highlighted the analytical techniques that have been developed in the past few years for analyzing acyl-CoAs. Clearly, a lot of progress has been made, however more studies are required particularly focusing on ways to increase the stability and simplifying the analytical strategies of these compounds. These methodologies can not only be beneficial for FAOD but for other metabolic diseases, cancer, etc. The correlation of acyl-CoAs with other metabolites can also be helpful in predicting the different metabolic pathways involved in various other disorders.

Author contributions

Madhulika Singh: Conceptualization, Writing-original draft and editing; Hyung L. Elfrink: Writing-Review & editing; Amy C. Harms: Supervision, Review & editing; Thomas Hankemeier: Funding acquisition, Supervision, Review & editing. The manuscript was written through contributions of all authors. All authors have given approval to the final version of the manuscript.

Acknowledgements

References

[1]   R. Leonardi, Y.-M. Zhang, C.O. Rock, S. Jackowski, Coenzyme A: back in action, Prog Lipid Res. 44 (2005) 125–153. https://doi.org/10.1016/j.plipres.2005.04.001.

[2]   A.E. Jones, N.J. Arias, A. Acevedo, S.T. Reddy, A.S. Divakaruni, D. Meriwether, A Single LC-MS/MS Analysis to Quantify CoA Biosynthetic Intermediates and Short-Chain Acyl CoAs, Metabolites. 11 (2021) 468. https://doi.org/10.3390/metabo11080468.

[3]   T. Sanvictores, S. Chauhan, Vitamin B5 (Pantothenic Acid), in: StatPearls, StatPearls Publishing, Treasure Island (FL), 2023. http://www.ncbi.nlm.nih.gov/books/NBK563233/ (accessed April 3, 2023).

[4]   E.P. Brass, Overview of coenzyme A metabolism and its role in cellular toxicity, Chemico-Biological Interactions. 90 (1994) 203–214. https://doi.org/10.1016/0009-2797(94)90010-8.

[5]   T.J. Grevengoed, E.L. Klett, R.A. Coleman, Acyl-CoA Metabolism and Partitioning, Annu Rev Nutr. 34 (2014) 1–30. https://doi.org/10.1146/annurev-nutr-071813-105541.

[6]   N.W. Snyder, S.S. Basu, Z. Zhou, A.J. Worth, I.A. Blair, Stable isotope dilution liquid chromatography-mass spectrometry analysis of cellular and tissue medium- and long-chain acyl-coenzyme A thioesters, Rapid Commun Mass Spectrom. 28 (2014) 1840–1848. https://doi.org/10.1002/rcm.6958.

[7]   X. Yang, Y. Ma, N. Li, H. Cai, M.G. Bartlett, Development of a Method for the Determination of Acyl-CoA Compounds by Liquid Chromatography Mass Spectrometry to Probe the Metabolism of Fatty Acids, Anal Chem. 89 (2017) 813–821. https://doi.org/10.1021/acs.analchem.6b03623.

[8]   P. Zhu, T. Oe, I.A. Blair, Determination of cellular redox status by stable isotope dilution liquid chromatography/mass spectrometry analysis of glutathione and glutathione disulfide, Rapid Commun Mass Spectrom. 22 (2008) 432–440. https://doi.org/10.1002/rcm.3380.

[9]   G.R. Wagner, D.P. Bhatt, T.M. O'Connell, J.W. Thompson, L.G. Dubois, D.S. Backos, H. Yang, G.A. Mitchell, O.R. Ilkayeva, R.D. Stevens, P.A. Grimsrud, M.D. Hirschey, A Class of Reactive Acyl-CoA Species Reveals the Non-Enzymatic Origins of Protein Acylation, Cell Metab. 25 (2017) 823-837.e8. https://doi.org/10.1016/j.cmet.2017.03.006.

[10]   A.M. James, K. Hoogewijs, A. Logan, A.R. Hall, S. Ding, I.M. Fearnley, M.P. Murphy, Non-enzymatic N-acetylation of Lysine Residues by AcetylCoA Often Occurs via a Proximal S-acetylated Thiol Intermediate Sensitive to Glyoxalase II, Cell Rep. 18 (2017) 2105–2112. https://doi.org/10.1016/j.celrep.2017.02.018.

[11]   X. Liu, S. Sadhukhan, S. Sun, G.R. Wagner, M.D. Hirschey, L. Qi, H. Lin, J.W. Locasale, High-Resolution Metabolomics with Acyl-CoA Profiling Reveals Widespread Remodeling in Response to Diet, Mol Cell Proteomics. 14 (2015) 1489–1500. https://doi.org/10.1074/mcp.M114.044859.

[12]   L. Mignani, B. Gnutti, D. Zizioli, D. Finazzi, Coenzyme a Biochemistry: From Neurodevelopment to Neurodegeneration, Brain Sci. 11 (2021) 1031. https://doi.org/10.3390/brainsci11081031.

[13]   T. Migita, K. Takayama, T. Urano, D. Obinata, K. Ikeda, T. Soga, S. Takahashi, S. Inoue, ACSL3 promotes intratumoral steroidogenesis in prostate cancer cells, Cancer Sci. 108 (2017) 2011–2021. https://doi.org/10.1111/cas.13339.

[14]   S. Zhang, O.D. Nelson, I.R. Price, C. Zhu, X. Lu, I.R. Fernandez, R.S. Weiss, H. Lin, Long-chain fatty acyl coenzyme A inhibits NME1/2 and regulates cancer metastasis, Proceedings of the National Academy of Sciences. 119 (2022) e2117013119. https://doi.org/10.1073/pnas.2117013119.

[15]   S. Jackowski, R. Leonardi, Deregulated Coenzyme A, Loss of Metabolic Flexibility and Diabetes, Biochem Soc Trans. 42 (2014) 1118–1122. https://doi.org/10.1042/BST20140156.

[16]   J.E. Kanter, F. Kramer, S. Barnhart, M.M. Averill, A. Vivekanandan-Giri, T. Vickery, L.O. Li, L. Becker, W. Yuan, A. Chait, K.R. Braun, S. Potter-Perigo, S. Sanda, T.N. Wight, S. Pennathur, C.N. Serhan, J.W. Heinecke, R.A. Coleman, K.E. Bornfeldt, Diabetes promotes an inflammatory macrophage phenotype and atherosclerosis through acyl-CoA synthetase 1, Proceedings of the National Academy of Sciences. 109 (2012) E715–E724. https://doi.org/10.1073/pnas.1111600109.

[17]   C.C.C.R. De Carvalho, M.J. Caramujo, The Various Roles of Fatty Acids, Molecules. 23 (2018) 2583. https://doi.org/10.3390/molecules23102583.

[18]   C. Subramanian, J. Yao, M.W. Frank, C.O. Rock, S. Jackowski, A pantothenate kinase-deficient mouse model reveals a gene expression program associated with brain coenzyme a reduction, Biochimica et Biophysica Acta (BBA) - Molecular Basis of Disease. 1866 (2020) 165663. https://doi.org/10.1016/j.bbadis.2020.165663.

[19]   S.M. Houten, S. Violante, F.V. Ventura, R.J.A. Wanders, The Biochemistry and Physiology of Mitochondrial Fatty Acid β-Oxidation and Its Genetic Disorders, Annual Review of Physiology. 78 (2016) 23–44. https://doi.org/10.1146/annurev-physiol-021115-105045.

[20]   J.L. Merritt, E. MacLeod, A. Jurecka, B. Hainline, Clinical manifestations and management of fatty acid oxidation disorders, Rev Endocr Metab Disord. 21 (2020) 479–493. https://doi.org/10.1007/s11154-020-09568-3.

[21]   S.M. Houten, R.J.A. Wanders, A general introduction to the biochemistry of mitochondrial fatty acid β-oxidation, J Inherit Metab Dis. 33 (2010) 469–477. https://doi.org/10.1007/s10545-010-9061-2.

[22]   G.P. Mannaerts, P.P. Van Veldhoven, [Peroxisomal beta-oxidation], Verh K Acad Geneeskd Belg. 55 (1993) 45–78.

[23]   J. Demarquoy, F. Le Borgne, Crosstalk between mitochondria and peroxisomes, World J Biol Chem. 6 (2015) 301–309. https://doi.org/10.4331/wjbc.v6.i4.301.

[24]   W.-H. Kunau, V. Dommes, H. Schulz, β-Oxidation of fatty acids in mitochondria, peroxisomes, and bacteria: A century of continued progress, Progress in Lipid Research. 34 (1995) 267–342. https://doi.org/10.1016/0163-7827(95)00011-9.

[25]   P. Rinaldo, D. Matern, M.J. Bennett, Fatty Acid Oxidation Disorders, Annual Review of Physiology. 64 (2002) 477–502. https://doi.org/10.1146/annurev.physiol.64.082201.154705.

[26]   G.F. Cahill, R.L. Veech, Ketoacids? Good medicine?, Trans Am Clin Climatol Assoc. 114 (2003) 149–163.

[27]   G.F. Cahill, Fuel metabolism in starvation, Annu Rev Nutr. 26 (2006) 1–22. https://doi.org/10.1146/annurev.nutr.26.061505.111258.

[28]   E. Vargas, N.V. Joy, M.A. Carrillo Sepulveda, Biochemistry, Insulin Metabolic Effects, in: StatPearls, StatPearls Publishing, Treasure Island (FL), 2023. http://www.ncbi.nlm.nih.gov/books/NBK525983/ (accessed March 31, 2023).

[29]   M. Dashty Rahmatabady, A quick look at biochemistry: Carbohydrate metabolism, Clinical Biochemistry. 46 (2013). https://doi.org/10.1016/j.clinbiochem.2013.04.027.

[30]   L. Rui, Energy Metabolism in the Liver, Compr Physiol. 4 (2014) 177–197. https://doi.org/10.1002/cphy.c130024.

[31]   T. Hashimoto, W.S. Cook, C. Qi, A.V. Yeldandi, J.K. Reddy, M.S. Rao, Defect in Peroxisome Proliferator-activated Receptor α-inducible Fatty Acid Oxidation Determines the Severity of Hepatic Steatosis in Response to Fasting*, Journal of Biological Chemistry. 275 (2000) 28918–28928. https://doi.org/10.1074/jbc.M910350199.

[32]   M.J. Bennett, P. Rinaldo, A.W. Strauss, Inborn errors of mitochondrial fatty acid oxidation, Crit Rev Clin Lab Sci. 37 (2000) 1–44. https://doi.org/10.1080/10408360091174169.

[33]   I.M.S. Guerra, H.B. Ferreira, T. Melo, H. Rocha, S. Moreira, L. Diogo, M.R. Domingues, A.S.P. Moreira, Mitochondrial Fatty Acid β-Oxidation Disorders: From Disease to Lipidomic Studies—A Critical Review, Int J Mol Sci. 23 (2022) 13933. https://doi.org/10.3390/ijms232213933.

[34]   K.G. Sim, J. Hammond, B. Wilcken, Strategies for the diagnosis of mitochondrial fatty acid β-oxidation disorders, Clinica Chimica Acta. 323 (2002) 37–58. https://doi.org/10.1016/S0009-8981(02)00182-1.

[35]   L. Console, M. Scalise, N. Giangregorio, A. Tonazzi, M. Barile, C. Indiveri, The Link Between the Mitochondrial Fatty Acid Oxidation Derangement and Kidney Injury, Frontiers in Physiology. 11 (2020). https://www.frontiersin.org/articles/10.3389/fphys.2020.00794 (accessed August 16, 2023).

[36]   M.M. Adeva-Andany, N. Carneiro-Freire, M. Seco-Filgueira, C. Fernández-Fernández, D. Mouriño-Bayolo, Mitochondrial β-oxidation of saturated fatty acids in humans, Mitochondrion. 46 (2019) 73–90. https://doi.org/10.1016/j.mito.2018.02.009.

[37]   J.D. McGarry, N.F. Brown, The mitochondrial carnitine palmitoyltransferase system. From concept to molecular analysis, Eur J Biochem. 244 (1997) 1–14. https://doi.org/10.1111/j.1432-1033.1997.00001.x.

[38]   D.W. Foster, The Role of the Carnitine System in Human Metabolism, Annals of the New York Academy of Sciences. 1033 (2004) 1–16. https://doi.org/10.1196/annals.1320.001.

[39]   P. Ruiz-Sala, L. Peña-Quintana, Biochemical Markers for the Diagnosis of Mitochondrial Fatty Acid Oxidation Diseases, Journal of Clinical Medicine. 10 (2021) 4855. https://doi.org/10.3390/jcm10214855.

[40]   J.T. Talley, S.S. Mohiuddin, Biochemistry, Fatty Acid Oxidation, in: StatPearls, StatPearls Publishing, Treasure Island (FL), 2023. http://www.ncbi.nlm.nih.gov/books/NBK556002/ (accessed March 31, 2023).

[41]   G. Villani, G. Gallo, E. Scolamiero, F. Salvatore, M. Ruoppolo, "Classical organic acidurias": diagnosis and pathogenesis, Clinical and Experimental Medicine. 17 (2017). https://doi.org/10.1007/s10238-016-0435-0.

[42]   J.K. Hiltunen, Y.-M. Qin, β-Oxidation – strategies for the metabolism of a wide variety of acyl-CoA esters, Biochimica et Biophysica Acta (BBA) - Molecular and Cell Biology of Lipids. 1484 (2000) 117–128. https://doi.org/10.1016/S1388-1981(00)00013-5.

[43]   H. Schulz, W.-H. Kunau, Beta-oxidation of unsaturated fatty acids: a revised pathway, Trends in Biochemical Sciences. 12 (1987) 403–406. https://doi.org/10.1016/0968-0004(87)90196-4.

[44]   L. Laffel, Ketone bodies: a review of physiology, pathophysiology and application of monitoring to diabetes, Diabetes/Metabolism Research and Reviews. 15 (1999) 412–426. https://doi.org/10.1002/(SICI)1520-7560(199911/12)15:6<412::AID-DMRR72>3.0.CO;2-8.

[45]   V.A. Vishwanath, Fatty Acid Beta-Oxidation Disorders: A Brief Review, Ann Neurosci. 23 (2016) 51–55. https://doi.org/10.1159/000443556.

[46]   J.L. Merritt, M. Norris, S. Kanungo, Fatty acid oxidation disorders, Ann Transl Med. 6 (2018) 473. https://doi.org/10.21037/atm.2018.10.57.

[47]   Newborn screening: toward a uniform screening panel and system, Genet Med. 8 Suppl 1 (2006) 1S-252S. https://doi.org/10.1097/01.gim.0000223891.82390.ad.

[48]   A. Aynsley-Green, Hypoglycaemia in infants and children, Clin Endocrinol Metab. 11 (1982) 159–194. https://doi.org/10.1016/s0300-595x(82)80041-8.

[49]   R.S. Pildes, D.A. Patel, M. Nitzan, Glucose disappearance rate in symptomatic neonatal hypoglycemia, Pediatrics. 52 (1973) 75–82.

[50]   D.M. Bier, R.D. Leake, M.W. Haymond, K.J. Arnold, L.D. Gruenke, M.A. Sperling, D.M. Kipnis, Measurement of "true" glucose production rates in infancy and childhood with 6,6-dideuteroglucose, Diabetes. 26 (1977) 1016–1023. https://doi.org/10.2337/diab.26.11.1016.

[51]   E.S. Goetzman, Advances in the Understanding and Treatment of Mitochondrial Fatty Acid Oxidation Disorders, Curr Genet Med Rep. 5 (2017) 132–142. https://doi.org/10.1007/s40142-017-0125-6.

[52] N. Longo, C.A. di San Filippo, M. Pasquali, DISORDERS OF CARNITINE TRANSPORT AND THE CARNITINE CYCLE, Am J Med Genet C Semin Med Genet. 142C (2006) 77–85. https://doi.org/10.1002/ajmg.c.30087.

[53] A.A. Palladino, J. Chen, S. Kallish, C.A. Stanley, M.J. Bennett, Measurement of tissue acyl-CoAs using flow-injection tandem mass spectrometry: acyl-CoA profiles in short-chain fatty acid oxidation defects, Molecular Genetics and Metabolism. 107 (2012) 679–683. https://doi.org/10.1016/j.ymgme.2012.10.007.

[54] N. Longo, M. Frigeni, M. Pasquali, Carnitine transport and fatty acid oxidation, Biochimica et Biophysica Acta (BBA) - Molecular Cell Research. 1863 (2016) 2422–2435. https://doi.org/10.1016/j.bbamcr.2016.01.023.

[55] R.J.A. Wanders, G. Visser, S. Ferdinandusse, F.M. Vaz, R.H. Houtkooper, Mitochondrial Fatty Acid Oxidation Disorders: Laboratory Diagnosis, Pathogenesis, and the Complicated Route to Treatment, J Lipid Atheroscler. 9 (2020) 313–333. https://doi.org/10.12997/jla.2020.9.3.313.

[56] C.S. Tamvakopoulos, S. Willi, V.E. Anderson, D.E. Hale, Long-Chain Acyl-CoA Profiles in Cultured Fibroblasts from Patients with Defects in Fatty Acid Oxidation, Biochemical and Molecular Medicine. 55 (1995) 15–21. https://doi.org/10.1006/bmme.1995.1026.

[57] M. Pourfarzam, J. Schaefer, D.M. Turnbull, K. Bartlett, Analysis of fatty acid oxidation intermediates in cultured fibroblasts to detect mitochondrial oxidation disorders, Clinical Chemistry. 40 (1994) 2267–2275. https://doi.org/10.1093/clinchem/40.12.2267.

[58] R.S. Kler, S. Jackson, K. Bartlett, L.A. Bindoff, S. Eaton, M. Pourfarzam, F.E. Frerman, S.I. Goodman, N.J. Watmough, D.M. Turnbull, Quantitation of acyl-CoA and acylcarnitine esters accumulated during abnormal mitochondrial fatty acid oxidation, J Biol Chem. 266 (1991) 22932–22938.

[59] E. Martins, M.L. Cardoso, E. Rodrigues, C. Barbot, A. Ramos, M.J. Bennett, E.L. Teles, L. Vilarinho, Short-chain 3-hydroxyacyl-CoA dehydrogenase deficiency: the clinical relevance of an early diagnosis and report of four new cases, Journal of Inherited Metabolic Disease. 34 (2011) 835–842. https://doi.org/10.1007/s10545-011-9287-7.

[60] H. Yang, D. Yu, Clinical, biochemical and metabolic characterization of patients with short-chain enoyl-CoA hydratase(ECHS1) deficiency: two case reports and the review of the literature, BMC Pediatrics. 20 (2020) 50. https://doi.org/10.1186/s12887-020-1947-z.

[61] X.-Y. He, S.-Y. Yang, 3-hydroxyacyl-CoA dehydrogenase (HAD) deficiency replaces short-chain hydroxyacyl-CoA dehydrogenase (SCHAD) deficiency as well as medium- and short-chain hydroxyacyl-CoA dehydrogenase (M/SCHAD) deficiency as the consensus name of this fatty acid oxidation disorder, Mol Genet Metab. 91 (2007) 205–206. https://doi.org/10.1016/j.ymgme.2007.02.015.

[62] L.G. Rivera, M.G. Bartlett, Chromatographic methods for the determination of acyl-CoAs, Anal. Methods. 10 (2018) 5252–5264. https://doi.org/10.1039/C8AY01472H.

[63] J. Deutsch, E. Grange, S.I. Rapoport, A.D. Purdon, Isolation and quantitation of long-chain acyl-coenzyme A esters in brain tissue by solid-phase extraction, Anal Biochem. 220 (1994) 321–323. https://doi.org/10.1006/abio.1994.1344.

[64] P. Li, M. Gawaz, M. Chatterjee, M. Lämmerhofer, Targeted Profiling of Short-, Medium-, and Long-Chain Fatty Acyl-Coenzyme As in Biological Samples by Phosphate Methylation Coupled to Liquid Chromatography–Tandem Mass Spectrometry, Anal. Chem. 93 (2021) 4342–4350. https://doi.org/10.1021/acs.analchem.1c00664.

[65] X. Fu, S. Deja, B. Kucejova, J.A.G. Duarte, J.G. McDonald, S.C. Burgess, Targeted Determination of Tissue Energy Status by LC-MS/MS, Anal. Chem. 91 (2019) 5881–5887. https://doi.org/10.1021/acs.analchem.9b00217.

[66] R.W. Pearce, J.V. Kodger, Y.I. Sandlers, A liquid chromatography tandem mass spectrometry method for a semiquantitative screening of cellular acyl-CoA, Analytical Biochemistry. 640 (2022) 114430. https://doi.org/10.1016/j.ab.2021.114430.

[67] Y. Tsuchiya, U. Pham, I. Gout, Methods for measuring CoA and CoA derivatives in biological samples, Biochem Soc Trans. 42 (2014) 1107–1111. https://doi.org/10.1042/BST20140123.

[68] N. Cakić, B. Kopke, R. Rabus, H. Wilkes, Suspect screening and targeted analysis of acyl coenzyme A thioesters in bacterial cultures using a high-resolution tribrid mass spectrometer, Anal Bioanal Chem. 413 (2021) 3599–3610. https://doi.org/10.1007/s00216-021-03318-3.

[69] Q. Hu, Y. Sun, P. Yuan, H. Lei, H. Zhong, Y. Wang, H. Tang, Quantitative structure-retention relationship for reliable metabolite identification and quantification in metabolomics using ion-pair reversed-phase chromatography coupled with tandem mass spectrometry, Talanta. 238 (2022) 123059. https://doi.org/10.1016/j.talanta.2021.123059.

[70] A.M. James, A.A.I. Norman, J.W. Houghton, H.A. Prag, A. Logan, R. Antrobus, R.C. Hartley, M.P. Murphy, Native chemical ligation approach to sensitively probe tissue acyl-CoA pools, Cell Chem Biol. 29 (2022) 1232-1244.e5. https://doi.org/10.1016/j.chembiol.2022.04.005.

[71]   U. Keshet, T. Kind, X. Lu, S. Devi, O. Fiehn, Acyl-CoA Identification in Mouse Liver Samples Using the In Silico CoA-Blast Tandem Mass Spectral Library, Anal. Chem. 94 (2022) 2732–2739. https://doi.org/10.1021/acs.analchem.1c03272.

[72]   R. Speziale, C. Montesano, M.L. De Leonibus, F. Bonelli, P. Fezzardi, M.G. Beconi, E. Monteagudo, D. Elbaum, L. Orsatti, Determination of acetyl coenzyme A in human whole blood by ultra-performance liquid chromatography-mass spectrometry, Journal of Chromatography B. 1083 (2018) 57–62. https://doi.org/10.1016/j.jchromb.2018.02.039.

[73]   S. Li, Y.-Y. Chen, T.-T. Ye, Q.-F. Zhu, Y.-Q. Feng, Chemical isotope labeling assisted liquid chromatography-mass spectrometry method for simultaneous analysis of central carbon metabolism intermediates, Journal of Chromatography A. 1702 (2023) 464083. https://doi.org/10.1016/j.chroma.2023.464083.

[74]   S.M. Lam, T. Zhou, J. Li, S. Zhang, G.H. Chua, B. Li, G. Shui, A robust, integrated platform for comprehensive analyses of acyl-coenzyme As and acyl-carnitines revealed chain length-dependent disparity in fatty acyl metabolic fates across Drosophila development, Science Bulletin. 65 (2020) 1840–1848. https://doi.org/10.1016/j.scib.2020.07.023.

[75]   M. Wang, Y. Su, C. Hou, K. Ren, X. Liu, S. Zhao, Y. Wang, X. Liu, Targeted lipidomics analysis of lysine 179 acetylation of ACSF2 in rat hepatic stellate cells, Prostaglandins Other Lipid Mediat. 163 (2022) 106671. https://doi.org/10.1016/j.prostaglandins.2022.106671.

[76]   E.L. Varner, S. Trefely, D. Bartee, E. von Krusenstiern, L. Izzo, C. Bekeova, R.S. O'Connor, E.L. Seifert, K.E. Wellen, J.L. Meier, N.W. Snyder, Quantification of lactoyl-CoA (lactyl-CoA) by liquid chromatography mass spectrometry in mammalian cells and tissues, Open Biol. 10 (2020) 200187. https://doi.org/10.1098/rsob.200187.

[77]   L.L. Bieber, Quantitation of CoASH and Acyl-CoA, Analytical Biochemistry. 204 (1992) 228–230. https://doi.org/10.1016/0003-2697(92)90231-U.

[78]   P.B. Garland, Some kinetic properties of pig-heart oxoglutarate dehydrogenase that provide a basis for metabolic control of the enzyme activity and also a stoicheiometric assay for coenzyme A in tissue extracts, Biochem J. 92 (1964) 10C-12C. https://doi.org/10.1042/bj0920010c.

[79]   P.B. Garland, D. Shepherd, D.W. Yates, Steady-state concentrations of coenzyme A, acetyl-coenzyme A and long-chain fatty acyl-coenzyme A in rat-liver mitochondria oxidizing palmitate, Biochem J. 97 (1965) 587–594. https://doi.org/10.1042/bj0970587.

[80]   J.D. McGarry, M.J. Stark, D.W. Foster, Hepatic malonyl-CoA levels of fed, fasted and diabetic rats as measured using a simple radioisotopic assay., Journal of Biological Chemistry. 253 (1978) 8291–8293. https://doi.org/10.1016/S0021-9258(17)34394-6.

[81]   N. ALAM, E.D. SAGGERSON, Malonyl-CoA and the regulation of fatty acid oxidation in soleus muscle, Biochemical Journal. 334 (1998) 233–241. https://doi.org/10.1042/bj3340233.

[82]   D. Rabier, P. Briand, F. Petit, P. Kamoun, L. Cathelineau, Radioisotopic assay of picomolar amounts of coenzyme A, Analytical Biochemistry. 134 (1983) 325–329. https://doi.org/10.1016/0003-2697(83)90305-6.

[83]   J.B. Allred, D.G. Guy, Determination of coenzyme A and acetyl CoA in tissue extracts, Anal Biochem. 29 (1969) 293–299. https://doi.org/10.1016/0003-2697(69)90312-1.

[84]   A. Szutowicz, H. Bielarczyk, Elimination of CoASH interference from acetyl-CoA cycling assay by maleic anhydride, Analytical Biochemistry. 164 (1987) 292–296. https://doi.org/10.1016/0003-2697(87)90495-7.

[85]   T. Kato, CoA cycling: An enzymatic amplification method for determination of CoASH and acetyl CoA, Analytical Biochemistry. 66 (1975) 372–392. https://doi.org/10.1016/0003-2697(75)90605-3.

[86]   Y. Takamura, Y. Kitayama, A. Arakawa, S. Yamanaka, M. Tosaki, Y. Ogawa, Malonyl-CoA: acetyl-CoA cycling. A new micromethod for determination of acyl-CoAs with malonate decarboxylase, Biochimica et Biophysica Acta (BBA) - Lipids and Lipid Metabolism. 834 (1985) 1–7. https://doi.org/10.1016/0005-2760(85)90170-5.

[87]   Fred.C. Baker, D.A. Schooley, Analysis and purification of acyl coenzyme A thioesters by reversed-phase ion-pair liquid chromatography, Analytical Biochemistry. 94 (1979) 417–424. https://doi.org/10.1016/0003-2697(79)90384-1.

[88]   O. Rabin, J. Deutsch, E. Grange, K.D. Pettigrew, M.C.J. Chang, S.I. Rapoport, A.D. Purdon, Changes in Cerebral Acyl-CoA Concentrations Following Ischemia-Reperfusion in Awake Gerbils, Journal of Neurochemistry. 68 (1997) 2111–2118. https://doi.org/10.1046/j.1471-4159.1997.68052111.x.

[89]   J. Rosendal, J. Knudsen, A fast and versatile method for extraction and quantitation of long-chain acyl-CoA esters from tissue: Content of individual long-chain acyl-CoA esters in various tissues from fed rat, Analytical Biochemistry. 207 (1992) 63–67. https://doi.org/10.1016/0003-2697(92)90500-7.

[90]   M.J. Mangino, J. Zografakis, M.K. Murphy, C.B. Anderson, Improved and simplified tissue extraction method for quantitating long-chain acyl-coenzyme A thioesters with picomolar detection using high-

performance liquid chromatography, Journal of Chromatography B: Biomedical Sciences and Applications. 577 (1992) 157–162. https://doi.org/10.1016/0378-4347(92)80612-T.

[91]   J. Deutsch, S.I. Rapoport, T.A. Rosenberger, Coenzyme A and Short-Chain Acyl-CoA Species in Control and Ischemic Rat Brain, Neurochem Res. 27 (2002) 1577–1582. https://doi.org/10.1023/A:1021614422668.

[92]   A. Demoz, A. Garras, D.K. Asiedu, B. Netteland, R.K. Berge, Rapid method for the separation and detection of tissue short-chain coenzyme A esters by reversed-phase high-performance liquid chromatography, Journal of Chromatography B: Biomedical Sciences and Applications. 667 (1995) 148–152. https://doi.org/10.1016/0378-4347(94)00595-V.

[93]   K. Shibata, T. Nakai, T. Fukuwatari, Simultaneous high-performance liquid chromatography determination of coenzyme A, dephospho-coenzyme A, and acetyl-coenzyme A in normal and pantothenic acid-deficient rats, Analytical Biochemistry. 430 (2012) 151–155. https://doi.org/10.1016/j.ab.2012.08.010.

[94]   Y.I. Shurubor, M. D'Aurelio, J. Clark-Matott, E.P. Isakova, Y.I. Deryabina, M.F. Beal, A.J.L. Cooper, B.F. Krasnikov, Determination of Coenzyme A and Acetyl-Coenzyme A in Biological Samples Using HPLC with UV Detection, Molecules. 22 (2017) 1388. https://doi.org/10.3390/molecules22091388.

[95]   H.F. Sobhi, P.E. Minkler, C.L. Hoppel, Synthesis and characterization of cis-4-decenoyl-CoA, 3-phenylpropionyl-CoA, and 2,6-dimethylheptanoyl-CoA, Analytical Biochemistry. 401 (2010) 114–124. https://doi.org/10.1016/j.ab.2010.02.026.

[96]   B.E. Corkey, Analysis of acyl-coenzyme A esters in biological samples, Methods Enzymol. 166 (1988) 55–70. https://doi.org/10.1016/s0076-6879(88)66011-3.

[97]   L. Abrankó, G. Williamson, S. Gardner, A. Kerimi, Comprehensive quantitative analysis of fatty-acyl-Coenzyme A species in biological samples by ultra-high performance liquid chromatography–tandem mass spectrometry harmonizing hydrophilic interaction and reversed phase chromatography, Journal of Chromatography A. 1534 (2018) 111–122. https://doi.org/10.1016/j.chroma.2017.12.052.

[98]   B.A. Wolf, W. Conrad-Kessel, J. Turk, Long-chain fatty alcohol quantitation in subfemtomole amounts by gas chromatography-negative ion chemical ionization mass spectrometry. Application to long-chain acyl coenzyme A measurement, J Chromatogr. 509 (1990) 325–332. https://doi.org/10.1016/s0021-9673(01)93090-0.

[99]   M.R. Prasad, J. Sauter, W.E. Lands, Quantitative determination of acyl chain composition of subnanomole amounts of cellular long-chain acyl-coenzyme A esters, Anal Biochem. 162 (1987) 202–212. https://doi.org/10.1016/0003-2697(87)90028-5.

[100]   C.S. Tamvakopoulos, V.E. Anderson, Detection of acyl-coenzyme A thioester intermediates of fatty acid beta-oxidation as the N-acylglycines by negative-ion chemical ionization gas chromatography-mass spectrometry, Anal Biochem. 200 (1992) 381–387. https://doi.org/10.1016/0003-2697(92)90483-n.

[101]   P.G. Tardi, J.J. Mukherjee, P.C. Choy, The quantitation of long-chain acyl-CoA in mammalian tissue, Lipids. 27 (1992) 65–67. https://doi.org/10.1007/BF02537062.

[102]   T. Kasumov, W.Z. Martini, A.E. Reszko, F. Bian, B.A. Pierce, F. David, C.R. Roe, H. Brunengraber, Assay of the Concentration and 13C Isotopic Enrichment of Propionyl-CoA, Methylmalonyl-CoA, and Succinyl-CoA by Gas Chromatography–Mass Spectrometry, Analytical Biochemistry. 305 (2002) 90–96. https://doi.org/10.1006/abio.2002.5639.

[103]   J. Kopka, J.B. Ohlrogge, J.G. Jaworski, Analysis of in vivo levels of acyl-thioesters with gas chromatography/mass spectrometry of the butylamide derivative, Anal Biochem. 224 (1995) 51–60. https://doi.org/10.1006/abio.1995.1007.

[104]   L. Gao, W. Chiou, H. Tang, X. Cheng, H.S. Camp, D.J. Burns, Simultaneous quantification of malonyl-CoA and several other short-chain acyl-CoAs in animal tissues by ion-pairing reversed-phase HPLC/MS, Journal of Chromatography B. 853 (2007) 303–313. https://doi.org/10.1016/j.jchromb.2007.03.029.

[105]   T.R. Larson, I.A. Graham, Technical Advance: A novel technique for the sensitive quantification of acyl CoA esters from plant tissues, The Plant Journal. 25 (2001) 115–125. https://doi.org/10.1111/j.1365-313X.2001.00929.x.

[106]   D. Morin-Rivron, N. Christinat, M. Masoodi, Lipidomics analysis of long-chain fatty acyl-coenzyme As in liver, brain, muscle and adipose tissue by liquid chromatography/tandem mass spectrometry, Rapid Commun Mass Spectrom. 31 (2017) 344–350. https://doi.org/10.1002/rcm.7796.

[107]   S. Neubauer, D.B. Chu, H. Marx, M. Sauer, S. Hann, G. Koellensperger, LC-MS/MS-based analysis of coenzyme A and short-chain acyl-coenzyme A thioesters, Anal Bioanal Chem. 407 (2015) 6681–6688. https://doi.org/10.1007/s00216-015-8825-9.

[108]   C. Magnes, M. Suppan, T.R. Pieber, T. Moustafa, M. Trauner, G. Haemmerle, F.M. Sinner, Validated comprehensive analytical method for quantification of coenzyme A activated compounds in biological tissues by online solid-phase extraction LC/MS/MS, Anal Chem. 80 (2008) 5736–5742. https://doi.org/10.1021/ac800031u.

[109] A.U. Blachnio-Zabielska, C. Koutsari, M.D. Jensen, Measuring long-chain acyl-coenzyme A concentrations and enrichment using liquid chromatography/tandem mass spectrometry with selected reaction monitoring, Rapid Commun Mass Spectrom. 25 (2011) 2223–2230. https://doi.org/10.1002/rcm.5110.

[110] A.J. Frey, D.R. Feldman, S. Trefely, A.J. Worth, S.S. Basu, N.W. Snyder, LC-quadrupole/Orbitrap high-resolution mass spectrometry enables stable isotope-resolved simultaneous quantification and 13C-isotopic labeling of acyl-coenzyme A thioesters, Anal Bioanal Chem. 408 (2016) 3651–3658. https://doi.org/10.1007/s00216-016-9448-5.

[111] C. Zhao, Y. Wang, H. Yang, S. Wang, M.-C. Tang, D. Cyr, F. Parente, P. Allard, P. Waters, A. Furtos, G. Yang, G.A. Mitchell, Propionic acidemia in mice: Liver acyl-CoA levels and clinical course, Mol Genet Metab. 135 (2022) 47–55. https://doi.org/10.1016/j.ymgme.2021.11.011.

[112] A. Wakamatsu, K. Morimoto, M. Shimizu, S. Kudoh, A severe peak tailing of phosphate compounds caused by interaction with stainless steel used for liquid chromatography and electrospray mass spectrometry, Journal of Separation Science. 28 (2005) 1823–1830. https://doi.org/10.1002/jssc.200400027.

[113] R. Harmancey, C.R. Wilson, N.R. Wright, H. Taegtmeyer, Western diet changes cardiac acyl-CoA composition in obese rats: a potential role for hepatic lipogenesis, J Lipid Res. 51 (2010) 1380–1393. https://doi.org/10.1194/jlr.M001230.

[114] M.Y. Golovko, E.J. Murphy, An improved method for tissue long-chain acyl-CoA extraction and analysis, J Lipid Res. 45 (2004) 1777–1782. https://doi.org/10.1194/jlr.D400004-JLR200.

[115] S.S. Basu, C. Mesaros, S.L. Gelhaus, I.A. Blair, Stable Isotope Labeling by Essential Nutrients in Cell Culture for Preparation of Labeled Coenzyme A and Its Thioesters, Anal Chem. 83 (2011) 1363–1369. https://doi.org/10.1021/ac1027353.

[116] O. Hayashi, K. Satoh, Determination of acetyl-CoA and malonyl-CoA in germinating rice seeds using the LC-MS/MS technique, Biosci Biotechnol Biochem. 70 (2006) 2676–2681. https://doi.org/10.1271/bbb.60269.

[117] P.E. Minkler, J. Kerner, S.T. Ingalls, C.L. Hoppel, Novel isolation procedure for short-, medium-, and long-chain acyl-coenzyme A esters from tissue, Anal Biochem. 376 (2008) 275–276. https://doi.org/10.1016/j.ab.2008.02.022.

[118] F.-L. Liu, C.-B. Qi, Q.-Y. Cheng, J.-H. Ding, B.-F. Yuan, Y.-Q. Feng, Diazo Reagent Labeling with Mass Spectrometry Analysis for Sensitive Determination of Ribonucleotides in Living Organisms, Anal. Chem. 92 (2020) 2301–2309. https://doi.org/10.1021/acs.analchem.9b05122.

[119] Y. Zhu, P. Deng, D. Zhong, Derivatization methods for LC-MS analysis of endogenous compounds, Bioanalysis. 7 (2015) 2557–2581. https://doi.org/10.4155/bio.15.183.

[120] A. Logan, H.M. Cochemé, P.B. Li Pun, N. Apostolova, R.A.J. Smith, L. Larsen, D.S. Larsen, A.M. James, I.M. Fearnley, S. Rogatti, T.A. Prime, P.G. Finichiu, A. Dare, E.T. Chouchani, V.R. Pell, C. Methner, C. Quin, S.J. McQuaker, T. Krieg, R.C. Hartley, M.P. Murphy, Using exomarkers to assess mitochondrial reactive species in vivo, Biochim Biophys Acta. 1840 (2014) 923–930. https://doi.org/10.1016/j.bbagen.2013.05.026.

[121] H.-K. Woo, E.P. Go, L. Hoang, S.A. Trauger, B. Bowen, G. Siuzdak, T.R. Northen, Phosphonium labeling for increasing metabolomic coverage of neutral lipids using electrospray ionization mass spectrometry, Rapid Commun Mass Spectrom. 23 (2009) 1849–1855. https://doi.org/10.1002/rcm.4076.

[122] S. Neubauer, C. Haberhauer-Troyer, K. Klavins, H. Russmayer, M.G. Steiger, B. Gasser, M. Sauer, D. Mattanovich, S. Hann, G. Koellensperger, U13C cell extract of Pichia pastoris--a powerful tool for evaluation of sample preparation in metabolomics, J Sep Sci. 35 (2012) 3091–3105. https://doi.org/10.1002/jssc.201200447.

[123] S.S. Basu, I.A. Blair, SILEC: a protocol for generating and using isotopically labeled coenzyme A mass spectrometry standards, Nat Protoc. 7 (2011) 1–12. https://doi.org/10.1038/nprot.2011.421.

[124] S.-E. Ong, B. Blagoev, I. Kratchmarova, D.B. Kristensen, H. Steen, A. Pandey, M. Mann, Stable isotope labeling by amino acids in cell culture, SILAC, as a simple and accurate approach to expression proteomics, Mol Cell Proteomics. 1 (2002) 376–386. https://doi.org/10.1074/mcp.m200025-mcp200.

[125] N.W. Snyder, G. Tombline, A.J. Worth, R.C. Parry, J.A. Silvers, K.P. Gillespie, S.S. Basu, J. Millen, D.S. Goldfarb, I.A. Blair, Production of stable isotope-labeled acyl-coenzyme A thioesters by yeast stable isotope labeling by essential nutrients in cell culture, Anal Biochem. 474 (2015) 59–65. https://doi.org/10.1016/j.ab.2014.12.014.

[126] S. Trefely, K. Huber, J. Liu, M. Noji, S. Stransky, J. Singh, M.T. Doan, C.D. Lovell, E. von Krusenstiern, H. Jiang, A. Bostwick, H.L. Pepper, L. Izzo, S. Zhao, J.P. Xu, K.C. Bedi, J.E. Rame, J.G. Bogner-Strauss, C. Mesaros, S. Sidoli, K.E. Wellen, N.W. Snyder, Quantitative subcellular acyl-CoA analysis reveals distinct nuclear metabolism and isoleucine-dependent histone propionylation, Mol Cell. 82 (2022) 447-462.e6. https://doi.org/10.1016/j.molcel.2021.11.006.

[127] D.C. Lehotay, P. Hall, J. Lepage, J.C. Eichhorst, M.L. Etter, C.R. Greenberg, LC–MS/MS progress in newborn screening, Clinical Biochemistry. 44 (2011) 21–31. https://doi.org/10.1016/j.clinbiochem.2010.08.007.

[128] M.H. Gelb, K. Basheeruddin, A. Burlina, H.-J. Chen, Y.-H. Chien, G. Dizikes, C. Dorley, R. Giugliani, A. Hietala, X. Hong, S.-M. Kao, H. Khaledi, T. Klug, F. Kubaski, H.-C. Liao, M. Martin, A. Manning, J. Orsini, Y. Peng, E. Ranieri, A. Rohrwasser, N. Szabo-Fresnais, C.T. Turgeon, F.M. Vaz, L. Wang, D. Matern, Liquid Chromatography–Tandem Mass Spectrometry in Newborn Screening Laboratories, Int J Neonatal Screen. 8 (2022) 62. https://doi.org/10.3390/ijns8040062.

[129] J.Y. Yang, D.A. Herold, Chapter 13 - Evolving platforms for clinical mass spectrometry, in: H. Nair, W. Clarke (Eds.), Mass Spectrometry for the Clinical Laboratory, Academic Press, San Diego, 2017: pp. 261–276. https://doi.org/10.1016/B978-0-12-800871-3.00013-4.

[130] P.L. Hall, A. Wittenauer, A. Hagar, Newborn screening for medium chain acyl-CoA dehydrogenase deficiency: performance improvement by monitoring a new ratio, Mol Genet Metab. 113 (2014) 274–277. https://doi.org/10.1016/j.ymgme.2014.10.007.

[131] J.G. Okun, S. Kölker, A. Schulze, D. Kohlmüller, K. Olgemöller, M. Lindner, G.F. Hoffmann, R.J.A. Wanders, E. Mayatepek, A method for quantitative acylcarnitine profiling in human skin fibroblasts using unlabelled palmitic acid: diagnosis of fatty acid oxidation disorders and differentiation between biochemical phenotypes of MCAD deficiency, Biochimica et Biophysica Acta (BBA) - Molecular and Cell Biology of Lipids. 1584 (2002) 91–98. https://doi.org/10.1016/S1388-1981(02)00296-2.

[132] M.F. Browning, C. Larson, A. Strauss, D.L. Marsden, Normal acylcarnitine levels during confirmation of abnormal newborn screening in long-chain fatty acid oxidation defects, Journal of Inherited Metabolic Disease. 28 (2005) 545–550. https://doi.org/10.1007/s10545-005-0545-4.

[133] M.J. Miller, K. Cusmano-Ozog, D. Oglesbee, S. Young, ACMG Laboratory Quality Assurance Committee, Laboratory analysis of acylcarnitines, 2020 update: a technical standard of the American College of Medical Genetics and Genomics (ACMG), Genet Med. 23 (2021) 249–258. https://doi.org/10.1038/s41436-020-00990-1.

[134] I.M.L.W. Körver-Keularts, P. Wang, H.W.A.H. Waterval, L.A.J. Kluijtmans, R.A. Wevers, C.-D. Langhans, C. Scott, D.D.J. Habets, J. Bierau, Fast and accurate quantitative organic acid analysis with LC-QTOF/MS facilitates screening of patients for inborn errors of metabolism, Journal of Inherited Metabolic Disease. 41 (2018) 415–424. https://doi.org/10.1007/s10545-017-0129-0.

[135] C.G. Costa, W.S. Guérand, E.A. Struys, U. Holwerda, H.J. ten Brink, I. Tavares de Almeida, M. Duran, C. Jakobs, Quantitative analysis of urinary acylglycines for the diagnosis of beta-oxidation defects using GC-NCI-MS, J Pharm Biomed Anal. 21 (2000) 1215–1224. https://doi.org/10.1016/s0731-7085(99)00235-6.

[136] C.G. Costa, L. Dorland, U. Holwerda, I.T. de Almeida, B.T. Poll-The, C. Jakobs, M. Duran, Simultaneous analysis of plasma free fatty acids and their 3-hydroxy analogs in fatty acid beta-oxidation disorders, Clin Chem. 44 (1998) 463–471.

[137] G. Martínez, G. Jiménez-Sánchez, P. Divry, C. Vianey-Saban, E. Riudor, M. Rodés, P. Briones, A. Ribes, Plasma free fatty acids in mitochondrial fatty acid oxidation defects, Clinica Chimica Acta. 267 (1997) 143–154. https://doi.org/10.1016/S0009-8981(97)00130-7.

[138] S.S. Basu, E.C. Deutsch, A.A. Schmaier, D.R. Lynch, I.A. Blair, Human platelets as a platform to monitor metabolic biomarkers using stable isotopes and LC–MS, Bioanalysis. 5 (2013) 3009–3021. https://doi.org/10.4155/bio.13.269.

[139] B. Piskláková, J. Friedecká, E. Ivanovová, E. Hlídková, V. Bekárek, M. Prídavok, A. Kvasnička, T. Adam, D. Friedecký, Rapid and efficient LC-MS/MS diagnosis of inherited metabolic disorders: a semi-automated workflow for analysis of organic acids, acylglycines, and acylcarnitines in urine, Clinical Chemistry and Laboratory Medicine (CCLM). (2023). https://doi.org/10.1515/cclm-2023-0084.
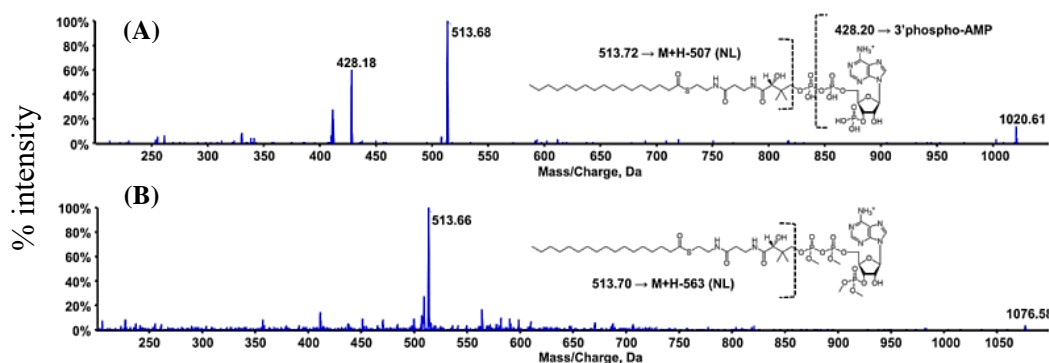
Supplementary Material

Figure S1. Product ion spectrum of (A) C17:0 CoA, (B) methylated C17:0 CoA. Phosphate methylation of CoA moiety will methylate all the phosphate groups of CoA leading to the neutral loss of 563 Da.
Reprinted with permission from, Li et al. Targeted Profiling of Short-, Medium-, and Long-Chain Fatty Acyl-Coenzyme As in Biological Samples by Phosphate Methylation Coupled to Liquid Chromatography–Tandem Mass Spectrometry, Anal. Chem. 93 (2021) 4342–4350, Copyright (2021) [1].
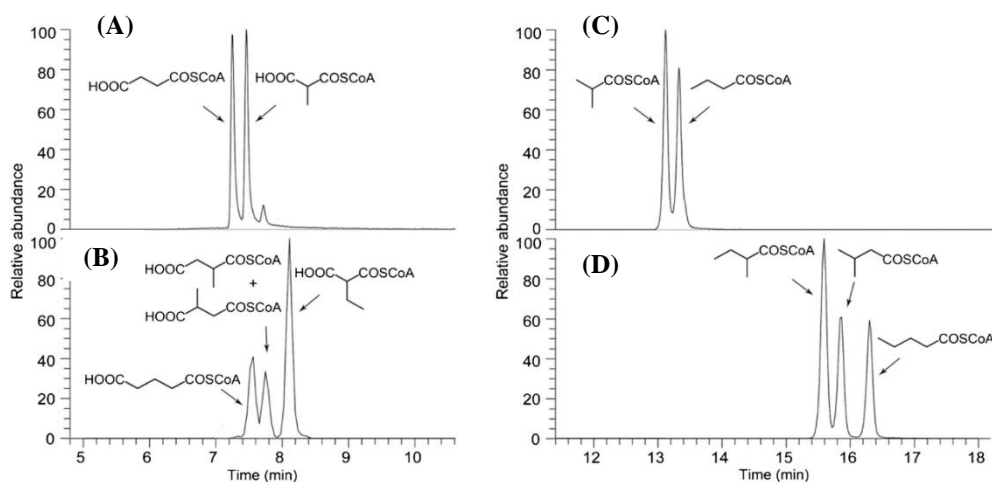

Figure S2. Separation of acyl-CoA thioesters isomers. XIC of acyl-CoA standards (A) Succinyl-CoA and methylmalonyl-CoA (m/z 361.1428); (B) Glutaryl-CoA, ethylmalonyl-CoA and a mixture of 2- and 3-methylsuccinyl-CoA (m/z 375.1584); (C) Butyryl- and isobutyryl-CoA (m/z 331.1686); (D) 2-methylbutyryl-CoA, isopentanoyl-CoA and pentanoyl-CoA (m/z 345.1844).
Reprinted from, Cakić et al. Suspect screening and targeted analysis of acyl-coenzyme A thioesters in bacterial cultures using a high-resolution tribrid mass spectrometer, Anal Bioanal Chem. 413 (2021) 3599–3610, under the terms of the Creative Commons CC-BY license [2].
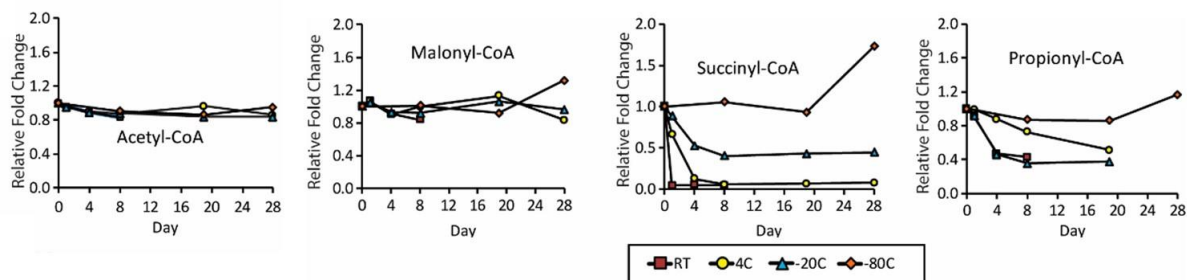
Figure S3. Assay stability using stable isotope labeled ISs at room temperature (RT), 4 °C, −20 °C, and −80 °C. Reprinted with permission from Fu et al. Targeted Determination of Tissue Energy Status by LC-MS/MS, Anal. Chem. 91 (2019) 5881–5887 [3], Copyright (2019), (https://pubs.acs.org/doi/10.1021/acs.analchem.9b00217) under the terms of ACS AuthorChoice License. Further permission related to the material excerpted should be directed to the ACS [3].

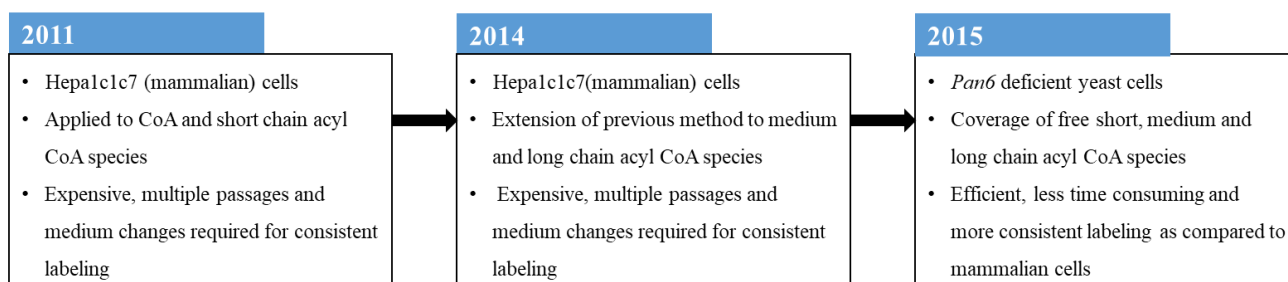| 2011	2014	2015
• Hepa1c1c7 (mammalian) cells • Applied to CoA and short chain acyl CoA species • Expensive, multiple passages and medium changes required for consistent labeling	• Hepa1c1c7(mammalian) cells • Extension of previous method to medium and long chain acyl CoA species • Expensive, multiple passages and medium changes required for consistent labeling	• *Pan6* deficient yeast cells • Coverage of free short, medium and long chain acyl CoA species • Efficient, less time consuming and more consistent labeling as compared to mammalian cells

Figure S4. Development of SILEC technology over the years.

References

[1] P. Li, M. Gawaz, M. Chatterjee, M. Lämmerhofer, Targeted Profiling of Short-, Medium-, and Long-Chain Fatty Acyl-Coenzyme As in Biological Samples by Phosphate Methylation Coupled to Liquid Chromatography–Tandem Mass Spectrometry, Anal. Chem. 93 (2021) 4342–4350. https://doi.org/10.1021/acs.analchem.1c00664.

[2] N. Cakić, B. Kopke, R. Rabus, H. Wilkes, Suspect screening and targeted analysis of acyl coenzyme A thioesters in bacterial cultures using a high-resolution tribrid mass spectrometer, Anal Bioanal Chem. 413 (2021) 3599–3610. https://doi.org/10.1007/s00216-021-03318-3.

[3] X. Fu, S. Deja, B. Kucejova, J.A.G. Duarte, J.G. McDonald, S.C. Burgess, Targeted Determination of Tissue Energy Status by LC-MS/MS, Anal. Chem. 91 (2019) 5881–5887. https://doi.org/10.1021/acs.analchem.9b00217.

Chapter 5

Development of targeted hydrophilic interaction liquid chromatography-tandem mass spectrometry method for acyl-Coenzyme A covering short- to long-chain species in a single analytical run

Based on

Development of targeted hydrophilic interaction liquid chromatography-tandem mass spectrometry method for acyl-Coenzyme A covering short- to long-chain species in a single analytical run

Madhulika Singh, Ligia Akemi Kiyuna, Christoff Odendaal, Barbara M. Bakker, Amy C. Harms, Thomas Hankemeier

Abstract

Acyl-CoAs play a significant role in numerous physiological and metabolic processes making it important to assess their concentration levels for evaluating metabolic health. Considering the important role of acyl-CoAs, it is crucial to develop an analytical method that can analyze these compounds. Due to the structural variations of acyl-CoAs, multiple analytical methods are often required for comprehensive analysis of these compounds, which increases complexity and the analysis time. In this study, we have developed a method using a zwitterionic HILIC column that enables the coverage of free CoA and short- to long-chain acyl-CoA species in one analytical run. Initially, we developed the method using an LC-QTOF instrument for the identification of acyl-CoA species and optimizing their chromatography. Later, a targeted HILIC-MS/MS method was created in scheduled multiple reaction monitoring mode using a QTRAP-MS detector. The performance of the method was evaluated based on various parameters such as linearity, precision, recovery and matrix effect. This method was applied to identify the difference in acyl-CoA profiles in HepG2 cells cultured in different conditions. Our findings revealed an increase in levels of acetyl-CoA, medium- and long-chain acyl-CoA while a decrease in the profile of free CoA in the starved state, indicating a clear alteration in the fatty acid oxidation process.

Keywords

Acyl-CoA; LC-MS; HILIC; HepG2; Biomarker

1. Introduction

Acyl-CoAs are thioester compounds that have a pivotal role in various metabolic processes such as fatty acid beta-oxidation, biosynthesis of lipids, signaling, and xenobiotics metabolism [1,2]. The most important biological function of acyl-CoAs is in the metabolism of fatty acids via beta-oxidation. The fatty acid beta-oxidation (FAO) process in the liver breaks down fatty acids (FA) to produce adenosine triphosphate (ATP) in low glucose conditions [3,4]. Acyl-CoAs are formed when a FA forms a thioester bond with Coenzyme-A (CoA) [5,6], which subsequently undergo FAO process inside the mitochondria. Fatty acid oxidation disorders (FAOD) occur due to the deficient activity of the enzymes or transporter proteins involved in the pathway, which results in the accumulation of acyl-CoA esters [3]. The acyl-CoA accumulation profile provides information on the type of fatty acid oxidation disorder (FAOD). Intracellular acyl-CoA levels are important reporters of metabolic health and their accumulation in case of FAOD makes them interesting biomarkers [7]. Apart from FAOD, these compounds are also involved in progression of cancer [8–10], diabetes [11–14], precursors for lipid synthesis and ketone bodies. Since acyl-CoA are involved in numerous physiological and pathophysiological pathways, it is important to develop analytical methods for their identification and quantitation.

Developing chromatographic methods for acyl-CoAs is challenging due to their structural complexity. These compounds exhibit significant variations in their physicochemical properties by factors such as carbon chain length, degree of saturation and the presence of functional groups [15–17]. Additionally, acyl-CoAs have low endogenous levels and are highly unstable in aqueous solutions. Due to these reasons they are susceptible to hydrolysis, making sample preparation challenging and resulting in poor recovery and low signal intensity [15,18]. The quantitation of acyl-CoAs has previously been accomplished using a variety of analytical techniques, such as gas chromatography, capillary electrophoresis, and reversed phase liquid chromatography (RPLC) coupled to UV or fluorescence detection [19–22]. However, liquid chromatography coupled to mass spectrometry (LC-MS) is the most widely used technique for acyl-CoA analysis due to its higher sensitivity and selectivity [17–19,23–25]. On the other hand, severe peak tailing, signal deterioration, and poor detection limits are common obstacles associated with this approach [26,27]. Various efforts have been made to cover the full range of acyl-CoAs. In RPLC, slightly acidic mobile phases were used for short- to medium-chain acyl-CoAs [28], while alkaline mobile phase was used for medium- to long-chain acyl-CoAs [26]. Liu et al. used this approach for comprehensive coverage by employing two analytical

runs [23]. The combination of RPLC and hydrophilic interaction liquid chromatography (HILIC) [26] or two-dimensional (2D) LC-MS [17] have also been used to cover short-, medium- and long-chain acyl-CoAs. However, these approaches introduce complexity and increase the analysis time due to the need for multiple chromatographic runs and inclusion of a second dimension of separation. This complexity and added analysis time, in turn, can impact the high-throughput. Another approach for comprehensive coverage is to use ion-pairing reagents such as triethylamine [29] or dimethylbutyl amine [16,25]. However, ion-pairing reagents are reported to decrease mass spectrometry signal intensity [30] and frequent cleaning of detectors is required. Furthermore, a RPLC-MS/MS technique based on phosphate methylation after acyl-CoA derivatization has been reported [15]. Nonetheless, derivatization complicates sample preparation and requires investigation for the evaluation of complete chemical conversion.

HILIC has become increasingly popular and promising for the separation of polar compounds, as HILIC allows class-based separation by hydrophilic interaction. Despite significant variations in chain length polarity, the presence of a similar hydrophilic headgroup in acyl-CoAs facilitates their elution within a relatively shorter time period. In HILIC chromatography, the compounds are separated on a polar stationary phase by gradually increasing mobile phase polarity [31–33]. The compounds with higher polarity have enhanced affinity for the polar stationary phase, thus resulting in prolonged retention, whereas compounds with lower polarity tend to elute earlier.

The aim of the present study is to develop a targeted HILIC-MS/MS method utilizing a zwitterionic HILIC column for the quantitation of free CoA and short- to long-chain acyl-CoA compounds in a single analytical run (covering the full analyte range from high to low polarity) and demonstrate the utility of this method in HepG2 cell application. To achieve this, the initial method development was done on an LC coupled to a high-resolution time-of-flight (QTOF) mass spectrometer (HRMS) for pre-screening of species and evaluating their retention times. The chromatography was optimized by studying the effects of different factors such as buffer concentration and injection solvents. After optimization of various LC-MS settings, a targeted method was created and validation parameters such as linearity, sensitivity, precision, recovery and matrix effect were examined to evaluate method performance in the HepG2 cells. Finally, the HILIC-MS/MS method was applied to compare the free CoA and acyl-CoA profile in HepG2 cells cultured in different conditions.

2. Materials and methods

2.1 Chemicals and reagents

Analytical grade solvents including acetonitrile, chloroform, isopropanol (IPA) and methanol (MeOH) were purchased from Biosolve BV (Valkenswaard, The Netherlands). Purified water was obtained using the Milli-Q Advantage A10 Water Purification System manufactured by Merck Millipore (Billerica, MA, USA). Ammonium acetate with a purity of 99% was supplied by Sigma-Aldrich (St. Louis, MO, USA). Acyl-CoA standards, such as acetyl-CoA (C2:0-CoA) and propionyl-CoA (C3:0-CoA) as sodium salts, octanoyl-CoA (C8:0-CoA), pentadecanoyl-CoA (C15:0-CoA), palmitoyl-CoA (C16:0-CoA), heptadecanoyl-CoA (C17:0-CoA), and 11Z-octadecenoyl-CoA (C18:1(n7)-CoA) as ammonium salts, were purchased from Avanti Polar Lipids (Alabaster, AL, USA). Acetyl-1,2-$^{13}C_2$-CoA (C2:0($^{13}C_2$)-CoA) and n-heptanoyl-CoA (C7:0-CoA) in the form of lithium salts were obtained from Sigma-Aldrich (St. Louis, MO, USA). Additional acyl-CoA standards, including free CoA (CoA), butyryl-CoA (C4:0), hexanoyl-CoA (C6:0), decanoyl-CoA (C10:0), lauroyl-CoA (C12:0), myristoyl-CoA (C14:0), and stearoyl-CoA (C18:0), were provided by collaborators from University Medical Center Groningen (Groningen, The Netherlands).

Dulbecco's Modified Eagle Medium (DMEM) (Product No. P04-01500) and glucose-free DMEM (Product No. P04-01548S1) were purchased from PAN Biotech™. Fetal bovine serum (FBS) and phosphate-buffered saline (PBS) were purchased from Gibco while L-carnitine (Product No. C0283) and palmitate (Product No. P9767) were purchased from Sigma-Aldrich.

2.2 Cell culture

Wildtype HepG2 cells were maintained in DMEM with 5 mM glucose, 3.7 g L^{-1} NaHCO$_3$, 1 mM sodium pyruvate and amino acids, supplemented with 3 mM glutamine, and 10% FBS. The cells were kept at 37 °C and 5% CO$_2$. To test the individual and combined effects of glucose depletion and fatty acid stimulation on the free CoA level and acyl-CoA profile, the cells were incubated for 24 h in two different conditions. In condition 1 the cells were cultured in DMEM (5 mM glucose, 1 mM pyruvate supplemented with 3 mM glutamine and 10% FBS) with additional supplements 2 mM L-carnitine and 0.5 mM BSA-bound palmitate. Condition 2 was with glucose-free DMEM (no glucose, no glutamine, no pyruvate, 10% FBS) supplemented with 2 mM L-carnitine and 0.5 mM BSA-bound palmitate. After 24 h, the cells were washed twice with ice-cold PBS and harvested for further analysis. Condition 1 cells were

"supplemented cells" with multiple carbon sources, while condition 2 cells were "starved cells" with fewer carbon sources.

2.3 Sample preparation

Acyl-CoAs from HepG2 cells were extracted by a two-step protocol using chloroform/methanol/water based on the Bligh and Dyer approach [34]. 10 μL of acyl-CoA internal standard (IS) containing mixture of C2:0($^{13}C_2$)-CoA, C7:0-CoA, C15:0-CoA and C17:0-CoA with concentration of 3 μM were spiked in the HepG2 cell extracts containing 1×10^6 cells in 100 μL of methanol. To this extract, 220 μL of cold methanol and 100 μL of cold water was added and sonicated for 3 min. After sonication, 320 μL of chloroform and 188 μL of cold water was added. Samples were vortexed for 2 min, left to partition on ice for 10 min, and centrifuged at 15800 rcf for 15 min at 4 °C. 450 μL of the upper aqueous layer was transferred to a new Eppendorf tube. Samples were evaporated to dryness with a Labconco CentriVap vacuum concentrator (Kansas City, MO, USA). The dried samples were reconstituted in 100 μL of methanol/water/isopropanol (1:1:1), vortexed and centrifuged for 10 min. The supernatant was transferred to HPLC vial for LC-MS analysis.

2.4 HILIC-HRMS (HILIC-TOF-MS) analysis

The Waters Synapt G2-S quadrupole time-of-flight mass spectrometer with an electrospray ionization (ESI) source (Milford, MA, USA) was coupled to an Acquity UPLC system (Waters). The chromatographic separation was performed on SeQuant® ZIC®-cHILIC (100 mm x 2.1 mm, 100 Å pore size, 3 μm) column. The column oven and autosampler temperatures were set at 40 °C and 10 °C respectively. Mobile phase A (MP-A) consisted of acetonitrile:water (9:1) containing 5 mM ammonium acetate and acetonitrile:water (1:9) with 5 mM ammonium acetate was used for mobile phase B (MP-B). The flow rate was 0.25 mL/min and injection volume was 5 μL. The gradient program is shown in **Table S1**. The autosampler injection needle was washed with a weak needle wash consisting of acetonitrile:water (9:1, v/v) and strong needle wash consisting of acetonitrile:water (1:9, v/v).

For the MS analysis, a TOF-MS scan was performed. The mass spectrometer was set to scan a mass range from 300 to 1200 Da in both positive and negative ESI ionization modes. To ensure accurate mass measurement, 0.1 mg/L leucine-enkephalin in water:MeOH:formic acid (50:50:0.1, v/v/v) was used as a lock-mass calibrant with the infusion flow rate of 10 μL/min. The mass spectrometer was operated with the following parameters: the capillary voltage was set at 2.50 kV in both positive and negative mode of ionization; the sampling cone voltage was

set to 30 V and the source offset voltage was 100 V. The source temperature was maintained at 125 °C, while the desolvation temperature was set at 500 °C. Gas flows were controlled as follows: the cone gas flow rate was set to 50 L/h; the desolvation gas flow rate was 500 L/h, and the nebulizer gas flow rate was adjusted to 6 Bar.

2.5 HILIC-QTRAP (HILIC-MS/MS) analysis in scheduled MRM mode

The targeted HILIC-MS/MS analysis was performed on a Waters Acquity UPLC I-class system from Waters (Milford, MA, USA) coupled to an AB Sciex QTRAP 6500 mass spectrometer (Concord, ON, Canada). The needle wash was acetonitrile:water (1:1, v/v). The column, mobile phase, autosampler temperature and column oven temperature were the same as described in section *2.4.* with a slight modification in the gradient program as shown in **Table 1**.

Table 1. Gradient for HILIC-MS/MS analysis.

Time (min)	Flow rate (mL min^{-1})	MP-A (%)	MP-B (%)
Initial	0.25	95	5
2.3	0.25	95	5
8.5	0.25	25	75
13.00	0.25	15	85
15.5	0.25	15	85
15.6	0.25	95	5
20	0.25	95	5

The MS/MS experiments were conducted on a Turbo V source. The analysis was conducted in positive ion mode and analytes were monitored in scheduled multiple reaction monitoring (sMRM) mode. The mass spectrometer was operated at the following settings: the curtain gas (N_2) pressure was set to 25 psi, and the collision gas (N_2) was maintained at a medium level. The spray voltage was set at 4000 V in positive ion mode. The source temperature was maintained at 325 °C. The GS1 and GS2 pressures both were set at 60 psi. The target scan time was of 0.35 sec. The delustering potential (DP) and collision energy (CE) were optimized to achieve maximum response.

2.6 Method validation

Method validation of the HILIC-MS/MS method was performed using non-endogenous acyl-CoA standards- C2:0($^{13}C_2$)-CoA, C7:0-CoA, C15:0-CoA and C17:0-CoA. These standards were either isotopically labeled or had odd chains to be free from interference of endogenous species.

2.6.1 Calibration curves

The calibration curves were freshly prepared on three different days to assess the linearity of the method. For this purpose, an 8-point calibration line was created by serially diluting the standards. The concentrations of these calibration points are presented in **Table S2**. Three types of calibration lines were prepared: 1) Neat solvents; 2) Spiking standards in HepG2 cells before performing the extraction as described in the sample preparation section; 3) Spiking standards in HepG2 cells after extraction. To determine the linear range, an unweighted linear regression model was employed. The calculation of various validation parameters was performed using cal-3 (low), cal-5 (medium), and cal-7(high) concentration levels.

2.6.2 Limit of detection (LOD) and limit of quantitation (LOQ)

LOD and LOQ were calculated by using equation 1 and equation 2 respectively.

$$LOD = \frac{\frac{3 \times SD_{areac_{S/N>3}} + area_{blank}}{area_{c_{S/N>3}}}}{\left[c_{S/N>3}\right]} \quad (1)$$

$$LOQ = \frac{\frac{10 \times SD_{areac_{S/N>3}} + area_{blank}}{area_{c_{S/N>3}}}}{\left[c_{S/N>3}\right]} \quad (2)$$

where $SD_{areac_{S/N>3}}$ represents the standard deviation of area of the lowest concentration with signal-to-noise ratio greater than 3 ($C_{S/N>3}$), $area_{blank}$ are the peak area of the blank and $\frac{area_{c_{S/N>3}}}{\left[c_{S/N>3}\right]}$ represents the ratio between peak area and concentration at $C_{S/N>3}$ [35].

2.6.3 Precision

Precision was assessed by calculating the relative standard deviation (RSD %). Low, medium and high concentration levels were used for this analysis. Intraday precision was determined by conducting three consecutive measurements on the same day. Interday precision, on the other hand, was evaluated by measuring the samples on three different days. The precision was calculated by equation 3 [36].

$$RSD \ (\%) = \frac{Standard \ deviation}{Mean} \times 100 \quad (3)$$

2.6.4 Extraction Recovery

The response of standards at low, medium and high levels (measured in triplicate) was calculated in the samples spiked before and after extraction in HepG2 cells and equation 4 was used to calculate the recovery.

$$Recovery(\%) = \frac{Response\ of\ standards\ in\ HepG2\ cells\ before\ extraction}{Response\ of\ standards\ in\ HepG2\ cells\ after\ extraction} \times 100 \quad (4)$$

2.6.5 Matrix effect

Matrix effect is a prevalent issue encountered in mass spectrometry measurements. It refers to a phenomenon where the response of an analyte is suppressed or amplified due to the presence of a matrix or other interfering components that affect the ionization process of compounds. This was calculated by equation 5 at low, medium and high level (measured in triplicate).

$$Matrix\ effect(\%) = \frac{Response\ of\ standards\ in\ HepG2\ cells\ after\ extraction}{Response\ of\ standards\ in\ neat\ solvents} \times 100 \quad (5)$$

2.6.6 Carryover

Carryover refers to the presence of analytes in the blank samples after injection of the highest calibration standards [37]. This was evaluated by comparing the peak area of standards in the blank solvents to the peak area of standards spiked in high concentration in HepG2 cells, analyzed before the blank solvents.

2.6.7 Repeatability

The repeatability of our method was assessed by calculating RSD (%) of endogenous acyl-CoA species in the quality control (QC) samples inserted at regular intervals in the batch of study samples.

2.7 Quantitation

The odd-chain or isotopic labeled non-endogenous standards were used as internal standards for the quantitation of endogenous acyl-CoA species. C2:0($^{13}C_2$)-CoA was used for the quantitation of short-chain species, C7:0-CoA was used for the quantitation of medium-chain species while C15:0-CoA and C17:0-CoA were used for the quantitation of long-chain species. These standards were used for the quantitation of both saturated and unsaturated species. In this study, we find that the abundance of unsaturated species in the biological samples was very low and hence their contribution to isotopic interference was less than 1%. Therefore, we do not require any isotopic correction in this study.

2.8 Data processing

Data acquisition was performed using MassLynx (version 4.1) for the Synapt G2-S (HILIC-TOF-MS) and Analyst (version 1.6.2) for the QTRAP (HILIC-MS/MS). Peak integration was performed using TargetLynx (version 4.1) and Sciex OS (version 2.1.6) for HILIC-TOF-MS and HILIC-MS/MS respectively. The peak asymmetry factor was used to determine the effect of different conditions during method development and was calculated by equation 6 [38].

$$A_s = b/a \qquad (6)$$

where A_s = peak asymmetry factor, b = half width of peak (distance from peak midpoint to the trailing edge at 10% of the full peak height), a = front half width (distance from peak midpoint to leading edge at 10% of the peak height). A_s is lower than 1 for a fronting peak and higher than 1 for a tailing peak.

GraphPad Prism (version 9) was used to calculate statistical significance between the groups using t-test and plot graphs.

3. Results and Discussion

Representative standards C2:0-CoA (short-chain), C8:0-CoA (medium-chain), C16:0-CoA and C18:1-CoA (long-chain) from each chain length were used for method optimization.

3.1 Mass spectrometry parameters optimization

The TOF-MS scan on the Synapt G2-S was performed in both positive ESI mode (ESI$^+$) and negative ESI (ESI$^-$) mode by injecting a mixture of four representative acyl-CoA standards. Firstly, the observed mass of the representative standards was confirmed with their accurate masses in protonated $[M+H]^+$, deprotonated $[M-H]^-$ and doubly charged negative ions $[M-2H]^{2-}$ form. The corresponding m/z values of these acyl-CoA standards are presented in **Table S3** and the sensitivity of acyl-CoA standards in different ionization modes is shown in **Figure S1.** Doubly charged ions in the negative mode $[M-2H]^{2-}$ have slightly higher sensitivity for these standards compared to their protonated form $[M+H]^+$ while intensities were very low in singly negative charged ion $[M-H]^-$. Despite the slightly higher sensitivity observed in the doubly charged ions in negative mode, we decided to measure protonated species utilizing positive ionization mode for our analysis. This choice was based on the previously reported studies [16–18] and the fragmentation patterns observed in positive ionization mode provide a more straightforward approach for analyzing acyl-CoAs. Additionally, when dealing with doubly charged negative ions, there may be greater susceptibility to background interference, which

can disrupt the linearity of the analysis. **Table S4** presents the observed m/z of all the targets with their retention times in the HILIC-TOF-MS method.

3.2 Chromatographic separation for acyl-CoAs

We started the chromatographic separation with a 20 min long gradient elution as reported in **Table S1.** In order to achieve the quantitation of all acyl-CoA species in a single analytical run, we employed a ZIC-cHILIC column which contains a phosphorylcholine group **(Figure S2)** that consists of a negatively charged inner moiety and a positively charged outer moiety [39]. We chose to use this ZIC-cHILIC column for the chromatography optimization of acyl-CoA as it was reported to effectively separate various compounds containing phosphate groups like ATP, ADP, NAD, sugar phosphates, etc. [40–42]. The presence of a zwitterionic stationary phase requires lower concentrations of buffer compared to other types of stationary phases, as the zwitterionic stationary phase contains both positive and negative charges. This causes weak electrostatic interactions with the analytes and hence only a low concentration of buffer is needed [39]. The peak tailing observed in the acyl-CoA species can be attributed to the presence of the phosphate group on CoA moiety [43]. This phenomenon might occur due to the interactions of phosphate groups and metal surfaces in path of LC flow [44]. Additionally, these phosphate groups have a tendency to adhere to the stainless steel parts of the LC-MS instrumentation, further contributing to the challenges in analysis [43]. The buffer salts such as ammonium acetate and ammonium formate are known to maintain the ionization of analytes and decrease the interaction between stationary phase and analytes [31,45–47]. We have used ammonium acetate buffer as this is one of the most commonly used buffers for metabolomics studies employing HILIC chromatography [46–48]. In this study, we investigated the impact of different concentrations of ammonium acetate on the peak shape, separation and retention of acyl-CoAs. Mobile phases were prepared with concentrations of 2.5 mM, 5 mM, and 10 mM ammonium acetate and the buffer concentration was kept same in both mobile phases to maintain consistent ionic strength throughout the gradient elution. **Figure 1** displays the peaks of the acyl-CoA standards for each buffer concentration and peak asymmetry factors were calculated and summarized in **Table 2**. Notably, as the concentration of ammonium acetate increased, the peak tailing of the acyl-CoAs decreased. After evaluating different concentrations of ammonium acetate, a final concentration of 5 mM was chosen, as it resulted in satisfactory peak shapes. Additionally, maintaining a lower salt concentration helps in preventing excessive salt precipitation within the instrument, ensuring its proper functionality and long-term stability. Furthermore, we assessed the influence of pH variation and flow rate

on peak tailing but did not observe any significant effects (data not shown). As a result, a flow rate of 0.25 mL/min was chosen for chromatographic separation with the presence of 5 mM ammonium acetate in the mobile phases.
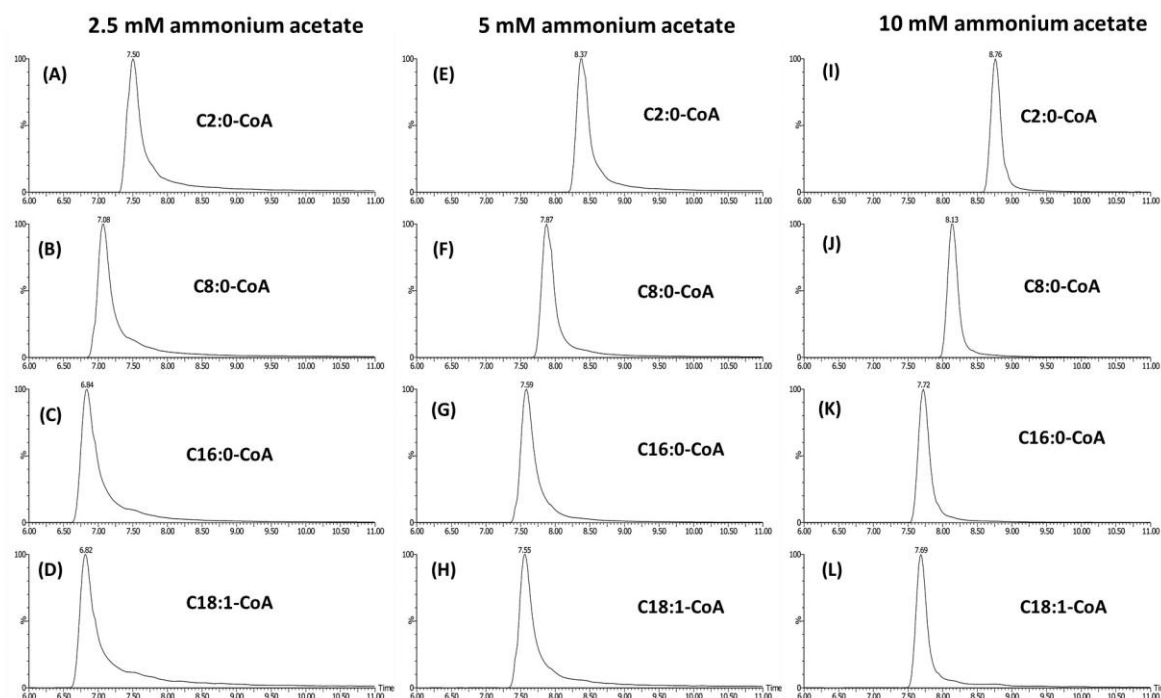

Figure 1. Extracted ion chromatograms of representative acyl-CoA standards (C2:0-CoA, C8:0-CoA, C16:0-CoA and C18:1-CoA) separated in mobile phases containing 2.5 mM ammonium acetate (A-D), 5 mM ammonium acetate (E-H) and 10 mM ammonium acetate (I-L). X-axis represents time (min) and Y-axis represents intensity.

Table 2. Peak asymmetry factor of acyl-CoA standards with 2.5 mM ammonium acetate, 5 mM ammonium acetate and 10 mM ammonium acetate.

Concentration of ammonium acetate (mM)	C2:0-CoA	C8:0-CoA	C16:0-CoA	C18:1-CoA
2.5	7.00	5.71	6.38	6.78
5	4.29	3.29	4.38	2.57
10	3.40	2.14	2.57	1.78

Further, we tested the effect of cell matrix on peak tailing by spiking four representative acyl-CoA standards in HepG2 cells after extraction. The ammonium acetate concentration of the mobile phase was kept at 5 mM, and peak asymmetry factor was compared between acyl-CoA standards spiked in the cell samples and the neat standards. It was observed that peak tailing and subsequently asymmetry factor has been reduced due to the presence of cell matrix **(Figure 2, Table 3)**. One possible explanation behind the reduction of peak tailing in the presence of

cell matrix is that the components within the cell samples can act as masking agents, thus disrupting the secondary interactions between analytes and LC system. As a result, the interaction between the acyl-CoA molecules and the column is reduced, leading to a decrease in peak tailing during chromatographic analysis. However, additional investigations are required to confirm this hypothesis. This can also be valuable as understanding the role of the cell matrix in reducing peak tailing can provide valuable insights for optimizing analytical methods and can be helpful in developing strategies to minimize peak tailing and improve the overall performance of chromatographic analyses.
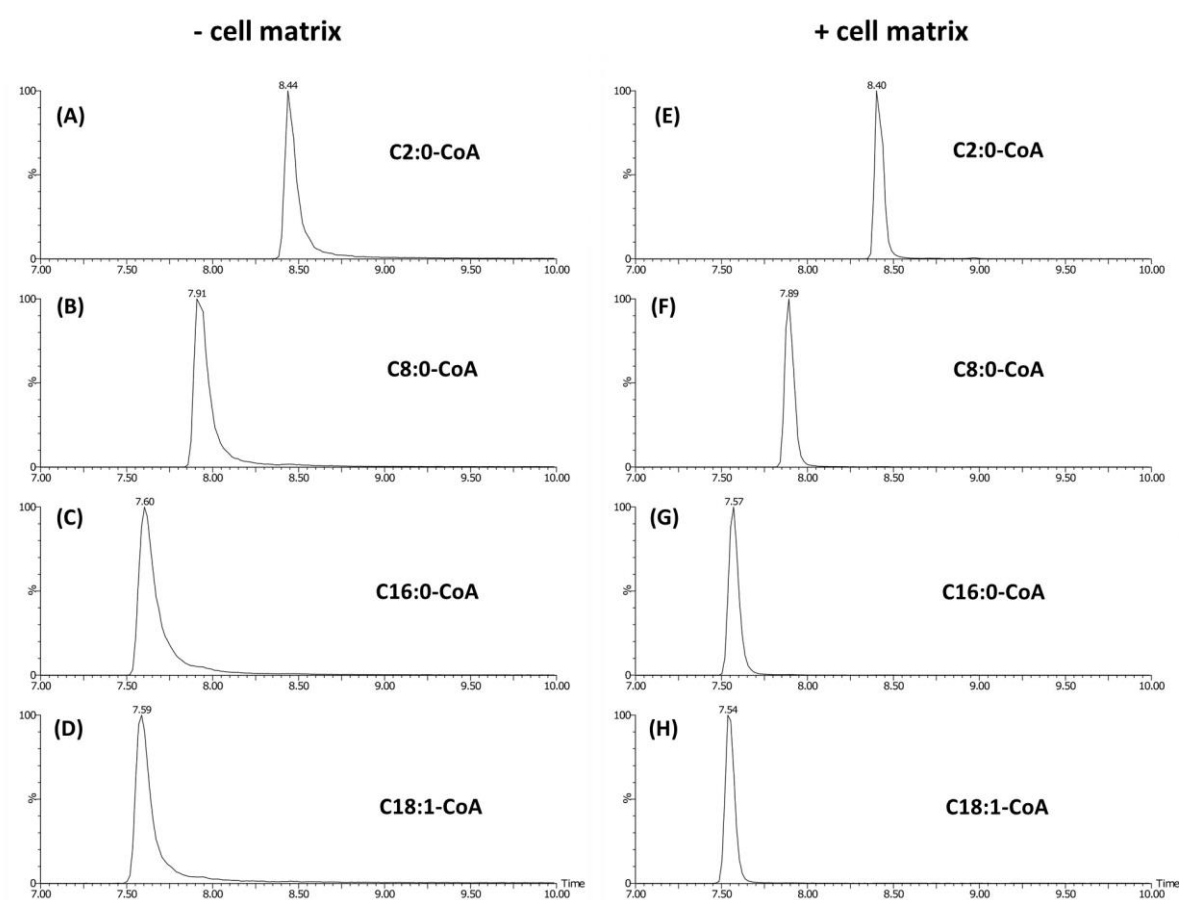

Figure 2. Extracted ion chromatograms of representative acyl-CoA standards (C2:0-CoA, C8:0-CoA, C16:0-CoA and C18:1-CoA) in 5 mM ammonium acetate, without (A-D) and with (E-H) cell matrix. X-axis represents time (min) and Y-axis represents intensity.

Table 3. Peak asymmetry factor of acyl-CoA standards with and without cell matrix.

Cell matrix	C2:0-CoA	C8:0-CoA	C16:0-CoA	C18:1-CoA
Absent (-)	2.32	2.00	3.50	2.28
Present (+)	2.00	1.40	1.33	1.60

3.3 Optimization of injection solvent for sample reconstitution

Acyl-CoAs are highly unstable in alkaline and strongly acidic solutions [18]. It is important to check the stability of acyl-CoAs in the injection solvents to assess degradation rate and determining the time window for stable sample analysis. As mentioned previously in literature, methanol was considered to have good stability for acyl-CoA for 24 h [18]. For this experiment, the four representative acyl-CoA standards (C2:0-CoA, C8:0-CoA, C16:0-CoA and C18:1-CoA) were reconstituted in 5 different solutions, MeOH:Water (1:5,v/v), MeOH:Water:IPA (1:1:1,v/v/v), MeOH:50 mM ammonium acetate (1:1,v/v), MeOH:Water (1:1,v/v) and methanol (100%). The presence of water in the injection solvents is necessary for the solubility of acyl-CoA especially for the short-chain species. The four acyl-CoA standards were dissolved in solvents, placed in the autosampler, and analyzed with the HILIC-TOF-MS method at three different time points: 0 h, 6 h and 24 h **(Figure 3).**

The stability of acyl-CoAs in the various solvents was assessed by measuring the change in response at 6 and 24 h, expressed as a percentage relative to the response observed at 0 h. Both MeOH:Water (1:5, v/v) and MeOH:Water:IPA (1:1:1, v/v/v) showed acceptable stability over time for the acyl-CoAs. The response with the injection solvent MeOH:50 mM ammonium acetate (1:1,v/v) decreased at 6 and 24 h, except for C2:0-CoA, which had a higher response at these time points. MeOH:Water (1:1,v/v) and methanol (100%) showed increase in response at 24 h as compared to 6 h especially for C2:0-CoA and C8:0-CoA. Methanol (100%) also shows a high variation in response for C2:0-CoA. The exact reason behind this observation is not clearly understood, however, solubility could be one of the contributing factors. For our method, we chose methanol:water:isopropanol (1:1:1, v/v/v) as the injection solvent as it has acceptable stability and the inclusion of slightly less polar solvent (isopropanol) in the injection solvent can increase the solubility of long-chain acyl-CoAs.
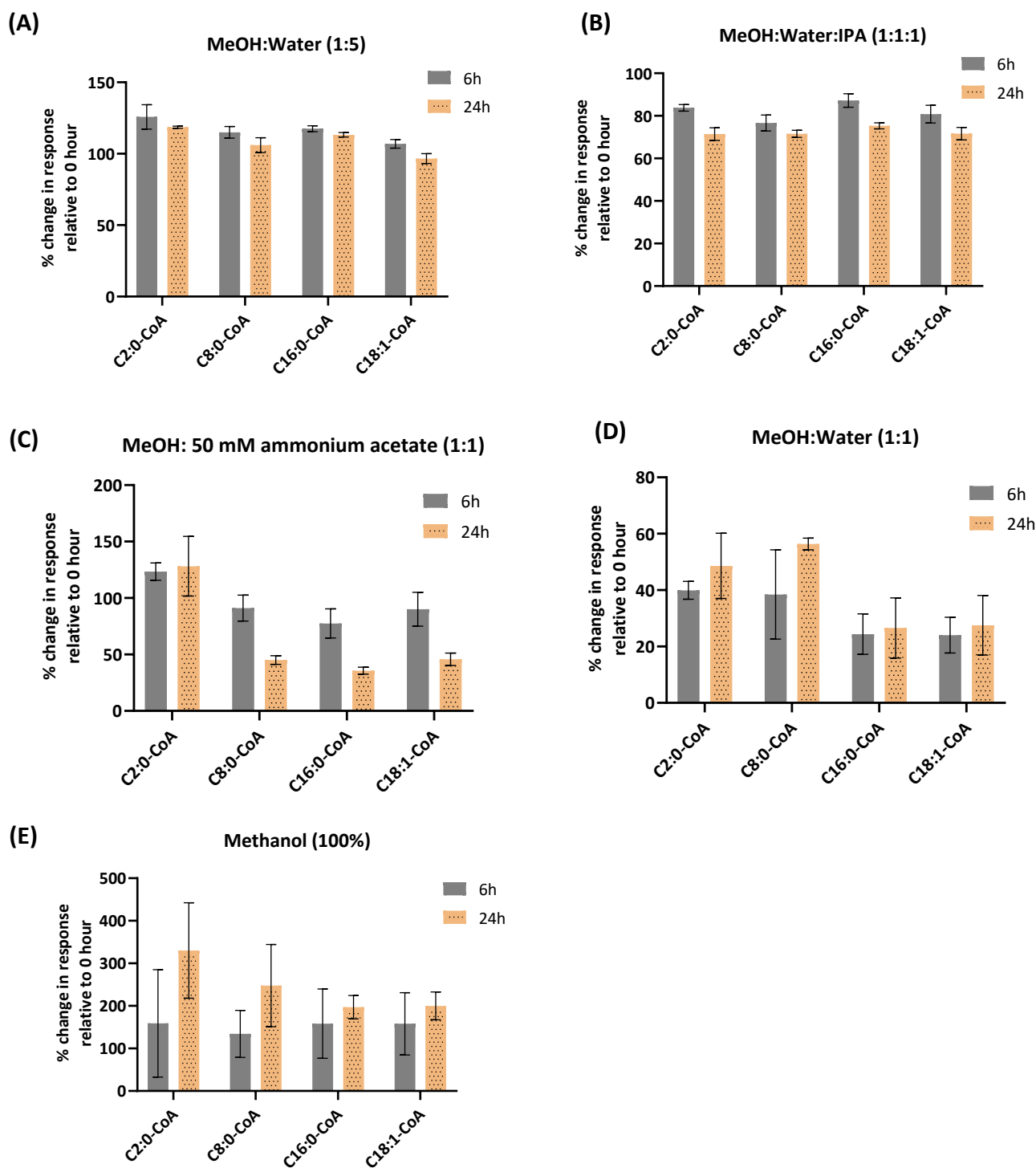
Figure 3. Stability of representative acyl-CoA standards (C2:0 CoA, C8:0 CoA, C16:0 CoA and C18:1 CoA) in different injection solvents. (A) MeOH:Water (1:5, v/v); (B) MeOH:Water:IPA (1:1:1, v/v/v); (C) MeOH:50 mM ammonium acetate (1:1, v/v); (D) MeOH:Water (1:1, v/v); (E) Methanol (100%).

3.4 HILIC-MS/MS QTRAP analysis

Following the optimization of chromatographic and mass spectrometry conditions, a targeted method was created using the sMRM mode on the QTRAP instrument in positive ion mode. We made slight modifications and finalized the gradient program as presented in **Table 1**. The formation of water-rich layer on the surface of stationary phase is quite important for interaction with the analytes to ensure consistent retention of compound. Hence, we specifically extended the equilibration time as it is a critical step in HILIC for a stable chromatography. **Figure 4(A)** shows the representative chromatogram of acyl-CoA standards.

The fragmentation pattern was examined for the selection of product ion (Q3). Acyl-CoA species exhibit two important fragments [15,17–19]. The first is the neutral loss of 507 Da $[M+H-507]^+$, which occurs as a result of the loss of the 3'-phosphate-adenosine-5'-diphosphate moiety from the acyl-CoA precursor molecular ion. Additionally, m/z 428 is another distinctive fragment present in all acyl-CoA species which is the representative CoA moiety. These findings were confirmed in **Figure 4(B),** which presents the fragmentation pattern of C7:0-CoA. **Figure 4(C)** illustrates the structural sites for fragmentation of acyl-CoA. The neutral loss of 507 was chosen as the product ion (Q3) for the sMRM mode as it was the most intense and common fragment among acyl-CoAs, as observed in our study and supported by other publications [15,19].

In the HILIC-TOF-MS method, the focus was primarily on detecting saturated species, however with the use of highly sensitive QTRAP instrument we were able to detect a few additional monounsaturated species. The identification of these monounsaturated species was confirmed by evaluating the pattern of their retention times (**Figure 5**). The intensity of these species was much lower compared to their saturated form, nevertheless their detection can provide additional information and contribute to understanding the biological context of the study samples. The targets along with their sMRM parameters have been mentioned in **Table 4.**
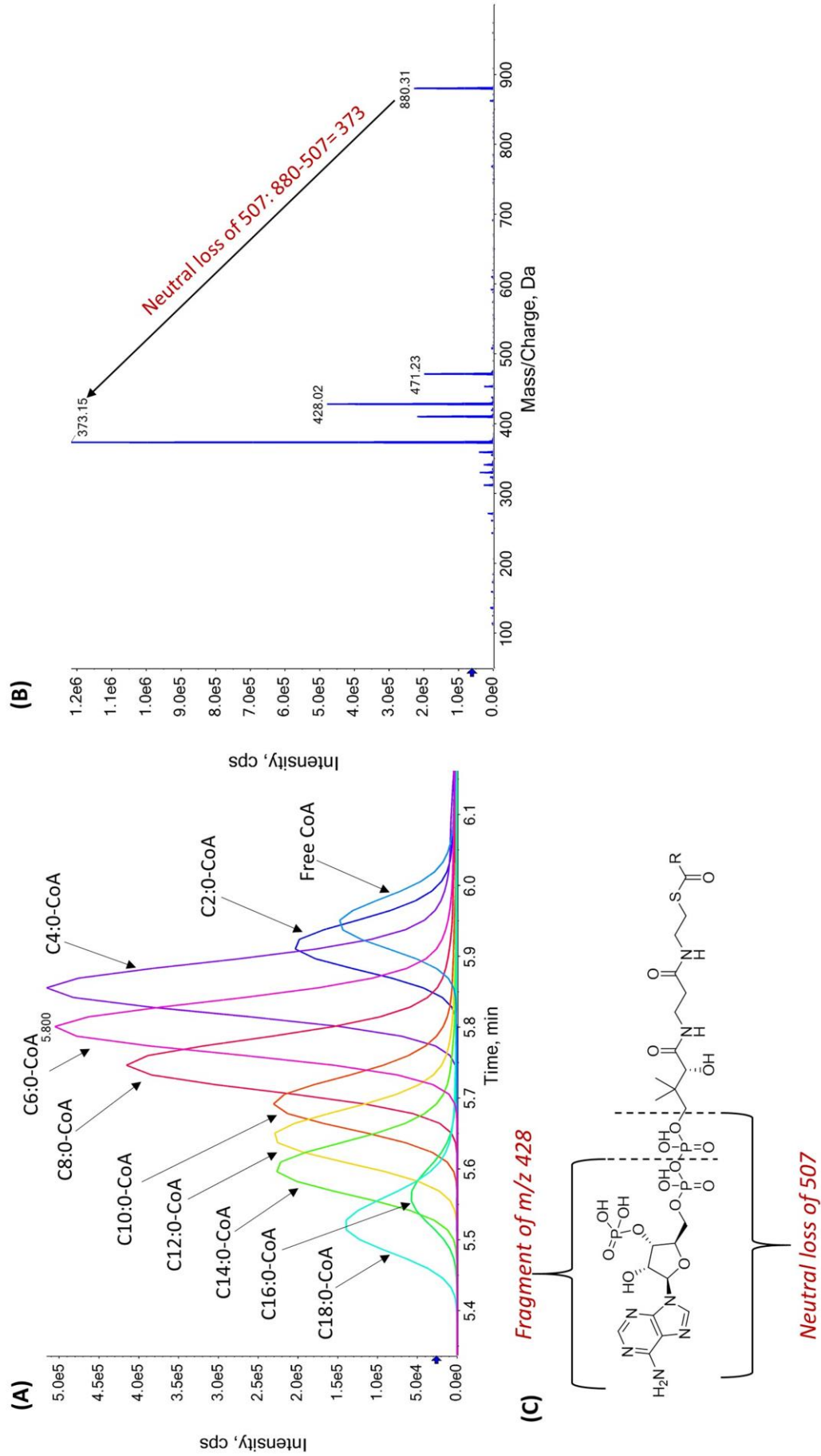
Figure 4. (A) Representative chromatogram of acyl-CoA standards; (B) Mass spectrum showing fragmentation of C7:0-CoA; (C) Structural sites of acyl-CoA fragmentation.

147

Table 4. sMRM parameters for acyl-CoA targets in HILIC-MS/MS method.

Targets	Q1	Q3	RT	DP	CE
CoA (Free CoA)	768.1	261.1	5.99	100	40
C2:0-CoA (Acetyl-CoA)	810.1	303.1	5.95	100	40
C3:0-CoA (Propionyl-CoA)	824.2	317.2	5.90	100	40
C4:1-CoA	836.2	329.2	ND	100	40
C4:0-CoA	838.2	331.2	5.88	100	40
C6:1-CoA	864.2	357.2	ND	100	40
C6:0-CoA (Hexanoyl-CoA)	866.2	359.2	5.82	100	40
C8:1-CoA	892.2	385.2	5.79	100	40
C8:0-CoA(Octanoyl-CoA)	894.2	387.2	5.76	100	40
C10:1-CoA	920.2	413.2	5.72	100	40
C10:0-CoA (Decanoyl-CoA)	922.3	415.3	5.71	100	40
C12:1-CoA	948.3	441.3	5.68	100	45
C12:0-CoA (Lauroyl-CoA)	950.3	443.3	5.65	100	45
C14:1-CoA	976.3	469.3	5.63	100	45
C14:0-CoA (Myristoyl-CoA)	978.3	471.3	5.61	100	45
C16:1-CoA	1004.3	497.3	5.59	100	45
C16:0-CoA (Palmitoyl-CoA)	1006.4	499.4	5.56	100	45
C18:1-CoA	1032.4	525.4	5.55	100	45
C18:0-CoA (Steraoyl-CoA)	1034.4	527.4	5.54	100	45
C2:0-CoA($^{13}C_2$) (Acetyl-1,2-$^{13}C_2$-CoA)*	812.1	305.1	5.95	100	40
C7:0-CoA (Heptanoyl-CoA)*	880.2	373.2	5.78	100	40
C15:0-CoA (Pentadecanoyl-CoA)*	992.3	485.3	5.58	100	45
C17:0-CoA (Heptadecanoyl-CoA)*	1020.4	513.4	5.55	100	45

*, Internal standard; ND, not detected

3.5 Retention time pattern

The identification and confirmation of acyl-CoA species were further supported by analyzing their retention time pattern. In HILIC chromatography, the gradient initiates with an organic mobile phase and subsequently transitions to a more aqueous phase. As a result, acyl-CoA species with longer carbon chains elute first, followed by medium- and short-chain species, as depicted in **Figure 5.** Similarly, species with a higher number of double bonds but the same number of carbon atoms elute later compared to species with a lower number of double bonds. For example, C16:0-CoA elutes at 5.56, while C16:1-CoA elutes at 5.59. This distinct retention time pattern is highly valuable for the identification and confirmation of a wide range of acyl-CoA species.
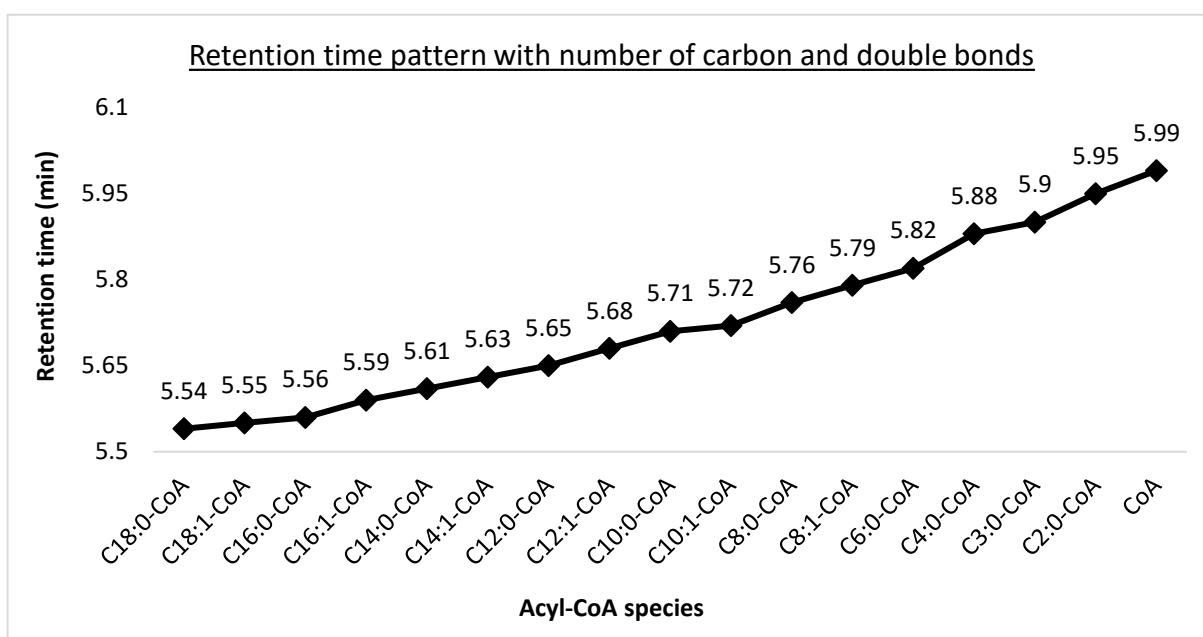

Figure 5. Retention time pattern of acyl-CoA species.

3.6 Method validation of targeted HILIC-MS/MS method

The targeted HILIC-MS/MS method was validated for quantitation of acyl-CoA compounds in HepG2 cells. Representative non-endogenous standards from short-(C2:0($^{13}C_2$)-CoA), medium-(C7:0-CoA) and long-chain (C15:0-CoA and C17:0-CoA) species were chosen for the validation. The calibration curves of non-endogenous standards spiked in pure solvent and in HepG2 cells (before and after extraction) are shown in **Figure 6.** The values of linearity, LOD, LOQ, precision, recovery, matrix effect and carryover are reported in **Table 5**. The linear regression coefficients (R^2) were above 0.99 for all spiked standards. The LODs and LOQs were in the range of (1.3-12.4) pmol mL^{-1} and (3.1-26.6) pmol mL^{-1} respectively which makes our method sensitive enough to detect the acyl-CoAs in ~1×10^6 HepG2 cells. In comparison to

previous studies, reporting LODs in the range of (0.5-2.4) pmol mL^{-1} [26], (3-133) pmol mL^{-1} [7] and (1.2-4.6) pmol mL^{-1} [15], our reported LODs were comparable and, in some cases, even lower. It is worth noting that in our method development, we tried to achieve sensitivity without compromising on reliability and throughput. The intraday and interday precisions were determined at low, medium and high concentration levels. Almost all the classes have RSD (%) below 20% except for C15:0 CoA with slightly higher value of 22.9% at low level. The recovery was in the range of (53-123)% for all standards. It was observed that recovery of long-chain acyl-CoA species is slightly lower. The reason for this may be that long-chain acyl-CoA species have lower polarity compared to short- and medium-chain species, which could result in their migration to the non-polar lower layer. The matrix effect was in the range of (85-133)%. The carryover was analyzed in the blank samples placed right after the highest calibration point in HepG2 cells before extraction and was below 1% for all standards. We are using non-endogenous compounds as internal standards based on the chain length of endogenous targets. These standards elute in close proximity to the endogenous compounds present in the sample. Hence, the issues related to poor recovery, ion suppression and matrix effects can be compensated as internal standards and endogenous compounds will parallelly go through the same processing.

The repeatability evaluates the consistency and reliability of the results, ensuring that there is minimal deviation or variability in the analysis. The repeatability of our HILIC-MS/MS method was determined by measuring the RSD (%) of endogenous acyl-CoA species in QC samples. It was found that out of 19 targets, 7 species show RSD below 5%. The RSD of (5-10)% and (10-15)% was shown by 7 and 1 species respectively while 2 species show RSD in between (15-25)%. Two species were not detected in these samples. In total, 17 acyl-CoA species show RSD below 25% **(Figure S3).** We further tested the stability of non-endogenous acyl-CoA standards in HepG2 cells over 3 days. The extracted samples of HepG2 cells containing these standards were analyzed on day 1. The samples were then stored at -80 °C and analyzed again on day 3. We compared the peak area of these standards on both days **(Table S5)** and found that the deviation over 3-day period, ranges from (5-10)%, indicating good stability during this time. However, for a more comprehensive assessment, further experiments are required by storing samples for longer periods under different conditions.

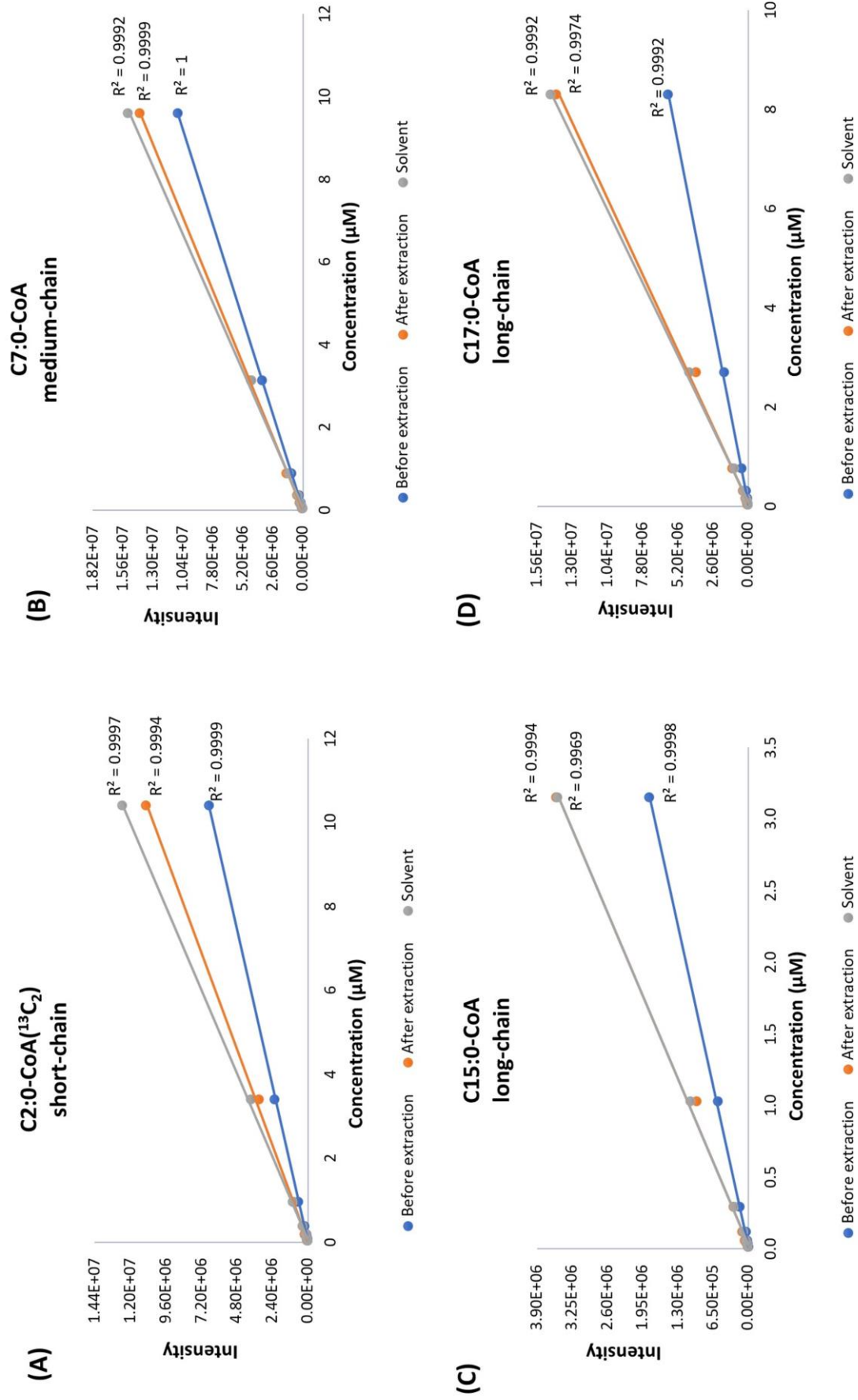**Figure 6.** Calibration curves of non-endogenous acyl-CoA standards spiked in pure solvent, spiked in HepG2 cells before and after extraction. (A) C2:0-CoA($^{13}C_2$): short-chain; (B) C7:0-CoA: medium-chain; (C) C15:0-CoA: long-chain; (D) C17:0-CoA: long-chain.

Table 5. Summary of the validation parameters.

Non-endogenous acyl-CoA standards	Linearity	LOD (μM)	LOQ (μM)	Intraday precision [%]			Interday precision [%]			Recovery [%]			Matrix effect [%]			Carryover [%]
				Low	Medium	High	Low	Medium	High	Low	Medium	High	Low	Medium	High	
C2:0-CoA($^{13}C_2$)	0.9999	0.0013	0.0031	2.2	2.2	1.0	4.7	3.3	2.5	100.0	88.7	92.2	114.7	101.4	85.7	0.4
C7:0-CoA	1	0.0076	0.0136	4.1	3.4	5.2	12.7	17.4	20.3	123.4	100.1	105.4	124.8	113.0	101.1	0.3
C15:0-CoA	0.9998	0.0110	0.0266	9.5	6.5	4.4	22.9	14.2	11.4	73.1	62.0	80.3	129.9	122.2	89.5	0.3
C17:0-CoA	0.9992	0.0124	0.0230	7.0	5.7	3.0	18.4	6.2	14.1	80.9	53.5	62.5	133.1	113.6	89.0	0.2

3.7 Acyl-CoA profile in HepG2 cells cultured in supplemented and starved state

We applied our HILIC-MS/MS method to analyze acyl-CoA profile of wildtype HepG2 cells cultured under two different conditions. In Condition 1 (supplemented cells), the cells were cultured in a medium containing glucose, pyruvate, glutamine with supplementation of carnitine and palmitate. On the other hand, Condition 2 (starved cells) involved culturing the cells in a glucose-free medium with no pyruvate and glutamine, but with the addition of carnitine and palmitate, aiming to simulate a state of starvation. **Figure 7(A)** shows the profile of free CoA and short- to long-chain acyl-CoAs in HepG2 cells cultured under both supplemented (condition 1) and starved conditions (condition 2). **Figure 7(B)** displays the fold change in acyl-CoA levels between the supplemented and starved states. We observed a decrease in the free CoA level ($p<0.05$) during the starvation state of HepG2 cells while there has been an increase in the acetyl-CoA ($p<0.0001$) in starved cells as compared to supplemented ones. The medium chain acyl-CoA also showed an increase in their profile in starved conditions for C6:0-CoA ($p<0.0021$), C8:0-CoA ($p<0.05$) and C10:0-CoA ($p<0.0002$). Furthermore, we observed an increase in the profile of long-chain acyl-CoA such as C12:0-CoA, C14:0-CoA and C16:0-CoA with $p<0.0001$.

The change in the profile of acyl-CoAs in our study shows an activation of fatty acid oxidation. During starvation conditions, cells shift in the survival mode due to decrease in glucose level, activating the FAO process. In FAO, free fatty acids are activated to long-chain acyl-CoA and enter inside the mitochondria for fatty acid oxidation process, thus leading to an increase in the level of long-chain acyl-CoA. A study has reported an increase in the expression of acyl-CoA synthetase (ACS) and carnitine palmitoyltransferase-1 (CPT-1) while decrease in the level of acetyl-CoA carboxylase (ACC) during fasting conditions [49]. ACS increases the formation of fatty acyl-CoA from fatty acid and CPT-1 is responsible for converting acyl-CoAs into acylcarnitines. The increase in the level of both of these enzymes suggests an increase in the transportation of long-chain acyl-CoA inside mitochondria. Our data also reflects the same with increase in the profile of long-chain acyl-CoAs in the starved state. On the contrary, ACC controls the rate-limiting step of FAO by facilitating the formation of malonyl-CoA, an inhibitor of CPT-1. The decrease in its level further supports the formation of long-chain acyl-CoA. Acetyl-CoA (C2:0-CoA) is the final product of FAO pathway. We observed an increase in acetyl-CoA levels, indicating an activation of the FAO pathway. This increased acetyl-CoA formation supports ATP synthesis and promotes the production of ketone bodies [50]. The

activation of FAO relative to downstream Krebs cycle and oxidative phosphorylation further contributes to the accumulation of acetyl-CoA during the state of starvation.

Our observations also indicate a decrease in the profile of free CoA during starvation conditions. One hypothesis to support this observation is an increased utilization of CoA for fatty acid activation by formation of acyl-CoA esters and subsequent FAO processes. This reduction in free CoA levels can be associated with the higher demand for acyl-CoA formation due to the observed increase of acyl-CoA thioesters in our study. Another possible hypothesis could be the inhibition of pantothenate kinase, an enzyme responsible for catalyzing the initial biosynthetic step of free CoA. It is known that higher concentrations of long-chain acyl-CoA and acetyl-CoA can inhibit this enzyme [51]. Consequently, this inhibition of pantothenate kinase may also contribute to the decrease in CoA biosynthesis and subsequently lead to a reduction in free CoA levels.
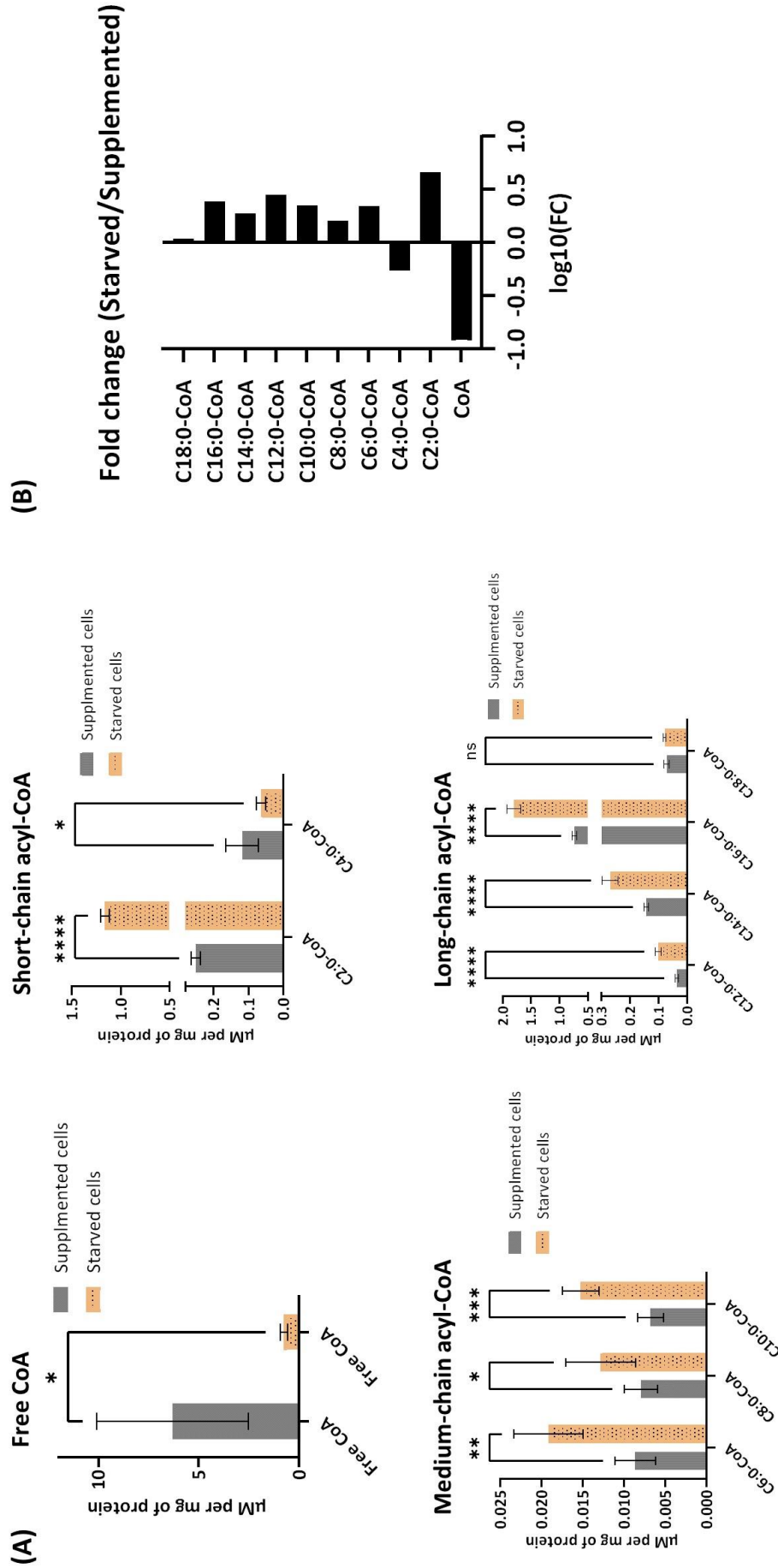
Figure 7. Acyl-CoAs profile in supplemented *vs* starved conditions in wildtype HepG2 cells.(A) Bar graph showing concentration (μM per mg of protein) of free CoA; short-chain acyl-CoA; medium-chain acyl-CoA and long-chain acyl-CoA in supplemented and starved state (* *p*<0.05; ** *p*<0.0021; *** *p*<0.0002; **** *p*<0.0001; ns, not significant).; (B) Fold change of acyl-CoAs in starved/supplemented conditions.

4. Conclusion

We have developed a HILIC-MS/MS method utilizing a zwitterionic ZIC-cHILIC column, covering short- to long-chain acyl-CoA species in one analytical run with the use of lower concentration of ammonium acetate. This HILIC-MS/MS method did not require the use of an ion-pairing reagent, which has several disadvantages like contamination of the MS, nor other complicated derivatization, etc. The characterization of the analytical performance was successful and the method appeared to be sensitive, linear and repeatable. We demonstrated the potential of the method by evaluating the change in acyl-CoA profile in wildtype HepG2 cells cultured in supplemented and starved state. We observed an increase in the profile of acetyl-CoA, medium- and long-chain acyl-CoA while decrease in the level of free CoA in HepG2 cells cultured in starved state. These findings suggest an increase in the fatty acid oxidation process in starved state, relative to the downstream metabolic processes.

The comprehensive analysis of acyl-CoA species in one run is highly beneficial for high-throughput analysis of biological samples and has the potential for integration in clinical settings because of its simplicity and robustness. This HILIC-MS/MS method can be further extended in the future to cover very long-chain acyl-CoA species. However, the separation and identification of isomers such as butyryl and isobutryl-CoA, succinyl-CoA and methylmalonyl-CoA, etc., or the identification of position of double bond in species such as C10:1-CoA or C18:1-CoA is the current limitation associated with this method and therefore, these species were reported by the carbon chain composition instead of their names. Hence, in future additional research should be performed for the separation of these isomeric species, which can involve exploring the use of ion-mobility mass spectrometry and electron-activated dissociation (EAD) techniques.

Author contributions

Madhulika Singh: Investigation, Conceptualization, Methodology, Data curation, Visualization, Writing – original draft & editing. Ligia Akemi Kiyuna: Methodology, Investigation, Writing – review & editing. Christoff Odendaal: Methodology, Writing – review & editing. Barbara M. Bakker: Writing – review & editing. Amy C. Harms: Supervision, Writing – review & editing. Thomas Hankemeier: Supervision, Funding acquisition, Writing – review & editing.

Declaration of competing interests

The authors declare no competing financial interests.

Acknowledgements

References

[1]   C.C.C.R. de Carvalho, M.J. Caramujo, The Various Roles of Fatty Acids, Molecules. 23 (2018) 2583. https://doi.org/10.3390/molecules23102583.

[2]   E.P. Brass, Overview of coenzyme A metabolism and its role in cellular toxicity, Chemico-Biological Interactions. 90 (1994) 203–214. https://doi.org/10.1016/0009-2797(94)90010-8.

[3]   J.L. Merritt, E. MacLeod, A. Jurecka, B. Hainline, Clinical manifestations and management of fatty acid oxidation disorders, Rev Endocr Metab Disord. 21 (2020) 479–493. https://doi.org/10.1007/s11154-020-09568-3.

[4]   S.M. Houten, R.J.A. Wanders, A general introduction to the biochemistry of mitochondrial fatty acid β-oxidation, J Inherit Metab Dis. 33 (2010) 469–477. https://doi.org/10.1007/s10545-010-9061-2.

[5]   P.A. Watkins, Fatty acid activation, Prog Lipid Res. 36 (1997) 55–83. https://doi.org/10.1016/s0163-7827(97)00004-0.

[6]   J.M. Ellis, C.E. Bowman, M.J. Wolfgang, Metabolic and Tissue-Specific Regulation of Acyl-CoA Metabolism, PLOS ONE. 10 (2015) e0116587. https://doi.org/10.1371/journal.pone.0116587.

[7]   Q. Li, S. Zhang, J.M. Berthiaume, B. Simons, G.-F. Zhang, Novel approach in LC-MS/MS using MRM to generate a full profile of acyl-CoAs: discovery of acyl-dephospho-CoAs, J Lipid Res. 55 (2014) 592–602. https://doi.org/10.1194/jlr.D045112.

[8]   T.J. Grevengoed, E.L. Klett, R.A. Coleman, Acyl-CoA Metabolism and Partitioning, Annu Rev Nutr. 34 (2014) 1–30. https://doi.org/10.1146/annurev-nutr-071813-105541.

[9]   T. Migita, K. Takayama, T. Urano, D. Obinata, K. Ikeda, T. Soga, S. Takahashi, S. Inoue, ACSL3 promotes intratumoral steroidogenesis in prostate cancer cells, Cancer Sci. 108 (2017) 2011–2021. https://doi.org/10.1111/cas.13339.

[10] S. Zhang, O.D. Nelson, I.R. Price, C. Zhu, X. Lu, I.R. Fernandez, R.S. Weiss, H. Lin, Long-chain fatty acyl coenzyme A inhibits NME1/2 and regulates cancer metastasis, Proceedings of the National Academy of Sciences. 119 (2022) e2117013119. https://doi.org/10.1073/pnas.2117013119.

[11]   S. Jackowski, R. Leonardi, Deregulated Coenzyme A, Loss of Metabolic Flexibility and Diabetes, Biochem Soc Trans. 42 (2014) 1118–1122. https://doi.org/10.1042/BST20140156.

[12]   J.E. Kanter, F. Kramer, S. Barnhart, M.M. Averill, A. Vivekanandan-Giri, T. Vickery, L.O. Li, L. Becker, W. Yuan, A. Chait, K.R. Braun, S. Potter-Perigo, S. Sanda, T.N. Wight, S. Pennathur, C.N. Serhan, J.W. Heinecke, R.A. Coleman, K.E. Bornfeldt, Diabetes promotes an inflammatory macrophage phenotype and atherosclerosis through acyl-CoA synthetase 1, Proceedings of the National Academy of Sciences. 109 (2012) E715–E724. https://doi.org/10.1073/pnas.1111600109.

[13] A. Michno, A. Raszeja-Specht, A. Jankowska-Kulawy, T. Pawelczyk, A. Szutowicz, Effect of L-Carnitine on Acetyl-CoA Content and Activity of Blood Platelets in Healthy and Diabetic Persons, Clinical Chemistry. 51 (2005) 1673–82. https://doi.org/10.1373/clinchem.2005.050328.

[14]   S. HORIE, M. ISOBE, T. SUGA, Changes in CoA Pools in Hepatic Peroxisomes of the Rat, under Various Conditions, The Journal of Biochemistry. 99 (1986) 1345–1352. https://doi.org/10.1093/oxfordjournals.jbchem.a135602.

[15] P. Li, M. Gawaz, M. Chatterjee, M. Lämmerhofer, Targeted Profiling of Short-, Medium-, and Long-Chain Fatty Acyl-Coenzyme As in Biological Samples by Phosphate Methylation Coupled to Liquid Chromatography–Tandem Mass Spectrometry, Anal. Chem. 93 (2021) 4342–4350. https://doi.org/10.1021/acs.analchem.1c00664.

[16] L. Gao, W. Chiou, H. Tang, X. Cheng, H. Camp, D. Burns, Simultaneous quantification of malonyl-CoA and several other short-chain acyl-CoAs in animal tissues by ion-pairing reversed-phase HPLC/MS, Journal of Chromatography. B, Analytical Technologies in the Biomedical and Life Sciences. 853 (2007) 303–13. https://doi.org/10.1016/j.jchromb.2007.03.029.

[17] S. Wang, Z. Wang, L. Zhou, X. Shi, G. Xu, Comprehensive Analysis of Short-, Medium-, and Long-Chain Acyl-Coenzyme A by Online Two-Dimensional Liquid Chromatography/Mass Spectrometry, Anal Chem. 89 (2017) 12902–12908. https://doi.org/10.1021/acs.analchem.7b03659.

[18] X. Yang, Y. Ma, N. Li, H. Cai, M.G. Bartlett, Development of a Method for the Determination of Acyl-CoA Compounds by Liquid Chromatography Mass Spectrometry to Probe the Metabolism of Fatty Acids, Anal. Chem. 89 (2017) 813–821. https://doi.org/10.1021/acs.analchem.6b03623.

[19] L.G. Rivera, M.G. Bartlett, Chromatographic methods for the determination of acyl-CoAs, Anal. Methods. 10 (2018) 5252–5264. https://doi.org/10.1039/C8AY01472H.

[20] P.G. Tardi, J.J. Mukherjee, P.C. Choy, The quantitation of long-chain acyl-CoA in mammalian tissue, Lipids. 27 (1992) 65–67. https://doi.org/10.1007/BF02537062.

[21] G. Liu, J. Chen, P. Che, Y. Ma, Separation and Quantitation of Short-Chain Coenzyme A's in Biological Samples by Capillary Electrophoresis, Anal. Chem. 75 (2003) 78–82. https://doi.org/10.1021/ac0261505.

[22] A. Demoz, A. Garras, D.K. Asiedu, B. Netteland, R.K. Berge, Rapid method for the separation and detection of tissue short-chain coenzyme A esters by reversed-phase high-performance liquid chromatography, Journal of Chromatography B: Biomedical Sciences and Applications. 667 (1995) 148–152. https://doi.org/10.1016/0378-4347(94)00595-V.

[23] X. Liu, S. Sadhukhan, S. Sun, G.R. Wagner, M.D. Hirschey, L. Qi, H. Lin, J.W. Locasale, High-Resolution Metabolomics with Acyl-CoA Profiling Reveals Widespread Remodeling in Response to Diet, Mol Cell Proteomics. 14 (2015) 1489–1500. https://doi.org/10.1074/mcp.M114.044859.

[24] M. Singh, H.L. Elfrink, A.C. Harms, T. Hankemeier, Recent developments in the analytical approaches of acyl-CoAs to assess their role in mitochondrial fatty acid oxidation disorders, Molecular Genetics and Metabolism. (2023) 107711. https://doi.org/10.1016/j.ymgme.2023.107711.

[25] A.E. Jones, N.J. Arias, A. Acevedo, S.T. Reddy, A.S. Divakaruni, D. Meriwether, A Single LC-MS/MS Analysis to Quantify CoA Biosynthetic Intermediates and Short-Chain Acyl CoAs, Metabolites. 11 (2021) 468. https://doi.org/10.3390/metabo11080468.

[26] L. Abrankó, G. Williamson, S. Gardner, A. Kerimi, Comprehensive quantitative analysis of fatty-acyl-Coenzyme A species in biological samples by ultra-high performance liquid chromatography–tandem mass spectrometry harmonizing hydrophilic interaction and reversed phase chromatography, Journal of Chromatography A. 1534 (2018) 111–122. https://doi.org/10.1016/j.chroma.2017.12.052.

[27] N.W. Snyder, S.S. Basu, Z. Zhou, A.J. Worth, I.A. Blair, Stable isotope dilution liquid chromatography-mass spectrometry analysis of cellular and tissue medium- and long-chain acyl-coenzyme A thioesters, Rapid Commun Mass Spectrom. 28 (2014) 1840–1848. https://doi.org/10.1002/rcm.6958.

[28] S. Neubauer, D.B. Chu, H. Marx, M. Sauer, S. Hann, G. Koellensperger, LC-MS/MS-based analysis of coenzyme A and short-chain acyl-coenzyme A thioesters, Anal Bioanal Chem. 407 (2015) 6681–6688. https://doi.org/10.1007/s00216-015-8825-9.

[29] S.M. Lam, T. Zhou, J. Li, S. Zhang, G.H. Chua, B. Li, G. Shui, A robust, integrated platform for comprehensive analyses of acyl-coenzyme As and acyl-carnitines revealed chain length-dependent disparity in fatty acyl metabolic fates across Drosophila development, Science Bulletin. 65 (2020) 1840–1848. https://doi.org/10.1016/j.scib.2020.07.023.

[30] M. Holcapek, K. Volná, P. Jandera, L. Kolárová, K. Lemr, M. Exner, A. Církva, Effects of ion-pairing reagents on the electrospray signal suppression of sulphonated dyes and intermediates, J Mass Spectrom. 39 (2004) 43–50. https://doi.org/10.1002/jms.551.

[31] B. Buszewski, S. Noga, Hydrophilic interaction liquid chromatography (HILIC)--a powerful separation technique, Anal Bioanal Chem. 402 (2012) 231–247. https://doi.org/10.1007/s00216-011-5308-5.

[32] R. Li, J. Huang, Chromatographic behavior of epirubicin and its analogues on high-purity silica in hydrophilic interaction chromatography, J Chromatogr A. 1041 (2004) 163–169. https://doi.org/10.1016/j.chroma.2004.04.033.

[33] P. Hemström, K. Irgum, Hydrophilic interaction chromatography, Journal of Separation Science. 29 (2006) 1784–1821. https://doi.org/10.1002/jssc.200600199.

[34] H. Wu, A.D. Southam, A. Hines, M.R. Viant, High-throughput tissue extraction protocol for NMR- and MS-based metabolomics, Anal Biochem. 372 (2008) 204–212. https://doi.org/10.1016/j.ab.2007.10.002.

[35]   T. Van Der Laan, A.-C. Dubbelman, K. Duisters, A. Kindt, A.C. Harms, T. Hankemeier, High-Throughput Fractionation Coupled to Mass Spectrometry for Improved Quantitation in Metabolomics, Anal. Chem. 92 (2020) 14330–14338. https://doi.org/10.1021/acs.analchem.0c01375.

[36]   N. Kadian, K.S.R. Raju, M. Rashid, M.Y. Malik, I. Taneja, M. Wahajuddin, Comparative assessment of bioanalytical method validation guidelines for pharmaceutical industry, Journal of Pharmaceutical and Biomedical Analysis. 126 (2016) 83–97. https://doi.org/10.1016/j.jpba.2016.03.052.

[37]   D. Wolrab, M. Chocholoušková, R. Jirásko, O. Peterka, M. Holčapek, Validation of lipidomic analysis of human plasma and serum by supercritical fluid chromatography-mass spectrometry and hydrophilic interaction liquid chromatography-mass spectrometry, Anal Bioanal Chem. 412 (2020) 2375–2388. https://doi.org/10.1007/s00216-020-02473-3.

[38]   M. Azim, M. Moloy, P. Bhasin, HPLC METHOD DEVELOPMENT AND VALIDATION: A REVIEW, International Research Journal of Pharmacy. 4 (2015) 39–46. https://doi.org/10.7897/2230-8407.04407.

[39]   merck_sequant-zic-chilic_brochure.pdf, (n.d.). https://mz-at.de/fileadmin/user_upload/Brochures/merck_sequant-zic-chilic_brochure.pdf (accessed June 8, 2023).

[40]   F. Hosseinkhani, L. Huang, A.-C. Dubbelman, F. Guled, A.C. Harms, T. Hankemeier, Systematic Evaluation of HILIC Stationary Phases for Global Metabolomics of Human Plasma, Metabolites. 12 (2022) 165. https://doi.org/10.3390/metabo12020165.

[41]   S. Arase, S. Kimura, T. Ikegami, Method optimization of hydrophilic interaction chromatography separation of nucleotides using design of experiment approaches I: Comparison of several zwitterionic columns, J Pharm Biomed Anal. 158 (2018) 307–316. https://doi.org/10.1016/j.jpba.2018.05.014.

[42]   E. Zborníková, Z. Knejzlík, V. Hauryliuk, L. Krásný, D. Rejman, Analysis of nucleotide pools in bacteria using HPLC-MS in HILIC mode, Talanta. 205 (2019) 120161. https://doi.org/10.1016/j.talanta.2019.120161.

[43]   A. Wakamatsu, K. Morimoto, M. Shimizu, S. Kudoh, A severe peak tailing of phosphate compounds caused by interaction with stainless steel used for liquid chromatography and electrospray mass spectrometry, Journal of Separation Science. 28 (2005) 1823–1830. https://doi.org/10.1002/jssc.200400027.

[44]   J. Zhang, Q. Wang, B. Kleintop, T. Raglione, Suppression of peak tailing of phosphate prodrugs in reversed-phase liquid chromatography, Journal of Pharmaceutical and Biomedical Analysis. 98 (2014) 247–252. https://doi.org/10.1016/j.jpba.2014.05.027.

[45]   H.-L. Koh, A.-J. Lau, E.C.-Y. Chan, Hydrophilic interaction liquid chromatography with tandem mass spectrometry for the determination of underivatized dencichine (beta-N-oxalyl-L-alpha,beta-diaminopropionic acid) in Panax medicinal plant species, Rapid Commun Mass Spectrom. 19 (2005) 1237–1244. https://doi.org/10.1002/rcm.1928.

[46]   I. Kohler, M. Verhoeven, R. Haselberg, A.F.G. Gargano, Hydrophilic interaction chromatography – mass spectrometry for metabolomics and proteomics: state-of-the-art and current trends, Microchemical Journal. 175 (2022) 106986. https://doi.org/10.1016/j.microc.2021.106986.

[47]   Y. Du, Y. Li, X. Hu, X. Deng, Z. Qian, Z. Li, M. Guo, D. Tang, Development and evaluation of a hydrophilic interaction liquid chromatography-MS/MS method to quantify 19 nucleobases and nucleosides in rat plasma, Biomedical Chromatography. 31 (2017) e3860. https://doi.org/10.1002/bmc.3860.

[48]   X. Liu, Z. Ser, J.W. Locasale, Development and Quantitative Evaluation of a High-Resolution Metabolomics Technology, Anal. Chem. 86 (2014) 2175–2184. https://doi.org/10.1021/ac403845u.

[49]   M.-H. Ryu, J.W. Daily, Y.-S. Cha, Effect of starvation on hepatic acyl-CoA synthetase, carnitine palmitoyltransferase-I, and acetyl-CoA carboxylase mRNA levels in rats, Nutrition. 21 (2005) 537–542. https://doi.org/10.1016/j.nut.2004.08.015.

[50]   L. Shi, B.P. Tu, Acetyl-CoA and the Regulation of Metabolism: Mechanisms and Consequences, Curr Opin Cell Biol. 33 (2015) 125–131. https://doi.org/10.1016/j.ceb.2015.02.003.

[51]   Y.-M. Zhang, C.O. Rock, S. Jackowski, Feedback Regulation of Murine Pantothenate Kinase 3 by Coenzyme A and Coenzyme A Thioesters, Journal of Biological Chemistry. 280 (2005) 32594–32601. https://doi.org/10.1074/jbc.M506275200.

Chapter 5

Supplementary material

Table S1. Gradient table for HILIC-TOF-MS chromatographic separation of acyl-CoAs in high-resolution mode.

Time (min)	Flow rate (mL min^{-1})	MP-A (%)	MP-B (%)
Initial	0.25	100	0
2.3	0.25	100	0
14	0.25	25	75
15.5	0.25	25	75
15.6	0.25	0	100
17.5	0.25	0	100
18.5	0.25	100	0
20	0.25	100	0

Table S2. Concentration (µM) of non-endogenous standards used for preparing the calibration curves for validation.

Standards	cal-1	cal-2	cal-3	cal-4	cal-5	cal-6	cal-7	cal-8
C2:0-CoA($^{13}C_2$)	0.042	0.063	0.117	0.193	0.386	0.964	3.396	10.410
C7:0-CoA	0.039	0.059	0.108	0.178	0.356	0.890	3.133	9.604
C15:0-CoA	0.013	0.019	0.035	0.058	0.117	0.292	1.028	3.150
C17:0-CoA	0.034	0.051	0.093	0.154	0.308	0.769	2.708	8.302

Table S3. Accurate and observed m/z values of representative acyl-CoA standards in protonated **[M+H]$^+$**, deprotonated **[M-H]$^-$** and doubly charged **[M-2H]$^{2-}$** ionization modes.

Standards	[M+H]$^+$		[M-H]$^-$		[M-H]$^{2-}$	
	Accurate mass	**Observed mass**	**Accurate mass**	**Observed mass**	**Accurate mass**	**Observed masss**
C2:0-CoA	**810.133**	810.140	**808.119**	808.123	**403.556**	403.551
C8:0-CoA	**894.227**	894.234	**892.212**	892.211	**445.603**	445.607
C16:0-CoA	**1006.352**	1006.362	**1004.338**	1004.338	**501.665**	501.666
C18:1-CoA	**1032.368**	1032.367	**1030.353**	1030.353	**514.673**	514.678

Table S4. Accurate and observed m/z values with the retention time of the targets in protonated [M+H]$^+$ form.

Free CoA/Acyl-CoA Species	Accurate [M+H]$^+$	Observed [M+H]$^+$	Retention Time (min)
Free CoA	768.12378	768.1254	6.52
C2:0-CoA	810.1331	810.136	6.44
C3:0-CoA	824.1487	824.1458	6.39
C4:0-CoA	838.1644	838.1579	6.35
C6:0-CoA	866.1957	866.193	6.3
C8:0-CoA	894.227	894.2336	6.09
C10:0-CoA	922.2583	922.2548	6
C12:0-CoA	950.2896	950.2924	5.91
C14:0-CoA	978.3209	978.3266	5.84
C16:0-CoA	1006.3522	1006.35	5.78
C18:0-CoA	1034.3835	1034.3823	5.75

Table S5. Deviation in the peak area of non-endogenous acyl-CoA standards over 3 days after storing at -80 °C.

Non-endogenous acyl-CoA standards	Area measured on day-1	Area measured on day-3	RSD (%)
C2:0-CoA(^{13}C$_2$)	2.14E+06	2.38E+06	7.61
C7:0-CoA	3.53E+06	4.07E+06	10.07
C15:0-CoA	1.02E+06	9.35E+05	5.86
C17:0-CoA	8.10E+05	7.34E+05	6.94

(A)

C2:0-CoA

(B)

C8:0-CoA

(C)

C16:0-CoA
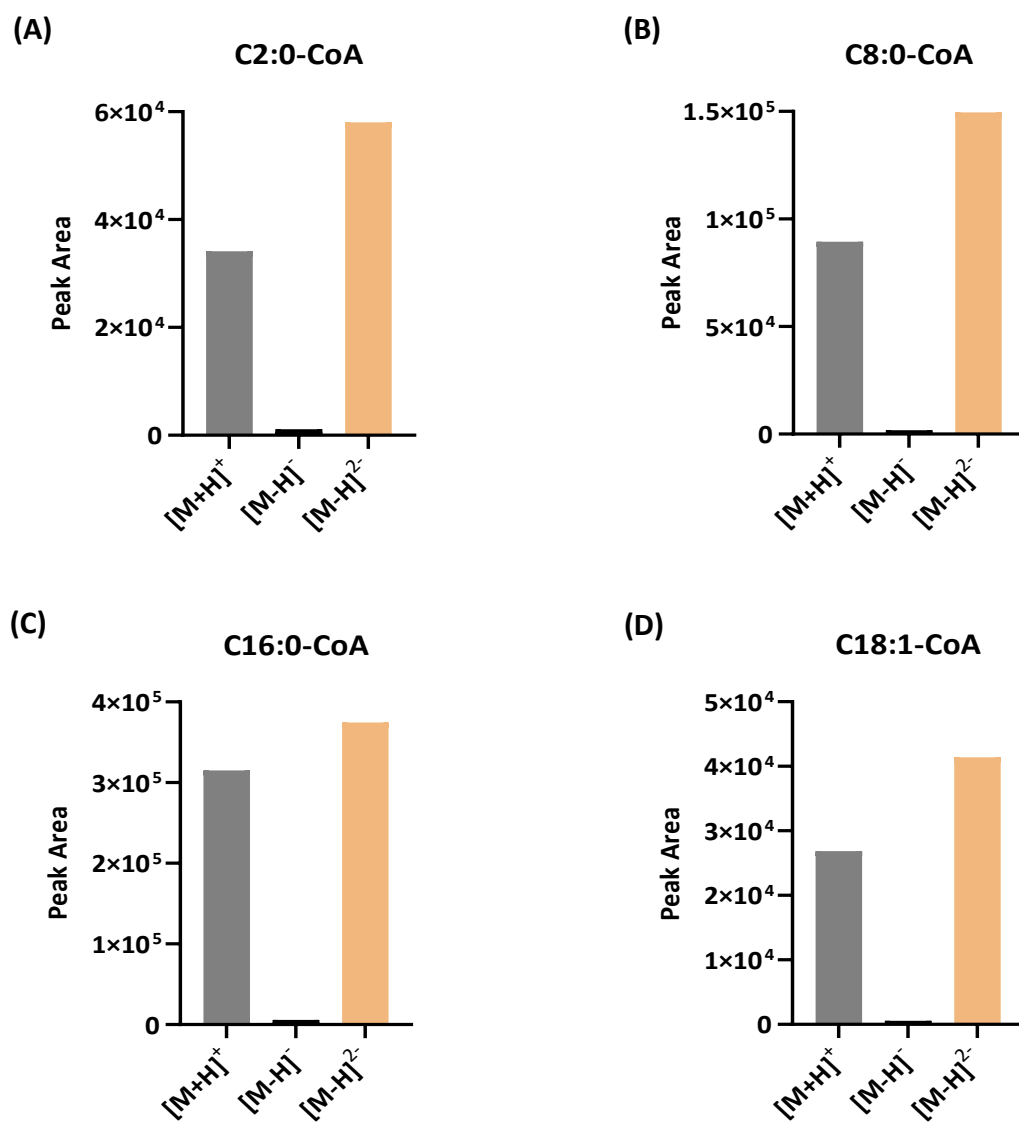

(D)

C18:1-CoA

Figure S1. Sensitivity of representative acyl-CoA standards in positive and negative ion mode. (A) C2:0-CoA; (B) C8:0-CoA; (C) C16:0-CoA; (D) C18:1-CoA.
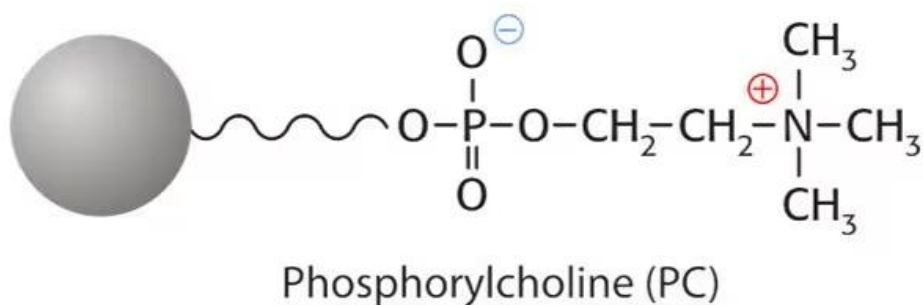

Phosphorylcholine (PC)

Figure S2. Zwitterionic stationary phase of ZIC-cHILIC column consists of phosphorylcholine group.
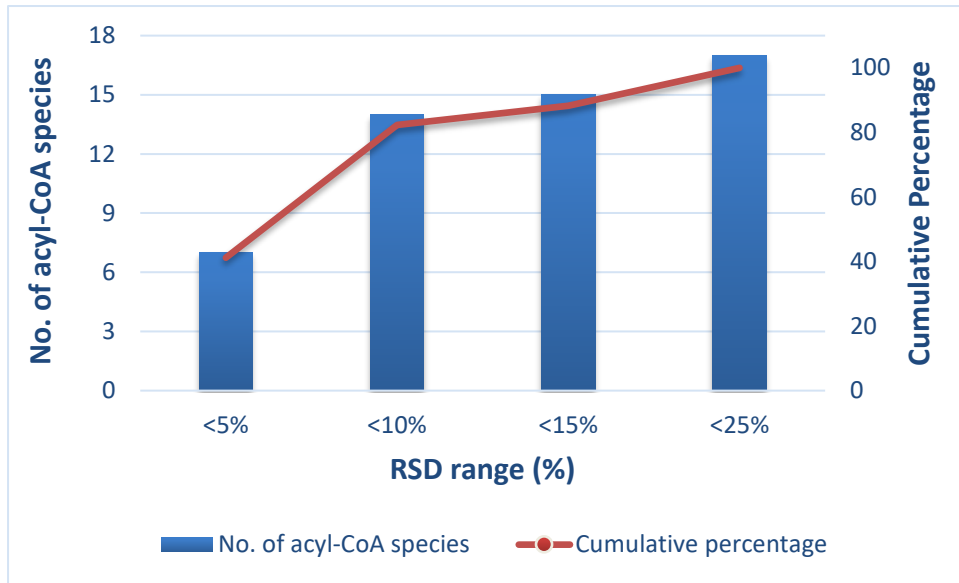
Figure S3. Repeatability of identified acyl-CoA species in HepG2 cells.

Chapter 6

An old new player in MCADD: reduced free coenzyme A availability in medium-chain acyl-CoA dehydrogenase deficiency

(To be revised according to manuscript in preparation)

Christoff Odendaal*, Ligia Akemi Kiyuna*, **Madhulika Singh***, Albert Gerding, Miriam Langelaar-Makkinje, Marianne van der Zwaag, Asmara Drachman, Vladimíra Cetkovská, Gaby Liem Foeng Kioen, Anne-Claire M.F. Martines, Nicolette C. A. Huijkman, Hein Schepers, Bart van de Sluis, Dirk-Jan Reijngoud, Ody C.M. Sibon, Amy C. Harms, Thomas Hankemeier, Barbara M. Bakker

 *authors contributed equally

Abstract

Background: Medium-chain acyl-CoA dehydrogenase deficiency (MCADD) is the most prevalent mitochondrial fatty-acid oxidation (mFAO) disorder. Among its symptoms, life-threatening hypoketotic hypoglycemia remains poorly understood. Using a computational model of hepatic mFAO, we predicted that MCADD leads to an increased risk of free coenzyme A (CoASH) depletion due to sequestration into medium-chain acyl-CoA esters, which may in turn impact glucose production. Therefore, we aimed to quantify the acyl-CoA esters and the CoA pool in MCAD-deficient cells and mouse liver. Moreover, we investigated the existence of compensatory mechanisms that would respond to such CoA sequestration.

Methods: Free CoA, acyl-CoA and acylcarnitine profiles were measured in wildtype (WT) and MCAD knockout (KO) HepG2 cells. $^{13}C_3^{15}N_1$- labeled pantothenate (precursor of free CoA) was used to estimate the CoA synthesis rate. Total CoA (sum of the free CoA fraction and CoA thioesters) and the expression of proteins involved in CoA turnover were analyzed in HepG2 cells as well as in the liver of WT & MCAD KO mice (C57BL/6, exposed to 14 h overnight fasting at room temperature followed by 4 h fasting at 4 °C).

Results: Compared to WT, MCAD-KO cells presented increased levels of C6-C10 acyl-CoAs, and reduced levels of free CoA, short- and long-chain acyl-CoAs. The changes in the acyl-CoA profile were mirrored in the cognate acylcarnitines. Under cold exposure, hepatic total CoA was strongly increased in MCAD-KO mice compared to the WT group, coinciding with an upregulation of acyl-CoA thioesterases (ACOTs), carnitine acyltransferases and pantothenate kinases. Computational simulations predicted recovery of free CoA and reduction in C8-CoA accumulation in the MCAD-KO model on increasing total CoA and ACOT levels simultaneously.

Discussion: Validating the computational simulations, free CoA was reduced in MCAD-KO cells due to its sequestration into medium-chain acyl-CoAs. Altogether, the experimental and modelling results suggest the role of multiple compensatory mechanisms in MCAD deficiency, specifically the upregulation of CoA biosynthesis and ACOT expression, which would work towards increasing the free CoA fraction and relieving the accumulation of acyl-CoA species, respectively.

Keywords

MCADD; *in silico*; *in vitro*; *in vivo*; Acyl-CoA esters; Total CoA; Free CoA/CoASH

1. Introduction

Coenzyme A (CoA) is vital for many metabolic pathways, particularly in the mitochondria. The most recent genome-scale reconstruction of human metabolism, Human1, contained 1044 reactions that consume or produce CoA – 8% of all its reactions [1]. It is essential for the mitochondrial fatty acid oxidation (mFAO), the oxidation of branched-chain amino acids and the tricarboxylic acid cycle, among others. Classically, symptoms of a metabolic disease are attributed to the function of the pathway in which a defect is found. For instance, an impairment of the mFAO limits the availability of energy from fat. It has been hypothesized, however, that a range of diseases in which CoA is implicated might also exert their pathogenicity via the accumulation of metabolites bound to CoA (acyl-CoA esters) and the consequent depletion of the free form of CoA (free CoA, also referred as CoASH). This hypothesis has been called CASTOR for Coenzyme A Sequestration, Toxicity and Redistribution [2–4]. Common symptoms of CASTOR diseases include acidosis, hypoglycemia and hyperammonemia, often with liver, heart or multiple organ dysfunction. These common symptoms are attributed to a lack of CoA required for gluconeogenesis and oxidative phosphorylation, as well as ureagenesis [2,5].

Medium-chain acyl-CoA dehydrogenase deficiency (MCADD, #OMIM 201450) is the most prevalent inborn error of mitochondrial fatty acid oxidation [6]. In humans, the medium-chain acyl-CoA dehydrogenase (MCAD) enzyme catalyzes the conversion of acyl-CoA esters with a chain length of 6-12 carbons into the corresponding enoyl-CoA esters. It is considered the most important enzyme for the oxidation of medium-chain fatty acids. Around 80% of clinically presenting patients are homozygous for the c.985A>G missense mutation in the *ACADM* gene, with less than 1% residual MCAD activity [7,8]. In blood and serum of patients, elevated levels of acylcarnitine esters of 6-10 carbon-atom chain length are observed, as well as an elevated ratio of C8/10 acylcarnitines [7]. These are thought to correspond to elevated levels of the corresponding acyl-CoA esters in the liver [9,10]. Before MCADD was included in the newborn screening programmes of many countries [11–14], it was typically diagnosed through life-threatening hypoketotic hypoglycemia in the first five years of life, or via a symptomatic sibling [15–17]. This hypoglycemia in combination with the accumulation of medium-chain acyl-CoA esters would make MCADD a typical CASTOR disease [2].

Direct evidence for accumulation of CoA esters and depletion of free CoA in putative CASTOR diseases is limited [3,4,18]. Most often the cognate carnitine esters are measured [3,4]. Propionyl-CoA carboxylase deficiency (propionic acidemia) is an example of

mitochondrial disorder resulting in reduced metabolism of propionyl-CoA. Like other CASTOR diseases, propionic acidemia is associated with metabolic acidosis, hypoglycemia, and hyperammonemia [19]. A study conducted measurements of both CoA and carnitine metabolites and demonstrated an elevated level of propionyl carnitine, propionyl-CoA and reduced free CoA in mouse model of these disorders [20,21]. Furthermore, this study also revealed that the metabolite concentration of free CoA can be restored by pharmacological activation of CoA biosynthesis [20]. A further piece of theoretical evidence of CoA metabolism comes from computational models of the mitochondrial fatty-acid oxidation in rodents. Model simulations predicted that the loss of MCAD activity causes severe reduction of free CoA due to its sequestration into medium-chain acyl-CoAs [22,23]. The simulations suggest that the mFAO pathway is particularly vulnerable to the CASTOR phenotype, due to the promiscuity of mFAO enzymes for substrates of different acyl-chain lengths, which may lead to a vicious cycle of acyl-CoA accumulation and free CoA depletion [24].

Quantitative and simultaneous analysis of acyl-CoA esters and free CoA is challenging due to the technical difficulty associated with the measurement of these compounds such as use of multiple methods for covering short-to long-chain species (high to low polarity) [25]. Recently, hydrophilic interaction liquid chromatography coupled with tandem mass spectrometry (HILIC-MS/MS) was shown to achieve a comprehensive analysis of free CoA and short- to long-chain acyl-CoA (covering carbon chain lengths from 2 to 18) in a single analytical run with good linearity, precision, and recovery [26]. This method allowed to explore the CASTOR hypothesis in MCADD experimentally in a convenient and direct way.

The levels of free CoA are not solely regulated by sequestration into CoA esters. Free CoA sequestration may be relieved by hydrolysis via thioesterases [27] or conversion into the cognate carnitine esters by acyltransferases [28–30]. Additionally, CoA can be synthesized *de novo* from pantothenate (vitamin B5) [31]. The biosynthesis of CoA may be inhibited by high levels of acyl-CoA species. Pantothenate kinase (PANK) is the first enzyme of CoA synthesis from pantothenate. Particularly, the hepatic PANK3 is inhibited by medium-chain acyl-CoA species. Last but not least, local free CoA levels may be affected by rerouting of acyl-CoA into the peroxisomal beta-oxidation [32]. The ability to redistribute CoA across the organelles has been proposed, for instance by purported peroxisomal CoA carrier SLC25A17 [33], and its mitochondrial cognates SLC25A16 [34] and SLC25A42 [35]. It is well known that this surrounding metabolic network (**Figure 1A**) of CoA release, biosynthesis and redistribution is regulated by gene expression in response to feeding/fasting cycles [36,37], cold [38] and

pharmacological intervention (e.g. HoPan) [29]. It is not known, however, how the network is regulated in response to CASTOR diseases, such as MCADD.

Addressing the overarching question of how free and total CoA are impacted by MCADD, the present study used *in silico*, *in vitro* and *in vivo* models. In agreement with previous reports, the *in silico* model of human liver (**Figure 1B**) suggests that an accumulation in C8-CoA dominates the CoA pool in mitochondria in MCADD conditions [22,23], which was experimentally tested in *in vitro* (wildtype (WT) and MCAD-knockout (KO) HepG2 cells) using the recently developed HILIC-MS/MS method [26]. Stable isotope labelling which could be detected by the HILIC-MS/MS method, was employed to track any possible changes in CoA synthesis in WT and MCAD-KO conditions. Similar experiments were performed in *in vivo* (WT and MCAD-KO mice liver) under physiologically relevant conditions. Gene expression levels involved in CoA turnover were also analyzed both *in vitro* and *in vivo*. Taken together, our study shows how multi-scale experimental and computational tools can be used to untangle systemic changes in MCADD.
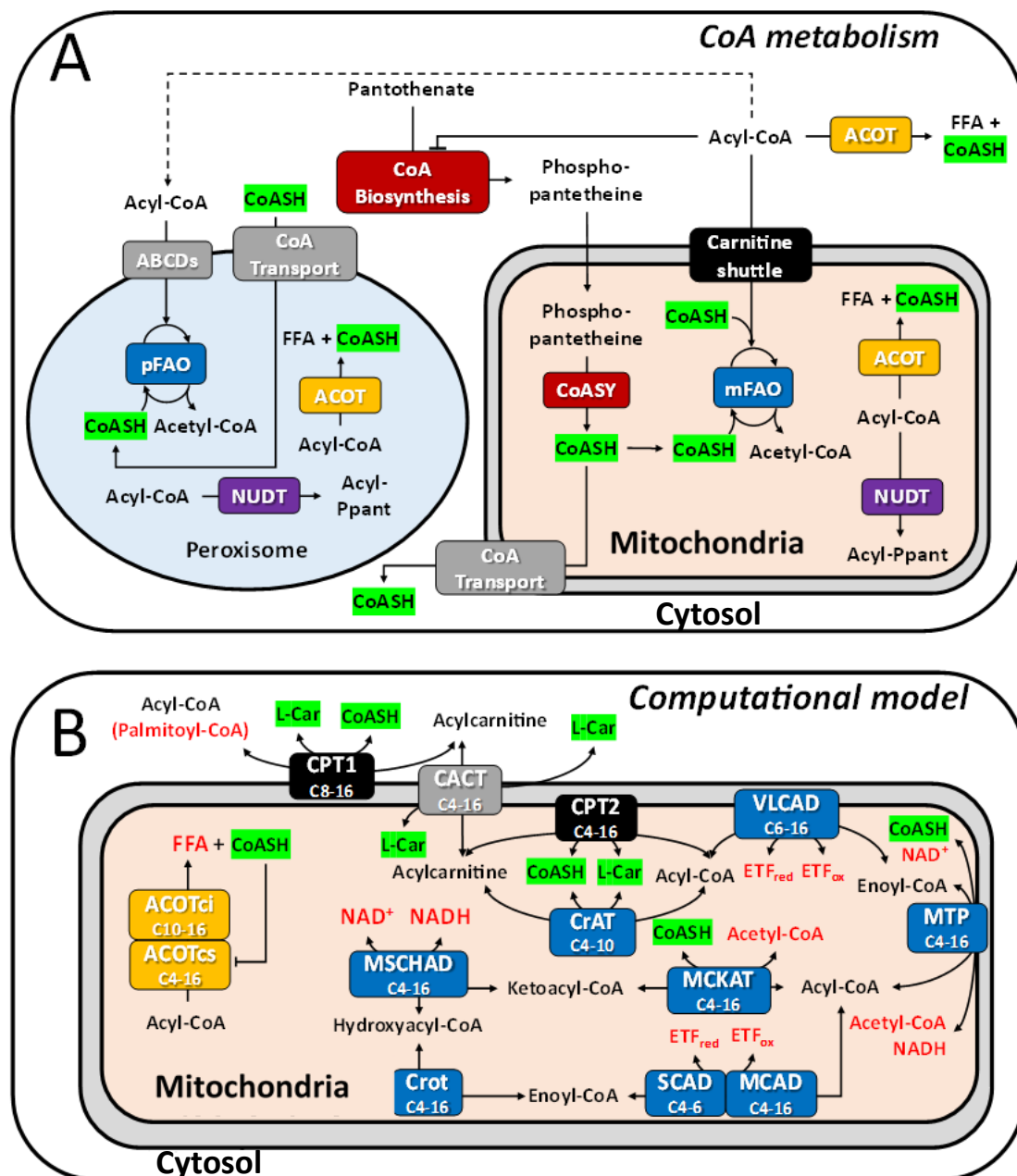
Figure 1. Coenzyme A compartmentalization, synthesis and sequestration. Boxes indicate pathways or individual enzymes: carnitine acyltransferases in black, transporters in grey, thioesterases in yellow, nudix hydrolases in purple, fatty acid oxidation in blue and CoA biosynthesis in red. Metabolites are in black text. CoASH and L-Car (highlighted green) represent free CoA and L-carnitine, respectively. **A.** Pathways investigated in this study span three compartments: the cytosol, mitochondrion, and peroxisome. pFAO = peroxisomal fatty acid oxidation, CoASY = bifunctional CoA synthase, ABCD = ATP-binding cassette domain transporter, NUDT = nudix hydrolase (nucleoside diphosphate linked moiety X-type motif), FFA = free fatty acid.; **B.** Reactions included in the kinetic computational model of human liver mFAO. Red metabolites have fixed concentrations in the model. Subscript indicates the chain-length specificity of each of the reactions. CPT1/2 = carnitine palmitoyltransferase 1/2, CACT = carnitine acylcarnitine translocase, CrAT = carnitine acetyltransferase, VLCAD/MCAD/SCAD = very long-/medium-/short-chain acyl-CoA dehydrogenase, MTP = mitochondrial trifunctional protein, Crot = crotonase, MSCHAD = medium- and short-chain hydroxyacyl-CoA dehydrogenase, MCKAT = medium-chain ketoacyl-CoA thiolase, ACOTci/cs = CoASH-insensitive/-sensitive ACOT, ETFred/ox = reduced/oxidised electron-transferring flavoprotein.

2. Materials and Methods

2.1 Chemicals and reagents

Liquid chromatography-mass spectrometry (LC-MS) grade solvents, namely acetonitrile, methanol, isopropanol and chloroform, were procured from BioSolve BV (Valkenswaard, The Netherlands). Ammonium acetate ($\geq$99%), was purchased from Sigma-Aldrich (St. Louis, MO, USA). Purified water was obtained through the Milli-QR Advantage A10 Water Purification System from Merck Millipore (Billerica, MA, USA). Formic acid (>98%) was bought from Acros Organics (Geel, Belgium). Pentadecanoyl-CoA (C15:0-CoA) and heptadecanoyl-CoA (C17:0-CoA) in ammonium salt form were purchased from Avanti Polar Lipids (Alabaster, AL, USA). Acetyl-1,2-^{13}C$_2$-CoA (C2:0(^{13}C$_2$)-CoA) and n-heptanoyl-CoA (C7:0-CoA) as lithium salts were obtained from Sigma-Aldrich (St. Louis, MO, USA). Acylcarnitines deuterium labeled standards, L-carnitine-d$_3$, propionyl-L-carnitine-d$_3$, butyryl-L-carnitine-d$_3$, octanoyl-L-carnitine-d$_3$ and octadecanoyl-L-carnitine-d$_3$ as hydrochloride salts were purchased from CDN Isotopes (Pointe-Claire, QC, Canada). Fetal bovine serum (FBS) and phosphate-buffered saline (PBS) were purchased from Gibco. Dulbecco's Modified Eagle Medium (DMEM) was purchased from PAN Biotech™. L-carnitine (Product No. C0283), palmitate (Product No. P9767) and labeled pantothenate (^{13}C$_3$-^{15}N$_1$-pantothenate, Product No. 705837) were obtained from Sigma-Aldrich.

2.2 Computational modelling

The human liver computational model was developed by adapting a previous model of mFAO in rat liver [10]. The kinetic constants were adjusted to align with human parameters, and enzymes crucial for CoA metabolism, such as carnitine acetyl-CoA transferase and acyl-CoA thioesterase, were incorporated. In this model, metabolites were distributed based on their solubility between the mitochondrial matrix and the inner membrane. Detailed modeling conditions can be found in previous publication [23], and the complete model is accessible on the JWS Online Biological Systems Modelling repository [39]. It can be viewed, downloaded, and simulated directly through JWS Online [40].

2.3 Cell lines

HepG2 cells, wildtype (WT) and MCAD-knockout (KO), were used for all *in vitro* experiments. In each individual experiment, WT and 3 MCAD-KO clones (3 biological replicates- KO4, KO9, KO21) were tested in parallel. The cell lines, their generation and validation of the knockout are described in detail elsewhere [23].

2.4 *In vitro* experiments

HepG2 cells were cultured in maintencance medium **(Table 1)**, unless stated otherwise, and kept at 37 °C and 5% CO_2. For the experiments, 2-4 x10^6 cells were seeded in 100 mm plates and kept for 24-48 h in maintenance medium until reaching ~70% confluency. On the day of the experiment, cells were washed 2 times with PBS, and the maintenance medium was replaced by the condition medium: *high-fat low-glucose medium* or *high-fat no-glucose medium* **(Table 1)**. After 24 h, the cells were washed twice with ice-cold PBS. Then, 200 µL of ice-cold MeOH was added and the adherent cells were further scraped from the plates using a pipet tip and transferred to a tube. The samples were divided into two equal parts of 100 µL each. Samples were immediately frozen at -80 ℃ until further analysis. One part was used for LC-MS analysis, while the other was used for protein quantification. These samples were used for free CoA, acyl-CoA esters and acylcarnitine analysis. Protein was quantified using the BCA assay (Thermo Scientific, 23225).

For label incorporation experiments, *high-fat low-glucose medium* **(Table 1)** was made using pantothenate free DMEM (PAN Biotech™) supplemented with 16 µM of $^{13}C_3$-$^{15}N_1$-pantothenate. This was equal to the unlabeled pantothenate concentration in the maintenance media. Moreover, dialysed FBS (Fisher scientific, Product Code 11521841) was used instead of normal FBS. The remaining steps in the procedure were same as described above. These samples were used for the analysis of free CoA and labeled free CoA.

Table 1. Composition of the media used for *in vitro* experiments.

Medium components	Maintenance	high-fat low-glucose	high-fat no-glucose
DMEM	P04-01500	P04-01500	P04-01548S1
FBS	10%	10%	10%
Glucose	1.0 g L^{-1}	1.0 g L^{-1}	-
Pyruvate	1 mM	1 mM	-
Glutamine	3 mM	3 mM	-
L-Carnitine	-	2 mM	2 mM
BSA-bound Palmitate	-	0.5 mM	0.5 mM

A different protocol, described by Srinivasan et al. [41] has been used for the analysis of total CoA (sum of the free CoA fraction and acyl-CoA thioesters). HepG2 cells were incubated in *high-fat low-glucose* medium supplemented with $^{13}C_3$-$^{15}N_1$-pantothenate (16 µM) for 24 h. The cells kept in the maintenance medium **(Table 1)** were used as control (0 h).The cells were collected in ice-cold medium and washed twice in ice-cold PBS. The pellet was reconstituted in 600 µL MilliQ H_2O and the lysate was sonicated using a Sonics Vibra cell VCX130 (25 sec, 50% amplitude, 2 times). Lysates were centrifuged at 14000 rpm for 15 min at 4 °C. In a new

tube, 80 µL Tris (2-carboxyethyl)phosphine hydrochloride (10 mM) was added to 400 µL supernatant and incubated for 15 min at room temperature. Next, samples were spun down (14000 rpm, 15 min, 4 °C). In a new tube, 40 µL ammonia solution (12.5% v/v) was added to 400 µL supernatant and incubated while shaking at 500 rpm at 60°C for 60 min. Lastly, samples were dried using a SpeedVac (Eppendorf) and reconstituted in 100 µL ice-cold methanol. These samples were further extracted and analyzed for total CoA and labeled total CoA analysis using the previously reported LC-MS/MS method [26].

For all *in vitro* experiments, we had 5 technical replicates (5 plates per condition). We conducted each experiment at least three times. In total, for each cell line, 15-18 separate cell cultures were assayed in 3-4 rounds of measurements.

Further details about MCAD overexpression in MCAD-KO HepG2 cells, protein extraction and immunoblotting have been mentioned in **Supplementary information**.

2.5 Acyl-CoA and acylcarnitine extraction from HepG2 cells and LC-MS/MS analysis

Sample preparation was performed using protocol based on Bligh and Dyer method [42]. A detailed protocol is available in **Supplementary information.**

For acyl-CoA and acylcarnitine profiling, an Acquity UPLC system from Waters (Milford, MA, USA) coupled to an AB Sciex QTRAP 6500 mass spectrometer equipped with Turbo V source (Concord, ON, Canada) was utilized. Both acyl-CoA and acylcarnitine analysis were conducted using positive electrospray ionization (ESI) in scheduled multiple reaction monitoring (sMRM) mode. The acyl-CoA profiling was performed using HILIC-MS/MS conditions according to the previously published study [26], employing a SeQuant® ZIC®-cHILIC-HPLC (100 x 2.1 mm) column, with a particle size of 3.0 µm and a pore size of 100Å (Merck, Darmstadt, Germany). The detailed explanation is provided in **Supplementary information.**

The acylcarnitine profiling was performed using a reversed-phase liquid chromatography-tandem mass spectrometry (RPLC-MS/MS) method using the AccQ-Tag[TM] Ultra C18 column with dimensions of 2.1 x 100 mm and a particle size of 1.7 µm from Waters (Milford, MA, USA). The settings and configurations are described in detail in **Supplementary information.**

2.6 *In vivo* experiments

Male MCAD-KO and wildtype (WT) littermate mice on a C57BL/6J background were kept in the housing facility under temperature 21 °C and light-controlled (12 h light) conditions, and had free access to food and drinking water. All experiments were approved by the Ethics

Committee for Animal Experiments of the University of Groningen (Netherlands). In the first experiment, 8-week old WT and MCAD-KO mice were divided in two groups: (1) fed and (2) 14 h fasted. Both groups were fed with commercially available laboratory chow diet (V1554-703, Ssniff). For the fasted group, on the day of the experiment, WT and MCAD-KO mice were transferred to a new cage without food, but with free access to water. The animals were overnight fasted for 14 h at 21 °C, and sacrificed. In a second experiment, 8-week old WT and MCAD-KO mice were exposed to a third condition, (3) 14 h fasted and cold-exposed. For condition (3), prior to the start of the experiment, at the age of 4-week, mice were fed with a chow-like semi-synthetic diet (D12450B, Research Diet Services) for 4 weeks. On the experiment day, 8 week WT and MCAD-KO mice were 14 h overnight fasted at 21 °C, then transferred to a 4 °C environment for 4 h, also fasted (total of 18 h fasting). For all the experimental conditions (1. Fed; 2. Fasted; 3. Fasted and cold-exposed), mice were terminated via cardiac puncture under isoflurane anesthesia, and the liver was collected for biochemical analysis.

The sample preparation and HPLC analysis protocol for measuring total CoA, phosphopantetheine (P-Pant) and dephospho-CoA (dPCoA) in mice samples were described in a previously reported study [41]. The details have been provided in the **Supplementary information**.

2.7 RNA extraction and quantitative real-time qPCR

RNA was isolated using the RNeasy® Plus Universal Mini Kit (Qiagen, 73404). Forward and reverse primers for human and murine genes are annotated in **Table S2 and S3**, respectively. RT-PCR was performed using FastStart Universal Sybr Green (Roche, 0413914001) on QuantStudio™ 7 (Applied Biosystems). The thermal cycling consisted of 10 min hold at 95 °C, followed by 40 cycles of 15 sec at 95 °C, 30 sec at 60 °C and 30 sec at 72 °C. The Ct values were expressed relative to YWHAZ (HepG2 cells) and 36B4 (mouse), and normalized to the expression level in the WT controls.

2.8 Statistical analysis and data representation

The results are shown as mean ± standard error of the mean (SEM). Analysis of differences between two groups were done using an unpaired Student's t-test. For the comparison of three or four groups, we performed one-way Brown-Forsythe ANOVA followed by the Dunnett's T3 posthoc test. Briefly, Brown-Forsythe ANOVA is a variation of the ordinary ANOVA, which does not assume the same standard deviations across the groups, and the Dunnett's T3

test corrects for the multiple comparisons performed against one control group. These analyses were performed using GraphPad Prism version 9.1 for Windows (GraphPad Software). The results were considered statistically significant when the p-value was smaller than 0.05.

All the mouse data are shown as mean ± standard error of the mean (SEM). Regarding the HepG2 cells (WT, MCAD-KO4, MCAD-KO9, MCAD-KO21), the results were presented in a distinct way. For all the HepG2 analyses, (I) the experiments were repeated up to three times (independent experiments/biological repeats), (II) independent experiments consisted of 4-5 technical replicates (parallel cell cultures), and (III) the results obtained consisted of values relative to the control WT group within each experiment, instead of absolute values. In other words, assuming the control WT group to be 1, the values indicated how much the MCAD-KO cells varied (or not) in relation to the control. As a consequence, the average of the WT group across experiments was 1, which did not allow for the performance of statistical test of combined experiments due to the lack of variance in the control group. To circumvent this issue, we performed statistical analysis per experiment instead. The significance scores per experiment and per MCAD-KO clone are detailed in the supplement **(Tables S4-S7)**.

3. Results

We employed *in silico*, *in vitro* and *in vivo* models to investigate the impact of MCADD on CoA metabolism. The findings from *in silico* simulations were validated through cellular *(in vitro)* and animal *(in vivo)* experiments. Additionally, gene expression analysis was conducted to observe the influence on CoA metabolism and identify potential compensatory mechanisms.

3.1 MCAD deficiency causes sequestration of CoA into medium-chain acyl-CoA esters

We first investigated how the complete deficiency of MCAD activity would affect the concentrations of free CoA and acyl-CoA esters. To this end we used a previously constructed and experimentally validated computational model [23] that simulates the oxidation of saturated, even-chain fatty acids in human liver mitochondria. The model starts from palmitoyl-CoA (a CoA ester with an acyl chain of 16 carbon atoms). It is based on detailed kinetic equations for each of the enzymes depicted in **Figure 1B**. Kinetic parameters were taken as much as possible from human enzymes and were obtained under physiological conditions. The model accurately predicts the biochemical characteristics of inherited mFAO deficiencies, including short-, medium-, and very long-chain acyl-CoA dehydrogenase deficiency (SCADD, MCADD and VLCADD). The model predicted a strong increase of the C8-CoA concentration and a lesser increase of C6-CoA (**Figure 2A**), while all other acyl-CoA ester concentrations

were significantly decreased in the MCAD-KO relative to the wildtype control (WT) (**Figure 2A**). In agreement with the CASTOR hypothesis, free CoA was decreased in the MCAD-KO relative to WT. Only acetyl-CoA (C2-CoA) was unchanged in the simulations, as it had a fixed boundary concentration in the model. The elevated C6- and C8-CoA concentrations were expected, since these compounds are the main substrates of MCAD. In contrast, the decline of long-chain acyl-CoA esters was counterintuitive: in linear metabolic pathways, accumulation of upstream metabolites is expected in response to an enzyme defect. However, mFAO is not a linear pathway. In its first step in the mitochondrial matrix, free CoA is required for the conversion of palmitoylcarnitine to palmitoyl-CoA by carnitine palmitoyltransferase 2 (CPT2) (**Figure 1B**). Therefore, if decreased, free CoA may limit the entry of substrate into the mFAO pathway, which in turn explains the observed reduction in long-chain acyl-CoA esters.

To validate the model predictions, we used a previously generated HepG2 MCAD-KO cell line [23]. The three clones (KO4, KO9, K21) had no detectable residual MCAD protein. Overexpression of the *ACADM* gene in KO9 and KO21 led to a partial complementation of the MCAD protein and reduced the C8-carnitine level, demonstrating that the phenotype was indeed caused by the MCAD mutation (**Figure S1**). Subsequently, WT and three MCAD-KO clones were incubated in a medium without glucose, pyruvate and glutamine, but in the presence of mFAO substrates palmitate and L-carnitine, condition named as *high-fat no-glucose*. Interestingly, MCAD-KO versus WT cells showed a similar pattern in the acyl-CoA levels as predicted in the simulations (**Figure 2B**). C8-CoA and the C8/C10 acyl-CoA ester ratios strongly increased in the MCAD-KO cells compared to the WT, while free CoA and C2-C4-CoAs were decreased (**Figure S2, Table S4**). Also, in agreement with the simulations, C14-CoA was reduced in the MCAD-KO relative to the WT. A more detailed analysis showed a broader range of medium-chain acyl-CoA species (C6 and C10) upregulated in the MCAD-KO cells, but not observed in the simulations (**Figure 2A and 2B**). The acylcarnitine profile (**Figure 2C**) exhibited a similar pattern as the acyl-CoA profile, with the only difference in the C12-carnitine that reduced in the MCAD-KO relative to the WT, thus mirroring the simulations even better (**Figure S3, Table S5**). We would like to emphasize that each data point in **Figure 2B and 2C** represents a different MCAD-KO clone, with at least 3 biological replicates (independent experiments), consisting of 4-5 technical replicates (parallel cell cultures).

To even further consolidate the results, the experiment was replicated in a culture medium which not only contain mFAO substrates (palmitate and L-carnitine), but also glucose, pyruvate and glutamine were present (named *high-fat low-glucose*), with essentially the same

results (**Figure S4**). In conclusion, loss of MCAD activity leads to an increase of medium-chain acyl-CoA esters, and a decrease in free CoA, short- and long-chain acyl-CoA, in agreement with the predicted sequestration of free CoA into medium-chain acyl-CoA esters.
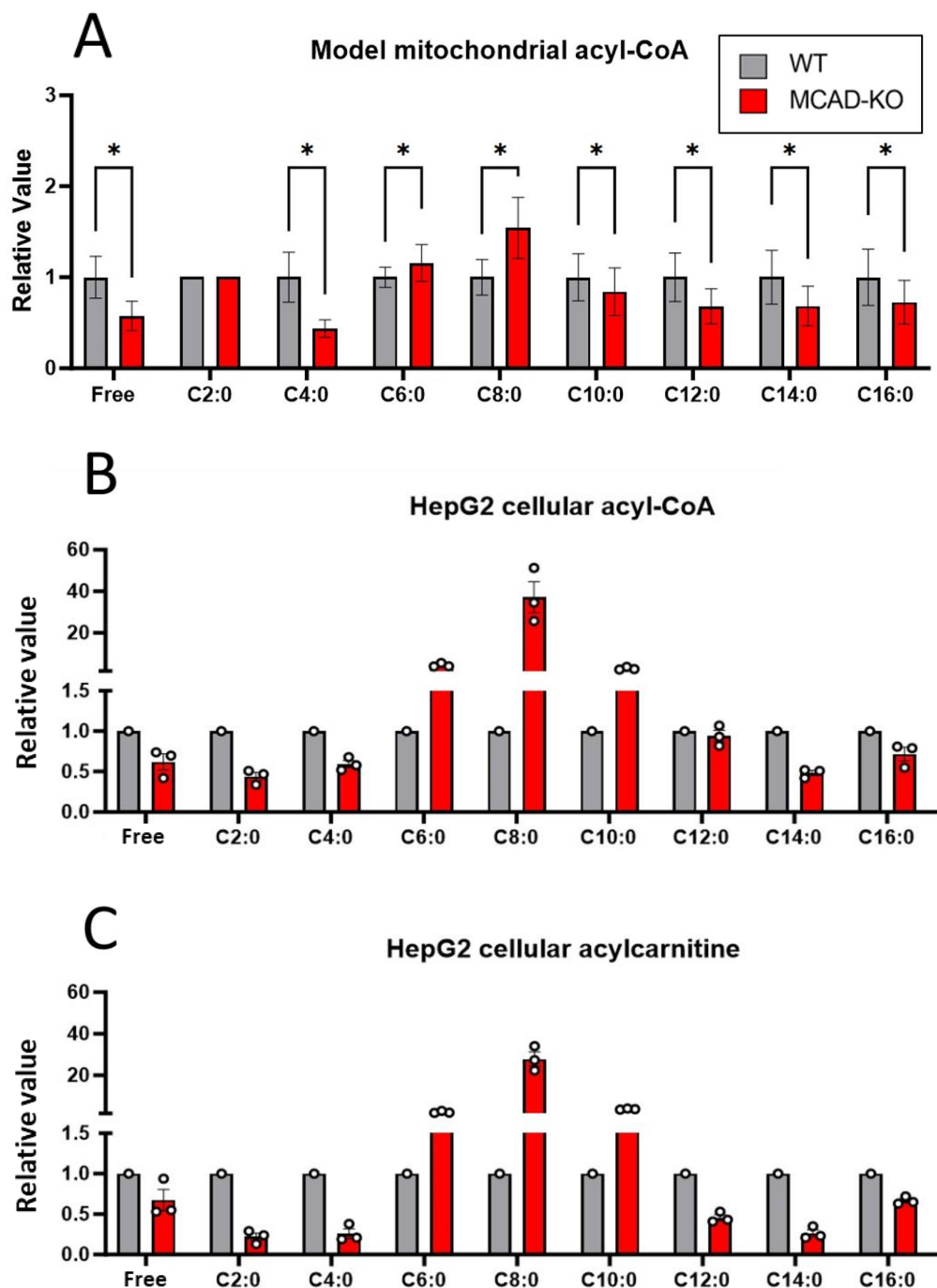
Figure 2. Acyl-CoA and acylcarnitine profile in computational model and HepG2 cells. A. Mitochondrial acyl-CoAs predicted by computational simulations of mFAO in human liver.* $p<0.05$, matched-pair Wilcoxon tests.; **B.** Acyl-CoA esters in HepG2 cells.; **C.** Acylcarnitines in HepG2 cells. WT and MCAD-KO cells were cultured in *high-fat no-glucose medium* for 24 h (DMEM, 0 mM glucose, 0 mM pyruvate, 0 mM glutamine, supplemented with 0.5 mM palmitate and 2 mM L-carnitine). The grey bar represents WT cells while red bar represents MCAD-KO clone (each data point represent one KO clone-KO4, KO9, KO21). The data consists of mean of 3 independent experiments. In turn, each independent experiment consisted of 4-5 parallel cell cultures/technical replicates. (Error) bar represents median and range of the data. Expanded data sets are presented in **Figure S2 and S3**. The significance scores per experiment and per MCAD-KO clone for acyl-CoA and acylcarnitnes in the HepG2 cells are detailed in the supplement **(Tables S4-S5).**

3.2 Loss of MCAD does not affect CoA biosynthesis

PANK, the first enzyme in the biosynthetic pathway of CoA, has been reported to be inhibited by acyl-CoA esters [2]. Therefore, we interrogated if CoA biosynthesis was affected by the knockout of MCAD in HepG2 cells. At time 0 h, mFAO substrates (palmitate and L-carnitine) were added and pantothenate, the precursor of CoA, was replaced by isotopically labelled $^{13}C_3^{15}N_1$-pantothenate **(Figure 3A)**. Confirming previous observations **(Figure 2B)**, after 24 h incubation in the presence of palmitate and L-carnitine, MCAD-KO cells had lower levels of free CoA than their WT counterparts **(Figure 3B)**. At time 0 h, without the addition of mFAO substrates, there was no difference between WT and MCAD-KO, demonstrating that the effect was depended on an active mFAO pathway **(Figure 3B)**. The total CoA pool (acylated plus free fraction) did not differ between WT and MCAD-KO cells **(Figure 3C)**. In line with this, there was no difference between the groups in the percentage of label incorporation over the course of 24 h, neither into the free fraction nor into the total CoA pool **(Figure 3D and 3E)**. Remarkably, we detected approximately 10 times more label incorporation into the free CoA fraction than into the total CoA pool **(Figure 3D and 3E)**, suggesting the existence of a large inert pool that is replaced at a much slower rate than the metabolically active pool. In conclusion, the fact that label incorporation and total CoA were not affected by the MCAD knockout, demonstrates that loss of MCAD did not affect the CoA biosynthesis rate in these HepG2 cells under the conditions studied.

Therefore, the reduced free CoA observed in MCAD-KO was not caused by a smaller total CoA pool, but the CoA sequestration into medium-chain acyl-CoA esters.
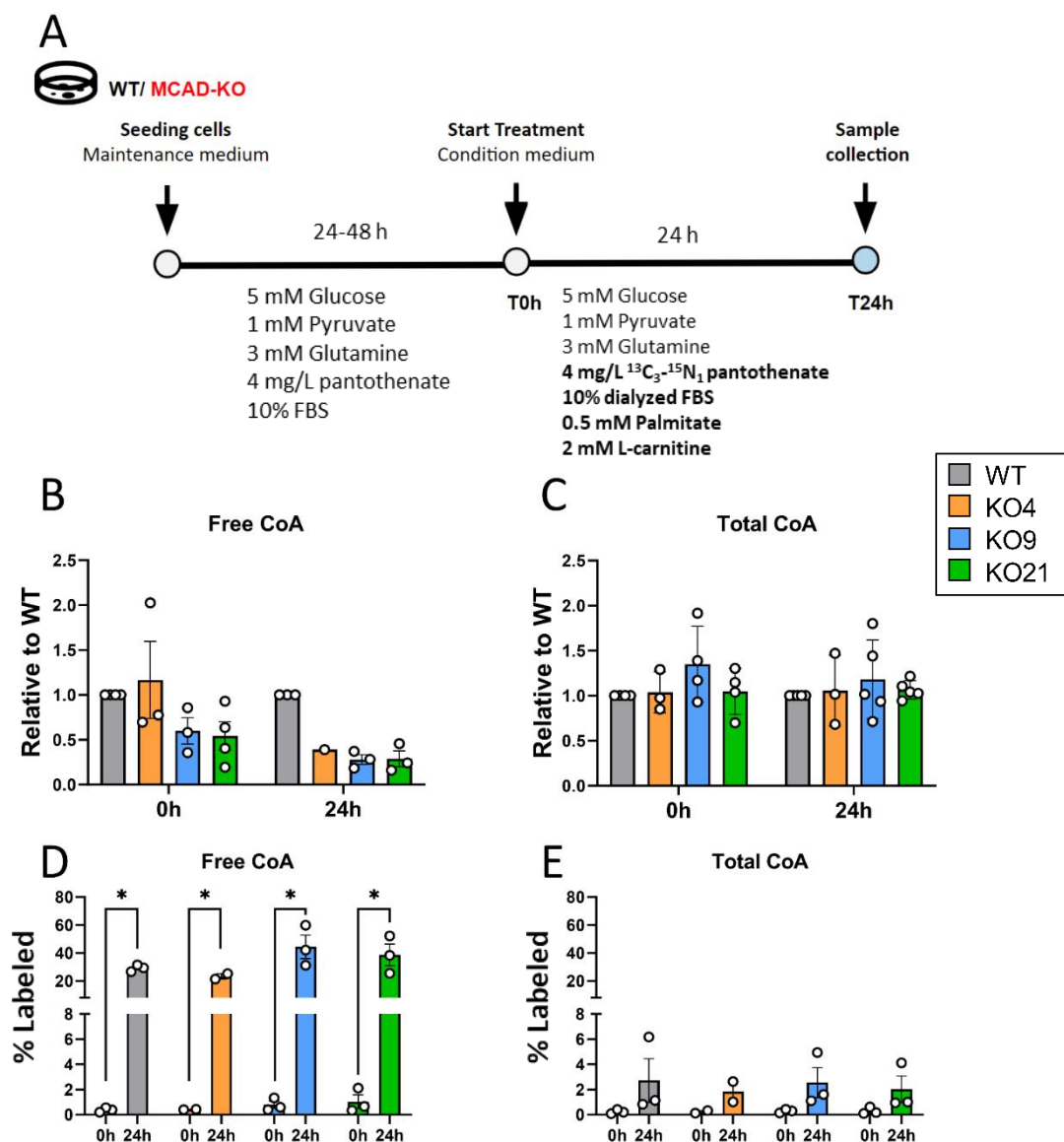
Figure 3. CoA biosynthesis in MCAD-KO cells. A. Simplified scheme of study design; After seeding, cells were precultured in maintenance medium (DMEM 5 mM glucose, 1 mM pyruvate, 3 mM glutamine, 4 mg/L pantothenate, 10% FBS). At T0h, the maintenance medium was replaced by a *high-fat low-glucose medium* (DMEM 5 mM glucose, 1 mM pyruvate, 3 mM glutamine, 10% dialyzed FBS, supplemented with 0.5 mM palmitate and 2.0 mM L-carnitine), in which non-labeled pantothenate was replaced by 4 mg/L stable isotope labeled pantothenate; After 24 h in condition medium, samples were collected at T24h.; **B & C.** Free and total CoA relative to WT.; **D & E.** Percentage label incorporation into the free and total CoA pools. * $p<0.05$ with an unpaired t-test. For all experimental data (**B-E**), each datapoint represents an independent experiment, using a different cell passage (n=1-3). In turn, each individual experiment consisted of 4-5 technical replicates (parallel cell cultures). Therefore, each datapoint represents the average of 4-5 technical replicates, per experiment. For **B-C**, the values shown are relative to the average of the WT within the same experiment.

3.3 MCAD-KO mice remodel CoA metabolism under severe energetic stress

After validating the simulations *in vitro*, we set to investigate the effect of MCAD deficiency on the CoA pool and metabolism *in vivo*. Previous studies have reported that MCAD-KO mice, as MCADD patients, shows resistance when subjected only to fasting [43,44]. Recently, Martines ACMF et al. reported that the combination of fasting and cold exposure triggers relevant disease phenotype in MCAD-KO mice, such as reduced blood glucose, reduced amino acids and triglycerides accumulation in the liver [45]. In this context, we investigated hepatic CoA metabolism in young (8-weeks old) MCAD-KO mice upon fasting and cold exposure. Our experimental groups comprised WT and MCAD-KO littermate mice in all the three conditions: (1) fed, (2) 14 h overnight fasted, and (3) 14 h overnight fasted plus 4 h fasted at 4 °C (total of 18 h fasting) (**Figure 4A**). First, total CoA and CoA biosynthesis intermediate levels consisting of phosphopantetheine (P-Pant) and dephospho-CoA (dPCoA) were measured in liver samples (**Figure 4B and 4C**). Due to methodological limitations, we were not able to accurately measure free CoA and acyl-CoA profile in mice samples. In alignment with the literature [46], in both WT and MCAD-KO, P-Pant and total CoA levels were increased in response to fasting. Notably, a significant increase in total CoA levels was detected in MCAD-KO mice compared to WT mice after fasting and cold exposure. Taken together, the results suggest that CoA biosynthesis is affected by loss of MCAD, and specifically under energetic stress conditions.

To explore this further, the expression of genes involved in CoA metabolism were quantified. Indeed, mRNA levels encoding isoenzymes of the first enzyme in the CoA biosynthesis pathway (*Pank1a, Pank1b,* and *Pank3*) were upregulated in MCAD-KO relative to WT mice, when exposed to fasting plus cold (**Figure 4D**). The mRNA encoding *Pank4*, an enzyme that counteracts CoA biosynthesis by converting phosphopantetheine back to pantetheine [47], was significantly downregulated (**Figure 4D and S5A**). All these adaptations are therefore consistent with an effort to increase CoA levels. At the same time, the mRNA levels encoding the carnitine acyltransferases *Cpt1a*, *Cpt2*, and *Crat* were upregulated in MCAD-KO relative to WT mice (**Figure 4E**). These enzymes can release mitochondrial CoA by transferring acyl-groups to L-carnitine, forming acylcarnitines, which can cross the mitochondrial membrane (**Figure 1B**) [48,49]. The mRNA encoding the peroxisomal acyl-CoA transporter *Abcd1* was also upregulated. This might also decrease the burden on the mitochondrial CoA pool, allowing, instead, the peroxisome to take over some of the beta-oxidation that would normally take place in the mitochondria [32,50]. Upregulation of *Nudt19*, potentially involved in

detoxification of acyl-CoA esters **(Figure 1A)**, was significant, but too small to be relevant (**Figure 4E)**).

Finally, mRNA of several ACOT isoenzymes were substantially and significantly upregulated (**Figure 4F**), with even a 2- to 4-fold increase of *Acot2* and *Acot3* expression. Smaller, but still significant changes were seen for mRNAs encoding other isoenzymes with a median increase between 40% (*Acot8*) and 64% (*Acot* 4 and *Acot7*). The same analyses were carried out in HepG2 cells under both *high-fat no-glucose* and *high-fat low-glucose medium* (**Figure S5 and S6, Table S6 and S7**), however, the changes were not consistent across the different MCAD-KO clones.

Altogether, the changes in gene expression observed in the liver of MCAD-KO mice exposed to fasting and cold seemed to work towards increasing the CoA synthesis and relieving the accumulation of acyl-CoA species.
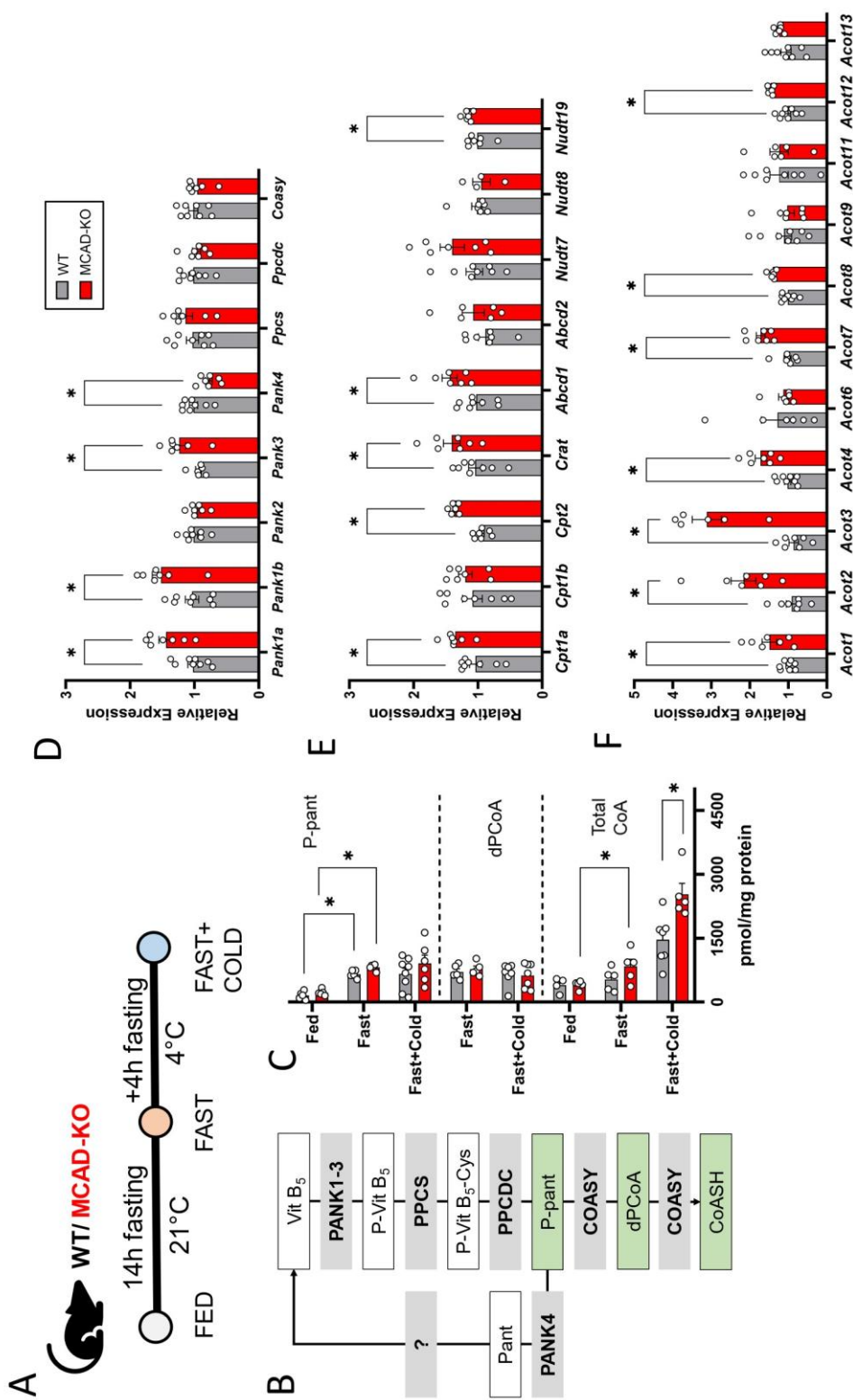
Figure 4. CoA metabolism in the liver of mice exposed to fasting and cold. A. Mice either had free access to food (fed), were fasted overnight for 14 h (fast), or fasted for 18 h of which the last 4 h at 4 °C (fast + cold).; **B.** CoA biosynthesis pathway. PANK (gene *Pank*) = pantothenate kinase, PPCS (gene *Ppcs*) = phosphopantothenate-cysteine ligase, PPCDC (gene *Ppcdc*) = phosphopantothenoylcysteine decarboxylase, COASY (gene *Coasy*) = bifunctional coenzyme A synthase, Vit B$_5$ = pantothenate, P-Vit B$_5$ = phosphopantothenate, P-Vit B$_5$-Cys = phosphopantothenoyl-cysteine, P-pant = phosphopantetheine, Pant = pantetheine, dPCoA = dephospho-CoA. Metabolites are shown in white or green boxes (green boxes correspond to data in panel C) and enzymes in grey.; **C.** Metabolites in the CoA biosynthesis pathway.; **D-F.** Hepatic gene expression in fasted, cold-exposed mice. mRNA levels relative to WT of CoA biosynthetic enzymes **(D)**, acyltransferases and peroxisomal enzymes **(E)** and acyl-CoA thioesterases **(F)**. * *p<0.05* using an unpaired t-test; ± standard error of the mean (SEM).

3.4 Combined upregulation of CoA biosynthesis and ACOT normalize CoA metabolites

Finally, we investigated how the increased total CoA levels in MCAD-KO relative to WT mice, and the upregulated *Acot* expression, affected the concentrations of free CoA and that of potentially toxic medium chain acyl-CoAs. The experimental analysis would only show the total cell average rather than the local mitochondrial concentration. Therefore, we turned again to the computational kinetic model of the mFAO. **Figure 5A** shows the simulated distribution of CoA over the acyl-CoA esters in WT and MCAD-KO in mitochondria. In agreement with **Figure 2**, C8-CoA sequestered most of the available CoA in the MCAD-KO, resulting in a reduced free CoA fraction. Interestingly, if the total CoA in the mutant was increased by 10%, from 3.60 mM to 3.96 mM (**Figure 5A**), the free CoA was restored to the WT level. Most of the extra CoA, however, ended up in the C8-CoA fraction, which was almost doubled.

Subsequently, we tested the effect of simultaneously increasing the total CoA concentration and the ACOT activity (**Figure 5B and 5C**). Again, at low ACOT activities, increasing total CoA almost doubled the levels C8-CoA in the MCAD-KO model (**Figure 5B**). Concomitantly, the free CoA fraction also increased, but to a smaller extent (**Figure 5C**). Increased ACOT activity reduced C8-CoA steeply, while at the same time increasing free CoA. The combined effect of elevated CoA and ACOT was more effective than either alone. However, a 20-fold increase of ACOT activity was required to completely normalize C8-CoA. Altogether, these results show that the observed upregulation of total CoA and ACOT are a powerful compensatory mechanism when MCAD activity is lost, yet not sufficient to fully normalize CoA metabolites.
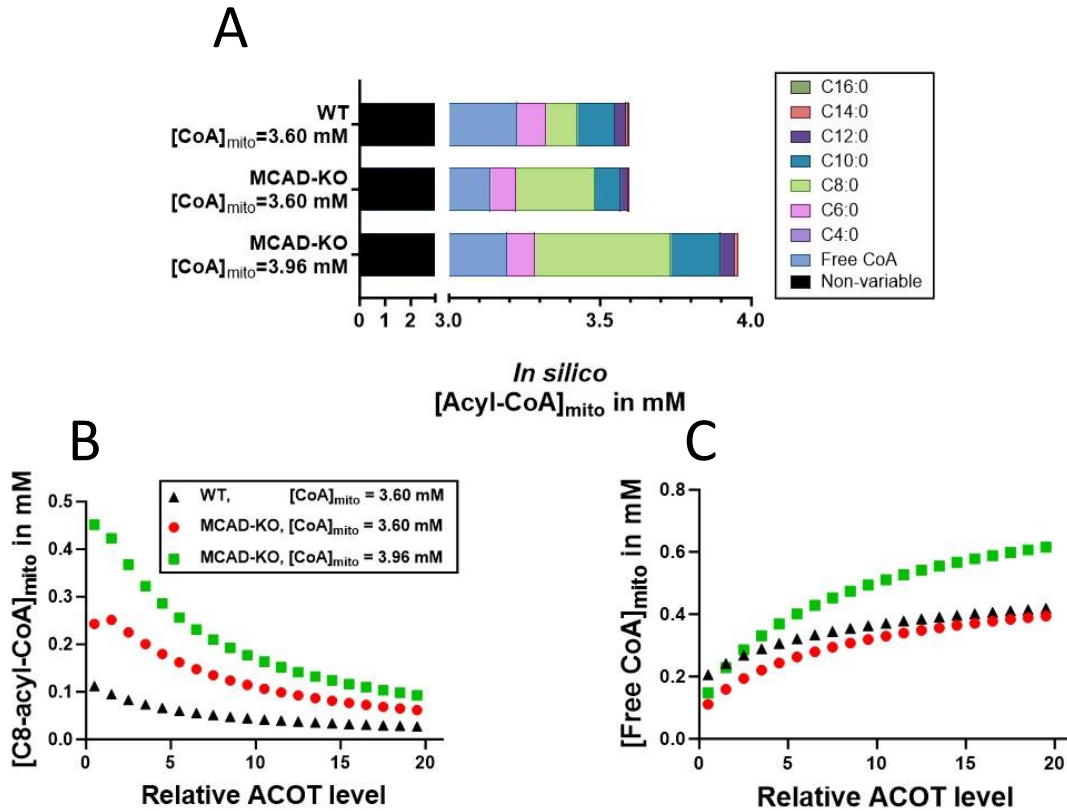
Figure 5. Increased total CoA and ACOT as compensation for free CoA depletion. *In silico* prediction of acyl-CoA and free CoA concentrations. Three models are compared: WT with 100% MCAD activity, MCAD-KO with 0% MCAD activity and MCAD-KO with elevated total CoA. **A.** Breakdown of the variable mitochondrial CoA pool. The non-variable pool represents a realistic amount of CoA that would be sequestered by mitochondrial pathways other than the mFAO.; **B & C**. Steady-state mitochondrial concentrations of C8-CoA **(B)** and free CoA **(C)**, at increasing ACOT activity.

4. Discussion

Although depletion of the free CoA pool has been proposed as a pathogenic mechanism in MCADD, experimental evidence of this is largely absent [2–4,22]. The present study combined *in silico*, *in vitro* and *in vivo* approaches to further investigate it. Our *in silico* results suggested the sequestration of CoA as medium-chain acyl-CoA esters coincides with a decrease in free CoA. Additionally, the simulations have also shown that this phenotype could be remedied by increasing *de novo* production of CoA and by releasing existing CoA from acyl-CoAs. Our experimental results, both in cells and in animals, corroborated these computational predictions. The accumulation of medium-chain acyl-CoAs and concomitant indications of free CoA depletion in cells confirmed the validity of MCADD as a CASTOR disease. Gene expression data in both MCAD-KO cells and mice, as well as CoA measurements in fasted, cold-exposed MCAD-KO mice demonstrated a reorganisation of the CoA metabolism that

could be interpreted as an adaptation to increase the availability of free CoA and relieve the excessive accumulation of C8-CoA.

Computational modelling results suggested an accumulation of C8-CoA which takes up most of the mitochondrial CoA pool in MCAD-KO, leading to decreased levels of all other chain-lengths relative to the WT model including, the free CoA species (**Figure 2A**). The same pattern was seen in MCAD-KO HepG2 cells exposed in both *high-fat low-glucose* and *high-fat no-glucose medium* for 24 h (**Figure 2B and Figure S4A**). This evidence was in favour of the hypothesis that an extensive sequestration of CoA as medium-chain species in MCADD might underlie some of the symptomatology of MCADD patients in crisis [22]. Interestingly, both longer- and shorter-chain acyl-CoAs were decreased in MCAD-KO cells, as in the computational model. One might expect longer chains to also accumulate as they are upstream of the medium chains that constitute the bottleneck. However, the finding that long chains also decrease might suggest that a depletion of free CoA hampers the import of new long-chain substrates into the pathway. The implications of this for an MCADD patient might be dire: it would mean that most of the beta-oxidation substrates are in the least useful form, as medium chains, of which the oxidation is most impaired. This finding is a good example of how models assist us in generating and understanding counter-intuitive pathway behaviours [51].

Another relevant finding of this study was the confirmation that the acyl-CoA profile was mirrored in the acylcarnitines in these cells (**Figure 2C and Figure S4B**). This is important, as acylcarnitines, which cross the cell membrane to enter the bloodstream, are important clinical markers of MCADD and have always been assumed to mirror the cellular acyl-CoA profile [9,52]. Our results provide evidence of the appropriateness of acylcarnitines as proxies for acyl-CoAs.

An important note is that the computational model did not make any predictions with regard to acetyl-CoA, as this metabolite is a fixed parameter. However, acetyl-CoA is a crucial metabolite, and it is interesting to reflect on how a variable acetyl-CoA is expected to compare to *in vitro* measurements. In the cells, acetyl-CoA was about halved in the MCAD-KO cells relative to the WT. Acetyl-CoA from the mFAO is also crucial for the production of ketone bodies in the liver during periods of fasting [53,54]. A reduction in acetyl-CoA levels is therefore also a potential link between MCADD and hypoketosis. Future investigations should take the role of this metabolite into account.

Having obtained evidence for the initial hypothesis of free CoA depletion in MCAD-KO, we shifted our attention to adaptations in the broader network. One logical adaptation would be the upregulation of CoA synthesis. In our results, we obtained a decrease in free CoA for MCAD-KO cell lines compared to WT after palmitate and L-carnitine supplementation in *high-fat low-glucose medium* (**Figure 3B**). Conversely, we did not observe any difference in total CoA pools in these cells (**Figure 3C**). Previous studies on computational modelling suggested that the extensive sequestration of acyl-CoA esters and depletion of free CoA under fat overload conditions is a property of the mFAO even without the loss of MCAD, as it is a substrate of the pathway [10,24,55]. In our study, despite the same level of total CoA, the MCAD-KO cells exhibited a lower free CoA content than the WT cells in *high-fat low-glucose medium*. This might indicate that the production of new CoA was less effective at increasing the free CoA levels in KO cells than in WT cells, as part of the newly synthesized CoA might be channeled into C8-CoA in MCAD-KO cells. We observed higher label incorporation in free CoA as compared to total CoA pool. Additionally, we did not observe any difference in the lable incorporation between WT and MCAD-KO groups (**Figure 3D and 3E**). Our observations suggest that the knockout of MCAD did not impact the rate of CoA biosynthesis or its total pool size in HepG2 cells under the examined conditions. If the total CoA pool was constantly used and recycled in the various CoA-consuming processes, then one would expect the fraction of labeled free and total CoA to be more or less equivalent. Instead, it seemed like there was a large portion of the total CoA pool which was not readily released as free CoA (which would reduce the fraction of labeled free CoA). The probable reasons might be that the CoAs are covalently attached to proteins (CoAlation [56]), or much of the cellular CoA is constituted of acyl-CoAs that are bound very tightly to high-affinity binding proteins that protect them from thioesterases and acyltransferases [57,58]. Further investigation is required to elucidate this question.

In vivo, the CoA level is dynamic, rapidly changing in response to the metabolic and feeding states. Under fasting condition, total CoA has been shown to increase in the liver [59], following a higher demand for this metabolite in active metabolic pathways such as fatty acid oxidation and gluconeogenesis. With regards to temperature, rats exposed to cold stress have been reported to present increased incorporation of labeled pantothenate and CoA synthesis in the liver [38]. Therefore, the combination of fasting and cold must impose a high demand for CoA on top of ATP requirements coming from thermogenesis [60]. Such condition might be particularly challenging in MCADD, which is predicted to have a lower mFAO flux and limited

CoA availability [10,22]. Indeed, despite their resistance to long-time fasting, MCAD KO mice have been shown to be cold-sensitive [43]. In our study, we observed a significant activation of CoA biosynthesis, carnitine acyltransferases and several ACOT enzymes that both release free CoA and alleviate excessive acyl-CoA accumulation highlighting both strategies and their relevance as compensatory mechanisms in MCADD. ACOTs are understood to have a regulatory function over the levels of acyl-CoAs, free fatty acids and free CoA in cells [61,62]. Most relevant for our hypothesis is the ACOTs ability to act as "a release valve when CoA is limiting" [27]. In HepG2 cells, MCAD-KO clone 9 (KO9) showed similar changes with those observed in the liver of MCAD KO-mice, suggesting an attempt to rescue the free CoA pool and alleviate excessive accumulation of C8-CoA. However, it should be noted that there was a considerable variation among the different MCAD-KO clones (**Figures S5 and S6, Table S6 and S7**). Unraveling the particularities of each MCAD-KO clone that led to its specific gene expression profile and investigating its precise impact on the acyl-CoA and free CoA levels were beyond the scope of this investigation.

The theme of our results has very much been one of simultaneous events having some shared underlying logic and mechanistic origin. The accumulation of medium-chain acyl-CoAs might have depleted the free CoA pool, which might trigger the production of more CoA. In the context of MCAD deficiency, however, the production of more CoA might simply lead to further accumulations in acyl-CoAs, possibly to toxic levels without much of a gain in free CoA [63]. Simultaneous processes for reducing the levels of acyl-CoA might therefore be engaged, for instance the upregulation of ACOTs. This hypothetical scenario was computationally modelled. However, one can imagine not two, but multiple mechanisms being simultaneously engaged to increase free CoA while avoiding the risk of lipotoxicity from an enlarged acyl-CoA pool. It is also possible, if not likely, that different MCAD-KO cell lines and animals, indeed different MCADD patients, might engage different sets of rescue mechanisms. This might be an important insight for understanding inter-patient heterogeneity better.

A significant limitation of the current study is that the models used differ in a number of important ways from an MCADD patient. Kinetic models by definition contain only a subset of the metabolic reactions and many potential adaptations and dangers might be excluded. In order to identify other possibilities, experimental models could be of great use. HepG2 cells, though useful and convenient to use, are only imperfect models of human liver cells. The development of 3D *in vitro* cultures, such as liver organoids [64–67] from induced pluripotent

stem cells might, in future, promise ways of generating more human liver-like *in vitro* cultures, especially if MCADD patient cells could be used. Another limitation is the broader physiological context: not only livers, but whole bodies are MCAD deficient, and this could have implications for the manifestation of the conditions. Animal models could help, but are also not perfect substitutes for human bodies. Patient studies like FiTtINg MCADD holds promise for yielding some human data collected under controlled conditions that might yield more insight [68].

5. Conclusion

In conclusion, we have described an approach in which *in silico*, *in vitro* and *in vivo* techniques were combined to confirm that loss of MCAD can indeed trigger a CASTOR phenotype. Our observations showed the sequestration of medium-chain acyl-CoA metabolites in MCAD-KO systems, potentially depletes free CoA during metabolic stress. We have also identified several rescue mechanisms that could mitigate this phenotype. Our gene expression analysis revealed the activation of CoA biosynthesis and acyl-CoA thioesterases as compensatory mechanisms that might increase free CoA levels, preventing excessive accumulation of acyl-CoA species. For future research, it is essential to consider the broader network in which MCADD and other CASTOR diseases operate. This broader network can respond, either in compensatory or in aggravating ways, to seemingly simple perturbations.

Author contributions

C.O., L.A.K., M.S., A.C.H., T.H., and B.M.B. designed the experiments. C.O., L.A.K., and M.S. performed the experiments, generated and interpreted the data, and wrote the manuscript. M.S. with the support of A.D., V.C. and G.L.F.K. developed, optimized and performed the HILIC-MS/MS protocol used in this work. C.O. performed all the computational simulations. M.L.M. supported with the *in vitro* experiments and qPCR analyses. M.v.d.Z. performed the HPLC analysis. A.C.M.F.M. and L.A.K. designed and conducted the animal experiments. N.C.A.H. and B.v.d.S. advised on the overexpression experiments, and N.C.A.H. and L.A.K. carried them out. A.G., H.S., D.J.R. and O.C.M.S provided important advice at various crucial junctures during experimental design and manuscript writing. A.C.H., T.H., and B.M.B. supervised the project and edited the draft manuscript. All authors commented on the text.

Declaration of competing interests

This paper has no conflict of interest with any of the other research groups, or organizations.

Acknowledgements

References

[1] J.L. Robinson, P. Kocabaş, H. Wang, P.-E. Cholley, D. Cook, A. Nilsson, M. Anton, R. Ferreira, I. Domenzain, V. Billa, A. Limeta, A. Hedin, J. Gustafsson, E.J. Kerkhoven, L.T. Svensson, B.O. Palsson, A. Mardinoglu, L. Hansson, M. Uhlén, J. Nielsen, An atlas of human metabolism, Sci Signal. 13 (2020) eaaz1482. https://doi.org/10.1126/scisignal.aaz1482.

[2] G.A. Mitchell, N. Gauthier, A. Lesimple, S.P. Wang, O. Mamer, I. Qureshi, Hereditary and acquired diseases of acyl-coenzyme A metabolism, Mol Genet Metab. 94 (2008) 4–15. https://doi.org/10.1016/j.ymgme.2007.12.005.

[3] H. Yang, C. Zhao, Y. Wang, S.P. Wang, G.A. Mitchell, Hereditary diseases of coenzyme A thioester metabolism, Biochem Soc Trans. 47 (2019) 149–155. https://doi.org/10.1042/BST20180423.

[4] H. Yang, C. Zhao, M.-C. Tang, Y. Wang, S.P. Wang, P. Allard, A. Furtos, G.A. Mitchell, Inborn errors of mitochondrial acyl-coenzyme a metabolism: acyl-CoA biology meets the clinic, Molecular Genetics and Metabolism. 128 (2019) 30–44. https://doi.org/10.1016/j.ymgme.2019.05.002.

[5] G.S. Ribas, F.F. Lopes, M. Deon, C.R. Vargas, Hyperammonemia in Inherited Metabolic Diseases, Cell Mol Neurobiol. 42 (2022) 2593–2610. https://doi.org/10.1007/s10571-021-01156-6.

[6] E.A. Jager, M.M. Kuijpers, A.M. Bosch, M.F. Mulder, E.R. Gozalbo, G. Visser, M. de Vries, M. Williams, H.R. Waterham, F.J. van Spronsen, P.C.J.I. Schielen, T.G.J. Derks, A nationwide retrospective observational study of population newborn screening for medium-chain acyl-CoA dehydrogenase (MCAD) deficiency in the Netherlands, J Inherit Metab Dis. 42 (2019) 890–897. https://doi.org/10.1002/jimd.12102.

[7] U. Spiekerkoetter, J. Vockley, Mitochondrial Fatty Acid Oxidation Disorders, in: N. Blau, C. Dionisi Vici, C.R. Ferreira, C. Vianey-Saban, C.D.M. van Karnebeek (Eds.), Physician's Guide to the Diagnosis, Treatment, and Follow-Up of Inherited Metabolic Diseases, Springer International Publishing, Cham, 2022: pp. 929–957. https://doi.org/10.1007/978-3-030-67727-5_48.

[8] K. Tanaka, I. Yokota, P.M. Coates, A.W. Strauss, D.P. Kelly, Z. Zhang, N. Gregersen, B.S. Andresen, Y. Matsubara, D. Curtis, Mutations in the medium chain acyl-CoA dehydrogenase (MCAD) gene, Hum Mutat. 1 (1992) 271–279. https://doi.org/10.1002/humu.1380010402.

[9] M.A. Nada, W.J. Rhead, H. Sprecher, H. Schulz, C.R. Roe, Evidence for Intermediate Channeling in Mitochondrial β -Oxidation (∗), Journal of Biological Chemistry. 270 (1995) 530–535. https://doi.org/10.1074/jbc.270.2.530.

[10] K. van Eunen, S.M.J. Simons, A. Gerding, A. Bleeker, G. den Besten, C.M.L. Touw, S.M. Houten, B.K. Groen, K. Krab, D.-J. Reijngoud, B.M. Bakker, Biochemical Competition Makes Fatty-Acid β-Oxidation Vulnerable to Substrate Overload, PLoS Comput Biol. 9 (2013) e1003186. https://doi.org/10.1371/journal.pcbi.1003186.

[11] B. Wilcken, M. Haas, P. Joy, V. Wiley, M. Chaplin, C. Black, J. Fletcher, J. McGill, A. Boneh, Outcome of neonatal screening for medium-chain acyl-CoA dehydrogenase deficiency in Australia: a cohort study, Lancet. 369 (2007) 37–42. https://doi.org/10.1016/S0140-6736(07)60029-4.

[12] T.G.J. Derks, T.S. Boer, A. van Assen, T. Bos, J. Ruiter, H.R. Waterham, K.E. Niezen-Koning, R.J.A. Wanders, J.M.M. Rondeel, J.G. Loeber, L.P. Ten Kate, G.P.A. Smit, D.-J. Reijngoud, Neonatal screening for medium-chain acyl-CoA dehydrogenase (MCAD) deficiency in The Netherlands: the importance of enzyme analysis to ascertain true MCAD deficiency, J Inherit Metab Dis. 31 (2008) 88–96. https://doi.org/10.1007/s10545-007-0492-3.

[13] M. Pourfarzam, A. Morris, M. Appleton, A. Craft, K. Bartlett, Neonatal screening for medium-chain acyl-CoA dehydrogenase deficiency, Lancet. 358 (2001) 1063–1064. https://doi.org/10.1016/S0140-6736(01)06199-2.

[14] M.L. Couce, D.E. Castiñeiras, J.D. Moure, J.A. Cocho, P. Sánchez-Pintos, J. García-Villoria, D. Quelhas, N. Gregersen, B.S. Andresen, A. Ribes, J.M. Fraga, Relevance of expanded neonatal screening of medium-chain acyl co-a dehydrogenase deficiency: outcome of a decade in galicia (Spain), JIMD Rep. 1 (2011) 131–136. https://doi.org/10.1007/8904_2011_28.

[15] A.K. Iafolla, R.J. Thompson, C.R. Roe, Medium-chain acyl-coenzyme A dehydrogenase deficiency: clinical course in 120 affected children, J Pediatr. 124 (1994) 409–415. https://doi.org/10.1016/s0022-3476(94)70363-9.

[16] B. Wilcken, J. Hammond, M. Silink, Morbidity and mortality in medium chain acyl coenzyme A dehydrogenase deficiency., Arch Dis Child. 70 (1994) 410–412.

[17] E.H. Touma, C. Charpentier, Medium chain acyl-CoA dehydrogenase deficiency., Arch Dis Child. 67 (1992) 142–145.

[18] N. Gauthier, J.W. Wu, S.P. Wang, P. Allard, O.A. Mamer, L. Sweetman, A.B. Moser, L. Kratz, F. Alvarez, Y. Robitaille, F. Lépine, G.A. Mitchell, A Liver-Specific Defect of Acyl-CoA Degradation Produces Hyperammonemia, Hypoglycemia and a Distinct Hepatic Acyl-CoA Pattern, PLOS ONE. 8 (2013) e60581. https://doi.org/10.1371/journal.pone.0060581.

[19] O.A. Shchelochkov, N. Carrillo, C. Venditti, Propionic Acidemia, in: M.P. Adam, J. Feldman, G.M. Mirzaa, R.A. Pagon, S.E. Wallace, L.J. Bean, K.W. Gripp, A. Amemiya (Eds.), GeneReviews®, University of Washington, Seattle, Seattle (WA), 1993. http://www.ncbi.nlm.nih.gov/books/NBK92946/ (accessed November 16, 2023).

[20] C. Subramanian, M.W. Frank, R. Tangallapally, M.-K. Yun, A. Edwards, S.W. White, R.E. Lee, C.O. Rock, S. Jackowski, Pantothenate kinase activation relieves coenzyme A sequestration and improves mitochondrial function in mice with propionic acidemia, Sci Transl Med. 13 (2021) eabf5965. https://doi.org/10.1126/scitranslmed.abf5965.

[21] C. Subramanian, M.W. Frank, R. Tangallapally, M.-K. Yun, S.W. White, R.E. Lee, C.O. Rock, S. Jackowski, Relief of CoA sequestration and restoration of mitochondrial function in a mouse model of propionic acidemia, J Inherit Metab Dis. 46 (2023) 28–42. https://doi.org/10.1002/jimd.12570.

[22] K. van Eunen, C.M.L. Volker-Touw, A. Gerding, A. Bleeker, J.C. Wolters, W.J. van Rijt, A.-C.M.F. Martines, K.E. Niezen-Koning, R.M. Heiner, H. Permentier, A.K. Groen, D.-J. Reijngoud, T.G.J. Derks, B.M. Bakker, Living on the edge: substrate competition explains loss of robustness in mitochondrial fatty-acid oxidation disorders, BMC Biol. 14 (2016) 1–15. https://doi.org/10.1186/s12915-016-0327-5.

[23] C. Odendaal, E.A. Jager, A.-C.M.F. Martines, M.A. Vieira-Lara, N.C.A. Huijkman, L.A. Kiyuna, A. Gerding, J.C. Wolters, R. Heiner-Fokkema, K. van Eunen, T.G.J. Derks, B.M. Bakker, Personalised modelling of clinical heterogeneity between medium-chain acyl-CoA dehydrogenase patients, BMC Biol. 21 (2023) 1–22. https://doi.org/10.1186/s12915-023-01652-9.

[24] A.-C.M.F. Martines, K. van Eunen, D.-J. Reijngoud, B.M. Bakker, The promiscuous enzyme medium-chain 3-keto-acyl-CoA thiolase triggers a vicious cycle in fatty-acid beta-oxidation, PLoS Comput Biol. 13 (2017) e1005461. https://doi.org/10.1371/journal.pcbi.1005461.

[25] M. Singh, H.L. Elfrink, A.C. Harms, T. Hankemeier, Recent developments in the analytical approaches of acyl-CoAs to assess their role in mitochondrial fatty acid oxidation disorders, Molecular Genetics and Metabolism. (2023) 107711. https://doi.org/10.1016/j.ymgme.2023.107711.

[26] M. Singh, L.A. Kiyuna, C. Odendaal, B.M. Bakker, A.C. Harms, T. Hankemeier, Development of targeted hydrophilic interaction liquid chromatography-tandem mass spectrometry method for acyl-Coenzyme A covering short- to long-chain species in a single analytical run, Journal of Chromatography A. (2023) 464524. https://doi.org/10.1016/j.chroma.2023.464524.

[27] C. Bekeova, L. Anderson-Pullinger, K. Boye, F. Boos, Y. Sharpadskaya, J.M. Herrmann, E.L. Seifert, Multiple mitochondrial thioesterases have distinct tissue and substrate specificity and CoA regulation, suggesting unique functional roles, J Biol Chem. 294 (2019) 19034–19047. https://doi.org/10.1074/jbc.RA119.010901.

[28] J.D. McGarry, C. Robles-Valdes, D.W. Foster, Role of carnitine in hepatic ketogenesis., Proc Natl Acad Sci U S A. 72 (1975) 4385–4388.

[29] Y.-M. Zhang, S. Chohnan, K.G. Virga, R.D. Stevens, O.R. Ilkayeva, B.R. Wenner, J.R. Bain, C.B. Newgard, R.E. Lee, C.O. Rock, S. Jackowski, Chemical knockout of pantothenate kinase reveals the metabolic and genetic program responsible for hepatic coenzyme A homeostasis, Chem Biol. 14 (2007) 291–302. https://doi.org/10.1016/j.chembiol.2007.01.013.

[30] R.R. Ramsay, R.D. Gandour, F.R. van der Leij, Molecular enzymology of carnitine transfer and transport, Biochimica et Biophysica Acta (BBA) - Protein Structure and Molecular Enzymology. 1546 (2001) 21–43. https://doi.org/10.1016/S0167-4838(01)00147-9.

[31] R. Leonardi, Y.-M. Zhang, C.O. Rock, S. Jackowski, Coenzyme A: back in action, Prog Lipid Res. 44 (2005) 125–153. https://doi.org/10.1016/j.plipres.2005.04.001.

[32] M. Schrader, J. Costello, L.F. Godinho, M. Islinger, Peroxisome-mitochondria interplay and disease, J Inherit Metab Dis. 38 (2015) 681–702. https://doi.org/10.1007/s10545-015-9819-7.

[33] G. Agrimi, A. Russo, P. Scarcia, F. Palmieri, The human gene SLC25A17 encodes a peroxisomal transporter of coenzyme A, FAD and NAD+, Biochem J. 443 (2012) 241–247. https://doi.org/10.1042/BJ20111420.

[34] F. Palmieri, M. Monné, G. Fiermonte, L. Palmieri, Mitochondrial transport and metabolism of the vitamin B-derived cofactors thiamine pyrophosphate, coenzyme A, FAD and NAD +, and related diseases: A review, IUBMB Life. 74 (2022) 592–617. https://doi.org/10.1002/iub.2612.

[35] G. Fiermonte, E. Paradies, S. Todisco, C.M.T. Marobbio, F. Palmieri, A Novel Member of Solute Carrier Family 25 (SLC25A42) Is a Transporter of Coenzyme A and Adenosine 3′,5′-Diphosphate in Human Mitochondria, J Biol Chem. 284 (2009) 18152–18159. https://doi.org/10.1074/jbc.M109.014118.

[36] S.D. Vickers, S.A. Shumar, D.C. Saporito, A. Kunovac, Q.A. Hathaway, B. Mintmier, J.A. King, R.D. King, V.M. Rajendran, A.M. Infante, J.M. Hollander, R. Leonardi, NUDT7 regulates total hepatic CoA levels and the composition of the intestinal bile acid pool in male mice fed a Western diet, J Biol Chem. 299 (2023) 102745. https://doi.org/10.1016/j.jbc.2022.102745.

[37] S.A. Shumar, E.W. Kerr, P. Fagone, A.M. Infante, R. Leonardi, Overexpression of Nudt7 decreases bile acid levels and peroxisomal fatty acid oxidation in the liver, J Lipid Res. 60 (2019) 1005–1019. https://doi.org/10.1194/jlr.M092676.

[38] M. Tsujikawa, S. Kimura, Effect of exposure to cold on pantothenic acid metabolism in rat liver, Tohoku J Exp Med. 133 (1981) 457–460. https://doi.org/10.1620/tjem.133.457.

[39] M. Peters, J.J. Eicher, D.D. van Niekerk, D. Waltemath, J.L. Snoep, The JWS online simulation database, Bioinformatics. 33 (2017) 1589–1590. https://doi.org/10.1093/bioinformatics/btw831.

[40] JWS Online: odendaal1. Available from: https:// jjj. bio. vu. nl/ models/ odend aal1/ simulate/., (n.d.).

[41] B. Srinivasan, M. Baratashvili, M. Van Der Zwaag, B. Kanon, C. Colombelli, R.A. Lambrechts, O. Schaap, E.A. Nollen, A. Podgoršek, G. Kosec, H. Petković, S. Hayflick, V. Tiranti, D.-J. Reijngoud, N.A. Grzeschik, O.C.M. Sibon, Extracellular 4′-phosphopantetheine is a source for intracellular coenzyme A synthesis, Nat Chem Biol. 11 (2015) 784–792. https://doi.org/10.1038/nchembio.1906.

[42] H. Wu, A.D. Southam, A. Hines, M.R. Viant, High-throughput tissue extraction protocol for NMR- and MS-based metabolomics, Anal Biochem. 372 (2008) 204–212. https://doi.org/10.1016/j.ab.2007.10.002.

[43] R.J. Tolwani, D.A. Hamm, L. Tian, J.D. Sharer, J. Vockley, P. Rinaldo, D. Matern, T.R. Schoeb, P.A. Wood, Medium-Chain Acyl-CoA Dehydrogenase Deficiency in Gene-Targeted Mice, PLoS Genet. 1 (2005) e23. https://doi.org/10.1371/journal.pgen.0010023.

[44] H. Herrema, T.G.J. Derks, T.H. van Dijk, V.W. Bloks, A. Gerding, R. Havinga, U.J.F. Tietge, M. Müller, G.P.A. Smit, F. Kuipers, D.-J. Reijngoud, Disturbed hepatic carbohydrate management during high metabolic demand in medium-chain acyl–CoA dehydrogenase (MCAD)–deficient mice, Hepatology. 47 (2008) 1894–1904. https://doi.org/10.1002/hep.22284.

[45] Martines A-C. Exploring the mechanisms underlying the phenotype of MCAD deficiency with Systems Medicine: from computational model to mice to man. [Groningen]: Rijksuniversiteit Groningen, 2019. 275 p., (n.d.).

[46] R. Leonardi, J.E. Rehg, C.O. Rock, S. Jackowski, Pantothenate Kinase 1 Is Required to Support the Metabolic Transition from the Fed to the Fasted State, PLOS ONE. 5 (2010) e11107. https://doi.org/10.1371/journal.pone.0011107.

[47] C.C. Dibble, S.A. Barritt, G.E. Perry, E.C. Lien, R.C. Geck, S.E. DuBois-Coyne, D. Bartee, T.T. Zengeya, E.B. Cohen, M. Yuan, B.D. Hopkins, J.L. Meier, J.G. Clohessy, J.M. Asara, L.C. Cantley, A. Toker, PI3K drives the de novo synthesis of coenzyme A from vitamin B5, Nature. 608 (2022) 192–198. https://doi.org/10.1038/s41586-022-04984-8.

[48] S. Violante, L. Ijlst, H. Te Brinke, I. Tavares de Almeida, R.J.A. Wanders, F.V. Ventura, S.M. Houten, Carnitine palmitoyltransferase 2 and carnitine/acylcarnitine translocase are involved in the mitochondrial synthesis and export of acylcarnitines, FASEB J. 27 (2013) 2039–2044. https://doi.org/10.1096/fj.12-216689.

[49] C. Indiveri, V. Iacobazzi, A. Tonazzi, N. Giangregorio, V. Infantino, P. Convertini, L. Console, F. Palmieri, The mitochondrial carnitine/acylcarnitine carrier: function, structure and physiopathology, Mol Aspects Med. 32 (2011) 223–233. https://doi.org/10.1016/j.mam.2011.10.008.

[50] M. Fransen, C. Lismont, P. Walton, The Peroxisome-Mitochondria Connection: How and Why?, Int J Mol Sci. 18 (2017) 1126. https://doi.org/10.3390/ijms18061126.

[51] P.A. Saa, L.K. Nielsen, Formulation, construction and analysis of kinetic models of metabolism: A review of modelling frameworks, Biotechnology Advances. 35 (2017) 981–1003. https://doi.org/10.1016/j.biotechadv.2017.09.005.

[52] E.P. Brass, C.L. Hoppel, Relationship between acid-soluble carnitine and coenzyme A pools in vivo, Biochem J. 190 (1980) 495–504.

[53] J.A. Fletcher, S. Deja, S. Satapati, X. Fu, S.C. Burgess, J.D. Browning, Impaired ketogenesis and increased acetyl-CoA oxidation promote hyperglycemia in human fatty liver, JCI Insight. 4 (n.d.) e127737. https://doi.org/10.1172/jci.insight.127737.

[54] C. Des Rosiers, F. David, M. Garneau, H. Brunengraber, Nonhomogeneous labeling of liver mitochondrial acetyl-CoA, Journal of Biological Chemistry. 266 (1991) 1574–1578. https://doi.org/10.1016/S0021-9258(18)52332-2.

[55] F. Abegaz, A.-C.M.F. Martines, M.A. Vieira-Lara, M. Rios-Morales, D.-J. Reijngoud, E.C. Wit, B.M. Bakker, Bistability in fatty-acid oxidation resulting from substrate inhibition, PLoS Comput Biol. 17 (2021) e1009259. https://doi.org/10.1371/journal.pcbi.1009259.

[56] I. Gout, Coenzyme A, protein CoAlation and redox regulation in mammalian cells, Biochem Soc Trans. 46 (2018) 721–728. https://doi.org/10.1042/BST20170506.

[57] C.A. Jolly, D.C. Wilton, F. Schroeder, Microsomal fatty acyl-CoA transacylation and hydrolysis: fatty acyl-CoA species dependent modulation by liver fatty acyl-CoA binding proteins, Biochim Biophys Acta. 1483 (2000) 185–197. https://doi.org/10.1016/s1388-1981(99)00170-5.

[58] J.T. Rasmussen, N.J. Faergeman, K. Kristiansen, J. Knudsen, Acyl-CoA-binding protein (ACBP) can mediate intermembrane acyl-CoA transport and donate acyl-CoA for beta-oxidation and glycerolipid synthesis, Biochem J. 299 (Pt 1) (1994) 165–170. https://doi.org/10.1042/bj2990165.

[59] P. Naquet, E.W. Kerr, S.D. Vickers, R. Leonardi, Regulation of coenzyme A levels by degradation: the 'Ins and Outs,' Prog Lipid Res. 78 (2020) 101028. https://doi.org/10.1016/j.plipres.2020.101028.

[60] F. Haman, F. Péronnet, G.P. Kenny, D. Massicotte, C. Lavoie, C. Scott, J.-M. Weber, Effect of cold exposure on fuel utilization in humans: plasma glucose, muscle glycogen, and lipids, Journal of Applied Physiology. 93 (2002) 77–84. https://doi.org/10.1152/japplphysiol.00773.2001.

[61] B. Kirkby, N. Roman, B. Kobe, S. Kellie, J.K. Forwood, Functional and structural properties of mammalian acyl-coenzyme A thioesterases, Prog Lipid Res. 49 (2010) 366–377. https://doi.org/10.1016/j.plipres.2010.04.001.

[62] M.C. Hunt, S.E.H. Alexson, The role Acyl-CoA thioesterases play in mediating intracellular lipid metabolism, Prog Lipid Res. 41 (2002) 99–130. https://doi.org/10.1016/s0163-7827(01)00017-0.

[63] Roe CR, Roe CR, Ding J. Mitochondrial fatty acid oxidation disorders. In: Scriver CR, Beaudet AL, Sly WS, Valle D, Childs B, Kinzler KW, et al., editors. The Metabolic and Molecular Bases of Inherited Disease. 8th ed. New York, NY: McGraw-Hill; 2001. p. 2297–326., in: The Metabolic and Molecular Bases of Inherited Disease., 8th ed., McGraw-Hill, n.d.: pp. 2297–326.

[64] F. Sampaziotis, M.C. de Brito, P. Madrigal, A. Bertero, K. Saeb-Parsy, F.A.C. Soares, E. Schrumpf, E. Melum, T.H. Karlsen, J.A. Bradley, W.T. Gelson, S. Davies, A. Baker, A. Kaser, G.J. Alexander, N.R.F. Hannan, L. Vallier, Cholangiocytes derived from human induced pluripotent stem cells for disease modeling and drug validation, Nat Biotechnol. 33 (2015) 845–852. https://doi.org/10.1038/nbt.3275.

[65] Y. Guan, D. Xu, P.M. Garfin, U. Ehmer, M. Hurwitz, G. Enns, S. Michie, M. Wu, M. Zheng, T. Nishimura, J. Sage, G. Peltz, Human hepatic organoids for the analysis of human genetic diseases, JCI Insight. 2 (2017) e94954, 94954. https://doi.org/10.1172/jci.insight.94954.

[66] S. Wang, X. Wang, Z. Tan, Y. Su, J. Liu, M. Chang, F. Yan, J. Chen, T. Chen, C. Li, J. Hu, Y. Wang, Human ESC-derived expandable hepatic organoids enable therapeutic liver repopulation and pathophysiological modeling of alcoholic liver injury, Cell Res. 29 (2019) 1009–1026. https://doi.org/10.1038/s41422-019-0242-8.

[67] F. Wu, D. Wu, Y. Ren, Y. Huang, B. Feng, N. Zhao, T. Zhang, X. Chen, S. Chen, A. Xu, Generation of hepatobiliary organoids from human induced pluripotent stem cells, J Hepatol. 70 (2019) 1145–1158. https://doi.org/10.1016/j.jhep.2018.12.028.

[68] T.G.J. Derks, Fasting Tolerance in Patients With Medium-chain Acyl-CoA Dehydrogenase Deficiency (MCADD) in the First Six Months of Life: an Investigator-initiated Human Pilot-study, clinicaltrials.gov, 2019. https://clinicaltrials.gov/study/NCT03761693 (accessed January 1, 2023).

Chapter 6

Supplementary material

MCAD overexpression in MCAD-KO HepG2 cells

HepG2 cells overexpressing *ACADM* were generated using the Polyethylenimine (PEI) transfection system and lentivirus. HEK293 cells were used as a lentivirus-producer cell line. Briefly, HEK293 cells were cultured in DMEM, supplemented with Glutamax I (Gibco, 31966-047), 10% FBS (Hyclone, SV30160) and 1% Penicillin-Streptomycin (10000 U/mL; Gibco, 15140122), and kept at 37 °C, 5% CO_2. For transfection, HEK293 cells were seeded into a 6-well plate at ~70% confluence. HEK293 cells were co-transfected with a mix of plasmids containing genes encoding lentivirus envelope (pHCMV-G, encoding for VSV-G behind a H-CMV promoter; ATCC, 75497), packaging (pMDLg/pRRE, include Gag and Pol genes; Addgene, 12251; pRSV-Rev, includes Rev gene; Addgene, 12253), and pGenLenti containing the target human *ACADM* gene (Genscript, U4143IC010) or control vector. Empty transfer vector (pCDH-CMV-MCS-EF1, System Biosciences, CD510B-1) was used as a negative control. EGFP-expressing plasmid (pLenti 9) was used as a positive control for transfection and transduction. The DNA-PEI mix contained: 440 µL DMEM (Glutamax I, 1% Penicillin-Streptomycin, no FBS), 60 µL PEI (1 mg/ml, pH 7.9, linear MW-25,000; Polysciences, 23966-2), and 3 µg of each plasmid. HEK293 cells were incubated with the mix for 24 h, and the supernatant was collected, filtered and supplemented with 5 µL Polybrene (8 mg/ml in H2O; Sigma, H9268-5G). The filtered medium-containing virus was added to the target HepG2 cells, which were incubated for 24 h at 37 °C, 5% CO_2. This step was repeated 2 times. In total, HepG2 cells were incubated with a medium-containing virus for 48 h. Then this medium was replaced for DMEM medium (10% FBS, Glutamax I, 1% Penicillin-Streptomycin). Lastly, transduced HepG2 cells were selected using Puromycin for approximately 5-7 days (1.5 µg/ml).

Protein extraction and Immunoblotting

Cells were lysed in RIPA buffer (1% IGEPAL CA-630, 0.1% SDS, and 0.5% sodium deoxycholate in PBS) supplemented with Phosphatase Inhibitor Cocktail 2 (Sigma, P5726) and Cocktail 3 (Sigma, P0044) and Complete Protease Inhibitor Cocktail (Sigma, 1186145001). Lysate was sonicated using Sonics Vibra cell VCX130 (Sonics & Materials Inc.) (30 sec; pulses 1 sec on, 1 sec off; 40% amplitude), then centrifuged at 12000 rcf for 10 min at 4 °C. Protein content was determined using Pierce BCA Protein Assay Kit (ThermoScientific, 23225). Lysates were adjusted with Laemmli loading buffer (5X: 60 mM Tris-Cl pH 6.8, 10% glycerol, 1% SDS, 0.05% Bromophenol Blue, 1% beta-mercaptoethanol). Protein separation was done in SDS-PAGE 10% using a Mini PROTEAN Tetra Vertical Electrophoresis Cell system (Bio-Rad, 1658029FC). For immunoblotting, the following primary antibodies were used: MCAD (Abcam, AB92461) and HSP90.

Acyl-CoA and acylcarnitine extraction from HepG2 cells

HepG2 cells were subjected to a two-step extraction process using chloroform/methanol/water. HepG2 cells were provided with 100 µL of methanol. Prior to extraction, a mixture of 10 µL of acyl-CoA and acylcarnitine internal standards (Acetyl-1,2-$^{13}C_2$-CoA, C7:0 CoA, C15:0 CoA, C17:0 CoA, L-carnitine-d$_3$, propionyl-L-carnitine-d$_3$, butyryl-L-carnitine-d$_3$, octanoyl-L-carnitine-d$_3$ and octadecanoyl-L-carnitine-d$_3$) was added to the study samples and vortexed for 1 min. Subsequently, 220 µL of methanol and 100 µL of water were added to each sample, followed by vortexing for 2 min and sonication for 3 min. To each sample, 320 µL of chloroform and 188 µL of water were added, vortexed for 2 min, and allowed to partition on ice for 10 min. The samples were then

centrifuged for 15 min at 4 °C with a speed of 15800 rcf. The resulting upper aqueous layer (450 μL) was transferred to a new Eppendorf tube. Additionally, the lower organic layer (250 μL) was transferred to the same Eppendorf tube. The combined solution was completely evaporated using a Labconco CentriVap vacuum concentrator (Kansas City, MO, USA). Following evaporation, the samples were reconstituted in a mixture of methanol/water/isopropanol (1:1:1, v/v/v) to a final volume of 100 μL, vortexed and centrifuged for 10 min. The supernatant was transferred to the HPLC vial for LC-MS injection.

Settings and configuration of HILIC-MS/MS method for analyzing free CoA and acyl-CoAs

For the acyl-CoAs, the separation of compounds was achieved using a mobile phase system consisting of acetonitrile:water (9:1) and 5 mM ammonium acetate for mobile phase A (MP-A), and acetonitrile:water (1:9) and 5 mM ammonium acetate for mobile phase B (MP-B). The flow rate was set at 0.25 mL/min, the autosampler temperature was maintained at 10 °C, and the column temperature was set to 40 °C. A 5 μL injection volume was used. The gradient elution method, spanning a 20 min duration, is provided in **Table S1.1**.

Table S1.1. Gradient program for acyl-CoA profiling

Time (min)	0	2.3	8.5	13.0	15.5	15.6	20.0
MP-A (%)	95.0	95.0	25.0	15.0	15.0	95.0	95.0
MP-B (%)	5.0	5.0	75.0	85.0	85.0	5.0	5.0

The QTRAP 6500 mass spectrometer was used in positive electrospray ionization mode. The mass spectrometer was configured with the following settings: the curtain gas (N_2) pressure was set to 25 psi, and the collision gas (N_2) was maintained at a medium level. The ion spray voltage was set at 4000 V. The source temperature was maintained at 325 °C, while the GS1 and GS2 pressures were set 60 psi. Data acquisition for targeted analysis was performed using scheduled MRM (sMRM) with a target scan time of 0.35 sec.

Settings and configuration of RPLC-MS/MS method for analyzing acylcarnitines

For the separation of acylcarnitines by RPLC, the mobile phase A (MP-A) consisted of 0.1% formic acid in water, while mobile phase B (MPB) contained 0.1% formic acid in acetonitrile. The injection volume was set at 5 μL, and the autosampler temperature was maintained at 10 °C, while the column temperature was set to 60 °C. A flow rate of 0.7 mL/min was employed. The gradient elution profile is provided in **Table S1.2**.

Table S1.2. Gradient program for acylcarnitine profiling

Time (min)	0	1.10	1.11	2.00	8.00	8.01	9.01	9.20	11.00
MP-A (%)	95.0	95.0	89.0	89.0	30.0	0	0	95.0	95.0
MP-B (%)	5.0	5.0	11.0	11.0	70.0	100.0	100.0	5.0	5.0

The QTRAP 6500 mass spectrometer was operated with the following parameters: the curtain gas (N_2) pressure was set to 20 psi, and the collision gas (N_2) was maintained at a medium level. For positive ion mode, the ion spray voltage was set at 4500 V. The source temperature was maintained at 350 °C, while the GS1 and GS2 pressures were set to 80 and 70 psi, respectively. Data acquisition for targeted analysis was performed using scheduled MRM (sMRM) with a target scan time of 0.1 sec.

The peak integration for both acyl-CoA and acylcarnitines was performed using AB Sciex OS (version 2.1.6, AB SCIEX, Concord, ON, Canada).

Total CoA measurements in mice samples

500 μL MilliQ H_2O was added to 25-100 mg liver tissue (adjusted to a final concentration of 0.2 mg liver/μL), and the tissue was lysed using a tissue homogenizer (Precellys, Bertin Instruments) (6000 rpm, 15 sec, 2 times). Lysates were centrifuged at 14000 rpm for 15 min at 4 °C. In a new tube, 10 μL Tris (2-carboxyethyl)phosphine hydrochloride (10 mM) was added to 50 μL supernatant and, incubated for 15 min at room temperature. Next, 40 μL ammonium sulfate solution (0.6 M) was added, and samples were spun down. The clear supernatant (50 μL) was then derivatized with 45 μL SBD-F (ammonium 7-flurobenzo-2-oxa-1,3-doazole-4-sulfonate; 1 mg/mL in borax buffer: 0.1 M containing 1 mM EDTA, pH 9.5) plus 5 μL ammonia solution (12.5% v/v), and incubated shaking at 500 rpm at 60 °C for 1 h (protect from light). Lastly, samples were spun down (14000 rpm, 15 min, 4 °C), and the supernatant was measured using the HPLC method (employing Phenomenex Gemini NX-C18 analytical column, 4.6 × 150 mm; 3 μm particles) and fluorescence detection.

Table S2. List of human primer sequences used in RT-qPCR.

Gene Name	Forward and reverse primer sequence (5'- 3')
PANK1	Fwd: AGGTGTCAGCATTCTAGCCGTG Rev: GGTCTCACAACCAGTCAGCAAG
PANK2	Fwd: CGTGGAGATAGCACCAAAGTGG Rev: CAGGTCCTCTTTACTGACAGCC
PANK3	Fwd: TTGCCAGGTTGGGCTGTAGCAT Rev: GCACACATTCGTGCCACAGAAC
PANK4	Fwd: TCGTGGATTCCTACAGCGAGTG Rev: CTGTCCCTCTAAGGAGTAGCTC
PPCS	Fwd: TCCTGGCAGTAGAGTTCACCAC Rev: GGCATTTCAGAGACAGGAACATAG
PPCDC	Fwd: CAAGAAGCTGGTGTGCGGAGAT Rev: GTCAACTCTGCTGGAAGCCACT
COASY	Fwd: TGAGGTGTGGACTGCTGTCATC Rev: TGGCTCTGTTCCACAAGCTGCT
SLC25A42	Fwd: AGTTCAGCGCACACGAGGAGTA Rev: GTAGGTCAGTGAAGCGGCTGTC
SLC25A16	Fwd: ATGCTCCTACCCTTCTTGGCAG Rev: TTGCATTCGCCGACGAGTCACA
SLC25A17	Fwd: GGTGGTAAACACCAGACTGAAGC Rev: AGCCGAGATTCCTTCATCGCGA
CPT1b	Fwd: TGTATCGCCGTAAACTGGACCG Rev: TGTCTGAGAGGTGCTGTAGCAC
CPT2	Fwd: GCAGATGATGGTTGAGTGCTCC Rev: AGATGCCGCAGAGCAAACAAGTG
CRAT	Fwd: CCTACAGACCAACAAGGAGCCT Rev: TGCATCTAGGCACACGGTGAAG
CROT	Fwd: CTAGTGAGGAGCGAACTCGATG Rev: CCTCTGGTGTTACATGTGGACTG
ACOT1	Fwd: GGGTTTTGCTGTGATGGCTCTG Rev: CAGCCCAACTCCTGGACCTTTT
ACOT2	Fwd: ATGGAGACGCTCCATCTGGAGT Rev: GTGATGCCCTTCAGGAAAGAGG
ACOT4	Fwd: CTTTGCCACGTTGGCTCTAGCT Rev: CCTAGAGAAATGCCCAAAAGCCC
ACOT6	Fwd: GAGCAATCCACTGGAGGAACAC Rev: GAGCTTGTAGCCTTTCAGAGGC
ACOT7	Fwd: CTACACCTCCAAGCACTCTGTG Rev: CCTTGTCCACATTCTTCAGCGAC

ACOT8	Fwd: GCTGACCACTGGATGCTCTATG
	Rev: AGGTCACAGCTAGGACTCCATC
ACOT9	Fwd: ATCCACTCCGCCAAGATGTCTC
	Rev: GATGTCTTCCCGACCCAGCTAA
ACOT11	Fwd: TCTGGTGCTCAAAGCCATCGTG
	Rev: TCATCTGCGTCCAGGACCACAA
ACOT12	Fwd: GGAGGTTACCAGCACTGTGGAA
	Rev: GCCAAATGTGCTGGACTTCCCA
ACOT13	Fwd: CGGAGTCAGTGTCGATATGAACA
	Rev: GCCTTGTTGGTCAGATCCACAG
ABCD3	Fwd: GTTCCTTTAGCAACGCCAAATGG
	Rev: CTCTTTCCGCAGCCATTTGGAC
NUDT7	Fwd: CTCCGTCCTTTTGCCATTGGTG
	Rev: TGTCTGTAGGGTCACGCTTACC
NUDT8	Fwd: CTGGCAGTGCCCGAGGAGCA
	Rev: GCCTACACCAGCAAGCACTGG
NUDT19	Fwd: GCACCACTCGCCGCTTTGACA
	Rev: GTTGCCTCTGATGGAGATGACC
YWHAZ	Fwd: ACCGTTACTTGGCTGAGGTTGC
	Rev: CCCAGTCTGATAGGATGTGTTGG

Fwd, forward primer; Rev, reverse primer.

Table S3. List of murine primer sequences used in RT-qPCR.

Gene Name	Forward and reverse primer sequence (5'- 3')
Pank1a	Fwd: GTTCGCCCAGCATGATTCTC
	Rev: CTTAACCAGGGTTCCACCGAT
Pank 1b	Fwd: CTGAGCCTAACTCCATTCAACT
	Rev: TCCACCGATATCCATACCAAAC
Pank 2	Fwd: TTGGGCATACGTGGAGCTTT
	Rev: TCTCACATACATTTCAACAGGACAAG
Pank 3	Fwd: TCACTGGGAACCAAAGGATAAA
	Rev: CAGTGAGGGATACTTCCCATTATAG
Pank 4	Fwd: GAAAACGGCCTCGCACTAAA
	Rev: CGCTCTTCCCAGCCTAGTGA
Ppcs	Fwd: CTCTCAGTCCATTAGGCTCTTC
	Rev: GGATCTTGTGTTCAGGCATTTC
Ppcdc	Fwd: TAACAACAGAGAGAGCCAAACA
	Rev: GCTTCCACATCTCCCATTCA
Coasy	Fwd: GGAGGCCTTTGGAACAGATATT
	Rev: GAGGATCTTCATCTGCTTCTTGT
Cpt1a	Fwd: CCATCCTGTCCTGACAAGGTTTAG
	Rev: CCTCACTTCTGTTACAGCTAGCAC
Cpt1b	Fwd: GCACACCAGGCAGTAGCTTT
	Rev: CAGGAGTTGATTCCAGACAGGTA
Cpt2	Fwd: CAACTCGTATACCCAAACCCAGTC
	Rev: GTTCCCATCTTGATCGAGGACATC
Crat	Fwd: GCTGCCAGAACCGTGGTAAA
	Rev: CCTTGAGGTAATAGTCCAGGGA
Abcd1	Fwd: GCTGTGACCTCCTACACTCTCC
	Rev: AGTAGTGCCAGTTCCACCTCA
Abcd2	Fwd: GAACTACCCCTCAGCGACAC
	Rev: ATGGCCTCTGTGGAATATAGAAC
Acot1	Fwd: AACATCACCTTTGGAGGGGAG
	Rev: TCCCCAACCTCCAAACCATCA
Acot2	Fwd: AGTCAACGACGCAAAATGGTG
	Rev: GCTCTTCCAATCCTGTTGGC
Acot3	Fwd: GCTCAGTCACCCTCAGGTAA

	Rev: AAGTTTCCGCCGATGTTGGA
Acot4	Fwd: ACATCCAAAGGTAAAAGGCCCA
	Rev: TCCACTGAATGCAGAGCCATT
Acot6	Fwd: ATCCTCAGGTGAAAGGCCCAA
	Rev: AAGGACAGTGGCTGTGATGTT
Acot7	Fwd: ATCAGCACGCGGCACTGTAA
	Rev: TTGGTACCTGTGAGGATGTTCTCC
Acot8	Fwd: AAGTATCGAGTGGGGCTGAAC
	Rev: TGATGTCACCTTCCCCAATGT
Acot9	Fwd: GGGGCTTCTTACTCATGGCA
	Rev: CATGGTCTCTCCAGACTGTGG
Acot11	Fwd: GTGACCAGCGGCCCTTTAG
	Rev: AGAACATAGAGGCGAAGCCCCTT
Acot12	Fwd: CCGTGGCACTAAGGTCAGTT
	Rev: ACGTTACGGTGCACGAATTG
Acot13	Fwd: AGACTCTTGCTTTGCGTCCA
	Rev: GACAAGCGTCACCTTTTCCAA
Nudt7	Fwd: CCAAGTGGAGGTGGTCTCTC
	Rev: GATGAAATCACGGCCAGACT
Nudt8	Fwd: CAGTTTCCCAGGCGGTAAGT
	Rev: CACGTTGGCAAGTACTGGGA
Nudt19	Fwd: ATCTGTGCCATCCGCGAAGC
	Rev: CACAGCTGGAGGAAGCAGCG
36b4	Fwd: GGACCCGAGAAGACCTCCTT
	Rev: GCACATCACTCAGAATTTCAATGG

Fwd, forward primer; Rev, reverse primer.
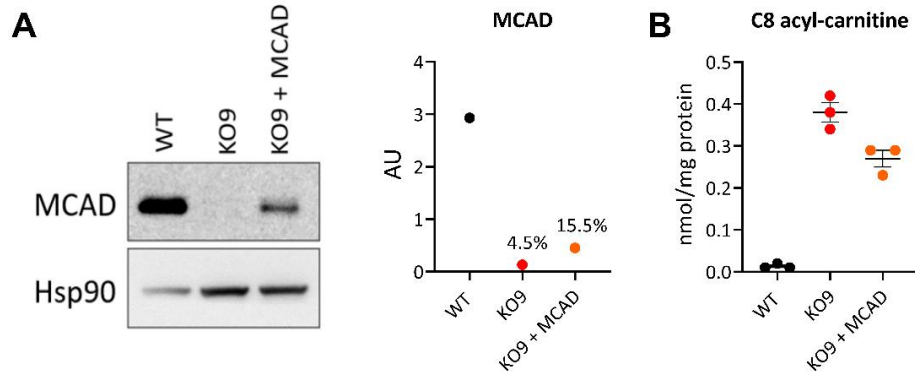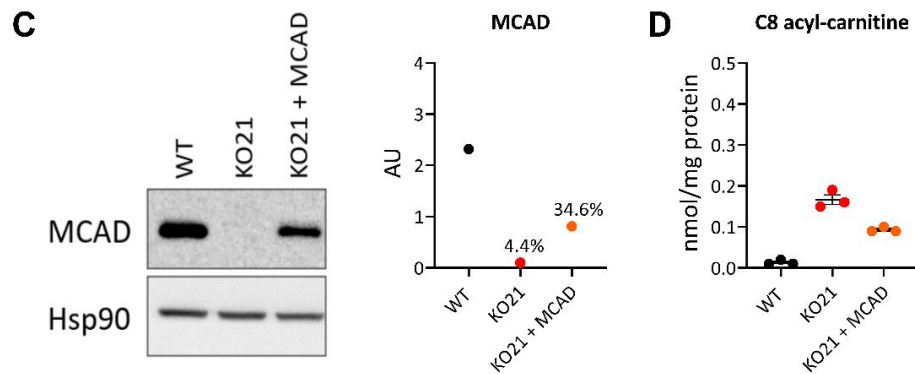
Figure S1. Partial MCAD reintroduction in MCAD-KO HepG2 cells partially restores phenotype.
A. Representative immunoblot image and respective quantification of MCAD protein in WT, MCAD-KO clone KO9 cells, and KO cells overexpressing MCAD (KO9 + MCAD); HSP90 (heat shock protein) was used as loading control.; **B.** Intracellular level of C8-carnitine; n=3 technical replicates.; **C.** Representative immunoblot image and respective quantification of MCAD protein in WT, MCAD-KO clone KO21 cells, and KO cells overexpressing MCAD (KO21 + MCAD).; **D.** Intracellular level of C8-carnitine; n=3 technical replicates.

HepG2 cellular acyl-CoA
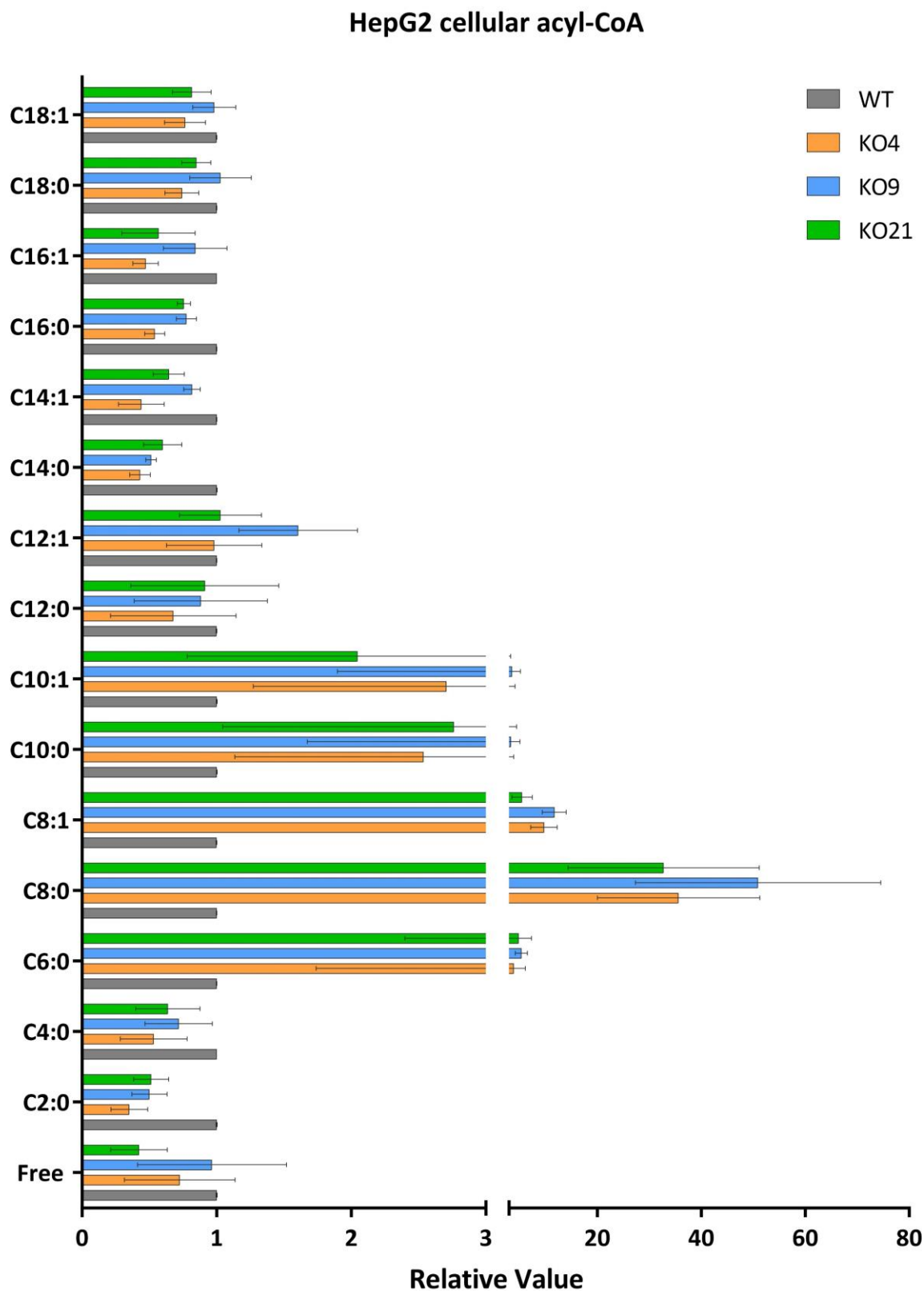
Figure S2. Full acyl-CoA profile in HepG2 cells incubated for 24 h in *high-fat no-glucose medium*. Values are relative to the mean WT value within each experiment. The data represents the average of independent experiments (n=3). Each independent experiment consisted of 4-5 technical replicates; ± standard error of the mean (SEM). Each colour represents one cell line – one WT and three MCAD-KO (KO4, KO9 and KO21).

Table S4. Statistical significance of differences in acyl-CoA levels between MCAD-KO clones and WT incubated in *high-fat no-glucose medium*. One-way Brown-Forsythe ANOVA adjusted by Dunnett's T3 multiple comparisons test was performed per individual experiment (n=3) on the data displayed in **Figure S2.** N1, N2, N3 denote the number of independent experiments. Each independent experiment in turn consists of 4-5 technical replicates. * $p<0.05$, ** $p<0.01$, *** $p<0.005$, **** $p<0.001$. Orange cells indicate cases where the KO had a higher value relative to the WT, while blue cells indicate a lower value in KO relative to the WT. *Black highlighted cells represent cases where no measurements were obtained for a given species.*

| MCAD-KO clones	KO4			KO9			KO21		
Acyl-CoAs	N1	N2	N3	N1	N2	N3	N1	N2	N3
Free		*			**		*	**	
C2:0	*	****	****		****	***		****	***
C4:0	**	**			**		*	**	
C6:0	*	***	****	**	****	***	***	****	**
C8:0	**	****	****	**	****	***	***	****	**
C8:1	■	*	**	■	**	**	■	**	**
C10:0		**	**		**	***		**	**
C10:1		*	**	*	*	*			*
C12:0	**			**			**		
C12:1					**				
C14:0	**	***		*	****		**	**	
C14:1	*	*					*		
C16:0	*	****			**			*	
C16:1	*	**			**			****	
C18:0		*							
C18:1		**						**	

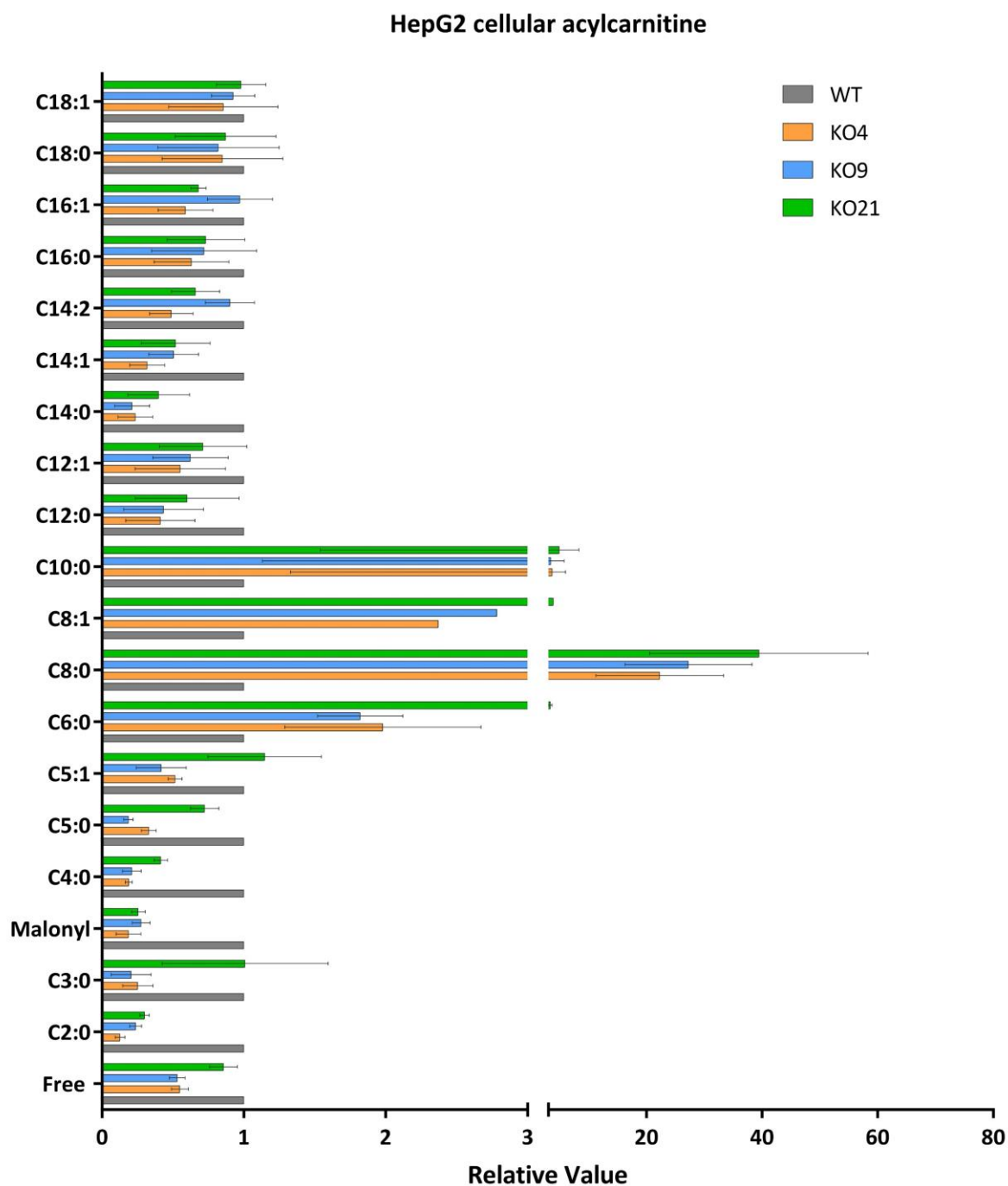**Figure S3. Full acylcarnitine profile in HepG2 cells incubated for 24 h in *high-fat no-glucose medium*.** Values are relative to the mean WT value within each experiment. The data represents the average of independent experiments (n=3). Each independent experiment consisted of 4-5 technical replicates; ± standard error of the mean (SEM). Each colour represents one cell line – one WT and three MCAD-KO (KO4, KO9, and KO21).

Table S5. Statistical significance of differences in acylcarnitine levels between MCAD-KO clones and WT incubated in *high-fat no-glucose medium*. One-way Brown-Forsythe ANOVA adjusted by Dunnett's T3 multiple comparisons test was performed per individual experiment (n=3) on the data displayed in **Figure S3.** N1, N2, N3 denote the number of independent experiments. Each independent experiment in turn consists of 4-5 technical replicates. * $p<0.05$, ** $p<0.01$, *** $p<0.005$, **** $p<0.001$. Orange cells indicate cases where the KO had a higher value relative to the WT, while blue cells indicate a lower value in KO relative to the WT. *Black highlighted cells represent cases where no measurements were obtained for a given species.*

MCAD-KO clones	KO4			KO9			KO21		
Acylcarnitines	N1	N2	N3	N1	N2	N3	N1	N2	N3
Free		**	****		*	****			
C2:0	**	****	****	**	****	****	*	****	****
C3:0	*	***	***	*	***	****	*	*	**
Malonyl	*	***	****		****	****	*	***	****
C4:0	**	***	****	*	***	****	*	**	****
C5:0	**	***	****	**	***	***		**	**
C5:1		***	***		***	****	*		
C6:0		**	***		****	***	***	****	****
C8:0	**	***	***	****	****	****	***	****	****
C8:1	**			***			****		
C10:0		****	****		****	****		****	****
C12:0	**	*	****	**	*	****	*		*
C12:1	*	*		*					
C14:0	****	***	****	****	***	****	****	***	***
C14:1	**	*	**	**	*		**		
C14:2	*	*					*		
C16:0	**	**	*	**			**		
C16:1	**		*				*	*	*
C18:0	**		**	***			**		*
C18:1	****			*					
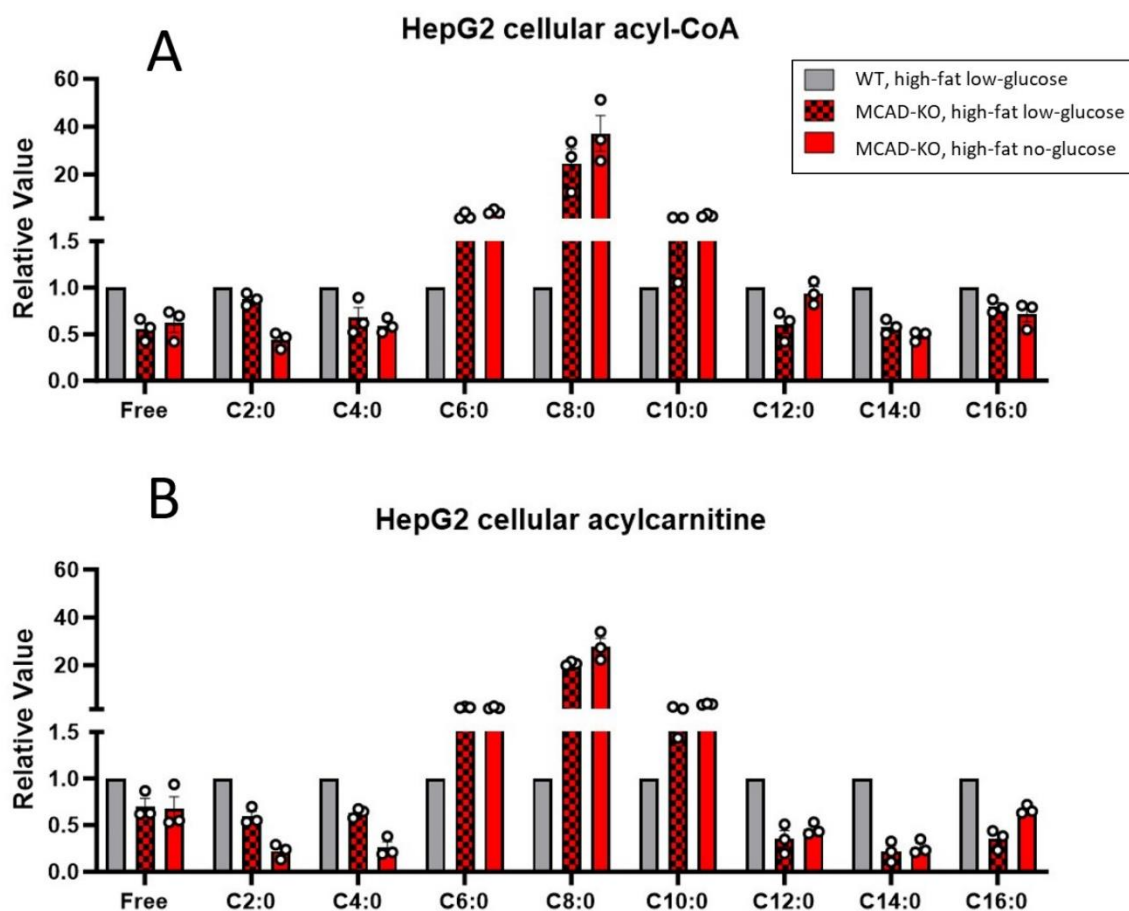
Figure S4. Acyl-CoA and acylcarnitine profiles of WT and MCAD-KO HepG2 cells grown under two conditions. Representative acyl-CoA and acylcarnitine accumulations in MCAD-KO relative to WT in HepG2 cells. Three KO-clones (KO4, KO9, KO21) and one WT cell line were investigated experimentally. Individual data points indicate the mean results for one cell line. The results consist of independent experiments (n=3) and technical replicates (n=4-5). The median and range are shown by the bar (error) bars. **A.** Acyl-CoA.; **B.** Acylcarnitines.

Figure S5. Gene expression data from MCAD-KO HepG2 cells in *high-fat no-glucose medium*. Relative expression of genes (relative to WT) in various pathways of CoA metabolism. Schemes of the relevant reactions are provided for clarity with three compartments: cytosol in white, mitochondria in pink, and peroxisomes in light blue. AcCoA = acetyl-CoA. **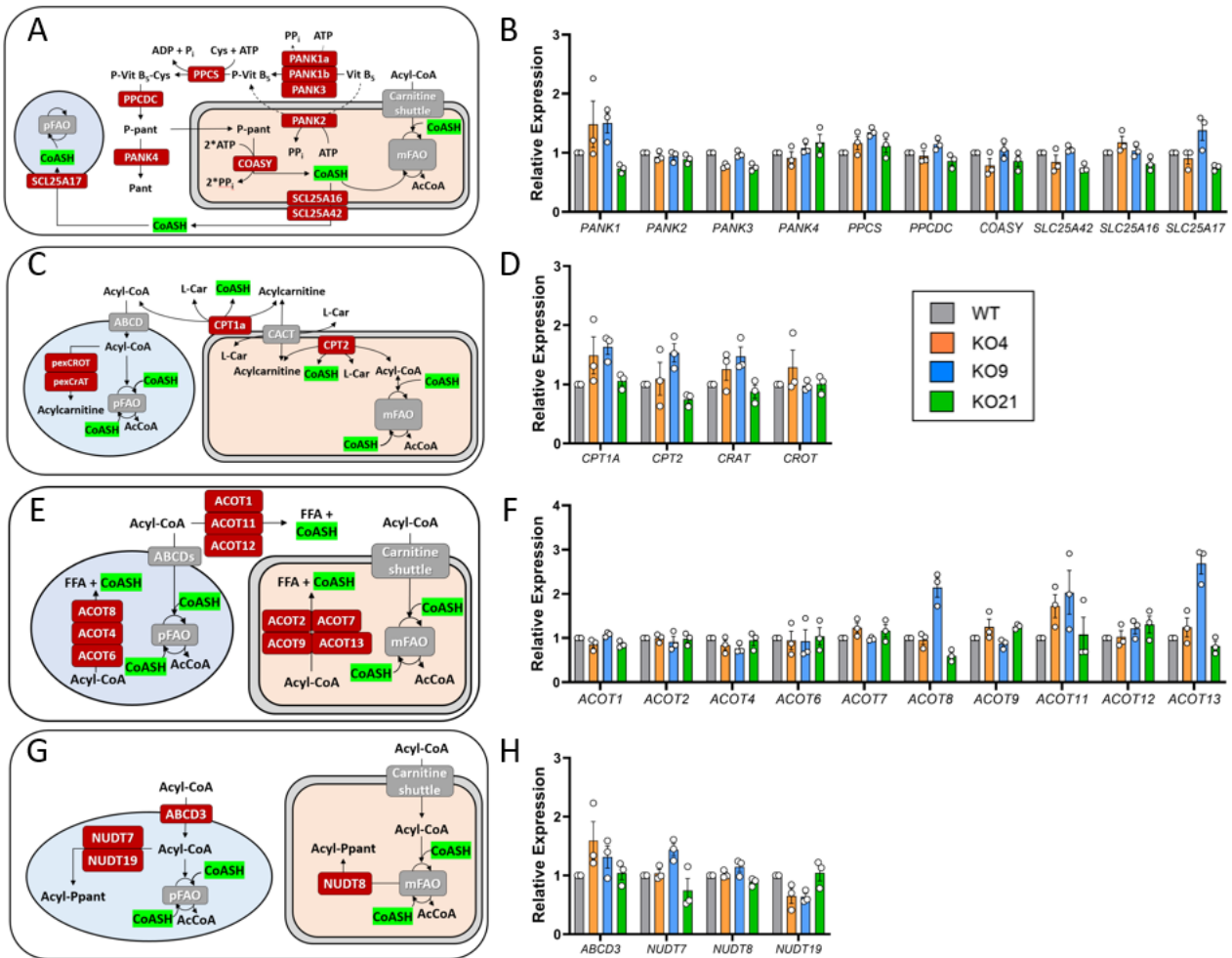A & B.** CoA biosynthesis and transport. *PANK* = pantothenate kinase, *PPCS* = phosphopantothenate-cysteine ligase, *PPCDC* = phosphopantothenoylcysteine decarboxylase, *COASY* = bifunctional coenzyme A synthase, Vit B$_5$ = pantothenate, P-Vit B$_5$ - = phosphopantothenate, P-Vit B$_5$-Cys = phosphopantothenoyl-cysteine, P-pant = phosphopantetheine, Pant = pantetheine, *SLC25A* = solute carrier family protein 25A.; **C & D.** Carnitine acyltransferases. *CPT* = carnitine palmitoyltransferase, *CRAT* = carnitine acetyltransferase, *CROT* = peroxisomal carnitine octanoyltransferase.; **E & F.** *ACOT* = Acyl-CoA thioesterases.; **G & H.** *ABCD3* = ATP-binding cassette domain protein 3, *NUDT* = nudix hydrolase. Expression values are relative to control WT (= 1); each data point represents the average of an independent experiment (3 experiments), which consisted of 4-5 technical replicates (cell cultures); ± standard error of the mean (SEM).

Table S6. Statistical significance of differences in mRNA expression between MCAD-KO clones and WT HepG2 cells incubated in *high-fat no-glucose medium*. One-way Brown-Forsythe ANOVA adjusted by Dunnett's T3 multiple comparisons test was performed per individual experiment (n=3) on the data displayed in **Figure S5.** These were therefore values relative to the WT mean within each experiment. Each experiment consisted of 4-5 technical replicates. Values were considered statistically significant when * $p<0.05$. Highlighted in orange are upregulated genes in KO relative to WT while in blue are downregulated genes in KO relative to WT.

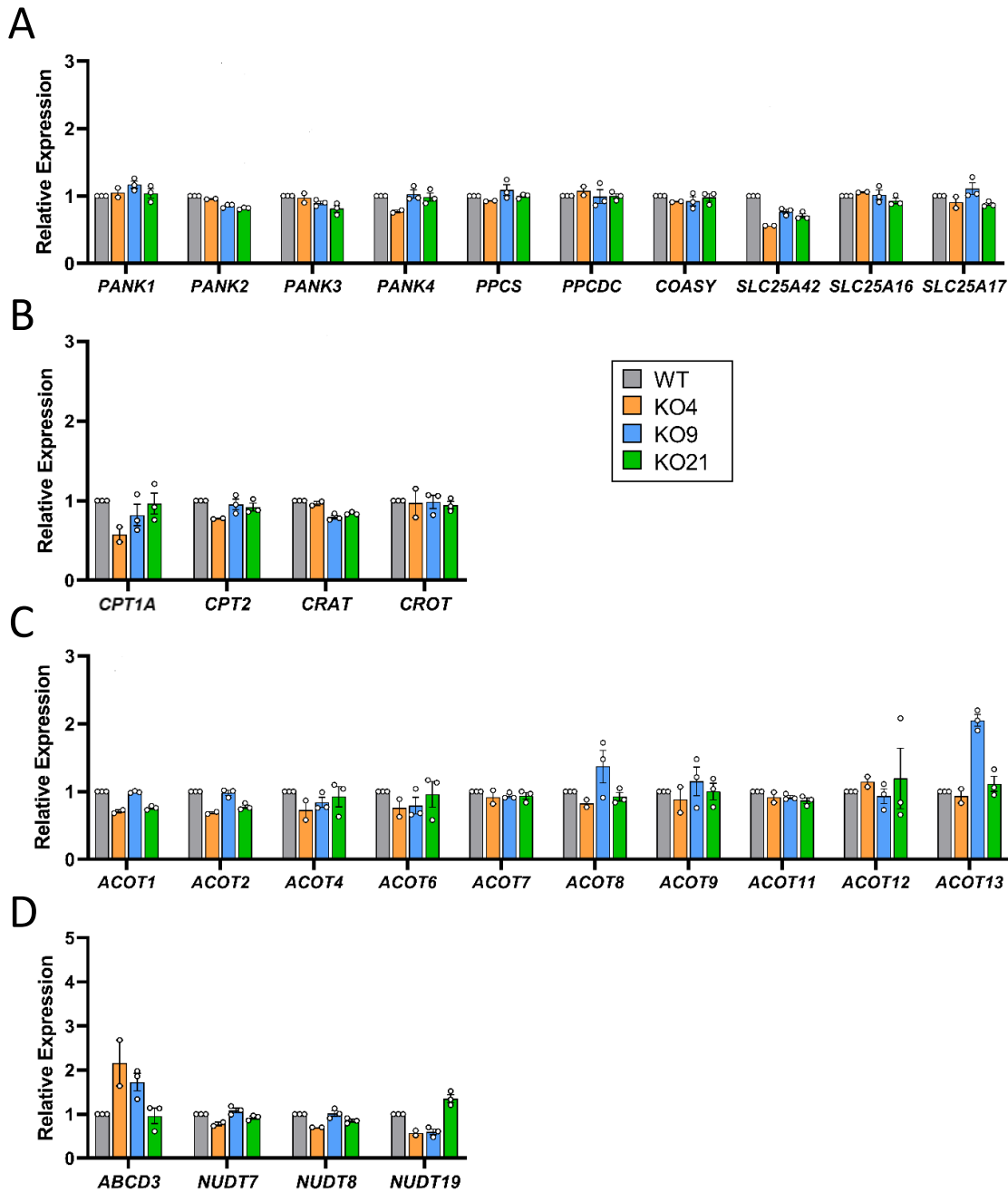| MCAD-KO clones	KO4			KO9			KO21		
Gene of Interest	N1	N2	N3	N1	N2	N3	N1	N2	N3
ACOT1		*						*	
ACOT2		*			*			*	*
ACOT4				*					
ACOT6		*			*				
ACOT7	*		*				*		
ACOT8				*	*	*	*	*	*
ACOT9	*			*				*	
ACOT11	*	*		*	*	*	*	*	*
ACOT12									
ACOT13			*	*	*	*		*	
NUDT7				*	*			*	*
NUDT8				*					*
NUDT19	*	*	*	*	*	*	*	*	
SLC25A42	*	*					*	*	
SLC25A16			*						*
SLC25A17	*				*	*	*	*	*
CRAT		*	*	*	*	*		*	
CROT			*				*		
CPT1A		*	*	*	*	*		*	
CPT2	*		*		*	*			*
PANK1		*	*	*				*	*
PANK2									
PANK3	*	*	*				*	*	*
PANK4		*	*				*		
PPCS	*			*	*	*	*	*	
PPCDC						*	*		
COASY	*	*		*			*		
ABCD3			*	*					

Figure S6. Gene expression data from MCAD-KO HepG2 cells in *high-fat low-glucose medium*. Relative expression of genes (relative to WT) in various pathways of CoA metabolism. **A .** CoA biosynthesis and transport. *PANK* = pantothenate kinase, *PPCS* = phosphopantothenate-cysteine ligase, *PPCDC* = phosphopantothenoylcysteine decarboxylase, *COASY* = bifunctional coenzyme A synthase, *SLC25A* = solute carrier family protein 25A.; **B.** Carnitine acyltransferases. *CPT* = carnitine palmitoyltransferase, *CRAT* = carnitine acetyltransferase, *CROT* = peroxisomal carnitine octanoyltransferase.; **C.** *ACOT* = Acyl-CoA thioesterases.; **D.** *ABCD* = ATP-binding cassette domain protein, *NUDT* = nudix hydrolase. Expression values are relative to control WT (= 1); each data point represents the average of an independent experiment (3 experiments), which consisted of 4-5 technical replicates (cell cultures); ± standard error of the mean (SEM).

Table S7. Statistical significance of differences in mRNA expression between MCAD-KO clones and WT HepG2 cells incubated in *high-fat low-glucose medium*. One-way Brown-Forsythe ANOVA adjusted by Dunnett's T3 multiple comparisons test was performed per individual experiment (n=3) on the data displayed in **Figure S6.** These were therefore values relative to the WT mean within each experiment. Each experiment consisted of 4-5 technical replicates. Values were considered statistically significant when * $p<0.05$. Highlighted in orange are upregulated genes in KO relative to WT while in blue are downregulated genes in KO relative to WT. *Experiment N3 in KO4 had technical issues due to which we were not able to perform the gene expression analysis.*

MCAD-KO clones	KO4			KO9			KO21		
Gene of Interest	N1	N2	N3	N1	N2	N3	N1	N2	N3
ACOT1	*								*
ACOT2	*	*						*	*
ACOT4		*							
ACOT6									*
ACOT7									
ACOT8	*	*		*	*	*			
ACOT9				*	*				*
ACOT11									
ACOT12								*	
ACOT13	*			*	*	*			*
NUDT7	*								
NUDT8		*							*
NUDT19	*	*		*	*	*	*	*	*
SLC25A42	*	*		*		*	*	*	*
SLC25A16									*
SLC25A17						*			*
CRAT				*	*	*	*	*	*
CROT	*								
CPT1A	*	*		*	*		*		
CPT2	*	*			*			*	
PANK1				*					
PANK2							*	*	*
PANK3							*	*	*
PANK4		*				*			
PPCS						*			
PPCDC									
COASY									*
ABCD3		*			*				*

Chapter 7

Conclusion and perspectives

Conclusion and perspectives

The liver, one of the body's largest organs, plays a pivotal role in all metabolic processes. It governs energy metabolism during both fed and fasted states, regulating essential functions such as glycolysis, lipogenesis, glycogenolysis, gluconeogenesis, fatty acid oxidation and ketogenesis [1]. These processes play key roles in maintaining lipid homeostasis through various cellular, biochemical and signaling pathways [2]. Disruptions in the normal metabolic processes can result from factors such as genetics and environmental influences, leading to liver metabolic diseases. Lipids have diverse roles in various essential cellular functions that are closely interconnected within chemical and genetic networks. As liver is the central organ for lipid metabolism, any deviation in the normal liver metabolic process will directly impact the lipid concentration levels. Hence, lipids are important biomarkers for elucidating the underlying pathophysiological mechanism associated with liver metabolic diseases, as previously discussed in chapter 1. The goal of this thesis is to develop technologies facilitating the measurement of different lipid classes and apply these technologies in biological models of liver metabolic diseases, to enhance our understanding of lipid biomarkers and associated biochemical pathways. The first part of thesis (**Chapter 2 and 3**) was focused on the development of methods for analyzing complex lipid classes and their application in cell models. The aim was to overcome shortcomings of current lipidomics methods and to improve coverage and quantitation. The developed method employed a liquid chromatography-tandem mass spectrometry (LC-MS/MS) and was subsequently applied to different *in vitro* liver matrices to compare their metabolic capabilities. The second part of thesis (**Chapter 4, 5 and 6**) centered on acyl-coenzyme A (acyl-CoA), belonging to the category of fatty acyl lipids. In this part, the emphasis was to study the significance of acyl-CoAs as diagnostic biomarkers for fatty acid oxidation disorders (FAOD) and the challenges associated with the measurement of these compounds. Further, we developed a targeted method for acyl-CoA analysis using LC-MS/MS to improve coverage for acyl-CoA profiling and applied this method to evaluate CoA metabolism in medium-chain acyl-CoA dehydrogenase deficiency (MCADD, a type of FAOD) and to explore its effect on relevant metabolic networks. The upcoming sections will provide a summary, discussion and future perspectives of this thesis.

Chapter 2 aimed at the development and validation of a hydrophilic interaction liquid chromatography-tandem MS (HILIC-MS/MS)-based lipidomics method, covering both non-polar and polar lipid classes and allows for the quantitation of lipid species at fatty acyl chain level. This method provided a comprehensive coverage of 1200 lipid transitions across 19-

(sub)classes belonging to categories glycerolipids, glycerophospholipids, sphingolipids and sterol lipids. The lipid species within these categories were evaluated on various cross-class (such as isobars, isomers and in-source fragments) and within-class interferences (including isotopes, different ion types and chromatographic separation) for unambiguous identification and to prevent over-reporting. The scores were assigned to indicate confidence in lipid identification. This HILIC-MS/MS method was validated on various parameters; the accurate quantitation strategy was evaluated by quantifying 608 lipid species with a high confidence score (score 4) in NIST SRM 1950 plasma samples using multiple internal standards per class followed by post-hoc correction. We demonstrated that our quantitation results shows good correlation (R^2 ranging from 0.64-0.84) with other reported studies [3–5]. The developed method was applied to coronavirus (COVID-19) patient samples to monitor the lipidome changes for disease severity assessment.

Future improvements in our HILIC method could include the ability to determine the positional isomers (sn-1 and sn-2 positions of fatty acyl chain), identifying double bonds locations in fatty acyl chains, and addressing cis-trans isomerization, as distinct isomers have different functions and properties with diverse biological implications [6]. Ion-mobility-mass spectrometry techniques are recognized for their ability to differentiate between isomeric or isobaric lipid species [7]. Recently, electron-activated dissociation (EAD) techniques, such as Electron-Induced Dissociation (EID) and Electron-Impact Excitation of Ions from Organics (EIEIO), have been introduced for the purpose of identifying the positions of double bonds within fatty acyl chains [8]. Ultraviolet Photodissociation (UVPD) activation mode has also been employed to identify sn-positional isomers and the positions of double bonds [9]. Calculating the variation in response factors based on differences in head group and fatty acyl chain compositions among various isomers is a crucial aspect for achieving absolute quantitation, especially due to the limited availability of commercial (internal)standards. Furthermore, there is a critical need to enhance high-throughput capabilities, particularly in the context of analyzing over 1000 lipid species and dealing with a large number of clinical samples. The traditional methods of manual sample preparation and peak integration are not only time-consuming but are also labor-intensive. These processes can cause significant delays in overall data analysis. Therefore, implementing automated tools for sample preparation and peak integration has the potential to streamline the sample analysis and preprocessing, and reduce the time required for analysis.

Research in liver metabolic diseases needs *in vitro* models that can effectively replicate the complex functions associated with liver. These models should be physiologically relevant and

accurate in mimicking metabolic processes and functions of liver. **Chapter 3** aimed at the characterization and evaluation of alternative *in vitro* models for energy metabolism studies in comparison to primary human hepatocytes (PHH) by assessing their metabolic capabilities. PHH are regarded as the gold standard liver-based *in vitro* models as they can replicate the metabolic processes and functionality of the human liver. However, there are several limitations associated with their culture such as loss of liver-specific functions, weak proliferation ability and rapid de-differentitation *in vitro* [10]. Therefore, there is a need for alternative sources that can perform functions at a similar level to PHH. We compared the metabolic capabilities of PHH with stem cell-derived hepatocytes (iPSC-Hep), human hepatocellular carcinoma cells (HepG2), immortalized upcyte-hepatocytes (Upcyte-Hep) and adult donor-derived liver organoids. These cells were cultured under fed conditions (supplemented with glucose) and glucose production (GP) challenge conditions (culturing them without glucose). These cell models were assessed on the basis of production of secreted glucose and induction of gluconeogenesis-related genes in GP-challenged conditions. The HILIC-MS/MS-based lipidomics method (developed in **Chapter 2**) was applied to analyze the lipid profile of these cell models and to observe changes in intracellular lipid composition in GP-challenged conditions. Among the cell models investigated, it was observed that when exposed to GP-challenging conditions, PHH exhibited the highest levels of glucose production and secretion, both intracellularly and extracellularly. Organoids and iPSC-Hep followed PHH in terms of intracellular glucose production, while Upcyte-Hep and HepG2 showed glucose production below the detection limit. Extracellularly, the ranking from highest to lowest glucose production was PHH, followed by organoids, iPSC-Hep, Upcyte-Hep and HepG2. Gluconeogenesis is the process of glucose production from non-carbohydrate sources after depletion of glycogen stores. Glucose-6-phosphatase (*G6PC*), phopshoenolpyruvate carboxykinase 1 (*PCK1*) and fructose 1,6-biphosphatase (*FBP1*) are the three key enzymes involved in the gluconeogenesis process. We observed that both G6PC and PCK1 were upregulated in all cell models when cultured in a GP medium compared to a fed medium. However, the regulation of FBP1 differed among the cell types. In PHH, iPSC-Hep and Upcyte-Hep, FBP1 expression showed minimal changes, while in organoids and HepG2 cells, it was downregulated. The lipid profiles of PHH closely resemble to those of organoids. Under GP-challenged conditions, both PHH and organoids exhibited decreased triglyceride (TG) levels, while minimal changes were observed in iPSC-Hep and HepG2 cells. Conversely, Upcyte-Hep cells showed a significant increase in several TG species under the same conditions. These findings suggested a correlation with glucose production and fatty acid oxidation rates. The reduction in TG levels implies the

activation of the fatty acid beta-oxidation pathway, potentially explaining the higher net glucose production in PHH and organoids. In contrast, the TG profiles in iPSC-Hep, HepG2, and Upcyte-Hep indicated a decrease in fatty acid beta-oxidation, reflecting reduced glucose production rates compared to PHH and organoids. Furthermore, there was significant alteration in the level of phospholipids, specifically phosphatidylethanolamine (PE) and phosphatidylcholine (PC) in GP conditions. PHH exhibited a decrease in PE, organoids demonstrated a reduction in both PC and PE, while an increase was observed in iPSC-Hep and Upcyte-Hep. This suggests an interconnection with metabolic processes aimed at maintaining energy homeostasis. The results presented in this chapter indicate that organoids may serve as a potential substitute for PHH. They have demonstrated the second highest net glucose production after PHH and exhibit a lipid profile similar to PHH. However, it is essential to conduct additional research to validate whether organoid models accurately represent fully mature, differentiated and metabolically proficient hepatocytes, and are suited to study liver metabolic diseases.

Future research in this direction should concentrate on exploring various experimental conditions and measuring metabolites involved in central carbon metabolism to deepen the understanding of energy metabolism in these hepatocyte models. One aspect would be to determine the ideal experimental parameters for these liver cell models, enabling the activation of both fatty acid oxidation and glucose production, and interpret the correlation between them. This may need the introduction of an initial fasting period to deplete the glycogen reserves or the application of fatty acid treatments to increase the cellular triglyceride levels before putting the matrices under glucose production challenge. Furthermore, there is need of additional studies that can enhance our understanding behind the complex process of lipid metabolism and the regulation of energy balance including the aspect of hormonal regulation. Different cell models require specific culture media tailored to their needs, which subsequently regulate the cell growth and proliferation. Examination of the effect of the medium on the profile of fatty acid chains in lipids, alterations in these chains at different stages of cell proliferation and maturation over various days and the correlation with the enzymes responsible for elongating and desaturating fatty acyl chains of lipid molecules can be another aspect of future research. The study of these three-dimensional (3D)-cell culture models have several challenges that should be carefully considered. Organoids are cultivated within Matrigel domes, requiring the extra washing steps prior to analysis due to the potential presence of residual glucose even after repeated washes. This residual glucose can compromise the accuracy of glucose production

assays. This chapter also highlighted the concerns about glucose and Matrigel traces during the incubation period of organoids, and further investigation needs to be conducted to establish robust glucose production assays for these three-dimensional (3D)-cell models. These hepatocyte models can be further investigated to study the disruption in energy metabolism and subsequently affected metabolic networks in liver metabolic diseases and can also be used for the assessment of treatment effectiveness, ultimately aiding in the development of novel therapies for these diseases.

Fatty acid oxidation disorders (FAOD) are a group of liver metabolic diseases that result from a deficiency in the activity of enzymes or transporter proteins involved in the fatty acid oxidation (FAO) pathway. The FAO pathway is crucial for human survival as it serves as an energy source in conditions of low glucose availability. Acyl-CoA molecules are central to this pathway and in FAOD, these molecules accumulate depending on the type of disorder. Acyl-CoAs, despite being the primary biomarkers, are not commonly used for diagnostic purposes. Instead, hospitals and clinics rely on secondary biomarkers such as acylcarnitines. The main reason for this preference is the significant technical challenges associated with the analysis of acyl-CoAs. **Chapter 4** provides a comprehensive overview on the technical challenges, recent analytical advancements for the measurement of these compounds, and potential measures that could be taken for improving the analysis. A major limitation in the analysis of acyl-CoAs is their intracellular location, making them inaccessible for measurement in readily available matrices like plasma and urine. Other obstacles include low endogenous level, instability and extreme variation in the physicochemical properties often leads to the need of using multiple chromatographic separation methods. To address these challenges, numerous efforts had been undertaken to improve the extraction of acyl-CoA from biological samples and perform their analysis. Protein precipitation, liquid-liquid extraction, solid-phase extraction or the combination of these techniques had been used for the extraction of acyl-CoA from biological matrices. Further, various methods had been explored for the separation and detection of these compounds including enzymatic assays, liquid chromatography with ultraviolet detection (LC-UV), gas chromatography coupled with mass spectrometry (GC-MS) and liquid chromatography-mass spectrometry (LC-MS). Among all these approaches, LC-MS is the most sensitive method, offering high resolution and comprehensive coverage, and is currently the most commonly employed technique. In recent years, several attempts such as ion-pairing [11], derivatization [12] and chemical ligation [13] have been made to improve the separation, peak shape and detection of these compounds. This chapter also emphasizes on the use of correct

internal standards for accurate quantitation of acyl-CoAs. Stable isotope labeling by essential nutrients in cell culture (SILEC) had been developed for the generation of labeled isotopic standards for acyl-CoA. These isotopic standards can be used as internal standards for the quantitation of corresponding endogenous acyl-CoA species. The generation of labeled internal standards is crucial for quantitation of unstable compounds like acyl-CoAs as both internal standards and endogenous species will undergo through the same process of degradation. In conclusion, this chapter outlines recent advancements in analytical techniques for acyl-CoA measurements and the need for further studies focusing on ways to increase the stability and simplifying the analytical strategies of these compounds.

Chapter 5 in this thesis addressed one of the technical challenges associated with the analysis of acyl-CoAs. As stated in **Chapter 4**, acyl-CoAs differ considerably in their physiochemical properties, often requiring multiple chromatographic methods or alternative strategies such as use of ion-pairing reagents or derivatization. However, these techniques also have disadvantages, ion-pairing are known to cause contamination in the mass spectrometers, while derivatization increases the complexity and analysis time, thus affecting the desired high-throughput of analysis. In **Chapter 5**, we developed an analytical method that can cover the entire range of acyl-CoA species in one analytical run. We employed a HILIC-MS/MS approach with the use of zwitterionic ZIC-cHILIC column. The initial method development was performed on a QTOF instrument to identify acyl-CoA species and determine their retention times. Various factors such as buffer concentration, effect of cell matrix and injection solvents were considered to optimize the chromatography. The ZIC-cHILIC column is composed of both negative and positive charged moieties, resulting in weak electrostatic interaction between the analyte and stationary phase, hence a lower concentration of buffer is needed for elution. After optimization of various parameters, 5 mM ammonium acetate was chosen for both organic and aqueous phase with a flow rate of 0.25 mL/min. The reconstitution solvent consisted of methanol:water:isopropanol (1:1:1, v/v/v). Further, a targeted method was created on a QTRAP instrument in scheduled multiple reaction monitoring mode. This method was successful in covering free CoA and short- to long-chain acyl-CoAs in one run. The performance of the method was evaluated on parameters such as linearity, precision, recovery and matrix effect for acyl-CoA quantitation in HepG2 cells. The method was further applied in wildtype (WT) HepG2 cells cultured in supplemented (high in carbon sources) and starved state (fewer carbon sources) to evaluate acyl-CoA profile. We observed an increase in the

concentration of short-, medium- and long-chain acyl-CoAs while decrease in the level of free CoA in starved state, thus indicating an activation in FAO process.

Our HILIC-MS/MS method for acyl-CoA analysis can be further explored for increasing the species coverage and separation of isomers. The current method was targeted on coverage of short- to long-chain acyl-CoAs, as our primary focus was on MCADD. However, the coverage of this method can further be extended to measure very long-chain acyl-CoA species (>20 carbon atoms) and can be applied to assess the acyl-CoA profile in very long-chain acyl-CoA dehydrogenase deficiency (VLCADD). Furthermore, ion-mobility mass spectrometry, EAD and UVPD techniques could be employed to distinguish between isomeric species, for instance, distinguishing between succinyl-CoA and methylmalonyl-CoA, and to determine the position of double bonds in species like C16:1 and C18:1. The endogenous concentrations of acyl-CoAs are very low which necessitates the use of highly sensitive techniques. In the future, there is potential for the utilization and further exploration of micro-LC-MS/MS and nano-LC-MS/MS techniques to achieve even greater sensitivity [14,15]. Additionally, it has been reported that acyl-CoAs exhibit suboptimal recovery rates when analyzed in tissue samples, attributed to their tendency to form anhydrides and S-acyl glutathione [13]. Consequently, it is essential to initiate efforts aimed at delving deeper into the recovery issue and gaining a comprehensive understanding of the factors contributing to the low recovery and degradation of acyl-CoAs. To address potential issues related to degradation, SILEC can be a valuable tool for achieving absolute quantitation of acyl-CoAs. This approach can help compensate for degradation problems and enhance the accuracy of the analysis, thus providing a reliable diagnostic approach. Presently, this method has been applied for the analysis of acyl-CoA species in HepG2 cells. In the future, its applicability can be extended to human samples, particularly tissue samples to have clinically relevant insight into liver metabolic diseases. Given that acyl-CoAs are primarily intracellular, obtaining tissue samples can be challenging, especially in the case of newborns. Therefore, alternative matrices like human fibroblasts, whole blood and platelets should be considered as a more accessible approach for biomarker analysis.

In **Chapter 6**, we extensively explored *in silico*, *in vitro* and *in vivo* models to gain insights into the CoA metabolism and systemic alterations caused by MCADD, and also to identify potential compensatory mechanisms. An *in silico* model of the human liver was developed to analyze changes in saturated and even-chain acyl-CoAs between the MCAD-knockout (KO) and WT conditions. The MCAD-KO model shows a marked increase in C6-CoA and C8-CoA levels, while all other species, including free CoA, decrease significantly. *In silico* simulations were

corroborated with experimental data, by culturing HepG2 MCAD-KO and WT cells in *high-fat low-glucose medium* (containing glucose, pyruvate, glutamine, palmitate and L-carnitine) and *high-fat no-glucose medium* (contains only palmitate and L-carnitine). We determined the intracellular levels of free CoA and acyl-CoA in HepG2 MCAD-KO and WT models using the HILIC-MS/MS method (developed in **Chapter 5**). Additionally, acylcarnitines were quantified using a RPLC (reversed-phase liquid chromatography)-MS/MS method. In both media formulations, MCAD-KO clones exhibited significant increases in medium-chain (C6-C10) acyl-CoA levels, particularly in the case of C8-CoA. In contrast, other saturated even-chain species and free CoA levels were reduced in all MCAD-KO compared to WT cells. The acylcarnitines exhibited a similar trend as acyl-CoA, with an increase in species containing (C6-10) chains and a decrease in other acylcarnitine esters and free carnitine in MCAD-KO samples. Further, we investigated the effect of MCAD-KO on CoA biosynthesis. We treated cells in a *high-fat low-glucose medium* with labeled pantothenate for 24 h. We observed an increase in label incorporation in newly synthesized CoA after 24 h indicating an increase in CoA biosynthesis, which were similar for both WT and MCAD-KO cells, suggesting an active CoA biosynthesis pathway in MCAD-KO conditions. In the same experiment, MCAD-KO cells exhibited lower unlabeled free CoA compared to WT, while total CoA remained unchanged. We conducted similar *in vivo* experiments under physiologically relevant conditions, involving MCAD-KO and WT mice in three states: fed, 14 h overnight fasted, and 14 h overnight fasted with additional 4 h of cold exposure. Total CoA levels and CoA biosynthesis intermediates were increased in both WT and MCAD-KO mice during fasting, with no significant difference between the two groups, indicating a comparable CoA biosynthesis rate. However, MCAD-KO mice exhibited a significant rise in total CoA levels when subjected to both fasting and cold conditions. These findings imply that higher metabolic stress tends to lead to an increase in total CoA levels.

We examined gene expression levels in both HepG2 cells and mouse samples across all study conditions. The upregulation of CoA biosynthesis enzymes and carnitine acyltransferases aligns with our findings from *in silico*, *in vitro* and *in vivo* experiments, suggesting that the accumulation of medium-chain acyl-CoAs could deplete the free CoA pool. This depletion might stimulate the production of more free CoA, however this increased production of free CoA, in turn, leads to further accumulations of acyl-CoAs. Another key finding was the upregulation of acyl-CoA thioesterases (ACOTs) enzymes in MCAD-KO conditions, suggesting an attempt to replenish the free CoA pool and mitigate the excessive buildup of acyl-

CoA esters. We used *in silico* experiments to show this compensatory mechanisms. Our computational model demonstrated that the simultaneous increase in total CoA and upregulating ACOTs in the MCAD-KO model effectively restored free CoA levels while reducing toxic C8-CoA, highlighting the concurrent activation of multiple compensatory mechanisms. These findings confirm the validity of MCADD as CoA sequestration, toxicity, and redistribution (CASTOR) disease.

The future directions of this study involve exploring various models for metabolic network analysis for MCADD. While HepG2 cells are readily accessible and convenient for use, they are not a perfect representation of human liver cells. In **Chapter 3**, we had already demonstrated their distinct response to PHH in terms of energy metabolism and response to challenged conditions. As discussed in **Chapter 3**, organoids and iPSC-Hep cells closely resemble to PHH. Therefore, it is recommended that future research places a priority on using these models for studying MCADD, as they offer a more accurate representation of the human hepatocyte system and allow for direct involvement of MCADD patient cells. Another limitation in the current study is the lack of broader physiological context, MCAD deficiency affects the entire body, which could influence the way the condition manifests. Patient studies such as "Fasting Tolerance in MCADD-infants (FiTtINg MCADD)" hold promise in providing human data collected under controlled conditions, which may offer deeper insights [16]. It is possible that various MCAD-KO cell lines, animals, and different MCADD patients may employ distinct compensatory mechanisms, offering valuable insights into inter-patient heterogeneity. Unraveling this heterogeneity and examining its precise effects on acyl-CoA and free CoA levels is another potential future direction for this study.

Final Perspectives

Understanding the lipid complexity and unveiling their involvement in metabolic disorders needs substantial amounts of research to fully explore the potential of lipidomics in deciphering the dynamics of lipid metabolism for early diagnosis of diseases, monitoring disease progression and efficiency of an intervention. To delve deeper into this field, it is important to engage in interdisciplinary research that incorporates other omics studies. The integration of multi-omics approaches will contribute significantly in gaining a systematic understanding of the pathological aspects related to liver metabolic diseases. Next-generation sequencing (NGS) has made it easier to identify disease-associated mutations, yet the diagnosis is only possible in (30-40)% cases with presumed hereditary abnormality. Many cases result in variants of unknown significance (VUS) without confirmed disease associations. The integration of NGS

with lipidomics can offer a promising approach to establish the pathogenicity of VUS and improve diagnostic accuracy. This combined approach has the potential to increase the diagnostic yield of NGS to (50-90)% [17].

Modern technologies for comprehensive coverage, better resolution, automation and quantitation of lipids are continuously being developed by researchers. These new technologies (including high-throughput technologies) support lipidomics research and broaden the scope of lipidomics from identification of disease-specific biomarkers to also include the monitoring of drug efficacy in the treatment of disorders, potentially leading to novel therapeutic approaches such as understanding the difference between responder and non-responders to interventions. An emerging field, tracer-based lipidomics, holds the potential for flux analysis, enabling a deeper understanding of reaction rates in lipid metabolism at molecular levels and aiding the reconstruction of metabolic pathways. These approaches allow us to link alterations in a patient's lipid profile with their specific gene variants, thereby revealing the connections between various metabolic networks. This knowledge can support in the development of personalized medicine, providing treatments based on individual needs and ensuring precise and effective healthcare.

This thesis primarily focuses on *in vitro* samples, but the next phase involves incorporating the technologies developed in **Chapters 2** and **5** into analysis of clinical samples. We have recently initiated the analysis of plasma and liver samples from patients at various stages of metabolic (dysfunction)-associated steatotic liver disease (MASLD) using the HILIC-MS/MS method described in **Chapter 2**. Patients have been categorized based on their SAF (steatosis, activity, and fibrosis) score, characterizing the disease severity [18]. Preliminary findings indicate promising lipid accumulation patterns linked to disease severity. The comprehensive dataset and associated biomarkers will be of great interest once the analysis is completed. Furthermore, correlating this data with a planned transcriptomics study in the future will enhance our understanding of the underlying pathophysiological mechanisms of MASLD. These analytical methods can also be extended to other liver metabolic diseases, including glycogen storage diseases (GSD) and various other types of fatty acid oxidation disorders.

In the present scenario, plasma is the most accessible and commonly utilized matrix in clinical studies. However, **Chapter 4** has highlighted the significance of acyl-CoA in cellular metabolic health. The challenge arises from the intracellular location of these compounds, making their analysis in clinical samples quite challenging. Therefore, there is urgent requirement for

investigation of alternative matrices for these metabolites. Harmonization in lipid quantitation is another crucial aspect. Lipid concentrations reported (even for the same sample) frequently differ between laboratories, posing an obstacle in establishing reference ranges. The standardized, or at least harmonized, workflows are necessary for data reproducibility and inter-laboratory comparability.

Overall, the research described in this thesis contributes to our understanding of how lipidomics can enhance our knowledge of liver metabolic diseases. We have developed analytical techniques to comprehensively study lipid molecules and to link them with biochemical pathways. These techniques have been applied to various *in vitro* models to gain insights into liver metabolism and to quantify alterations in lipid species in liver metabolic disease samples. In the future, this research shows potential for integrating lipidomics with multi-omics data, paving the way to a systems biology approach that could extend the possibilities of personalized medicine.

References

[1]   L. Rui, Energy Metabolism in the Liver, Compr Physiol. 4 (2014) 177–197. https://doi.org/10.1002/cphy.c130024.

[2]   M. Alves-Bezerra, D.E. Cohen, Triglyceride metabolism in the liver, Compr Physiol. 8 (2017) 1–8. https://doi.org/10.1002/cphy.c170012.

[3]   J.A. Bowden, A. Heckert, C.Z. Ulmer, C.M. Jones, J.P. Koelmel, L. Abdullah, L. Ahonen, Y. Alnouti, A.M. Armando, J.M. Asara, T. Bamba, J.R. Barr, J. Bergquist, C.H. Borchers, J. Brandsma, S.B. Breitkopf, T. Cajka, A. Cazenave-Gassiot, A. Checa, M.A. Cinel, R.A. Colas, S. Cremers, E.A. Dennis, J.E. Evans, A. Fauland, O. Fiehn, M.S. Gardner, T.J. Garrett, K.H. Gotlinger, J. Han, Y. Huang, A.H. Neo, T. Hyötyläinen, Y. Izumi, H. Jiang, H. Jiang, J. Jiang, M. Kachman, R. Kiyonami, K. Klavins, C. Klose, H.C. Köfeler, J. Kolmert, T. Koal, G. Koster, Z. Kuklenyik, I.J. Kurland, M. Leadley, K. Lin, K.R. Maddipati, D. McDougall, P.J. Meikle, N.A. Mellett, C. Monnin, M.A. Moseley, R. Nandakumar, M. Oresic, R. Patterson, D. Peake, J.S. Pierce, M. Post, A.D. Postle, R. Pugh, Y. Qiu, O. Quehenberger, P. Ramrup, J. Rees, B. Rembiesa, D. Reynaud, M.R. Roth, S. Sales, K. Schuhmann, M.L. Schwartzman, C.N. Serhan, A. Shevchenko, S.E. Somerville, L. St John-Williams, M.A. Surma, H. Takeda, R. Thakare, J.W. Thompson, F. Torta, A. Triebl, M. Trötzmüller, S.J.K. Ubhayasekera, D. Vuckovic, J.M. Weir, R. Welti, M.R. Wenk, C.E. Wheelock, L. Yao, M. Yuan, X.H. Zhao, S. Zhou, Harmonizing lipidomics: NIST interlaboratory comparison exercise for lipidomics using SRM 1950-Metabolites in Frozen Human Plasma, J Lipid Res. 58 (2017) 2275–2288. https://doi.org/10.1194/jlr.M079012.

[4]   J.J. Aristizabal-Henao, C.M. Jones, K.A. Lippa, J.A. Bowden, Nontargeted lipidomics of novel human plasma reference materials: hypertriglyceridemic, diabetic, and African-American, Anal Bioanal Chem. 412 (2020) 7373–7380. https://doi.org/10.1007/s00216-020-02910-3.

[5]   M. Ghorasaini, Y. Mohammed, J. Adamski, L. Bettcher, J.A. Bowden, M. Cabruja, K. Contrepois, M. Ellenberger, B. Gajera, M. Haid, D. Hornburg, C. Hunter, C.M. Jones, T. Klein, O. Mayboroda, M. Mirzaian, R. Moaddel, L. Ferrucci, J. Lovett, K. Nazir, M. Pearson, B.K. Ubhi, D. Raftery, F. Riols, R. Sayers, E.J.G. Sijbrands, M.P. Snyder, B. Su, V. Velagapudi, K.J. Williams, Y.B. de Rijke, M. Giera, Cross-Laboratory Standardization of Preclinical Lipidomics Using Differential Mobility Spectrometry and Multiple Reaction Monitoring, Anal Chem. 93 (2021) 16369–16378. https://doi.org/10.1021/acs.analchem.1c02826.

[6]   S.M. Camunas-Alberca, M. Moran-Garrido, J. Sáiz, A. Gil-de-la-Fuente, C. Barbas, A. Gradillas, Integrating the potential of ion mobility spectrometry-mass spectrometry in the separation and structural

characterisation of lipid isomers, Front. Mol. Biosci. 10 (2023) 1112521. https://doi.org/10.3389/fmolb.2023.1112521.

[7] G. Paglia, P. Angel, J.P. Williams, K. Richardson, H.J. Olivos, J.W. Thompson, L. Menikarachchi, S. Lai, C. Walsh, A. Moseley, R.S. Plumb, D.F. Grant, B.O. Palsson, J. Langridge, S. Geromanos, G. Astarita, Ion mobility-derived collision cross section as an additional measure for lipid fingerprinting and identification, Anal Chem. 87 (2015) 1137–1144. https://doi.org/10.1021/ac503715v.

[8] T. Baba, J.L. Campbell, J.C.Y. Le Blanc, PaulR.S. Baker, K. Ikeda, Quantitative structural multiclass lipidomics using differential mobility: electron impact excitation of ions from organics (EIEIO) mass spectrometry, Journal of Lipid Research. 59 (2018) 910–919. https://doi.org/10.1194/jlr.D083261.

[9] P.E. Williams, D.R. Klein, S.M. Greer, J.S. Brodbelt, Pinpointing Double Bond and sn-Positions in Glycerophospholipids via Hybrid 193 nm Ultraviolet Photodissociation (UVPD) Mass Spectrometry, J. Am. Chem. Soc. 139 (2017) 15681–15690. https://doi.org/10.1021/jacs.7b06416.

[10] S. Kammerer, J.-H. Küpper, Human hepatocyte systems for in vitro toxicology analysis, JCB. 3 (2018) 85–93. https://doi.org/10.3233/JCB-179012.

[11] A.E. Jones, N.J. Arias, A. Acevedo, S.T. Reddy, A.S. Divakaruni, D. Meriwether, A Single LC-MS/MS Analysis to Quantify CoA Biosynthetic Intermediates and Short-Chain Acyl CoAs, Metabolites. 11 (2021) 468. https://doi.org/10.3390/metabo11080468.

[12] P. Li, M. Gawaz, M. Chatterjee, M. Lämmerhofer, Targeted Profiling of Short-, Medium-, and Long-Chain Fatty Acyl-Coenzyme As in Biological Samples by Phosphate Methylation Coupled to Liquid Chromatography–Tandem Mass Spectrometry, Anal. Chem. 93 (2021) 4342–4350. https://doi.org/10.1021/acs.analchem.1c00664.

[13] A.M. James, A.A.I. Norman, J.W. Houghton, H.A. Prag, A. Logan, R. Antrobus, R.C. Hartley, M.P. Murphy, Native chemical ligation approach to sensitively probe tissue acyl-CoA pools, Cell Chem Biol. 29 (2022) 1232-1244.e5. https://doi.org/10.1016/j.chembiol.2022.04.005.

[14] B. He, X. Di, F. Guled, A.V.E. Harder, A.M.J.M. van den Maagdenberg, G.M. Terwindt, E.H.J. Krekels, I. Kohler, A. Harms, R. Ramautar, T. Hankemeier, Quantification of endocannabinoids in human cerebrospinal fluid using a novel micro-flow liquid chromatography-mass spectrometry method, Analytica Chimica Acta. 1210 (2022) 339888. https://doi.org/10.1016/j.aca.2022.339888.

[15] V. Kantae, S. Ogino, M. Noga, A.C. Harms, R.M. van Dongen, G.L.J. Onderwater, A.M.J.M. van den Maagdenberg, G.M. Terwindt, M. van der Stelt, M.D. Ferrari, T. Hankemeier, Quantitative profiling of endocannabinoids and related N-acylethanolamines in human CSF using nano LC-MS/MS, Journal of Lipid Research. 58 (2017) 615–624. https://doi.org/10.1194/jlr.D070433.

[16] T.G.J. Derks, Fasting Tolerance in Patients With Medium-chain Acyl-CoA Dehydrogenase Deficiency (MCADD) in the First Six Months of Life: an Investigator-initiated Human Pilot-study, clinicaltrials.gov, 2019. https://clinicaltrials.gov/study/NCT03761693 (accessed January 1, 2023).

[17] M. Zandl-Lang, B. Plecko, H. Köfeler, Lipidomics—Paving the Road towards Better Insight and Precision Medicine in Rare Metabolic Diseases, Int J Mol Sci. 24 (2023) 1709. https://doi.org/10.3390/ijms24021709.

[18] F. Nascimbeni, P. Bedossa, L. Fedchuk, R. Pais, F. Charlotte, P. Lebray, T. Poynard, V. Ratziu, LIDO (Liver Injury in Diabetes and Obesity) Study Group, Clinical validation of the FLIP algorithm and the SAF score in patients with non-alcoholic fatty liver disease, J Hepatol. 72 (2020) 828–838. https://doi.org/10.1016/j.jhep.2019.12.008.

Appendix

Nederlandse Samenvatting

Curriculum Vitae

List of Publications

Acknowledgements

<u>Samenvatting</u>

De lever – een van de grootste organen in het lichaam – heeft een cruciale rol bij het leveren van energie. De lever reguleert diverse metabole processen, zoals het afbreken van suikers en vetten, en is belangrijk bij het handhaven van homeostase in ons lichaam. Soms kunnen verstoringen in deze processen optreden door bijvoorbeeld genetische afwijkingen of omgevingsfactoren, wat tot leverziekten kan leiden. Vetten (lipiden) hebben een belangrijke rol in ons lichaam en de lever is, als het ware, het controlecentrum voor de verwerking ervan. Als de normale werking van de lever verstoord is, kan dit de lipidenniveaus in ons lichaam beïnvloeden, zoals beschreven in **hoofdstuk 1**. Hierdoor kan het bestuderen van lipiden (lipidomics) ons helpen begrijpen wat er gebeurt in het lichaam als er problemen zijn met de lever. Dit onderzoek gaat over de ontwikkeling van methoden om verschillende soorten lipiden te meten en het gebruik van deze methoden bij onderzoek naar leverziekten. Het eerste deel van dit proefschrift (**hoofdstuk 2 en 3**) was gericht op het ontwikkelen van methoden om lipiden te bestuderen en deze methode toe te passen op celmodellen. Het tweede deel (**hoofdstuk 4, 5 en 6**) richtte zich op een specifieke klasse lipide genaamd acyl-coënzym A (acyl-CoA), de rol van acyl-CoA in vetzuuroxidatiestoornissen (*fatty acid oxidation disorders*, FAOD, bepaalde leverziekten) en de uitdagingen die gepaard gaan met het meten van deze verbindingen. Er is een methode ontwikkeld om acyl-CoA's te meten en deze methode is toegepast om een specifiek type FAOD te bestuderen, genaamd midden-lang keten acyl-CoA dehydrogenase deficiëntie (*medium-chain acyl-CoA dehydrogenase deficiency*, MCADD).

In **hoofdstuk 2** richtten wij ons op de ontwikkeling en validatie van een methode om verschillende lipidenklassen te bestuderen. Dit is gedaan met behulp van een techniek genaamd hydrofiele interactie- vloeistofchromatografie-tandemmassaspectrometrie (HILIC-MS/MS). Deze methode stelt ons in staat om in het detail te kijken naar zowel polaire als apolaire lipiden, en meette 1200 verschillende lipiden in 19 (sub)klassen. Deze klassen omvatten categorieën zoals glycerolipiden, glycerofosfolipiden, sfingolipiden en sterolen. Er was hierbij rekening gehouden met verschillende factoren die potentieel tot meetfouten kunnen leiden. Na validatie van de methode door verscheidene testen, analyseerden wij monsters van COVID-19 patiënten om te bestuderen hoe de lipidensamenstelling verandert afhankelijk van de ernst van de ziekte. Er was nauwkeurige kwantificatie uitgevoerd met een gestandaardiseerde type bloedplasmamonster NIST SRM 1950. De lipidenconcentraties verkregen uit de NIST-bloedplasmamonsters met behulp van onze HILIC-MS/MS methode vertoonden goede overeenkomst met concentraties verkregen uit eerder onderzoek.

In **hoofdstuk 3** behandelden wij de zoektocht naar geschikte *in vitro* modellen die complexe functies van de lever accuraat nabootsten voor het onderzoek naar leverziektes. De gouden standaard voor zulke modellen is het gebruik van primaire humane hepatocyten (PHH). Echter, hebben deze cellen beperkingen zoals hun verlies van lever specifieke functies in de loop der tijd. Aldus hebben wij verschillende typen levercelmodellen vergeleken om te zien welke soortgelijke functies konden uitvoeren als PHH's, waaronder stamcelafgeleide hepatocyten (iPSC-Hep), humane hepatocellulaire carcinomacellen (HepG2), geïmmortaliseerde upcyte-hepatocyten (Upcyte-Hep) en leverorganoïden van volwassen donoren. Wij hebben getest hoe deze cellen functioneerden onder normale voedingsomstandigheden en uitdagende omstandigheden (door het weglaten van glucose).

Tevens hadden wij de in **hoofdstuk 2** ontwikkelde analysemethode ingezet om de lipidensamenstelling van deze cellen te onderzoeken. We hadden vastgesteld dat PHH's onder uitdagende omstandigheden zowel binnen als buiten de cellen de hoogste glucoseproductie vertoonden. Leverorganoïden waren daaropvolgend wat betreft de glucoseproductie, en hun lipidensamenstelling was vergelijkbaar met die van PHH's. Andere celtypen, zoals iPSC-Hep en HepG2 vertoonden een lagere glucoseproductie. Er zijn veranderingen in sleutelenzymen gerelateerd aan glucoseproductie geobserveerd en tevens veranderingen in lipidenprofielen in uitdagende omstandigheden, wat verschillen suggereerden in hoe deze cel. De resultaten impliceren dat leverorganoïden een goed alternatief kunnen zijn voor PHH bij het bestuderen van leverziekten. Maar er is meer onderzoek nodig om te bevestigen dat zij daadwerkelijk representatief zijn voor volledig functionerende en volgroeide levercellen.

FAOD's vormen een groep metabole leveraandoeningen die ontstaat door tekorten aan enzymen of eiwitten die verantwoordelijk zijn voor de afbraak van vetzuren, een essentieel proces voor het leveren van energie als de glucosespiegel laag is. Afhankelijk van het type FAOD hopen Acyl-CoA's en acylcarnitines zich op. Hoewel acyl-CoA's de primaire biomarkers voor FAOD's zijn, worden ze niet routinematig gebruikt voor diagnostisering, omdat de analyse ervan aanzienlijke technische uitdagingen met zich meebrengt. Acylcarnitines zijn afgeleiden van acyl-CoA's, die omgezet worden tijdens het vetzuurtransport naar de mitochondriën voor de vetzuuroxidatie. Acylcarnitines bewerkstelligen het transport van vetzuren over de mitochondriale membranen, waar zij uiteindelijk weer worden omgezet naar acyl-CoA's voor metabole processen. Omdat de analyse van acylcarnitines eenvoudiger is dan acyl-CoA's gebruiken ziekenhuizen bij voorkeur acylcarnitines voor de opsporing van FAOD's. **Hoofdstuk 4** geeft een uitgebreid overzicht van deze technische uitdagingen, recente

analytische voortuitgang bij de meting van acyl-CoA's en mogelijke maatregelen die genomen kunnen worden om de analyse te verbeteren. De voornaamste moeilijkheden bij de analyse van acyl-CoA's ontstaan door hun locatie binnenin de cel, de lage concentraties, instabiliteit en de uiteenlopende eigenschappen waarvoor meerdere scheidingsmethoden nodig zijn.

Om deze uitdagingen te overwinnen, hebben voorgaande onderzoeken verschillende technieken toegepast om acyl-CoA's uit biologische monsters te extraheren zoals, eiwitprecipitatie, vloeistof-vloeistof-extractie en vaste-fase-extractie. Er zijn verschillende methodes onderzocht voor de scheiding en detectie van deze verbindingen, waaronder enzymatische bepalingen, vloeistofchromatografie met ultravioletdetectie (LC-UV), gaschromatografie gekoppeld aan massaspectrometrie (GC-MS) en vloeistofchromatografie-massaspectrometrie (LC-MS). LC-MS is hiervan de gevoeligste en meest gebruikte methode. Recente inspanningen om de scheiding en detectie van acyl-CoA's te verbeteren, omvatten ionparen, derivatiseren en chemische ligatie. Het hoofdstuk benadrukt het belang van het gebruik van geschikte interne standaarden voor nauwkeurige kwantificatie. *Stable isotope labeling by essential nutrients in cell culture* (SILEC) is ontwikkeld om gelabelde isotopische standaarden voor acyl-CoA's te maken, die dienen als interne standaard voor nauwkeurige metingen. Dit is vooral cruciaal bij het kwantificeren van instabiele verbindingen zoals acyl-CoA's, aangezien zowel interne standaard als endogene varianten hetzelfde afbraakproces ondergaan. Samenvattend zette dit hoofdstuk recente vooruitgang uiteen in de analytische technieken voor het meten van acyl-CoA's en benadrukte het de noodzaak van verdere studies die gericht zijn op het vergroten van de stabiliteit en het vereenvoudigen van de analytische strategieën voor de meting van deze verbindingen.

In **Hoofdstuk 5** hadden wij één van de technische uitdagingen bij de analyse van acyl-CoA's aangepakt. Zoals vermeld in **hoofdstuk 4** hebben acyl-CoA's diverse eigenschappen, die vaak complexe chromatografische methoden of alternatieve technieken zoals ionparen of derivatisatie vereisen. Echter, gaan deze benaderingen gepaard met nadelen zoals verontreiniging en verhoogde complexiteit. In **hoofdstuk 5** was er een analysemethode ontwikkeld om het volledige scala aan acyl-CoA varianten in één enkele meting te dekken. Hierbij was een HILIC-MS/MS benadering met een zwitterionische ZIC-cHILIC kolom gebruikt. De ZIC-cHILIC kolom heeft zowel positief als negatief geladen deeltjes, wat leidt tot een zwakke elektrostatische interactie met het analyt, in dit geval acyl-CoA's. De methode werd in eerste instantie ontwikkeld op een QTOF (quadrupole-time-of-flight) massaspectrometer om acyl-CoA varianten te identificeren en hun retentietijden te bepalen. Factoren als

bufferconcentratie, matrixeffecten door cellen en injectieoplosmiddelen werden in achtgenomen bij de optimalisatie van de chromatografie. Vervolgens werd een gerichte methode gecreëerd op een QTRAP (quadrupole ion trap) massaspectrometer. Deze methode omvatte succesvol vrij CoA en acyl-CoA's met korte tot lange ketens in één enkele meting. Het presteren van de methode werd geëvalueerd aan de hand van parameters zoals lineariteit, precisie, opbrengst en matrixeffect voor kwantificatie van acyl-CoA's in HepG2 cellen. Deze methode werd vervolgens toegepast om wildtype HepG2 cellen te bestuderen die gekweekt waren in zowel voedselrijke als voedselarme toestand. De resultaten toonden een toename in concentratie van korte-, middellange en lange keten acyl-CoA's en een afname van het vrije CoA-gehalte onder voedselarme toestand, wat duidt op activatie van het vetzuuroxidatie proces.

In **hoofdstuk 6** hadden we een grondig onderzoek uitgevoerd van *in silico*, *in vitro* en *in vivo* modellen. Dit was gedaan om het CoA-metabolisme en systemische veranderingen, veroorzaakt door een metabole leveraandoening genaamd MCADD, te begrijpen, en ook om mogelijke compensatiemechanismen te identificeren. Allereerst werd er een *in silico* (computer-)model van de menselijke lever ontwikkeld om de veranderingen in acyl-CoA's onder normale omstandigheden en MCADD-omstandigheden te analyseren. Dit model wees op een significante toename van bepaalde acyl-CoA's, met name C6-CoA en C8-CoA onder MCADD-omstandigheden, terwijl andere soorten, waaronder vrij CoA, afnamen. Deze *in silico* bevindingen werden bevestigd aan de hand van experimentele gegevens op basis van HepG2 celmodellen (*in vitro*), waarbij er verhoogde niveaus van middellange keten (C6-C10) acyl-CoA's en acylcarnitines waren onder MCADD-omstandigheden. Tevens was de invloed van MCADD op biosynthese van CoA onderzocht door cellen te behandelen met gelabeld pantotheenzuur (vitamine B5), een precursor van CoA. We zagen labelinbouw in vrij CoA tussen de wildtype- en MCADD-groep in dezelfde mate, wat duidt op een actieve biosynthese van CoA onder MCADD-omstandigheden. Verder ontdekten we tijdens *in vivo* experimenten met zowel gezonde (controle) muizen als MCADD-muizen, een significante toename in totale CoA-waarden bij de MCADD-muizen tijdens vasten en blootstelling aan kou. Genexpressieanalyse in monsters verkregen uit cellen en muizen toonde aan dat zowel enzymen van de CoA-biosynthese als de carnitine acyltransferasen in MCADD-toestand omhoog waren gereguleerd, wat suggereerde dat de beschikbare vrije CoA's kunnen worden uitgeput door de ophoping van middellange keten acyl-CoA's. Interessant genoeg waren ook de Acyl-CoA thioesterases (ACOT's), verantwoordelijk voor het aanvullen van de vrije CoA-pool en het verminderen van overtollige opbouw van acyl-CoA's, verhoogd, wat duidde op een

compensatiemechanisme. Verder ondersteunden *in silico*-experimenten het idee dat de gelijktijdige toename van totaal CoA en omhoog regulatie van ACOT's effectief de niveaus van vrije CoA's herstelden terwijl de giftige opbouw van C8-CoA werd verminderd. Dit wees op de activatie van meerdere compensatiemechanismen. Concluderend hebben wij een aanpak beschreven waarbij *in silico*, *in vitro* en *in vivo* technieken werden gecombineerd om bevindingen te valideren en systemische veranderingen bij MCADD te ontrafelen.

Over het algemeen genomen draagt het onderzoek beschreven in dit proefschrift bij aan begrip over hoe lipidomics onze kennis van metabole leverziekten kan vergroten. Wij hebben analytische technieken ontwikkeld om lipidenmoleculen uitgebreid te bestuderen en ze in verband te brengen met biochemische routes. Deze technieken zijn toegepast op verschillende *in vitro* modellen om inzicht te krijgen in de stofwisseling van de lever en om veranderingen van lipidensoorten te kwantificeren in de monsters van metabole leverziekten. In de toekomst biedt dit onderzoek mogelijkheden voor de integratie van lipidomics met biologische gegevens uit andere *-omics* onderzoeksvelden, een *multi-omics* benadering. Dit opent de weg naar een systeembiologische aanpak die de mogelijkheden van gepersonaliseerde geneeskunde kan verbreden.

Curriculum Vitae

Madhulika Singh was born on the 5th of October, 1990, in Uttar Pradesh, India. Following her school education, she pursued a bachelor's degree in pharmacy (B.Pharm.) at Babu Banarasi Das National Institute of Technology and Management (BBDNITM) in Lucknow, Uttar Pradesh, India, from 2009 to 2013, and graduated with distinction. She received the award for being the top-ranking student throughout all four years of her B.Pharm. Subsequently, she was admitted to one of India's leading institutes for pharmacy education, the National Institute for Pharmaceutical Education and Research (NIPER) in Mohali, where she pursued a Master's in Medicinal Chemistry (M.S. Pharm.). During her master's program, Madhulika conducted her thesis research under the guidance of Prof. Asit K. Chakraborti. In her thesis, titled *"Design and Synthesis of 2-(2"-Arylphenyl) Benzoxazole Derivatives as Potential COX-2 Inhibitors"* Madhulika conducted molecular docking studies on various aryl phenyl benzoxazole derivatives to assess their binding affinity to COX-2. Subsequently, she synthesized these compounds and evaluated their *in vitro* enzymatic activity as potential COX-2 inhibitors. This comprehensive approach allowed her to establish a Structure-Activity Relationship (SAR) model. Madhulika received a scholarship from the Government of India during her M.S. studies. She was granted a patent titled "2-(2-aryl/alkyl phenyl) benzazole as selective COX-2 inhibitory scaffolds" for her M.S. (Pharm.) research Project (Patent Application No.: 2540/DEL/2015, Indian Patent Number: 387998). Following the completion of her master's degree, Madhulika ventured into industrial research where she worked as bioanalytical and metabolite identification scientist, in drug metabolism and pharmacokinetics (DMPK) field until June 2019. During this period, she worked in the discovery biology division of the biopharma company Syngene International Ltd., (daughter company of Biocon currently ranked 8th among Global Biotech Employers for 2022 by Science magazine).

In June 2019, she started her PhD under the supervision of Prof. dr. Thomas Hankemeier and Dr. Amy Harms at 'Metabolomics and Analytics Centre' (MAC), in the Leiden Academic Centre for Drug Research (LACDR). Madhulika worked as an early-stage researcher in the PoLiMeR consortium and her PhD research was funded through the European Union's Horizon 2020 research and innovation program under the Marie Skłodowska-Curie grant agreement. During her PhD, she developed lipidomics platforms, utilizing highly sensitive LC-MS/MS methods, aimed at investigating the role of lipids in liver metabolic diseases and gaining insights into the underlying pathophysiological mechanisms involved. Her academic involvement extended to active participation in various national and international conferences.

Appendix

She delivered both oral and poster presentations during PoLiMeR consortium meetings, which occurred semiannually. Furthermore, she presented her research findings through poster presentations at events such as CHAINS (2021), Euroanalysis (2023), the International Conference on the Bioscience of Lipids (2023) and the LACDR Spring Symposium (2020, 2021, 2023).

List of Publications

1. Zhang Z*, **Singh M***, Kindt A, Wegrzyn AB, Pearson MJ, Ali A, Harms AC, Baker P, Hankemeier T. Development of a targeted hydrophilic interaction liquid chromatography-tandem mass spectrometry-based lipidomics platform applied to a coronavirus disease severity study. Journal of Chromatography A, Volume 1708, 11 October 2023, 464342. https://doi.org/10.1016/j.chroma.2023.464342.

2. Bonanini F*, **Singh M***, Yang H, Kurek D, Harms AC, Mardinoglu A, Hankemeier T. A comparison between different human hepatocyte models reveals profound differences in net glucose production, lipid composition and metabolism *in vitro*. Experimental Cell Research, Volume 437, Issue 1, 1 April 2024, 114008. https://doi.org/10.1016/j.yexcr.2024.114008

3. **Singh M**, Elfrink HL, Harms AC, Hankemeier T. Recent developments in the analytical approaches of acyl-CoAs to assess their role in mitochondrial fatty acid oxidation disorders, *Molecular Genetics* and Metabolism. (2023) 107711. https://doi.org/10.1016/j.ymgme.2023.107711.

4. **Singh M**, Kiyuna LA, Odendaal C, Bakker BM, Harms AC, Hankemeier T. Development of targeted hydrophilic interaction liquid chromatography-tandem mass spectrometry method for acyl-Coenzyme A covering short- to long-chain species in a single analytical run. Journal of Chromatography A, Volume 1714, 11 January 2024, 464524. https://doi.org/10.1016/j.chroma.2023.464524.

5. Odendaal C*, Kiyuna LA*, **Singh M***, Gerding A, Langelaar-Makkinje M, Zwaag M van der, Drachman A, Cetkovská V, Kioen GLF, Martines ACMF, Huijkman NCA, Schepers H, Sluis B van de, Reijngoud DJ, Oosterveer MH, Sibon OCM, Harms AC, Hankemeier T, Bakker BM. An old new player in MCADD: reduced free coenzyme A availability in medium-chain acyl-CoA dehydrogenase deficiency. *(In preparation)*

(* authors contributed equally)

Others (not part of this thesis)

1. Horcas-Nieto JM, Kiyuna LA, Langelaar-Makkinje M, Gerding A,. Broekhuis MJC, Bonanini F, **Singh M**, Kurek D, Harms AC, Hankemeier T, Foijer F, Derks TGJ, Bakker B. iPSC-derived liver organoids as a tool to study Medium Chain Acyl-CoA Dehydrogenase deficiency. *(Submitted)*

2. Zhang Z, Karu N, Kindt A, **Singh M**, Lamont L, van Gammeren AJ, Ermens AAM, Harms AC, Portengen L, Vermeulen RCH, Dik WA, Langerak AW, van der Velden VHJ, Hankemeier T. Association of Altered Plasma Lipidome with Disease Severity in COVID-19 Patients. *Biomolecules* **2024**, *14*, 296 https://doi.org/10.3390/biom14030296.

3. Tanwar B, Kumar D, Kumar A, Ansari MI, Qadri MM, Vaja MD, **Singh M.** and Chakraborti AK. Friedlander annulation: Scope and limitations of metal Lewis acid catalysts in selectivity control for the synthesis of functionalised quinolines. New J. Chem., 2015,39, 9824-9833. https://doi.org/10.1039/C5NJ02010G

Appendix

4. **Patent:** "2-(2-aryl/alkylphenyl)benzazoles as selective COX- 2 inhibitory scaffolds" M.S. Pharm. Research Project Patent Application No.: 2540/DEL/2015 (Granted). **Indian Patent Number: 387998.**

Acknowledgements

The journey of my PhD has been truly unforgettable, as it has transformed me both on a personal and professional level. However, this journey would not be complete without the support of many people who have contributed in the completion of this thesis.

First and foremost, I extend my deepest appreciation to Prof. dr. Thomas Hankemeier for giving me the opportunity to pursue my PhD within his research group and for providing invaluable guidance, unwavering mentorship, constant support and encouragement throughout my entire PhD journey. I wish to express my gratitude to my co-promoter and daily supervisor, Dr. Amy Harms, for her continuous support and guidance over the years. She always gave me the freedom to explore my ideas and was always available for discussions and assistance. Her constructive feedback, input and collaborative brainstorming allowed me to have scientific flexibility and autonomy, have been immeasurable in shaping the outcomes of this research and aiding in the successful completion of my thesis. I am delighted and deeply grateful that she travelled to India to attend my wedding and became a part of this important day in my life.

I extend my heartfelt gratitude to my collaborators, Prof. Barbara Bakker and Dr. Dorota Kurek, for their wonderful collaboration and fruitful discussions on our projects. My appreciation also goes to Zhengzheng, who has not only been a great colleague but a dear friend. She helped me during the early stages of my PhD and was an excellent collaborator in our work on lipidomics. I also want to express my thanks to Flavio, Ligia, and Christoff for their contributions to our exciting projects and collaborations. I am also grateful to my PoLiMeR consortium members, with a special mention to Karen, for organizing unforgettable meetings that combined education training with social events.

I would also like to acknowledge the current and former members of the Metabolomics and Analytics Centre, specifically Tim, Gerwin, Sabine and Faisa for their invaluable assistance with the instruments. Their timely support with the equipment has been instrumental in keeping most of our PhD projects on track and I am truly thankful for that. I also extend my heartfelt thanks to my dedicated students Asmara, Mai, Vladka, Gaby and Nadieh for their hard work and commitment to their master's projects. It fills me with immense pride to be their supervisor and their contributions significantly contributed to my growth as a teacher.

I extend my thanks to my office companions, Farideh, Mengle, Simon, Guus, Marielle and Lu, for the enjoyable moments we have shared and for brightening up our work environment. I want to express my gratitude to my friends who have become more like family over time - Manchu,

Mariyana and Kanchana. Thanks for all the fun, laughter and after-office adventures. To Pingping, Bingshu, Barbara, Joyee and others for being a companion in my PhD journey. You all have been a blessing. I also want to thank Alida, Pascal and Michael, for the wonderful tools they have developed. To Hyung for a nice collaboration and for providing support with the Dutch summary of my thesis. Thanks to Cathy, Ina and Ariadne for their assistance whenever needed.

I would like to extend my heartfelt appreciation to my dearest friends, Pooja, Ankita, Preeti, Sameer and Pihu, for the countless conversations and laughter that brightened my days. My deepest gratitude goes to my parents, Anamika (sister) and Shivendra (brother), whose unconditional love, care, motivation and support have been my source of strength throughout my PhD journey. I also want to thank my parents-in-law for their encouragement and goodwill. Lastly, I want to express my profound gratitude to my husband and best friend, Ashok, for his help with the cover design of this thesis. He is a constant source of encouragement and entertainment that keeps me motivated. I eagerly anticipate all the adventures and fun that await us in the future.

In conclusion, I extend my sincere gratitude and thanks to all the individuals who have played a part in my journey, including those I may have forgot to mention. Your contributions and support have been deeply appreciated.